An Appraisal of the Characteristic Modes of Composite Objects

by

Hamad Alroughani

A thesis submitted to the
Faculty of Graduate and Postdoctoral Studies
in partial fulfillment of the requirements for the degree of

Master of Applied Science
in Electrical & Computer Engineering

Ottawa-Carleton Institute for Electrical and Computer Engineering
School of Electrical Engineering and Computer Science
Faculty of Engineering
University of Ottawa

ABSTRACT

The theory of electromagnetic characteristic modes was published roughly forty years ago, for both conducting and penetrable objects. However, while the characteristic mode analysis of conducting objects has found renewed interest as a tool for antenna designers, computed results for the characteristic mode eigenvalues, eigencurrents and eigenfields for penetrable objects have not appeared, not even in the seminal papers on the subject. In this thesis both volume and surface integral equation formulations are used to compute the characteristic modes of penetrable objects for what appears to be the first time. This opens the way for the use of characteristic mode theory in the design of antennas made of penetrable material whose polarization current densities constitute the main radiating mechanism of the antenna. Volume formulations are shown to be reliable but computationally burdensome. It is demonstrated that surface formulations are computationally more efficient, but obtrude some non-physical modes in addition to the physical ones. Fortunately, certain field orthogonality checklists can be used to provide a straightforward means of unambiguously selecting only the physical modes. The sub-structure characteristic mode concept is extended to problems involving both perfectly conducting and penetrable materials. It is also argued that sub-structure modes can be viewed as characteristic modes that implicitly use modified Green's functions, but without such Green's functions being needed explicitly. This makes the concept really practical, since the desired modified Green's functions are not known explicitly in most cases.

Keywords: characteristic modes, natural modes, penetrable objects, sub-structure characterisitic modes

Acknowledgements

I would like to express my thanks and great appreciation to my supervisor Dr. Derek A. McNamara for his total support throughout the duration of my research. I have found that his constructive criticism, comments, disagreement, and honesty were very essential to get the job done right. I also thank him for allowing me unfettered use of material from his graduate course notes for some of the background material used in this thesis.

I also would like to thank my professors who taught the graduate courses namely Dr. Aldo Petosa, Dr. Derek McNamara, and Dr. Rony Amaya for their superior efforts in conveying the necessary message and delivering the right information to their students. I have learned a lot from all of you.

Also, I want to thank my colleague Dr. Jonathan Either who has extensively shared with me his knowledge and thoughts on the theory of characteristic modes. Besides, I am grateful for my colleagues Esther Yu and Eqab Almajali providing me with their thoughtful advice and helpful comments.

Finally, and most importantly, I would like to thank my friends and family for their great support and encourage that they have been showing to me to continue pursuing my graduate studies even though I am thousands miles away from all of them. To my friends in Canada, you all have been great company throughout my stay in this great nation, and you all deserve at least the word “Thank you”.

Publications

- H.Alroughani, J.Ethier and D.A.McNamara, "An Appraisal of the Characteristic Modes of Dielectric Objects", *URSI Radio Science Meeting Digest*, Chicago, USA, July 2012.

- Table of Contents

List of Figures

List of Tables

List of Symbols

$\left[Y\right]$	admittance operator, discrete form
$\bar{E}_n$	characteristic electric fields
J_n	characteristic mode current density coefficients
λ_n	characteristic mode eigenvalue, perfect conductors
s_{mn}	complex frequency of natural modes
$\left[G\right]$	conductance operator, discrete form
$\nabla\times$	curl operator
$\delta\left(\underline{r}\right)$	delta function
$\nabla\cdot$	divergence operator
$\bar{J}$	electric current density vector
$\mathbb{G}_{\text{free space}}$	free-space Green's function
$\mathbb{G}_{\text{modi}\,fied}$	modified Green's function
η	free-space intrinsic impedance
μ_o	free-space permeability
ε_0	free-space permittivity
k	free-spcae wave number
f	frequency
∇	gradient operator
$H_n^{(2)}$	Hankel function of second kind of nth order
j	imaginary unit, $\sqrt{-1}$
$\mathcal{Z}$	impedance operator, continuous form
$\left[Z\right]$	impedance operator, discrete form
$\bar{J}^{imp}$	impressed electric current source
$\bar{M}^{imp}$	impressed magnetic current source

$\bar{E}^{inc}$	incident electric field
$\bar{M}^{inc}$	Incident magnetic field
$\bar{E}_{\tan}^{inc}$	incident tangential electric field
$\bar{M}_{\tan}^{inc}$	incident tangential magnetic field
δ_{mn}	Kronecker delta
$\bar{M}$	magnetic current density vector
V_n^i	modal excitation coefficient
α_n	modal expansion coefficient
$W_{net,n}$	modal net stored energy
$\mathbb{G}_{\text{modified}}$	modified Green's function
r	radial distance
ω	radial frequency
$\bar{r}$	radial vector, observation location
$\bar{r}'$	radial vector, source location
a	radius of circumscribing sphere
$\mathscr{X}$	reactance operator, continuous form
$[X]$	reactance operator, discrete form
$\mathscr{R}$	resistance operator, continuous form
$[R]$	resistance operator, discrete form
Φ	scalar potential
S_∞	sphere at infinity
$[B]$	substance operator, discrete form
$[X]_{sub}$	sub-structure reactance operator, discrete form
$[R]_{sub}$	sub-structure resistance operator, discrete form
c	velocity of light
λ	wavelength of free space

List of Acronyms

2-D	Two-Dimensional
3-D	Three-Dimensional
BOR	Body of Revolution
CDR	Circular Dielectric Resonator
CFIE	Combined Field Integral Equation
CM	Characteristic Mode
CR	Cognitive Radio
DR	Dielectric Resonator
DRA	Dielectric Resonator Antenna
EFIE	Electric Field Integral Equation
FDTD	Finite Difference Time Domain
FEM	Finite Element Method
HEM	Hybrid Electromagnetic
IE	Integral Equation
MFIE	Magnetic Field Integral Equation
MIMO	Multiple Input Multiple Output
MoM	Method of Moments
MS	Modal Significance
PEC	Perfectly Electrical Conductor
PMCHWT	Poggio-Miller-Chang-Harrington-Wu-Tsai
RDR	Rectangular Dielectric Resonator
SIE	Surface Integral Equation
TE	Transverse Electric
TM	Transverse Magnetic
VIE	Volume Integral Equation

CHAPTER 1 Introduction

1.1 THE CHARACTERISTIC MODE CONCEPT

Antennas are needed in all wireless (as opposed to wired) communications. Except for those on base-stations, wireless antennas must have broad radiation patterns (hence low directivity) because of the propagation issues extant in wireless networks. Such antennas must usually fit in the crammed environment of portable devices and so can be difficult to design. This difficulty is increased for the cognitive radio (CR) and multiple-input/multiple-output (MIMO) capabilities that will be used in future wireless systems to overcome spectrum scarcity, since these low-directivity antennas will need to be electronically reconfigurable, with more than one antenna located on a single device, and offer more than the traditional antenna performance characteristics. [VAIN09] states that future portable terminals could have more than 20 antennas, some forming adaptive sets. New configurations, design methods, and testing methods are therefore under development worldwide.

Computational electromagnetics is a key tool in antenna design. The source densities and electromagnetic fields obtained from such modelling incorporate all the physics associated with a particular configuration. The difficulty is to extract and exploit the information in the solutions as much as possible. Characteristic mode analysis allows one to “squeeze out” a little more of this information. The theory of characteristic modes (CMs) of perfectly-conducting objects was first devised by Garbacz at the Ohio State University [GARB65], and received an impetus with the work of the Harrington group at Syracuse University [HARR71a, HARR71b] that provided a means of actually computing such modes for objects of quite general shape using the method of moments, which had just begun to make inroads in electromagnetic engineering. Interest in the topic lay dormant for more than twenty years, until attempts to forge insightful design methods for new wireless antennas led to renewed interest in characteristic mode ideas. Examples include [ADAM11], [ETHI08d], [ETHI09a], [CABE03], [CABE07], [ETHI09b], [ETHI10c] and [ETHI12a], to name but a few. For instance, [ETHI10c] devised a method that performs a true shape synthesis of antennas using numerical optimization with a new characteristic mode based objective function. This allows one to start with a conducting sheet of some specified shape (eg. the shape of the "leftover space" in some device) and synthesize an antenna shape for operation with maximised radiation efficiency and bandwidth (low Q) at a specified frequency or even for multiband performance. The completely new aspect of this approach, only possible through adopting a characteristic mode point of view, is that the location of the feed point(s) is not specified beforehand. So, the synthesis problem is not over-constrained and the electromagnetics "tells us" after the synthesis process where to locate the feed point(s).

1.2 LIMITATIONS OF EXISTING WORK ON THE CHARACTERISTIC MODES OF DIELECTRIC OBJECTS

Methods for finding the characteristic modes of penetrable objects using equivalent volume current densities [HARR72a] and equivalent surface current densities [CHAN 77] were published within six years of the work on that for perfectly-conducting objects. However, these references do not provide actual numerical results showing actual characteristic mode eigenvalues, current density distributions and fields. Nor are we aware of such information appearing in the literature since that time. As a result, at this stage all published work (including the examples given in Section 1.1) on the use of characteristic modes in antenna design has concentrated on configurations made of (principally planar) conducting material. In this thesis we therefore examine means for the reliable computation of the characteristic modes of penetrable objects. Knowing how to do this will be needed in the future if the antenna shape synthesis techniques mentioned in Section 1.1 are to be used for dielectric antenna and the like.

1.3 OVERVIEW OF THE THESIS

The goal of this thesis is the clarification of some matters on the subject of the characteristic modes of perfectly-conducting objects, and the actual computation (for the first time in fact) of the characteristic modes of penetrable objects. The thesis is of its very nature a theoretical one, even though the foundations that its lays are for eventual antenna shape synthesis purposes. The work described here could only be undertaken after a thorough study of the existing theoretical concepts underlying characteristic mode analysis. Chapter 2 provides a review of what is needed as the starting point of the thesis.

The most significant contributions of this thesis are developed in Chapters 3, 4 and 5. When the author presented the paper [ALRO12], he was asked why natural modes could not be used instead. In order to fully answer this question it has been necessary to examine the relation of natural modes to characteristic modes, since such a direct comparison does not appear to have been discussed elsewhere. In fact many antenna engineers (as in the case of this author prior to the writing of this thesis) are not familiar with the fact that exterior natural modes, as opposed interior natural modes (cavity modes), can even be defined for a conducting object in the same way as is done for a dielectric object. Some quantitative investigation, albeit brief, has therefore been conducted as part of this thesis research, and is described in Chapter 3. This allows us to appreciate the difference between natural modes and characteristic modes.

Chapter 4 investigates and provides some answers to certain questions of interpretation that arose, in the present research work, on the topic of the characteristic modes of perfectly conducting objects. It also shows that the sub-structure mode concept can be extended to PEC objects in the presence of penetrable ones.

Chapter 5 deals with the problem of finding the computation of the characteristic modes of penetrable objects using integral equation models. It begins with the use of volume integral equation (VIE) models in which the penetrable object is represented by volume equivalent current densities. This is followed by the use of surface integral equation (SIE) models in which the penetrable object is represented by fictitious surface current densities. The SIE approach is computationally less burdensome than the VIE one. However, we will show that the SIE obtrudes certain non-physical characteristic modes, and how experience gained in the characteristic mode determination using the VIE computation has shown us how to exclude these modes. This is the first time actual numerical results have been presented for the characteristic modes of penetrable objects. We use in-house codes (developed as part of this thesis) for initial studies of two-dimensional (2-D) geometries using both the SIE and VIE approaches. After having developed an understanding of the problem issues we then proceed to the use of a commercial code (for which access to specific matrices is, unusually, provided by the vendor) for the determination of the characteristic modes of three-dimensional penetrable objects, once again via both the VIE and SIE methods[1]. The above-mentioned matrices are extracted from the code and exported to MATLAB for the eigenanalysis that yields the characteristic mode information. Details of the extent of the computational burden are provided.

---

[1] The commercial code in question does not itself determine the characteristic modes of penetrable objects though.

Finally, in Chapter 6, we conclude with a list of the contributions made by the work of this thesis. We also comment on future work that we envisage in the area of characteristic mode computation and applications.

CHAPTER 2 Review of the Characteristic Mode Concept and its Applications

2.1 INTRODUCTION

The purpose of this chapter is to introduce the essentials of characteristic mode theory and how they can be determined for objects of general shape. To the best of the author's knowledge, no texts have yet been written on the topic, and an attempt has therefore been made to bring together many aspects in this chapter. Some references on the application of characteristic modes in antenna design were listed in Chapter 1. There are many more than these available in the literature, but in order to keep this review to a manageable level only those papers concerned with the actual computation of characteristic modes (as opposed to their application), will be discussed in the present chapter. Such computation is, after all, the goal of the thesis.

Section 2.2 describes the fundamental characteristic mode concept. Section 2.3 provides a review of the integral equation approaches used for finding characteristic modes, and lists some of the desirable properties of such modes. Alternative, but not widely used, ways of determining these modes are briefly described in Section 2.4. The necessity of using so-called mode-tracking, when computing the characteristic modes of any object, is the subject of Section 2.5. Examples of results we have obtained for the characteristic modes of selected perfectly-conducting (PEC) are presented in Section 2.6; reference to the results obtained by others for some of these same objects provide some confirmation that such computations are being correctly done in the thesis. Although not actually used in this thesis, a characteristic mode formulation for apertures in PEC connecting two regions is discussed in Section 2.7, in order to show the possible breadth of application. Sections 2.8 and 2.9 describe the volume integral equation and surface integral equation for the determination of the characteristic modes of penetrable objects; these have not yet been used by others to actually find the modes of such objects. The sub-structure characteristic mode idea is reviewed in Section 2.10, and some concluding remarks on the chapter are made in Section 2.11.

2.2 FUNDAMENTAL DEFINITION OF THE CHARACTERISTIC MODES OF PERFECTLY CONDUCTING (PEC) OBJECTS

Consider the scattering of an arbitrary incoming electromagnetic wave by some PEC object. Expand this incoming field in terms of an infinite series of vector spherical waves. Let $[A]$ be an infinite-dimensional column matrix containing the complex amplitudes of these incoming vector spherical waves. Similarly, let $[B]$ be an infinite-dimensional column matrix containing the complex amplitudes of outgoing vector spherical waves. These could be used to write down the scattered field as an expansion in terms of outgoing spherical waves. The relationship between $[A]$ and $[B]$ is expressed in terms of the generalized scattering matrix $[S]$ of the object by the expression $[B]=[S][A]$. If the scattering object is a sphere then $[S]$ is a diagonal matrix; in other words the excitation of one incoming spherical wave is not influenced by any other spherical wave. The spherical wave functions were considered to be "characteristic modes" associated with spherical scatterers[1]. By considering diagonalization of the scattering matrix of an object[2] Garbacz [GARB65, GARB68] was the first to show that any arbitrary object has its own set of characteristic modes, by which we mean characteristic fields and characteristic currents. Also shown was the fact that characteristic modes have certain very useful properties and physical interpretations. The characteristic currents are a set of real currents induced on the surface of lossless conducting objects. These characteristic mode currents depend only upon the shape and size of the object and are independent of any specific excitation. These modal currents form an orthogonal set (for the lossless case) that can be used to expand the actual current on the object when it is excited by a specific incident field. The properties of characteristic modes will be considered in more detail in Section 2.3.

The definition of characteristic modes is independent of the manner in which they are actually determined. The original paper [GARB65] did not provide a routine way of actually finding the characteristic modes of objects of general shape. It only found (with difficulty) those for somewhat idealized objects such as one consisting of an arrangement of thin parallel infinitely long conducting wires. However, characteristic modes are now most directly computed using

---

[1] Cylindrical wave functions are the characteristic modes associated with infinite circular cylinders.

[2] Harrington et al. (eg. [HARR71a] and [HARR71b]) subsequently showed a connection between the theory of Garbacz and the impedance operator of the electric field integral equation, and so was able to use the method of moments as a means of computing characteristic modes. This forms the discussion in most of the rest of Chapter 2.

integral equation (IE) models for scattering from the object in question, in particular their solution using the method of moments. The IE approach also more easily reveals the general properties of the CMs. As a result, there is a tendency to regard the IE approach as defining the CM concept, but it should be remembered that this is not strictly so. Nevertheless, apart from brief descriptions in Section 2.4 on alternative ways to compute CMs, this thesis will indeed use IE methods only.

2.3 METHODS FOR DETERMINING THE CHARACTERISTIC MODES OF A PEC OBJECT – INTEGRAL EQUATION APPROACH

2.3.1 Introductory Remarks

A number of methods have been used to determine the characteristic modes of an object. However, integral equation methods are the most widely-used of these methods, and appear to be the most reliable and convenient. Thus, although it was chronologically not the first method to be used for such purposes, integral-equation-based methods will be described first, and in the most detail, since it is the approach used in this thesis. The alternative approaches will then be briefly described; they will not be used here for reasons that will be given along with the description provided for each approach.

2.3.2 Electric Field Integral Equation (EFIE) Approach

A Basic Ideas

The derivation of the general form of the EFIE for PEC objects in free space is well-known [PETE97]. It is written down here because of the fundamental role it plays in the discussion of the characteristic modes of PEC objects (and hence in this thesis), and the fact that a particular notation will be emphasized[3] in order to contrast it with the discussion to follow in Chapter 4 (and hence facilitate understanding of the concepts discussed in the latter chapter).

---

[3] Specifically, we emphasize that a free space Green's function $G_{\text{free space}}$ is being used here. In Section 4.4, It will be replaced by a modified Green's function G_{modified}. These Green's functions might be scalar, vector or dyadic

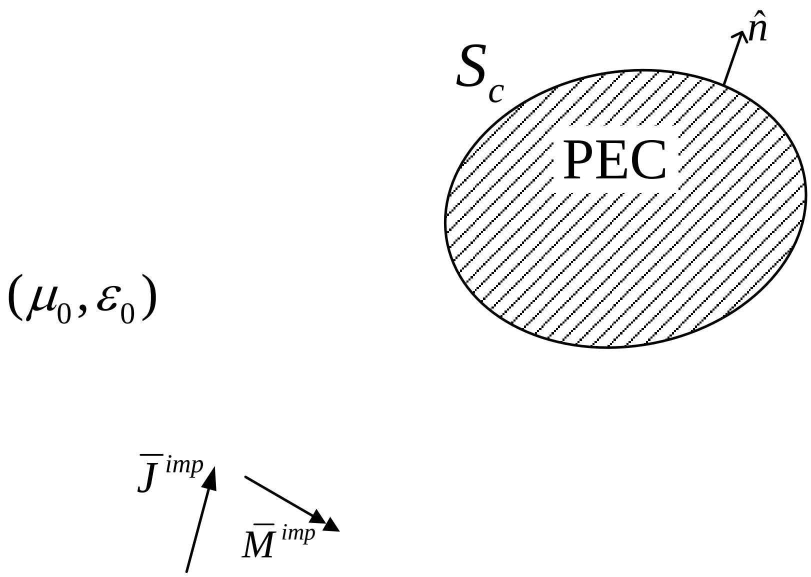

Figure 2.3-1: Representation of PEC Object Illuminated by Incident Fields Due to Impressed Sources

The EFIE for modeling scattering form a PEC object is

$$\hat{n}(\bar{r}_s)\times\bar{E}^{scat}\left\{\bar{r}_s,\bar{J}_s,\mathcal{G}_{\text{free space}}\right\}=-\hat{n}(\bar{r}_s)\times\bar{E}^{inc}\left\{\bar{r}_s,\bar{J}^{imp},\bar{M}^{imp},\mathcal{G}_{\text{free space}}\right\}\qquad \bar{r}_s\in S_c \quad (2.3\text{-}1)$$

$\bar{E}^{scat}\left\{\bar{r}_s,\bar{J}_s,\mathcal{G}_{\text{free space}}\right\}$ is the scattered field, and is an integral involving unknown electric surface current density $\bar{J}_s$ and a free space Green's function $\mathcal{G}_{\text{free space}}$, whereas $\bar{E}^{inc}\left\{\bar{r}_s,\bar{J}^{imp},\bar{M}^{imp},\mathcal{G}_{\text{free space}}\right\}$ is known. Integral equation (2.3-1) is often written as

$$\bar{E}^{scat}_{\tan}\left\{\bar{r},\bar{J}_s,\mathcal{G}_{\text{free space}}\right\}=-\bar{E}^{inc}_{\tan}\left\{\bar{r},\bar{J}^{imp},\bar{M}^{imp},\mathcal{G}_{\text{free space}}\right\}\qquad \bar{r}\in S_c \qquad (2.3\text{-}2)$$

where subscript "tan" on some quantity implies "take its component tangential to the surface S_c of the PEC object". The EFIE in (2.3-2) can be written in operator notation as

---

functions, depending on the specific integral equation formulation used. This is the reason for the notation used to denote it.

$$\mathcal{Z}\left\{\bar{J}_s\right\} = -\bar{E}_{\tan}^{inc} \tag{2.3-3}$$

with $\mathcal{Z}$ referred to as the impedance operator since its units are Ohms.

Following [HARR71a], we recognize that the most general form of eigenvalue problem involving this operator can be written

$$\mathcal{Z}\left\{\bar{J}_n\right\} = \nu_n \mathcal{K}\left\{\bar{J}_n\right\} \tag{2.3-4}$$

with the operator $\mathcal{K}$ yet to be determined. If $\mathcal{K}$ is selected to be the identity operator one obtains a set of eigenvectors (which will be eigencurrents) with No special properties such as orthogonality or otherwise. However, if $\mathcal{K}$ is chosen to be the real part of $\mathcal{Z}$, which we will denote by $\mathcal{R}$, we obtain eigencurrents and eigenfields with certain desirable orthogonality properties, as we will see shortly. With this choice for $\mathcal{K}$ the eigenvalue problem (2.3-4) is

$$\mathcal{Z}\left\{\bar{J}_n\right\} = \nu_n \mathcal{R}\left\{\bar{J}_n\right\} \tag{2.3-5}$$

Using a change of variables $\nu_n = 1 + j\lambda_n$ allows us to re-write the eigenvalue problem (2.3-5) in the form

$$\mathcal{Z}\left\{\bar{J}_n\right\} = \left(1 + j\lambda_n\right)\mathcal{R}\left\{\bar{J}_n\right\} \tag{2.3-6}$$

If we agree to write $\mathcal{Z}$ in terms of its real and imaginary parts as

$$\mathcal{Z}\left\{\bar{J}_n\right\} = \mathcal{R}\left\{\bar{J}_n\right\} + j\mathcal{X}\left\{\bar{J}_n\right\} \tag{2.3-7}$$

then (2.3-6) becomes

$$\mathcal{R}\left\{\bar{J}_n\right\} + j\mathcal{X}\left\{\bar{J}_n\right\} = \mathcal{R}\left\{\bar{J}_n\right\} + j\lambda_n \mathcal{R}\left\{\bar{J}_n\right\} \tag{2.3-8}$$

which reduces to

$$\mathcal{X}\left\{\bar{J}_n\right\} = \lambda_n \mathcal{R}\left\{\bar{J}_n\right\} \tag{2.3-9}$$

The operators $\mathcal{R}$ and $\mathcal{X}$ are both real symmetric operators, and hence the eigenvalues λ_n are real and the eigenvectors $\bar{J}_n$ real[4]. These are referred to as the characteristic mode eigenvalues and eigencurrents. Associated with each eigencurrent will be eigenfields $(\bar{E}_n, \bar{H}_n)$.

B Orthogonality Properties of Characteristic Modes Current Densities

Because the operators $\mathcal{R}$ and $\mathcal{X}$ are real symmetric operators (that is, Hermitian operators), various theorems from the mathematical discipline of functional analysis [TAYL82] then at once allow us to write down the following orthogonality properties of the eigencurrents :

$$\left\langle \bar{J}_m, \mathcal{R}\left\{\bar{J}_n\right\}\right\rangle = \left\langle \bar{J}_m^*, \mathcal{R}\left\{\bar{J}_n\right\}\right\rangle = 0 \qquad (2.3\text{-}10)$$

$$\left\langle \bar{J}_m, \mathcal{X}\left\{\bar{J}_n\right\}\right\rangle = \left\langle \bar{J}_m^*, \mathcal{X}\left\{\bar{J}_n\right\}\right\rangle = 0 \qquad (2.3\text{-}11)$$

$$\left\langle \bar{J}_m, \mathcal{Z}\left\{\bar{J}_n\right\}\right\rangle = \left\langle \bar{J}_m^*, \mathcal{Z}\left\{\bar{J}_n\right\}\right\rangle = 0 \qquad (2.3\text{-}12)$$

for $m \neq n$. The symmetric product $\langle ...,... \rangle$ signifies taking the dot product of the two functions involved and integrating it over the surface S_c of the PEC object.

Eigenanalysis always determines the eigencurrents (the eigenvectors) only to within a multiplicative factor. We can decide what this multiplicative factor must be, and will do so such that the radiated power of each mode is 1 Watt. In other words, we normalize the eigencurrents such that each mode radiates 1 Watt. A scaling factor is needed in order to do this

When there is an incident field $-\bar{E}_{\tan}^{inc}$ at points on a PEC object where the resulting induced current density is, the complex power radiated by the induced current is

---

[4] The eigenvector $\bar{J}_n$, for a given *n*, can in fact be complex, but its phase is the same at all points on the object. In other words, they are equiphasal. We will follow [HARR71b] and subsequent authors and refer to them as being real since the phase can always be made zero when considering one mode at a time.

$$P_{complex} = \left\langle \bar{J}_s^*, -\bar{E}_{\tan}^{inc} \right\rangle = \left\langle \bar{J}_s^*, \mathcal{Z}\left\{\bar{J}\right\} \right\rangle = \left\langle \bar{J}_s^*, \mathcal{R}\left\{\bar{J}\right\} \right\rangle + j\left\langle \bar{J}_s^*, \mathcal{X}\left\{\bar{J}\right\} \right\rangle \qquad (2.3\text{-}13)$$

The time-averaged power radiated by the n-th characteristic mode is thus

$$\mathrm{P}_{rad,n} = \left\langle \bar{J}_n, \mathcal{R}\left\{\bar{J}_n\right\} \right\rangle \qquad (2.3\text{-}14)$$

and is the quantity we want equal to unity. The normalized eigencurrent is therefore

$$\bar{J}_n^{norm} = \frac{\bar{J}_n}{\sqrt{\left|\left\langle \bar{J}_n, {}'\left\{\bar{J}_n\right\}\right\rangle\right|}} \qquad (2.3\text{-}15)$$

In other words, we then have

$$\begin{aligned} \mathrm{P}_{rad,n} = \left\langle \bar{J}_n^{norm}, {}'\left\{\bar{J}_n^{norm}\right\} \right\rangle &= \left\langle \frac{\bar{J}_n}{\sqrt{\left|\left\langle \bar{J}_n, {}'\left\{\bar{J}_n\right\}\right\rangle\right|}}, {}'\left\{\frac{\bar{J}_n}{\sqrt{\left|\left\langle \bar{J}_n, {}'\left\{\bar{J}_n\right\}\right\rangle\right|}}\right\} \right\rangle \\ &= \left\langle \frac{\bar{J}_n}{\sqrt{\left|\left\langle \bar{J}_n, {}'\left\{\bar{J}_n\right\}\right\rangle\right|}}, \frac{{}'\left\{\bar{J}_n\right\}}{\sqrt{\left|\left\langle \bar{J}_n, {}'\left\{\bar{J}_n\right\}\right\rangle\right|}} \right\rangle = 1 \end{aligned} \qquad (2.3\text{-}16)$$

where, for real quantity a, we have used the fact that $\mathcal{R}\left\{a\,\bar{J}_n\right\} = a\,\mathcal{R}\left\{\bar{J}_n\right\}$ because $\mathcal{R}\left\{...\right\}$ is a linear operator. We will in the remainder of the thesis assume that the eigencurrents are always normalized in this way, and will denote them simply by $\bar{J}_n$. The orthogonality relationships (2.3-10) through (2.3-12) can now be written as

$$\left\langle \bar{J}_m, \mathcal{R}\left\{\bar{J}_n\right\} \right\rangle = \left\langle \bar{J}_m^*, \mathcal{R}\left\{\bar{J}_n\right\} \right\rangle = \delta_{mn} \qquad (2.3\text{-}17)$$

$$\left\langle \bar{J}_m, \mathcal{X}\left\{\bar{J}_n\right\} \right\rangle = \left\langle \bar{J}_m^*, \mathcal{X}\left\{\bar{J}_n\right\} \right\rangle = \lambda_n \delta_{mn} \qquad (2.3\text{-}18)$$

and

$$\left\langle \bar{J}_m, \mathcal{Z}\left\{\bar{J}_n\right\} \right\rangle = \left\langle \bar{J}_m^*, \mathcal{Z}\left\{\bar{J}_n\right\} \right\rangle = \left(1 + j\lambda_n\right)\delta_{mn} \qquad (2.3\text{-}19)$$

where δ_{mn} is the Kronecker delta

$$\delta_{mn} = \begin{cases} 0 & m \neq n \\ 1 & m = n \end{cases} \qquad (2.3\text{-}20)$$

C Orthogonality Properties of Characteristic Modes Far-Zone Fields

Using the complex Poynting theorem, Maxwell's equations, and the fact that each characteristic mode field over the sphere at infinity (S_∞) takes the form of purely outward traveling waves, can be used to show that the characteristic mode fields are mutually orthogonal. In other words,

$$\frac{1}{\eta} \oint\!\!\!\oint_{S_\infty} \bar{E}_m \cdot \bar{E}_n^* dS = \delta_{mn} \qquad (2.3\text{-}21)$$

and

$$\frac{1}{\eta} \oint\!\!\!\oint_{S_\infty} \bar{H}_m \cdot \bar{H}_n^* dS = \delta_{mn} \qquad (2.3\text{-}22)$$

where $\eta = \sqrt{\mu_o / \varepsilon_o}$ is the free-space intrinsic impedance.

In the remainder of the thesis the above expressions will be referred to as the *far-field orthogonality*.

D Characteristic Mode Expansions of Actual Object Currents and Fields

If the PEC object is illuminated by an incident field there will be an induced current density on its surface. This surface current density can be written as a linear sum of the characteristic mode currents

$$\bar{J}_s = \sum_{n=0}^{\infty} \alpha_n \bar{J}_n \qquad (2.3\text{-}23)$$

and thus the actual scattered field can be written as a linear sum of the characteristic mode fields. So given any excitation, it is possible to determine how much of each of the characteristic modes is excited. This excitation can be any incident electromagnetic wave or take the form of some antenna feeding mechanism (eg. voltage gap, coaxial feed). If we recall that (2.3-3) can be written as $\left[\mathcal{Z}\left\{\bar{J}_s\right\}-\bar{E}^i_{\tan}\right]=0$, substitute (2.3-23) into it, and take the inner product with $\bar{J}_m$, we arrive at the expression

$$\sum_{n=0}^{\infty}\alpha_n\left\langle\bar{J}_m,\mathcal{Z}\left\{\bar{J}_n\right\}\right\rangle-\left\langle\bar{J}_m,\bar{E}^i_{\tan}\right\rangle=0 \tag{2.3-24}$$

By the orthogonality properties of the modal currents, we end with

$$\alpha_n\left(1+j\lambda_n\right)=\left\langle\bar{J}_n,\bar{E}^i_{\tan}\right\rangle \tag{2.3-25}$$

where we define the *modal excitation* and *modal expansion coefficients* respectively as

$$V_n^i=\oiint_S\bar{J}_n\cdot\bar{E}^i_{\tan}dS=\left\langle\bar{J}_n,\bar{E}^i_{\tan}\right\rangle \tag{2.3-26}$$

and

$$\alpha_n=\frac{\left\langle\bar{J}_n,\bar{E}^i_{\tan}\right\rangle}{1+j\lambda_n}=\frac{V_n^i}{1+j\lambda_n} \tag{2.3-27}$$

The quantity

$$MS=\left|\frac{1}{1+j\lambda_n}\right| \tag{2.3-28}$$

has been called the modal significance factor. This quantity is equals to any value from zero when a mode is totally storing energy, to one, when the mode is totally radiating.

The orthogonality properties have allowed us to express any arbitrary surface current and its fields as expansions of the characteristic mode currents and fields, namely

$$\bar{J}_s=\sum_{n=1}^{\infty}\alpha_n\bar{J}_n=\sum_{n=1}^{\infty}\frac{V_n^i\bar{J}_n}{1+j\lambda_n} \tag{2.3-29}$$

$$\bar{E} = \sum_{n=1}^{\infty} \alpha_n \bar{E}_n = \sum_{n=1}^{\infty} \frac{V_n^i \bar{E}_n}{1 + j\lambda_n} \tag{2.3-30}$$

and

$$\bar{H} = \sum_{n=1}^{\infty} \alpha_n \bar{H}_n = \sum_{n=1}^{\infty} \frac{V_n^i \bar{H}_n}{1 + j\lambda_n} \tag{2.3-31}$$

E *Physical Meaning of the Characteristic Mode Eigenvalues*

The eigenvalue for the generalized eigenvalue problem can be expressed as (the so-called Rayleigh quotient)

$$\lambda_n = \frac{\left\langle \bar{J}_n^*, \mathscr{X}\left\{\bar{J}_n\right\}\right\rangle}{\left\langle \bar{J}_n^*, \mathscr{R}\left\{\bar{J}_n\right\}\right\rangle} = \frac{\mathrm{P}_{reac,n}}{\mathrm{P}_{rad,n}} = \frac{\omega W_{net,n}}{\mathrm{P}_{rad,n}} \tag{2.3-32}$$

where $W_{n,net}$ is the net stored energy of the specified mode 'n'. This interpretation of the eigenvalue λ_{n} explicitly shows the following properties [GARB65, HARR71a] :

- If λ_{n} > 0, the mode can be considered to be an *inductive mode* since it predominantly stores magnetic energy.
- If λ_{n} < 0, the mode can be considered to be a *capacitive mode* since it predominantly stores electrical energy.
- If $\lambda_{\mathrm{n}} = 0$, the mode has *No net stored energy* and is called *externally resonant*
- If $\lambda_{\mathrm{n}} \rightarrow \infty$, the mode has *No radiated power* and is called *internally resonant*

If we want (e.g. for a case where the PEC object is in fact an antenna) to excite an individual characteristic mode (say the n^{th} mode) at some specific frequency then the shape of the PEC object needs to be such that the specific mode has $\lambda_{\mathrm{n}} \approx 0$, with the characteristic mode eigenvalues of all other modes very much larger.

2.3.3 Characteristic Modes as the Solution of a Generalized Matrix Eigenvalue Problem after Discretization of the Integral Equation Using the Method of Moments

Use of a moment method formulation to solve the EFIE for scattering from a perfectly conducting (PEC) structure converts the EFIE into a matrix equation [PETE97]

$$[Z][J]=[V^{inc}] \tag{2.3-33}$$

Column vector $[J]$ contains the coefficients of the expansion functions for the unknown electric current density on the structure, $[V^{inc}]$ is the excitation vector that is related to the incident electric field, and $[Z]$ is the moment method impedance matrix. The elements of the various matrices are[5]

$$Z_{pq}=\left\langle \bar{E}_q^{scat}\left\{\bar{r},\bar{J}_q,\mathcal{G}_{\text{free space}}\right\},\bar{W}_p\left(\bar{r}\right)\right\rangle \tag{2.3-34}$$

$$V_p=\left\langle -\bar{E}^{inc}\left\{\bar{r},\bar{J}^{imp},\bar{M}^{imp},\mathcal{G}_{\text{free space}}\right\},\bar{W}_p\left(\bar{r}\right)\right\rangle \tag{2.3-35}$$

and

$$\left[J\right]=\left[I_1 \quad I_2 \quad \cdot \quad \cdot \quad \cdot \quad I_N\right]^T \tag{2.3-35}$$

where the $\bar{W}_p$ are the weighting functions. The surface current density is then

$$\bar{J}_s\left(\bar{r}\right)=\sum_{q=1}^{N} I_q \bar{J}_q\left(\bar{r}\right) \tag{2.3-37}$$

Expression (2.3-20) is the discretized form of the EFIE; we are now dealing with discrete operators and finite dimensional vectors. It is therefore possible to write down, in matrix notation, the discrete equivalents of the characteristic mode eigenvalue problem and characteristic mode properties, for the discrete case by inspection. The characteristic mode eigenvalue problem is[6]

$$[X][J_n]=\lambda_n[R][J_n] \tag{2.3-38}$$

---

[5] We have stated these here for the convenience of the reader. It will not be necessary to always do this in later sections of this chapter.

[6] Note that $\left[J_n\right]$ denotes the complete column vector of expansion function coefficients for the n-th characteristic mode. In order to avoid notational confusion we have used subscript symbol q in (2.3-44) to denote the q-th expansion function $\bar{J}_q\left(\bar{r}\right)$.

for the currents $[J_n]$ of the n-th characteristic mode and its eigenvalue λ_n, with $[Z]=[R]+j[X]$ separating $[Z]$ into its real and imaginary parts. The current density orthogonality relations (2.3-17) through (2.3-19) can now be written in matrix notation

$$[J_m]^T[R][[J_n] = [J_m^*]^T[R][[J_n] = \delta_{mn} \tag{2.3-39}$$

$$[J_m]^T[X][[J_n] = [J_m^*]^T[X][[J_n] = \lambda_n\delta_{mn} \tag{2.3-40}$$

$$[J_m]^T[Z][[J_n] = [J_m^*]^T[Z][[J_n] = \left(1+j\lambda_n\right)\delta_{mn} \tag{2.3-41}$$

The far-zone field orthogonality relationships are unchanged.

2.3.4 Orthogonality and Degenerate Modes

Assume we have modes 'm' and 'n' with eigencurrents J_m and J_n. We know that the modes individually satisfy the expressions

$$[X][J_m] = \lambda_m[R][J_m] \tag{2.3-42}$$

and

$$[X][J_n] = \lambda_n[R][J_n] \tag{2.3-43}$$

regardless of orthogonality (they are not measures between modes, but rather for each mode individually). Take the Hermitian transpose of equation (2.3-42)

$$\begin{aligned} \left([X][J_m]\right)^H &= \left(\lambda_m[R][J_m]\right)^H \\ [J_m]^H[X]^H &= \lambda_m^*[J_m]^H[R]^H \end{aligned} \tag{2.3-44}$$

where $[X]^H = [X]$ and $[R]^H = [R]$ for lossless objects

Take the inner product of (2.3-44) with respect to J_n

$$[J_m]^H[X][J_n]^H = \lambda_m^*[J_m]^H[R][J_n] \tag{2.3-45}$$

Now take the inner product of (2.3-43) with respect to J_m

$$[J_n]^H[X][J_n]^H = \lambda_n[J_m]^H[R][J_n] \tag{2.3-46}$$

Notice that the left hand side in (2.3-45) and (2.3-46) are identical. Hence, we can equate and write:

$$\lambda_m^*[J_m]^H[R][J_n] = \lambda_n[J_m][R][J_n] \tag{2.3-47}$$

or equivalently

$$\left\{\lambda_m^* - \lambda_n\right\}[J_m]^H[R][J_n] = [0] \tag{2.3-48}$$

This property holds true if $J_m^H R J_n = 0$ or in other words, for distinct eigenvalues the modes are orthogonal.

Unfortunately, another condition is possible, i.e. $\lambda_m^* - \lambda_n = 0$, and since the eigenvalues are real, $\lambda_m = \lambda_n$. So if the eigenvalues are degenerate, then the condition (2.3-39) holds true, but it also implies $[J_m]^H[R][J_n] = [0]$ needn't be true and hence the orthogonality condition of the modes is not necessarily true for degenerate pairs. On the other hand, there is nothing stopping both conditions to be true (i.e. $\lambda_m = \lambda_n$ and $[J_m]^H[R][J_n]$) simultaneously.

If two modes have eigenvalues that are numerically identical (say up to the 16th decimal place), then they are obviously degenerate and so might not be orthogonal. The situation can also arise where two degenerate modes which are orthogonal have eigenvalues that are only approximately equal (say to the 3rd decimal place) due to arithmetical inaccuracies and their "coupling terms" may then not be precisely zero but close to zero. Judgment has to be exercise.

2.3.5 Magnetic Field Integral Equation Approach

The magnetic field integral equation for the PEC object in Fig.2.3-1 is derived in a manner similar to that of the EFIE except that the magnetic field boundary condition $\hat{n}\times\bar{H}=\bar{J}_s$ is used. The result is an integral equation [PETE97]

$$\bar{J}_s\left(\bar{r}_s\right)-\hat{n}\left(\bar{r}_s\right)\times\bar{H}^{scat}\left\{\bar{r}_s^{\,+},\bar{J}_s,G_{\text{free space}}\right\}=\hat{n}\left(\bar{r}_s\right)\times\bar{H}^{inc}\left(\bar{r}_s\right)\qquad \bar{r}_s\in S_c \qquad (2.3\text{-}49)$$

When we wish to apply the MFIE in a specific situation, and have to deal with the details of the expression for $\bar{H}^{scat}\left\{\bar{r}_s^{\,+},\bar{J}_s,G_{\text{free space}}\right\}$, we will have to perform the limiting operation denoted by the symbol $\bar{r}_s^{\,+}$, meaning that the limit must be taken as $\bar{r}_s^{\,+}\to\bar{r}_s$. Application of the method of moments reduces the integral equation to a matrix equation of the form

$$[M][J]=[I^{inc}] \qquad (2.3\text{-}50)$$

The [J] has the same meaning as for the EFIE, but the elements of the column matrix $[I^{inc}]$ are related to the incident magnetic field rather than the incident electric field. The moment method matrix $[M]$ is neither an impedance matrix nor an admittance matrix. Thus matrix equation (2.3-50) cannot be used directly, using the "recipe" given in Section 2.3.3 for the EFIE case, to find the characteristic modes. There appears to be only a single reference, namely [NALB 82], that has discussed the use of an MFIE to determine the characteristic modes of a PEC (or indeed any) object. There does not seem to be any particular advantage in using the MFIE to find the characteristic modes of a PEC object compared to using the EFIE.

2.3.6 Combined Field Integral Equation Approach

The EFIE and MFIE are susceptible to the so-called "internal resonance problem" when scattering by a closed-object is being considered. These "internal resonances" do not necessarily correspond to actual physical resonances associated with the object. They are best seen as specific frequencies at which the EFIE and MFIE are not able to provide unique solutions to the physical problem. This problem can be avoided if the so-called combined field integral equation

(CFIE) is used. However, it is not certain how a CFIE can be used to determine the characteristic modes of an object. Firstly, the CFIE includes the MFIE operator for which, as commented in Section 2.3.4, the CM eigenvalue equation is not as straightforward as for the EFIE case. Secondly, the complete moment method matrix of the CFIE is not symmetric, and would need to be symmetrized using some transformation.

2.3.7 Important Note on the Notation to be Used

The notation in later sections can become quite cumbersome, and so for convenience we will use the symbol $\lambda_{\mathrm{CM}}^{(n)}\left\{[A]\right\}$ to denote the characteristic mode eigenvalues that are obtained when solving the eigenvalue problem[7] $\{\mathrm{Im}[A]\}[J]=\lambda\{\mathrm{Re}[A]\}[J]$, for any complex matrix [A]. Thus, for example, the characteristic mode eigenvalues described in Section 2.3.3 would be $\lambda_{\mathrm{CM}}^{(n)}\left\{[Z]\right\}$.

2.4 METHODS OF DETERMINING THE CHARACTERISTIC MODES OF A PEC OBJECT – ALTERNATIVE APPROACHES

A Finite-Difference Time-Domain (FDTD) Method Approach

Details of the method used in [SURI04] and [SURI05] are not given in the said papers, and so only a rough description of the technique, gleaned from these references, can be provided here. The finite-difference time-domain (FDTD) method is used to model the PEC object. In order to compute the characteristic modes, the papers' authors generate initial conditions for the magnetic fields using a random number generator of uniform distribution. The resonant behavior "is then captured by observing" the discrete Fourier transform spectrum of the electric or magnetic field components of the induced surface currents on structure. The surface currents at the various resonant frequencies are examined to determine whether they are real and form an orthogonal

[7] In other words, $\lambda_{\mathrm{CM}}^{(n)}\left\{[A]\right\}$ is <u>not</u> the spectrum of matrix [A], which would be the solution of the eigenvalue problem $[A][J]=\lambda[J]$. The spectrum of [A] will simply be denoted by $\lambda\left\{[A]\right\}$.

set. Once this has been determine the corresponding far-zone patterns can be calculated. Not having additional details on this approach, we are not able to comment further on this method, although it does appear to be much more complicated than the moment method approach. It has not been adopted by others.

B Finite Element Approach

The eigenanalysis (by which we mean natural modes[8]) of a closed resonator is easily done using the finite element method (FEM) approach. In essence the wave equation is solved with zero excitation, and the demand for non-zero solutions produces a non-linear eigenvalue problem, which gives such non-zero solutions (the internal natural modes of the object) only at specific frequencies. Using the FEM for the eigenanalysis of an open resonator (that is, the PEC structure is viewed as an open resonator) requires special considerations. Commercial codes such as HFSS do not support such an eigenanalysis of open resonators. Means of using the FEM for the eigenanalysis of open resonators has been described in recent publications [MAXI 12], [ZEKI 13] and [KYRI 13], but mainly for two-dimensional structures, with the extension to three-dimensional structures on-going. Reference [MAXI 12] shows how their above-mentioned FEM approach for the eigenanalysis of open structures can be manipulated in a way that the only unknown is the electric current density on the PEC object (the open resonator), in effect making the equivalent of the moment method impedance matrix available. The latter is then used to find the characteristic modes of the PEC object. It is not certain at this stage what the advantage would be in adopting such a complicated approach instead of the integral equation one described in Section 2.3.3. The authors of [MAXI 12] have not clearly given such reasons.

C Estimation of Characteristic Mode Coefficients

Reference [SAFI 13] presents a method to reconstruct the modal current distribution on a PEC object from the known radiated far field and some ‘general knowledge’ about the characteristic modes involved. Any computational method is used to find the far-fields of some actual (eg. complicated) PEC structure when it is given some *specific excitation*. The method of moments is

[8] More will be said about natural modes in Chapter 3. Natural modes are not the same concept as characteristic modes.

then used to model a simplified version of the same PEC object, and the characteristic modes of the simplified structure found using the methods of Section 2.3.3. It is assumed that the characteristic modes of the actual structure are almost the same as those of the simplified structure. The simplified structure is then given the same excitation and the resulting complex amplitude coefficients of each of its characteristic modes determined. The correlations between the far-fields in the two cases are then used to find perturbed values of the amplitude coefficients of each of the simplified object's characteristic modes and assumed to apply to the actual object. We agree that this might be useful for certain antenna design problems, but is not really (and was not meant to be) a way to compute characteristic modes in a numerically rigorous fashion. The authors of [SAFI 13] remark that they devised the above approximate approach many commercial electromagnetic simulation codes are based on the FDTD method, using which the computation of characteristic modes is not easily done.

2.5 MODE TRACKING

A characteristic mode (CM) analysis is generally performed using a frequency sweep to observe the trends of an object's CM eigenvalues (capacitive or inductive) over frequency, and to determine the frequencies at which the modes have zero eigenvalues (the resonant frequencies of the modes). The CM eigenvalues are then sorted in ascending order according to their magnitude. As the magnitude gets lower, the more significant the mode is. In numerical work we are of course only able to compute the eigenvalues at discrete frequencies in some frequency range. Hence, at every frequency sample, solving of the CM equation, and subsequent sorting of the eigenvalues and eigencurrents, are required. The sign of the eigenvalues can change as the frequency varies; it can switch from negative to positive, or vice versa. Thus their magnitudes can decrease and then increase again. The first eigenvalue that goes through zero is said to be that of the dominant CM, but this dominant mode (first mode) does not always remain the CM with the lowest magnitude eigenvalue for the whole range of frequencies of interest. Therefore, it is essential to track and label these eigenvalues, based on their frequencies of first resonance. Several mode tracking methods [RAIN12, CAPE11, AKKE05] have been suggested in the literature. Due to the simplicity of implementation, faster run time, and minimum number of failures compared to the other two methods, this thesis uses the approach presented in [RAIN12].

The suggested approach rearranges the eigenvalues as a function of frequency. It associates the eigenvalues of one frequency sample with the previous one, and the associated eigenvectors are rearranged accordingly. Modes could simply be numbered according to their magnitude at the very first frequency used, but doing so results in a failure to correctly number the eigenvalues according to their first resonance occurrence. For example, when using the simplistic numbering mentioned in the previous sentence, λ_2 might resonate (go through zero) at a lower frequency than λ_1 even though λ_1 is lower in magnitude at frequencies lower than the frequency of resonance. Correct mode numbering should always be based on the starting frequency used in the computation; if this chosen starting frequency causes a first resonance to be missed then the numbering becomes incorrect. Therefore, two steps must be considered to properly numbering the CMs:

- Ensure mode numbering is based on resonance occurrence and not magnitude at the lower frequencies.
- When a frequency sweep is performed, choose a lower bound at a frequency that is lower than the first CM resonance, or take into account any previous occurrence of a resonance.

We here simplify the approach of, and will omit some extra procedures used in, reference [RAIN12], that may require computation of the CMs at more closely space frequency values if one begins with widely spaced values. Instead, we always use sufficiently closely spaced frequency samples. This is highly recommended since correlations between the eigencurrents at two adjacent frequencies have to be calculated. The correlation measure should provide a high value if an eigencurrent $J_m(f_{i+1})$ resembles $J_n(f_i)$, where n and m are mode indices, with n not necessarily equal to m. The correlation is calculated as [RAIN12]

$$\left[C\right] = \left|[J(f_{i+1})][J(f_i)]^{-1}\right| \tag{2.5-1}$$

where *i* is the frequency sample index, the modulus signs indicate that magnitudes must be taken of each of the individual matrix terms, and

$$[J(f_i)] = \left[[J_1(f_i)] \quad [J_2(f_i)] \quad \bullet \quad \bullet \quad \bullet \quad \bullet \quad [J_N(f_i)]\right] \tag{2.5-2}$$

It is convenient to use matrix notation as MATLAB is the common tool used for such analysis. At each frequency the eigenvalues (in ascending magnitude) are placed in a column vector, and these column vectors are placed "alongside each other" to form a matrix. This is done in two stages:

Stage#1 - We begin at the second frequency point, and move through all frequency points. At each stage we associate a given set of eigencurrents with the eigencurrents at the previous frequency using the correlation matrix defined in (2.5-1). Any terms in the correlation matrix that are high enough indicate that corresponding eigencurrents are correlated. A threshold value is usually set for acceptance of correlation; a recommended threshold value of 0.9 has found to be effective [RAIN12]. There are three possible outcomes from this stage :

(a) $Corr\left\{[J_n(f_{i+1})],[J_m(f_i)]\right\} \geq threshold$

(b) $Corr\left\{[J_n(f_{i+1})],[J_m(f_i)]\right\} < threshold$

(c) Correlation between an eigencurrent from a prior frequency sample gives a greater value than the threshold with multiple eigencurrents in the next sample or vice versa.

Outcomes (b) and (c) are resolved in the second stage.

Stage#2 - All eigencurrents left unassociated from Stage#1 are grouped for the next round of inspection. In this stage the set threshold of the correlation is not a factor. A higher correlation number between an eigencurrent from a previous sample and the present eigencurrents is the deciding factor in the association. Even though the [RAIN12] recommends resolving outcome (c) by dividing the frequency between f_i and f_{i+1} into more closely spaced samples and repeating Stage#1, we have found it sufficient to perform Stage#2.

This is not a perfect method, but it resolved the CM tracking problem for all the examples considered in this work. Fig.2.5-1 shows the eigenvalues of untracked CMs, whereas Fig.2.5-2 shows them when tracking has been applied, for a strip dipole in free space (to be discussed in Section 2.6.4). These have been included an example of how the tracking method works. At each frequency the eigenanalysis outputs a set of eigenvalues in a certain order. If we were to blindly use these in the order provided by the eigenanalysis the plots of the three CMs versus frequency would be as shown in Fig.2.5-1. In order to obtain the correct curves the eigenvalues must be tracked from one frequency to the next. In order to achieve this present tracking method swaps the first eigenvalue (output by the eigenanalysis routine) with the second between 3.4 and 5.3 GHz, and at higher frequencies swaps the first with the third. Frequency steps of 15 MHz were used over the range of frequencies shown; this was sufficient to resolve and track the lower order eigenvalues.

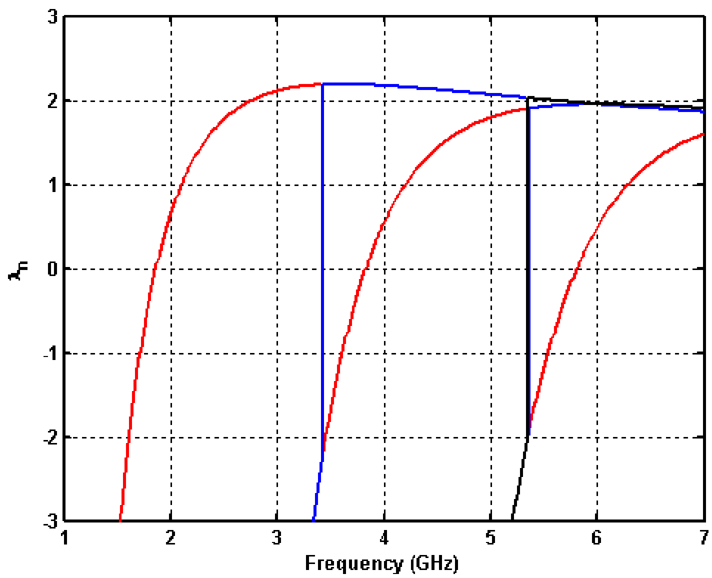

Figure 2.5-1: Untracked eigenvalues for the first three CMs – strip dipole in free space

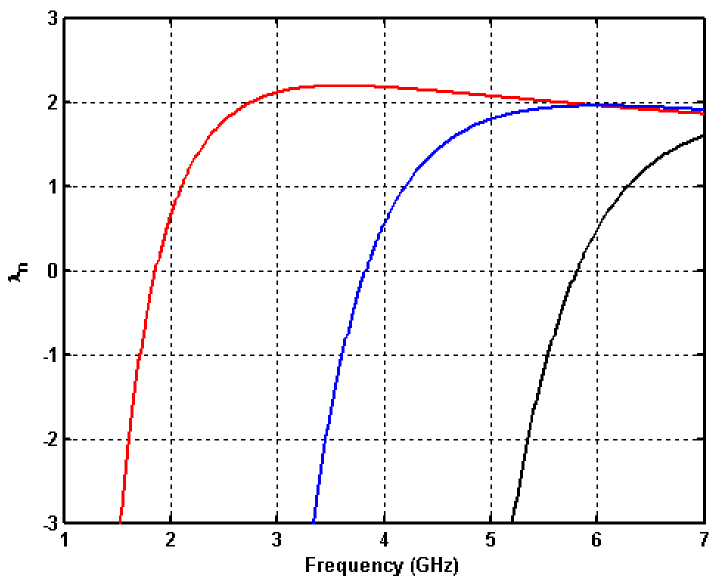

Figure 2.5-2: Tracked eigenvalues for the first three CMs – strip dipole in free space

2.6 EXAMPLES OF DETERMINING THE CHARACTERISTIC MODES OF A PEC OBJECT

We wish to demonstrate the use of the integral equation approach for the determination of the characteristic modes of various PEC objects. In order to do this it is necessary to explain exactly which integral equations are being used, and how their solutions are being obtained. This will be done in the present section.

2.6.1 Use of the EFIE for 2D PEC Objects of Arbitrary Cross-Section – TM Case

Characteristic modes of 2-D PEC objects of arbitrary cross section can be calculated using EFIE formulation presented in this section where only TM case is considered. The integral equation is derived using the argument of the following boundary condition:

$$\bar{M}_{eq}(\bar{r}) = -\hat{n}(\bar{r}) \times \bar{E}(\bar{r}) = 0 \qquad (2.6\text{-}1)$$

where the total tangential electric field vanishes at all points on the surface of a PEC object. The above expression is in general spatial coordinates, but only the transverse spatial coordinates $\bar{\rho}$ is considered for our 2-D TM case. Therefore, the total electric field at any observation point with this defined coordinate is

$$E_z\left\{\bar{\rho}, J_z(\bar{\rho})\right\} = E_z^{inc}\left(\bar{\rho}\right) + E_z^{scat}\left\{\bar{\rho}, J_z(\bar{\rho})\right\} \qquad (2.6\text{-}2)$$

where $\bar{\rho} = x\hat{x} + y\hat{y}$, and $J_z(\bar{\rho})$ is the equivalent electric current density, and it will produce a magnetic vector potential.

$$A_z\left(\bar{\rho}\right) = \frac{\mu_0}{4j}\int_{C_c} J_z\left(\bar{\rho}'\right) H_0^{(2)}\left(k\left|\bar{\rho} - \bar{\rho}'\right|\right) dC' \qquad (2.6\text{-}3)$$

where C_c is the contour of the 2-D object observed.

The current density and hence the electric field are entirely z-directed and in a function of the transverse spatial coordinates $\bar{\rho}$ only. The scattered field due to $J_z\left(\bar{\rho}\right)$ is simply equal to

$$E_z^{scat}\left\{\bar{\rho}, J_z(\bar{\rho})\right\} = -j\omega A_z\left\{\bar{\rho}, J_z(\bar{\rho})\right\} \qquad (2.6\text{-}4)$$

$E_z^{inc}(\bar{\rho})$ is the incident field of any arbitrary source. Using (2.6-2) and (2.6-3), the integral equation becomes as follows

$$-j\omega\left\{\frac{\mu}{4j}\int_{C_c} J_z(\bar{\rho}')H_0^{(2)}\left(k\left|\bar{\rho}-\bar{\rho}'\right|\right)dC'\right\} = -E_z^{inc}(\bar{\rho}) \qquad \bar{\rho}\in C_c \tag{2.6-5}$$

In terms of our general operator notation $\mathcal{L} f = g$, we have

$$f(\bar{\rho}) \equiv J_z(\bar{\rho}) \tag{2.6-6}$$

$$g(\bar{\rho}) \equiv -E_z^{inc}(\bar{\rho}) \tag{2.6-7}$$

$$\mathcal{L}\{f(\bar{\rho})\} \equiv -\frac{\omega\mu}{4}\int_{C_c} f(\bar{\rho}')H_0^{(2)}\left(k\left|\bar{\rho}-\bar{\rho}'\right|\right)dC' \tag{2.6-8}$$

The pulse function is chosen as the expansion function, and the point matching as the weighting function. Afterwards, the application of the method of moments will reduce the EFIE in (2.6-5) to the matrix equation $[Z][I]=[V]$, where

$$Z_{mn} = \left\langle E_{zn}^{scat}(\bar{\rho}), W_{zm}(\bar{\rho})\right\rangle = \left\langle -j\omega A_{zn}(\bar{\rho}), W_{zm}(\bar{\rho})\right\rangle \tag{2.6-9}$$

$$V_m = \left\langle -E_z^{inc}(\bar{\rho}), W_{zm}(\bar{\rho})\right\rangle \tag{2.6-10}$$

$$[I] = \begin{bmatrix} I_1 & I_2 & \cdot & \cdot & \cdot & I_N \end{bmatrix}^T \tag{2.6-11}$$

and

$$J_z(\bar{\rho}) = \sum_{n=1}^{N} I_n J_{zn}(\bar{\rho}) \tag{2.6-12}$$

The detailed expressions of the operator matrix and excitation vectors terms are included in Appendix II, and have been implemented in a code *2DCB* (in Matlab). Only the discretized operator matrix evaluated using the above expressions is needed for the CM computation.

A Rectangular Cross-Section PEC Cylinder

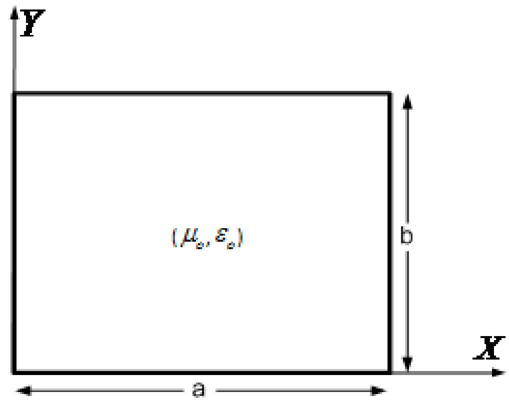

Figure 2.6-1: Two-Dimensional Rectangular Cavity

First, a rectangular cross-section infinite cylinder whose surface is made of PEC is considered for our CM analysis. The dimensions, based on Fig. 2.6-1, are a = 225 mm and b = 135 mm (which is 0.75 λ x 0.45 λ at 1 GHz). To observe the CMs of this structure, the eigenvalues and eigencurrents were numerically worked out using equation (2.3-45) at 281 frequency samples ranging from 100 to 1500 MHz. The behaviour of the eigenvalues can be studied at discrete frequencies by evaluating the impedance matrix followed by solving the eigenvalue equation (2.3-45) at each frequency step. This provides an insight in regards to the resonance of each mode, in addition to how significant the mode is over a frequency span of interest. For example, the first CM can be seen as inductive mode before it resonates at 410 MHz for this rectangular cylinder, as shown in Fig. 2.6-2. The same mode becomes capacitive right after its resonance and suffers from a sudden jump (asymptotic behaviour) at a frequency of 1.296 GHz. At this particular frequency, the EFIE undergoes numerical inaccuracies due to what is called the interior resonance problem, which will be discussed in Chapter 3. Another way to look at the eigenvalue of a CM is by calculating its modal significance using expression (2.3-28) at a frequency of interest. A CM may or may not stay significant throughout a wide bandwidth after it goes through a resonance; on the other hand, other CMs can become significant or less at those same frequencies. In Fig. 2.6-3, the modal significance of the first five CMs are shown revealing that λ_1 stays significant compared to other eigenvalues of the CMs at those frequencies around its first resonance. Table 2.6-1 gives the numerical values of their resonant frequencies.

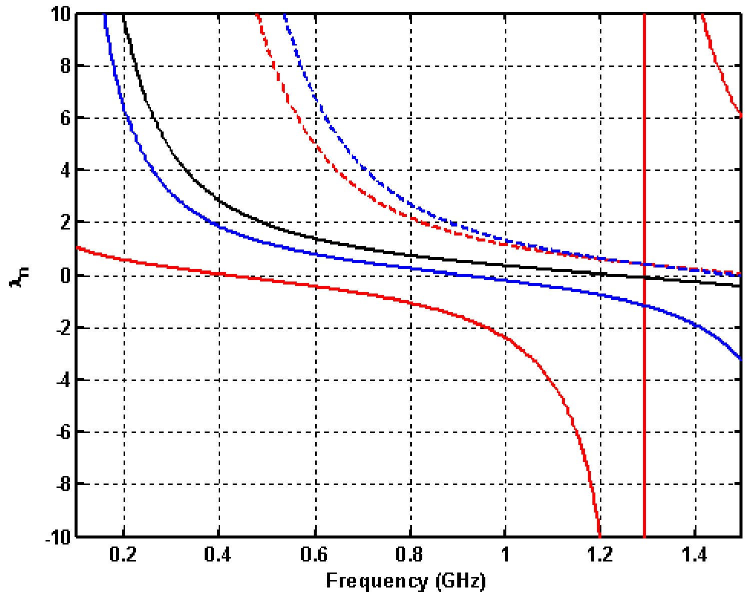

Figure 2.6-2: Eigenvalues of first five CMs - 2-D rectangular PEC cylinder. (——) λ_1, (——) λ_2, (——) λ_3, (– – –) λ_4, (– – –) λ_5.

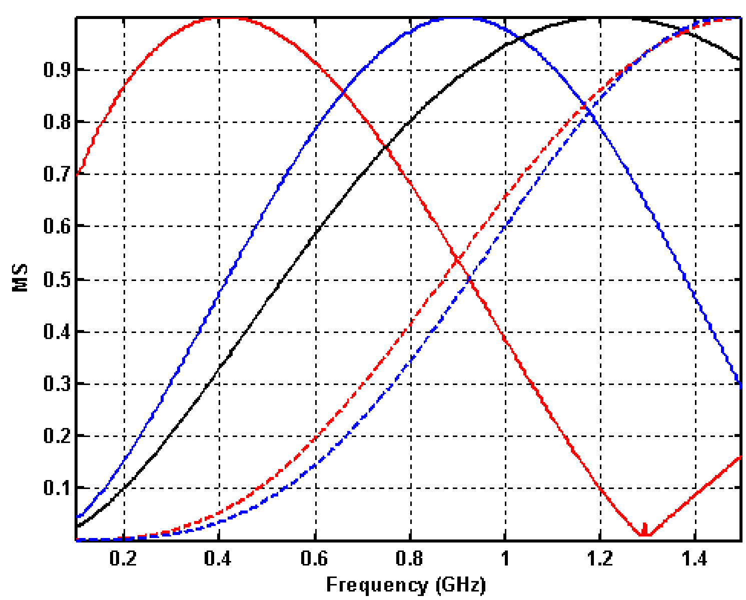

Figure 2.6-3: Modal Significance of the first CMs - 2-D rectangular PEC Cylinder. (——) λ_1, (——) λ_2, (——) λ_3, (– – –) λ_4, (– – –) λ_5.

Table 2.6-1: Resonance of the lowest CMs - 2-D rectangular PEC cylinder

	Resonant Frequency (GHz)
λ_1	0.410
λ_2	0.905
λ_3	1.220
λ_4	1.475
λ_5	>2.000

The eigenfields due to the first five eigencurrents were computed at 1 GHz; their corresponding eigenvalues are shown in Table 2.6-2. Their orthogonality to each other via expression (2.3-21) was checked by evaluating the field integral through using the approximation

$$\frac{1}{\eta}\oiint_{S_\infty} \bar{E}_m \cdot \bar{E}_n^* dS \simeq \frac{1}{\eta}\sum_i \bar{E}_m(\phi_i)\cdot \bar{E}_n^*(\phi_i)\Delta\phi \tag{2.6-13}$$

This is an excellent approximation if $\Delta\phi$ is made small. The values computed through this approximation using 361 samples in the phi direction are given in Table 2.6-3. Consequently, it can be stated that those CMs are indeed orthogonal. Moreover, the orthogonality of the eigencurrent was verified; they were properly normalized according to 2.3-15. The evaluation of expression (2.3-39) is given in Table 2.6-4. Despite the absence of degenerate modes, the reason behind the relatively high values of the coupling terms[9] between mode 4 and 5 is unclear; especially, the evaluation of the field integral did not yield a similar behavior. Finally, we show the radiation patterns, as depicted in Fig. 2.6-3, of every one of these modes, due to the modal currents calculated.

Table 2.6-2: First lowest eigenvalues computed at 1 GHz - 2-D rectangular PEC cylinder

CM#	**λ**
1	-0.218
2	0.345
3	1.149
4	1.331
5	-2.393

[9] By "coupling terms", we mean the m $\neq$n cases in (2.3-21), and (2.3-39)

Table 2.6-3: Evaluating expression[10] (2.3-21) for the lowest five CMs at 1 GHz - 2-D rectangular PEC cylinder

m/n	1	2	3	4	5
1	1.006+0.000i	0.000+0.000i	-0.000+0.000i	-0.000-0.000i	-0.000+0.000i
2	0.000-0.000i	0.972+0.000i	-0.000+0.000i	-0.000+0.000i	-0.000+0.000i
3	-0.000-0.000i	-0.000-0.000i	0.986+0.000i	0.000+0.000i	-0.000-0.000i
4	-0.000+0.000i	-0.000-0.000i	0.000-0.000i	1.011+0.000i	-0.000-0.000i
5	-0.000-0.000i	-0.000-0.000i	-0.000+0.000i	-0.000+0.000i	0.976+0.000i

Table 2.6-4: Evaluating expression (2.3-39) for the lowest five CMs at 1 GHz - 2-D rectangular PEC cylinder

m/n	1	2	3	4	5
1	1.000	0.000	0.000	0.000	0.000
2	0.000	1.000	0.000	0.000	0.000
3	0.000	0.000	1.000	0.000	0.000
4	0.000	0.000	0.000	1.000	-0.014
5	0.000	0.000	0.000	-0.037	1.000

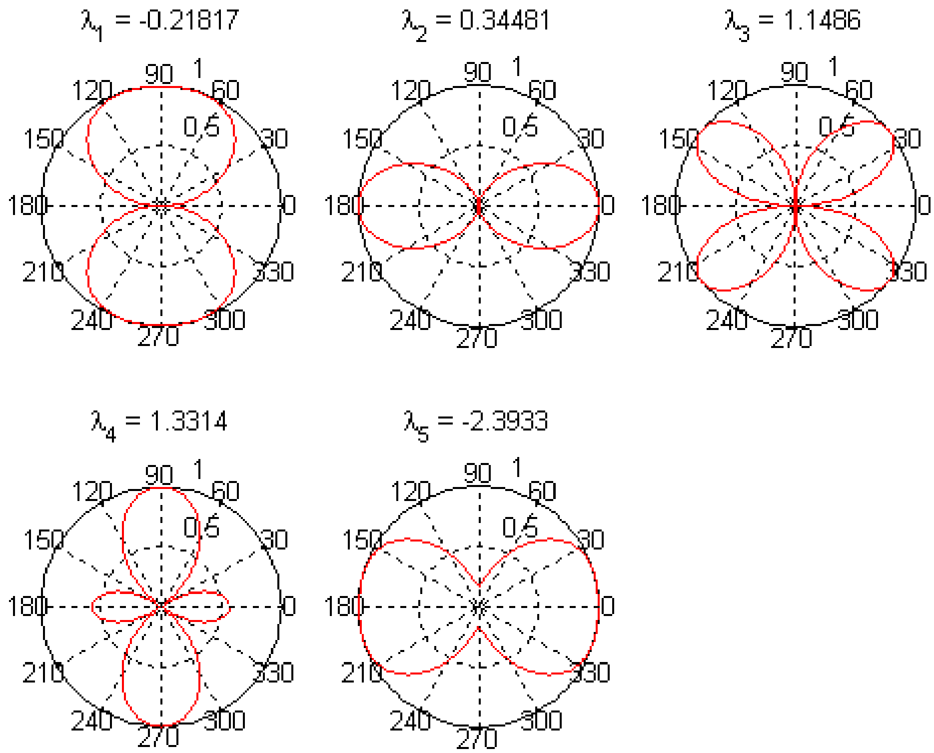

Figure 2.6-4: Radiation pattern[11] of the lowest five characteristic fields - 2-D rectangular PEC cylinder.

---

[10] For m≠n, the integration results in a very samll number (not exactly zero).

[11] The normalized magnitude of the scattered field is shown. The scale of the polar plot's grid is divided to 0, 0.5, and 1. All far-zone patterns for the CMs of 2-D objects are in the azimuthal plane, for which $\theta = 90^{\circ}$ and ϕ varies from 0° to 360°.

B Circular Cross-Section PEC Cylinder

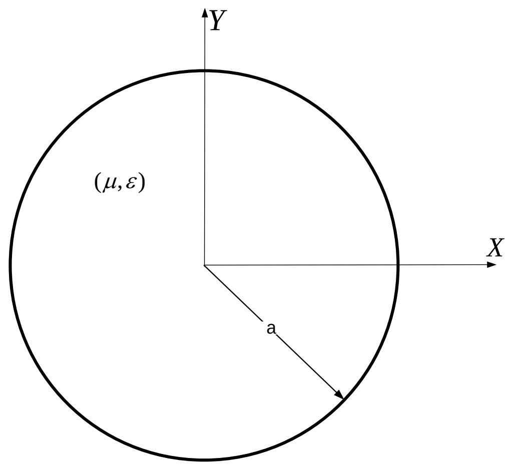

Figure 2.6-5: Two-Dimensional Circular Cavity

Next, a circular cross-section infinite cylinder whose surface is made of PEC is considered for analysing its CM. Its radius, a, is equal to 150 mm (0.5λ @ 1 GHz). Like the case with the rectangular cylinder, the eigenvalues and eigencurrents were numerically computed using equation (2.3-45) at 281 frequency samples ranging from 100 to 1500 MHz. In Fig. 2.6-6, the lowest CM eigenvalues are depicted at the specified range of frequency; degeneracy is evident for this rotationally symmetric structure. Eigenvalues λ_1 and λ_2 are degenerate modes, as λ_4 and $\lambda_{5,}$ which explains why only three eigenvalues are shown in the Fig. 2.6-6 even though five modes are mentioned. For this particular range of frequency, two interior resonances were spotted and numerically disturbed two different CMs. Nonetheless, all the five CMs went through resonance as Table 2.6-5 indicates.

Table 2.6-5: Resonant frequencies of the lowest five CMs for the 2-D circular PEC cylinder

	Resonant Frequency (GHz)
$\boldsymbol{\lambda_1}$ **&** $\boldsymbol{\lambda_2}$	0.285
$\boldsymbol{\lambda_3}$	0.700
$\boldsymbol{\lambda_4}$ **&** $\boldsymbol{\lambda_5}$	1.070

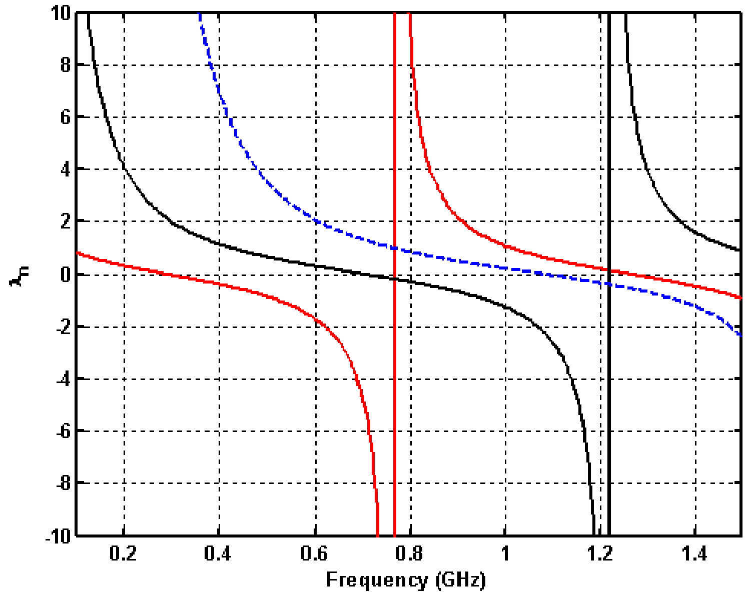

Figure 2.6-6: Eigenvalues of first five CMs for 2-D circular PEC cylinder. (——) λ_1, (——) λ_2, (——) λ_3, (– – –) λ_5, (– – –) λ_4.

In regard to degeneracy, we expect some discrepancies in evaluating either expression (2.3-15) or (2.3-21). Thus, we evaluated expression (2.3-21) at 1 GHz to examine the outcome for these degenerate CMs, as given in Table 2.6-7, and their corresponding eigenvalues are given in Table 2.6-6. The coupling terms associated to those degenerate modes suffered from numerical inaccuracies for a reason explained in Section 2.3.4; nonetheless, the modes can still be considered orthogonal. Finally, we show the lowest five CM eigenfields in Fig. 2.6-7. The degeneracy features are clear on the radiation pattern of the first and second CM besides the fourth and fifth one.

Table 2.6-6: First lowest eigenvalues computed at 1 GHz for 2-D circular PEC cylinder

CM#	λ
1	0.207
2	0.207
3	1.082
4	-1.257
5	-1.257

Table 2.6-7: Evaluating expression (2.3-21) for the lowest five CMs at 1 GHz for 2-D circular PEC cylinder

m/n	1	2	3	4	5
1	0.999+0.000i	0.039+0.000i	-0.000-0.000i	-0.000-0.000i	0.000+0.000i
2	0.039-0.000i	0.999+0.000i	-0.000-0.000i	0.000+0.000i	-0.000-0.000i
3	-0.000+0.000i	-0.000+0.000i	1.000+0.000i	-0.000+0.000i	-0.000+0.000i
4	-0.000+0.000i	0.000-0.000i	-0.000-0.000i	0.998+0.000i	-0.009-0.000i
5	0.000-0.000i	-0.000+0.000i	-0.000-0.000i	-0.009+0.000i	0.998+0.000i

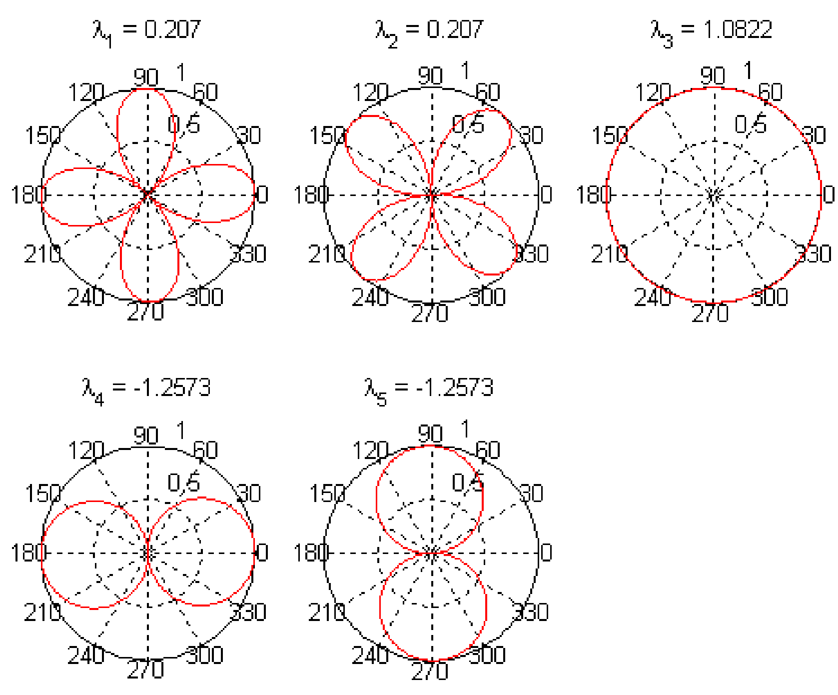

Figure 2.6-7: Eigenfields for the lowest five CMs for 2-D circular PEC cylinder

2.6.2 Use of the Analytical EFIE for 2-D PEC Objects of Circular Cross-Section

In Section 2.6.1, the determination of CMs of an arbitrary shaped object was performed numerically using EFIE by applying the MoM. Fortunately, the derivation of the analytical solution of EFIE is available in the literature for a 2-D circularly shaped cylinder as presented in Appendix I. Given the closed-form solution, the analytical computation of eigenvalues can be achieved using the expression (AI-21) provided in the same appendix. Therefore, we are enabled to verify those eigenvalues computed numerically in Section 2.6-1 for the circular cross-section cylinder. Figure 2.6-8 compares these eigenvalues computed both analytically and numerically; they were plotted in separate graphs to avoid the two solid line curves sitting on top of the dashed line curves which shows an excellent agreement between both results. Of course, the analytical solution does not produce degenerate eigenvalues; thus, the eigenvalues were ordered differently from those computed numerically.

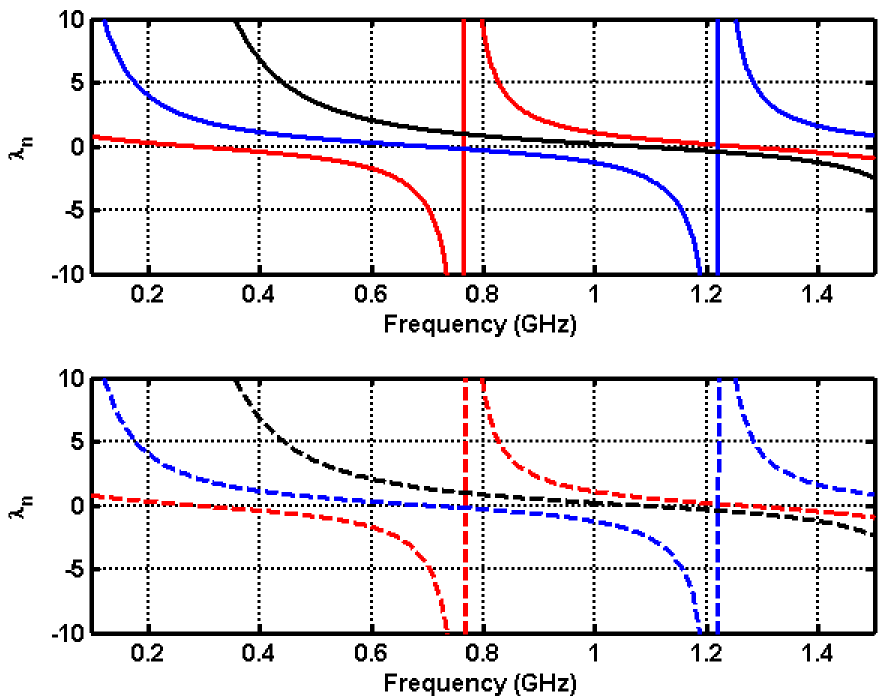

Figure 2.6-8: Eigenvalues of the lowest five CMs of the 2-D circular PEC cylinder computed analytically (top) and numerically (below). (———) λ_1, (———) λ_2, (———) λ_3, for those computed analytically. (— — —) λ_1, (— — —) λ_3, (— — —) λ_4 .

2.6.3 Use of the MFIE for 2-D PEC Objects of Arbitrary Shape

We have applied the MFIE to the case of finding the CMs of infinitely long PEC cylinders of circular cross-section. The details are provided in Appendix I. The expressions there show that they are identical to those obtained for the same object using the EFIE. Thus the graph of the CM eigenvalues versus frequency is identical to that found in Section 2.5.1 using the EFIE. This has been done to emphasize the fact that the CMs are a property of the object and hence, irrespective of the way they are found, they must be identical.

2.6.4 Use of the EFIE for 3-D PEC Objects of Arbitrary Shape

This section discusses CMs of three-dimensional objects simulated in [FEKO], which is a comprehensive three-dimensional (3-D) electromagnetic field simulator. This powerful tool commonly utilizes the method of moments to solve quite general electromagnetic problems. The advantage of FEKO over other commercially available codes that use the method of moments is that it allows one to extract the moment method matrix. We then use this matrix to perform the eigenanalysis "offline" using MATLAB software. Thereafter the CM currents (namely their coefficients) are sent back to FEKO, which is then used to find the CM fields.

In this section, we will attempt to analyze CMs of a PEC sphere, strip dipole, closed rectangular cavity, opened cavity, and finally opened-ends cylinder. Some of these objects are further analyzed in subsequent chapters from other perspectives. However, this section will only discuss the CMs of these objects and comment on their behavior.

A PEC Sphere

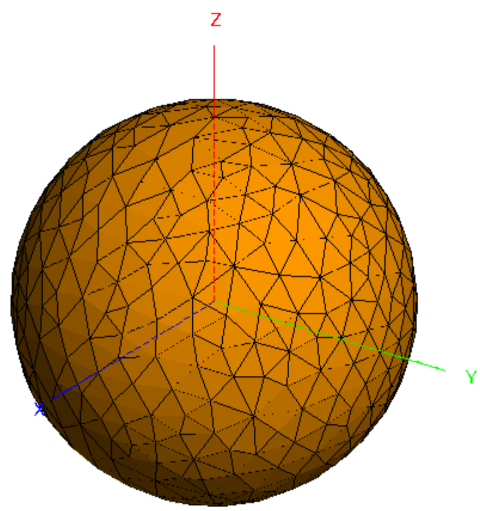

Figure 2.6-9: Sphere simulated in FEKO

A sphere is entirely enclosed and geometrically symmetric structure, and many consider this structure a classical problem in EM. We are interested in calculating the CMs of a sphere to examine the degeneracy of its modes besides comparing the eigenvalues of its CMs to those found analytically using the spherical wave functions theory. A PEC sphere of radius of 300 mm (0.2λ @ 2 GHz) was simulated in FEKO, so that the MoM discretized operator matrix can be obtained to perform CM analysis offline. The matrix was computed at a discrete number of 101 frequencies from 4 to 5 GHz using acceptable meshing (triangle edge length is λ/10 @ 5 GHz). As at this point, using fine mesh is not a necessary step since we are trying to study the general behavior of the CMs of this structure. By using the eigensolver[12] , eigenvalues were computed at all the frequency samples as shown in Fig. 2.6-10. As expected, degenerate modes have good presence for the sphere due to its symmetry. Though, the first CM is not degenerate, and its eigenvalue (red solid line) does go through resonance at a frequency below 4 GHz. The same eigenvalue exhibits an asymptotic behavior near the frequency of 4.390 GHz where the sphere surface happens to represent a cavity resonance which is called "interior resonance problem", as in part B of Section 2.6.1. The eigenvalues of the rest of CMs shown are degenerate, and only

[12] The function *EIG* in MATLAB is used at the eigensolver.

one of these degenerate eigenvalues is considered. The third CMs go through resonance at 4.470 GHz. It is worth noting that there were some capacitive and other inductive CMs for this structure particularly. Finally, we confirm that the orthogonality of the eigcurrents at all frequency samples was satisfied.

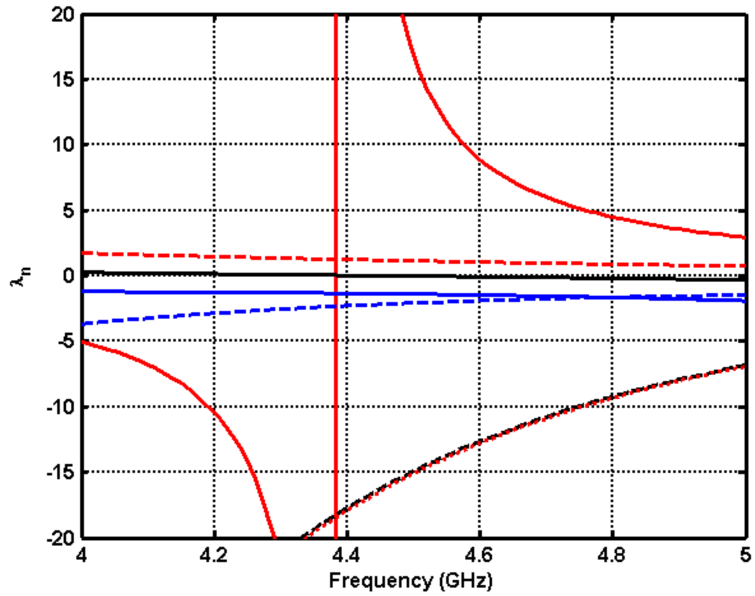

Figure 2.6-10: Eigenvalues of some selected CMs of the PEC sphere. (——) λ_1, (——) λ_4, (——) λ_9, (– – –) λ_{14}, (– – –) λ_{21}, (– – –) λ_{31}

Next, we want to compute the CM eigenvalues at 2 GHz when the physical radius is equal to 0.2λ and compare them to those computed using the spherical wave functions [HARR71b, Sec. III]. At this particular frequency, a finer mesh (triangle edge length is λ/25) was used to accurately compare a converged eigenvalues to those found analytically using the spherical wave functions. From Table 2.6-8, a conclusion can be drawn of a good agreement between both values. One must note that those eigenvalues whose values are repearted are degenerate in the Table. A list of the lowest thirty eigenvalues computed at this frequency is shown in Table 2.6-10.

Table 2.6-8: Comparison between the CM eigenvalues found analytically using spherical wave functions theory and CMs of a PEC sphere found numerically (a =0.2λ)

Spherical Wave Modes	**Characteristic Mode Eigenvalue Labels**	**Characteristic Mode Eigenvalues from Closed-Form Solution**	**Characteristic Mode Eigenvalues from Numerical Solution**
TE_{01}	λ_3	2.673	2.700
TE_{02}	λ_{12}	21.600	21.993
TM_{01}	λ_1	-1.082	-1.085
TM_{02}	λ_{17}	-284.4	-292.521
TE_{12}	λ_{13}	21.600	22.000
TM_{12}	λ_7	-11.00	-11.214
TE_{22}	λ_{14}	21.600	22.012
TM_{22}	λ_8	-11.00	-11.224

At the same frequency, we checked the orthogonality of the CMs by evaluating expression (2.3-21) given in Table 2.6-9. The far-field integral when m = n is evaluated via an accurate expression for total radiated power given in [DICH97], albeit in a context unrelated to CMs. The terms for m $\neq$ n are found by expressing the integration over the sphere by a simple summation as follows:

$$\frac{1}{\eta} \oiint_{S_\infty} \bar{E}_n \cdot \bar{E}_n^* dS \simeq \frac{1}{\eta} \sum_i \sum_j \bar{E}_n(\theta_i, \phi_j) \cdot \bar{E}_n^*(\theta_i, \phi_j) \Delta\theta \Delta\phi \tag{2.6-14}$$

Table 2.6-9: Expression (2.3-21) evaluated for the lowest five CMs - PEC sphere

m/n	1	2	3	4	5
1	1.000+0.000i	-0.001-0.000i	0.001-0.000i	-0.000-0.009i	-0.000+0.001i
2	-0.001+0.000i	1.000+0.000i	0.000+0.000i	0.000+0.001i	0.000-0.000i
3	0.001+0.000i	0.000-0.000i	1.000+0.000i	0.000+0.000i	-0.000+0.001i
4	-0.000+0.009i	0.000-0.001i	0.000-0.000i	1.000+0.000i	-0.001-0.000i
5	-0.000-0.001i	0.000+0.000i	-0.000-0.001i	-0.001+0.000i	1.000+0.000i

Table 2.6-10: the lowest thirty eigenvalues computed at 2 GHz for the PEC sphere

CM#	λ
1	-1.085
2	-1.086
3	-1.088
4	2.700
5	2.701
6	2.701
7	-11.214
8	-11.224
9	-11.233
10	-11.238
11	-11.249
12	21.993
13	22.000
14	22.012
15	22.012
16	22.015
17	-292.521
18	-292.865
19	-292.958
20	-293.129
21	-293.343
22	-293.637
23	-293.922
24	423.483
25	423.618
26	423.884
27	424.032
28	424.287
29	424.326
30	424.543

B PEC Strip Dipole

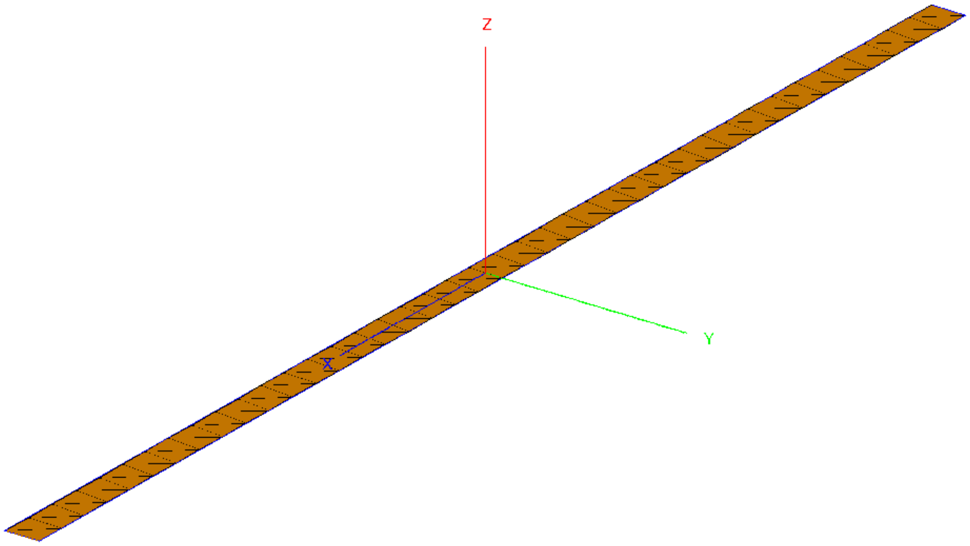

Figure 2.6-11: PEC strip dipole simulated in FEKO

A strip dipole made of infinitely thin PEC sheet with a length of (L=75mm) and width (W=2.5 mm) is studied to analyze its CMs. Some of the results shown in this section will again be referred to in Sections 2.10, 4.5, and 4.7. The characteristic modes of the isolated strip dipole were numerically computed between 1 to 7 GHz and compared to those found in [AKKE05]. Given in Table 2.6-11, the comparison shows a good agreement between the two results. The eigenvalues of theses CMs computed for the whole frequency range are shown in Fig. 2.6-12. Most of CMs computed are capacitive before they become resonant although few higher modes[13] were observed to be inductive. The fact that this is an open structure confirms that the interior resonance problem is not possible in this case. Thus, unlike the case with the sphere, No CM suffered from a numerical issue at any frequency.

Table 2.6-11: CM resonances of the strip dipole in free space. The computed values compared to [AKKE05]

CM	Resonant Frequency (GHz)		
	λ_1	λ_2	λ_3
[AKKE 05]	1.860	3.830	5.810
This Thesis	1.855	3.825	5.805

13 Though, the numerical accuracy of these higher modes can be questioned.

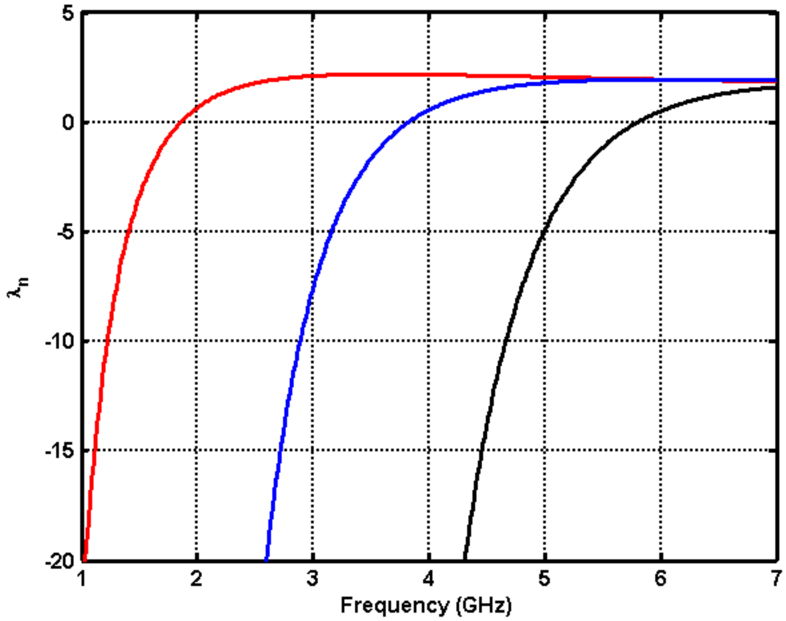

Figure 2.6-12: Eigenvalues of the lowest three CMs – PEC strip dipole. (——) λ_1, (——) λ_2, (——) λ_3

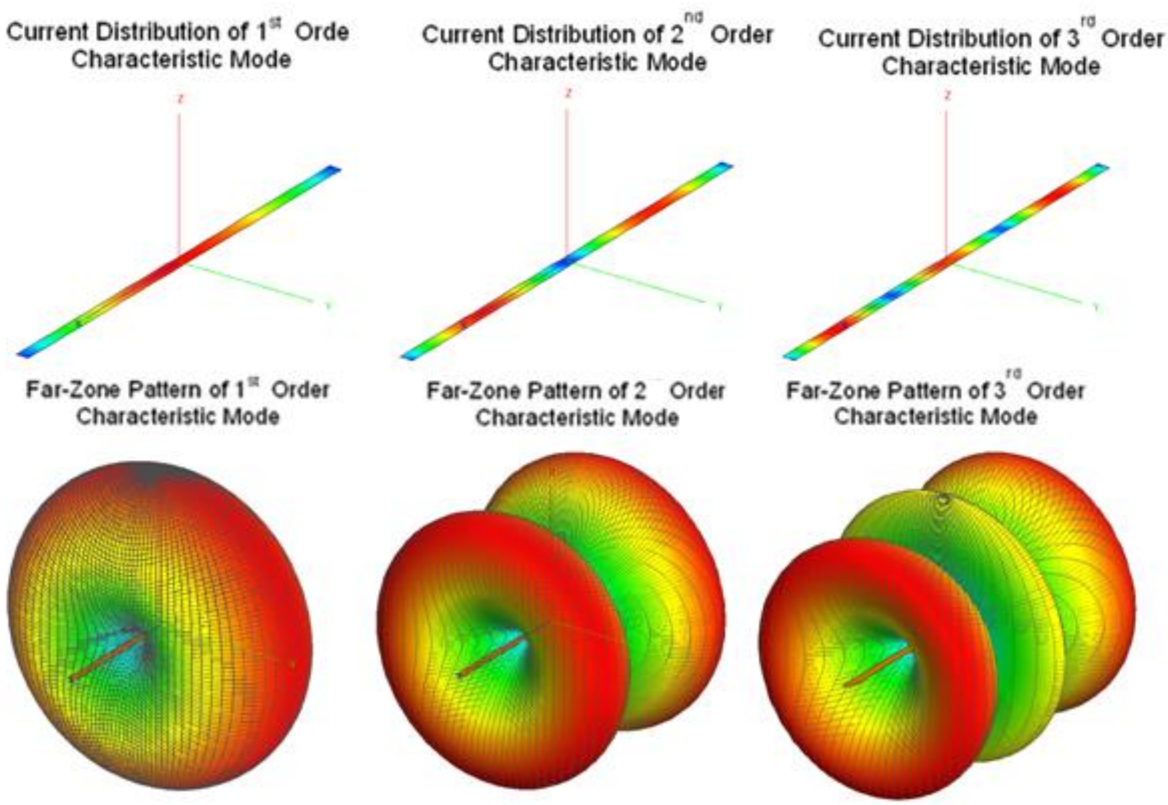

Figure 2.6-13: The modal current distribution and characteristic field radiation pattern for the lowest three CMs.

Theoretically speaking, a dipole antenna is expected to resonate at 0.48λ. For this strip dipole, the first CM resonates at 0.46λ (close enough to that 0.48 λ). Thus, the CMs can be seen as the modes that exhibit the same electromagnetic behavior of the structure itself.

The modal surface current and field radiation pattern for those three lowest CMs were calculated at the frequency of their resonance and plotted in FEKO[14] as shown in Fig. 2.6-13. Examination of the current distributions guides us on how each mode should be excited; for example, the lowest CM (possibly others but not as significant) can be excited by placing a feed in the center of the strip since the current is at its maximum at this point. The excitation of this mode would provide the radiation pattern of a donut shape which is a distinctive characteristic of a dipole. The orthogonality of the modal current and far-field was verified in a similar way it was done for the sphere.

C PEC Closed Rectangular Cavity

The 3-D object in Fig. 2.6-14 cannot be analyzed analytically, and so was simulated using FEKO to obtain the discretized operator matrix of EFIE to perform the typical CM analysis. The following are the dimensions of the rectangular cavity which is made of PEC: the width (in x axis) is 500 mm, the depth (in y axis) is 800 mm, and the height is 350 mm. The eigenvalues were computed for frequencies from 100 to 650 MHz; a coarse mesh (triangle edge length of λ/8 at 650 MHz) was used to speed up the computation time. Due to the fact the structure is electrically large, a tremendous number of unknowns would be required to represent the problem with a fine mesh.

[14] Even though FEKO currently features computation of characteristic modes of conductors, the eigenanalysis was performed in MATLAB through a code we have developed. Eigencurrents were fed back to FEKO as coefficients to calculate the surface currents and far-zone fields due those modes.

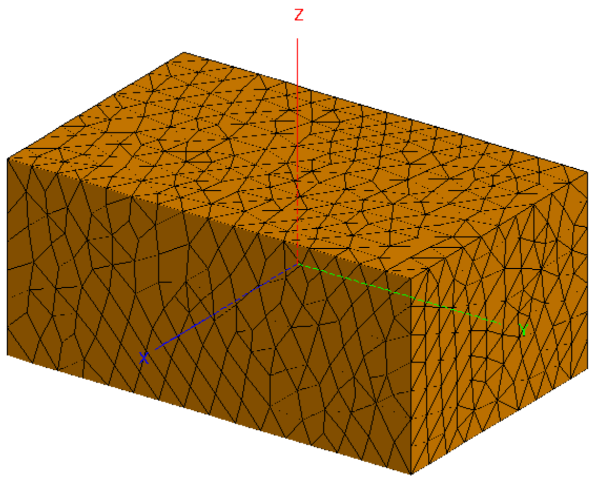

Figure 2.6-14: PEC closed rectangular cavity. The mesh that is visible is that set up by the code FEKO.

Figure 2.6-15 shows the ten lowest CM eigenvalues: our observation shows that only inductive CMs go through resonance, and thus the order of the CMs was done according to the resonance occurrence as depicted in Fig. 2.6-16. These resonances occur at 2.667, 3.186, 3.220, 3.220, and 3.600 Grad/s, respectively. Although the structure is entirely closed as the sphere, an asymptotic behavior was not spotted for any CMs at frequencies which the interior resonance problem would be expected. In addition, we ensured that FEKO used the EFIE formulation for this problem. However, the lowest capacitive modes were found to be affected near these frequencies (2.21, 3.01, and 4.00 Grad/s). Further discussion on this issue will be made in Chapter 3. Various CMs (including both capacitive and inductive) were verified to be orthogonal even near those frequencies at which interior resonances are believed to cause numerical inaccuracies. The modal currents for the lowest modes are shown in Fig. 2.6-17; we want to show the reader it is possible to calculate these distributions for any future work.

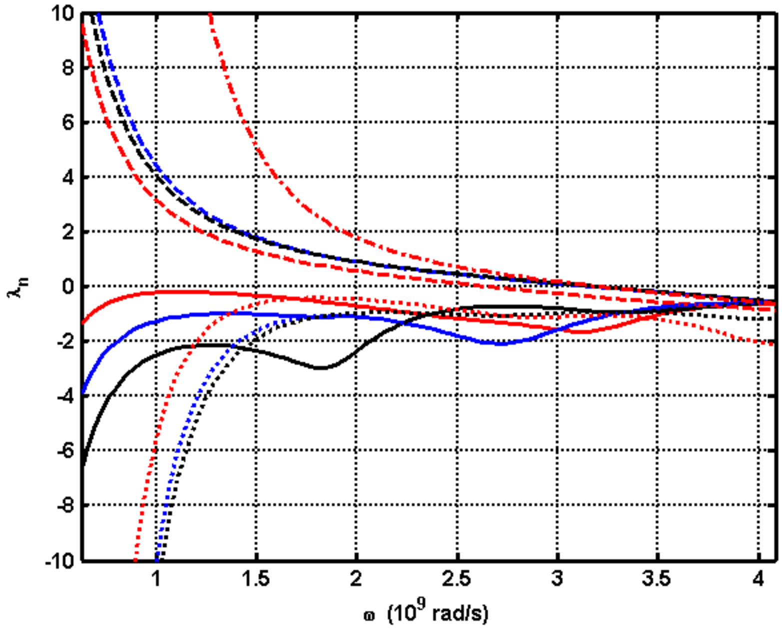

Figure 2.6-15: The lowest ten CM eigenvalues for closed rectangular PEC cavity

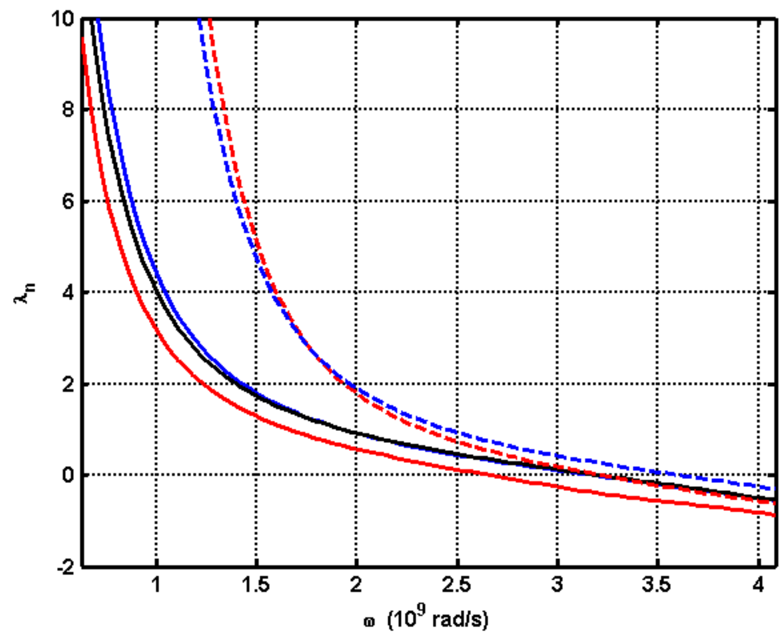

Figure 2.6-16: The lowest five (inductive) CM eigenvalues for closed rectangular PEC cavity. (——) λ_1, (——) λ_2, (——) λ_3, (– – –) λ_4, (– – –) λ_5.

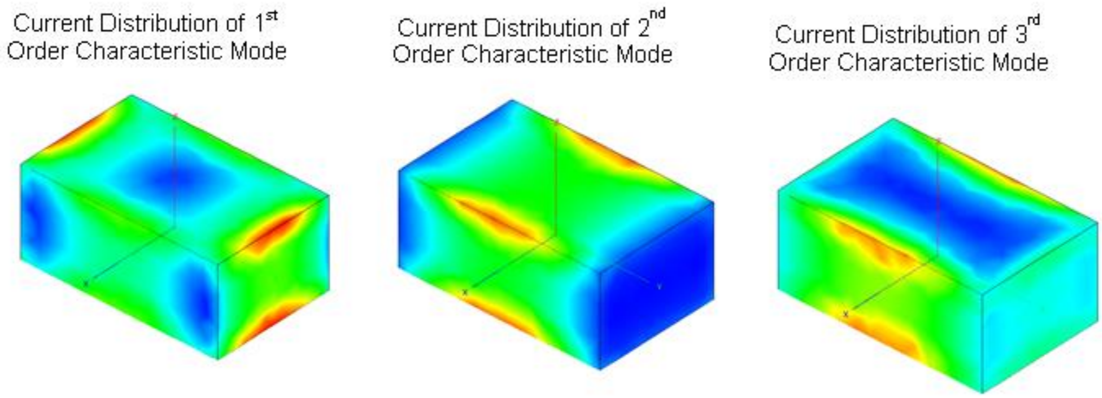

Figure 2.6-17: Modal current distribution of the lowest three CMs for closed rectangular PEC cavity

D Open PEC Rectangular Cavity

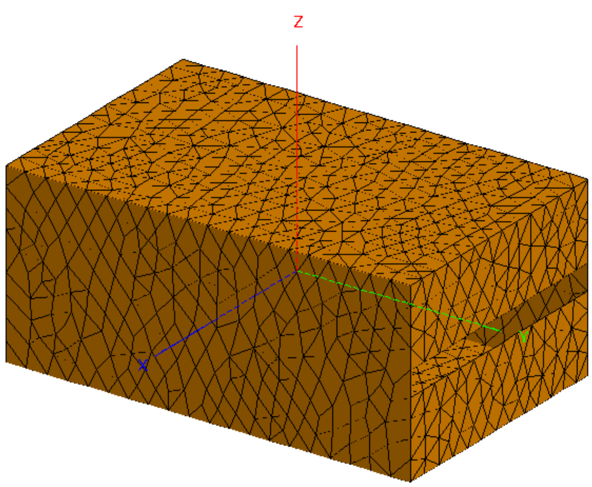

Figure 2.6-18: A slot opened in a rectangular PEC cavity. The mesh shown is that set up by the code FEKO.

A slot aperture opening was made to the previous structure considered as shown in Fig. 2.6-18. Due to the presence of the aperture, the change in the behavior of CM eigenvalues is evident by comparing Fig. 2.6-19 to 2.6-15. A new CM resonance at 1.7 GHz has resulted from opening a slot in the cavity, and it is believed it corresponds to the slot resonance [CHAU10]. The eigenvalue which is shown (black solid line) in Fig. 2.6-15 corresponds to the eigenvalue (green solid line) shown in Fig. 2.6-19. The slot causes this capacitive CM to resonate at 1.7 GHz, which did not previously happen in the case of the closed cavity. On the other hand, the same mode emerged with a capacitive mode resonating at 3.6 GHz similar to that resulted in Fig. 2.6-15. The described behavior of the mode (solid green) is due to the opening and has nothing to do with any modal tracking issue. Finally, one of those capacitive modes which resonated previously for the closed cavity failed to resonate in this case. We believe that all these changes to the behavior of the CMs are attributed to the slot opening.

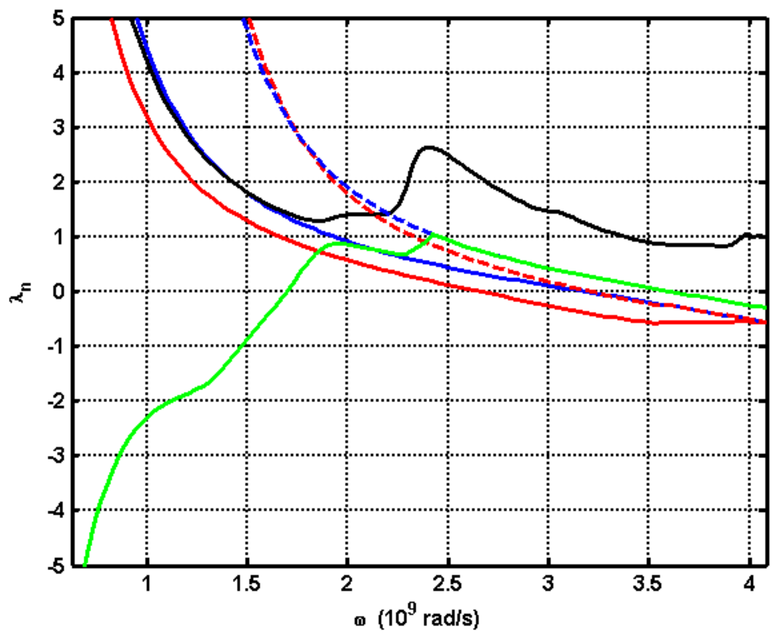

Figure 2.6-19: Eigenvalues of the lowest six CMs - open rectangular PEC cavity

E Open-ended Cylinder

The CMs of a cylinder with its both ends removed were computed for reasons that will be apparent in Chapter 4. The radius and height of the cylinder were set to 4.77 and 74.95 mm (ka = 0.2 and h = 0.5λ @ 2 GHz), respectively. The CMs were analyzed at frequencies between 1 and 3 GHz for the purpose of observing CM resonances as shown in Fig. 2.6-21. The eigenvalue of the first CM is equal to zero at 1.725 GHz while the rest of the eigenvalues continued approaching zero. No interior resonance problem was observed as expected since this structure is considered opened. The eigencurrents and eigenfields were checked to be orthogonal for these CMs.

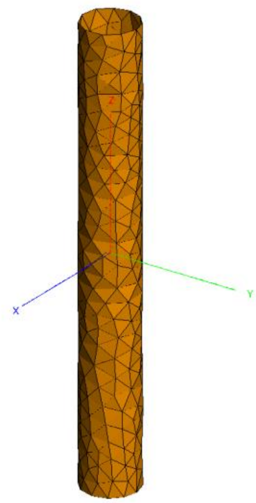

Figure 2.6-20: The PEC cylinder simulated in FEKO

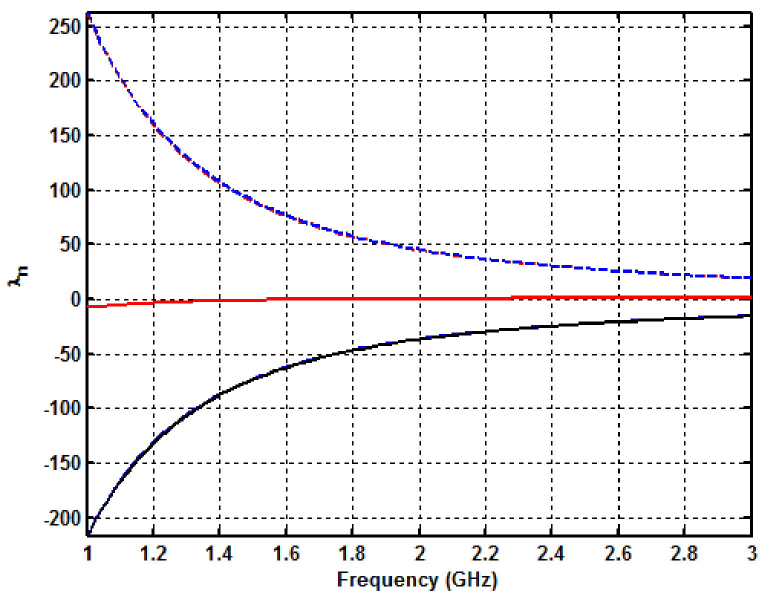

Figure 2.6-21: Eigenvalues of the lowest five CMs – open-ends PEC cylinder. (——) λ_1, (——) λ_2, (——) λ_3, (– – –) λ_4, (– – –) λ_5.

2.7 THE CHARACTERISTIC MODES OF APERTURES IN PERFECTLY CONDUCTING OBJECTS

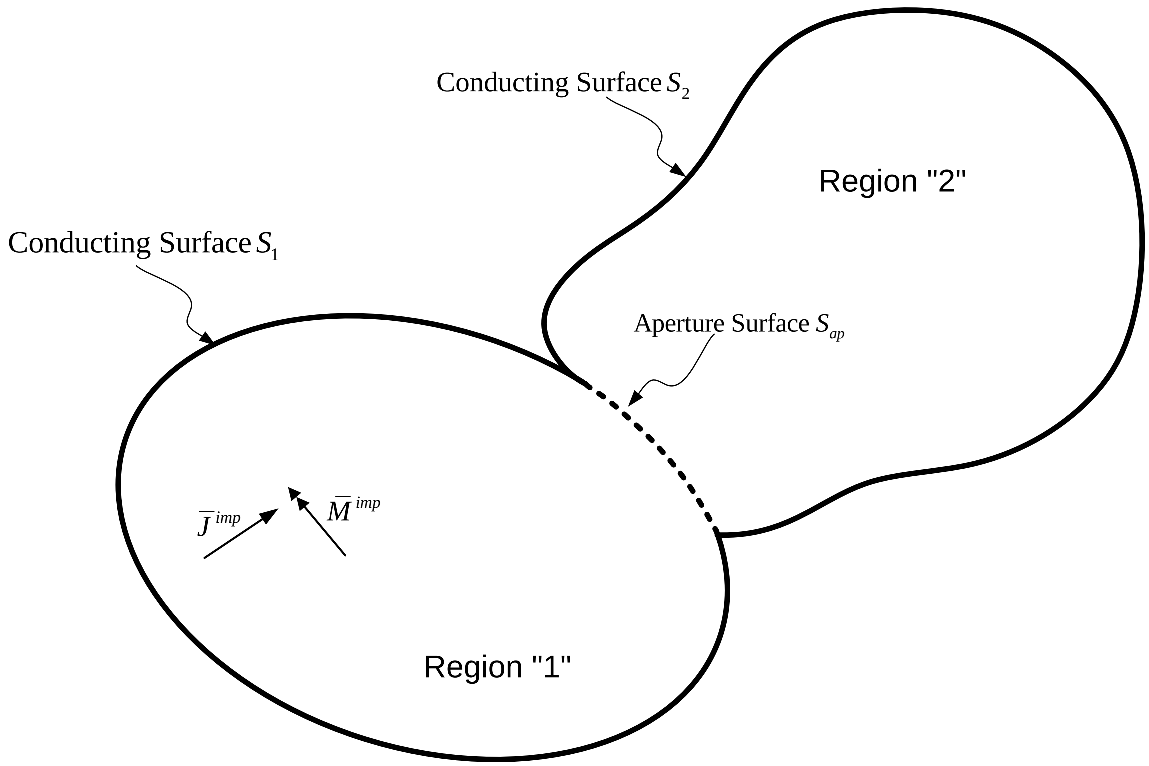

Figure 2.7-1: Two regions coupled through an aperture

Consider the problem shown in Fig.2.7-1, consisting of two regions connected through an aperture. The two regions need not be finite as shown, but could be infinitely large. There are impressed sources in one region and we wish to find the fields everywhere. The problem can be reduced to an integral equation in an unknown that is the magnetic current density $\bar{M}^{ap}$ over the aperture S_{ap}, and has the form [HARR76, HARR80]

$$\bar{H}_{1t}^{scat}\left\{S_{ap},\bar{M}^{ap}\right\}+\bar{H}_{2t}^{scat}\left\{S_{ap},\bar{M}^{ap}\right\}=-\bar{H}_{t}^{inc}\left\{S_{ap},\bar{J}^{imp},\bar{M}^{imp}\right\} \tag{2.7-1}$$

where the subscript "t" in $\bar{H}_{1t}^{scat}$ and $\bar{H}_{2t}^{scat}$ signifies "component tangential to S_{ap}". Use of the method of moments reduces this integral equation to a matrix equation

$$\left[Y\right]\left[V\right]=\left[I^{inc}\right] \tag{2.7-2}$$

The column matrix [V] is of the form

$$\left[V\right]=\begin{bmatrix} b_1 \\ b_2 \\ \vdots \\ b_N \end{bmatrix} \tag{2.7-3}$$

Once it is has been determined the magnetic current density over the aperture is known from

$$\bar{M}^{ap}\left(S_{ap}\right)=\sum_{q=1}^{N} b_q \bar{M}_q\left(S_{ap}\right) \tag{2.7-4}$$

where the $\bar{M}_q\left(S_{ap}\right)$ are the expansion functions for the unknown magnetic current density used in the method of moments formulation. The elements of column matrix $[I^{inc}]$ are related to the incident magnetic field. The moment method matrix $[Y]$ is an admittance matrix. The "recipe" given in Section 2.3.3 for the EFIE case can be used to find the characteristic modes of the aperture using the eigenvalue problem [HARR85]

$$[B][M_n]=\lambda_n[G][M_n] \tag{2.7-5}$$

for the currents $[M_n]$ of the n-th characteristic mode and its eigenvalue λ_n, with $[Y]=[G]+j[B]$ separating $[Y]$ into its real and imaginary parts.

2.8 CHARACTERISTIC MODES OF PENETRABLE OBJECTS – VOLUME INTEGRAL EQUATION FORMULATION

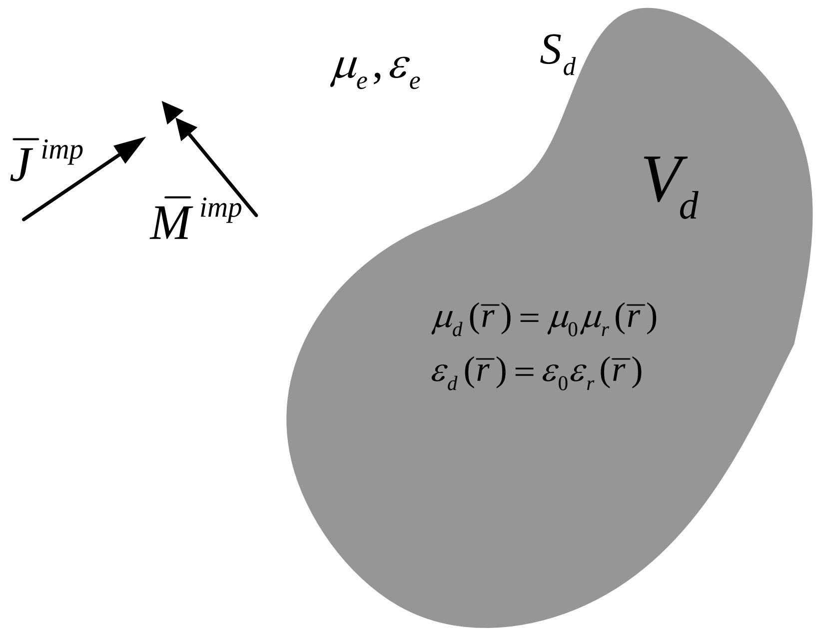

Figure 2.8-1: Scattering from a Penetrable Object

Consider the problem of impressed sources generating incident fields that are incident on the penetrable object (volume V_d) shown in Fig.2.8-1. Using the volume equivalence theorem it is possible to model the problem of scattering from such an object in terms of unknown volume equivalent current densities $\bar{J}_{eq}$ and $\bar{M}_{eq}$ that are solutions to the pair of coupled integral equations [SCHA84]

$$\frac{\bar{J}_{eq}(\bar{r})}{j\omega\left\{\varepsilon_d(\bar{r}) - \varepsilon_e\right\}} - \bar{E}^{scat}\left\{\bar{r}, \bar{J}_{eq}, \bar{M}_{eq}\right\} = \bar{E}^{inc}\left\{\bar{r}, \bar{J}^{imp}, \bar{M}^{imp}\right\} \text{ where } \bar{r} \in V_d \qquad (2.8\text{-}1)$$

$$\frac{\bar{M}_{eq}(\bar{r})}{j\omega\left\{\mu_d(\bar{r}) - \mu_e\right\}} - \bar{H}^{scat}\left\{\bar{r}, \bar{J}_{eq}, \bar{M}_{eq}\right\} = \bar{H}^{inc}\left\{\bar{r}, \bar{J}^{imp}, \bar{M}^{imp}\right\} \text{ where } \bar{r} \in V_d \qquad (2.8\text{-}2)$$

Application of the method of moments reduces this integral equation to the matrix form

$$\begin{bmatrix} [Z] & [C] \\ [D] & [Y] \end{bmatrix} \begin{bmatrix} [J] \\ [M] \end{bmatrix} = \begin{bmatrix} \left[V^{inc}\right] \\ \left[I^{inc}\right] \end{bmatrix} \tag{2.8-3}$$

where

$$[M] = \begin{bmatrix} V_1 \\ V_2 \\ \cdot \\ \cdot \\ V_N \end{bmatrix} \tag{2.8-4}$$

and

$$[J] = \begin{bmatrix} I_1 \\ I_2 \\ \cdot \\ \cdot \\ I_N \end{bmatrix} \tag{2.8-5}$$

are the coefficients of the expansion functions used to represent $\bar{J}_{eq}$ and $\bar{M}_{eq}$, respectively. $\left[V^{inc}\right]$ and $\left[I^{inc}\right]$ are related to the incident electric and magnetic fields, respectively. Partitions $[Z]$ and $[Y]$ of the moment method matrix are impedance and admittance matrices, respectively. Partitions $[C]$ and $[D]$ of the moment method matrix are dimensionless.

The moment method matrix in (2.8-3) is not symmetric, and thus the recipe described in Section 2.3.3 is not directly applicable. But the formulation details reveal that $[D] = -[C]$. It was shown in [HARR72a] that the matrix can be symmetrized into the form

$$\begin{bmatrix} [Z] & [jC] \\ [jC] & [Y] \end{bmatrix} \begin{bmatrix} [J] \\ [jM] \end{bmatrix} = \begin{bmatrix} \left[V^{inc}\right] \\ \left[jI^{inc}\right] \end{bmatrix} \tag{2.8-6}$$

and so the matrix eigenvalue problem for finding the CMs then becomes [CHAN 72]

$$\left[\begin{array}{c|c} [X] & [N_2] \\ \hline [N_2] & [B] \end{array}\right]\left[\begin{array}{c} [J_n] \\ \hline j[M_n] \end{array}\right] = \lambda_n \left[\begin{array}{c|c} [R] & [N_1] \\ \hline [N_1] & [G] \end{array}\right]\left[\begin{array}{c} [J_n] \\ \hline j[M_n] \end{array}\right] \tag{2.8-7}$$

where

$$[Y] = [G] + j[B] \tag{2.8-8}$$

and

$$j[C] = [N_1] + j[N_2] \tag{2.8-9}$$

The above formulation applies if the object has $\varepsilon_d \neq \varepsilon_o$ and $\mu_d \neq \mu_o$. This is because we then need both $\bar{J}_{eq}$ and $\bar{M}_{eq}$ to model the scattering problem. If the object has $\varepsilon_d \neq \varepsilon_o$ but $\mu_d = \mu_o$ then only $\bar{J}_{eq}$ is required, and the moment method matrix equation (2.7-3) reduces to $\left[Z\right]\left[J\right] = \left[V^{inc}\right]$. If the object has $\varepsilon_d = \varepsilon_o$ but $\mu_d \neq \mu_o$ then only $\bar{M}_{eq}$ is required, and the moment method matrix equation (2.8-3) becomes simply $\left[Y\right]\left[M\right] = \left[I^{inc}\right]$. In the latter two instances No special symmetrisation transformation is needed since the formulation gives matrices $\left[Z\right]$ and $\left[Y\right]$ that are symmetric.

Although formulated more than forty years ago, actual numerical results for the characteristic modes of penetrable object found using the above approach have not yet been published in the open literature; not even in the seminal publication [HARR85]. In oral conference presentations and discussions it has from time to time been stated that the determination of the CMs of penetrable objects is difficult, but without further comments as to why this is so. One of the aims of this thesis is to investigate this and perform actual computations for the CMs of such objects.

2.9 CHARACTERISTIC MODES OF PENETRABLE OBJECTS – SURFACE INTEGRAL EQUATION FORMULATION

We again consider the problem depicted in Fig.2.8-1. However, instead of using the physical volume current densities to model the penetrable object, the surface equivalence theorem and field continuity conditions are applied to arrive at a pair of coupled integral equations in which equivalent surface current densities $\bar{J}_s$ and $\bar{M}_s$ are the unknowns. Many possible forms of this coupled set of integral equations are available, but the most widely used (because it is free of the "internal resonance" problem mentioned in Section 2.3.5) is the so-called the PMCHWT[15] formulation

$$\hat{n}\times\bar{E}_e^{scat}\left\{S_d^-,\bar{J}_s,\bar{M}_s\right\}+\hat{n}\times\bar{E}_d^{scat}\left\{S_d^+,\bar{J}_s,\bar{M}_s\right\}=-\hat{n}\times\bar{E}^{inc}\left\{S_d^-,\bar{J}^{imp},\bar{M}^{imp}\right\} \qquad (2.9\text{-}1)$$

$$\hat{n}\times\bar{H}_e^{scat}\left\{S_d^-,\bar{J}_s,\bar{M}_s\right\}+\hat{n}\times\bar{H}_d^{scat}\left\{S_d^+,\bar{J}_s,\bar{M}_s\right\}=-\hat{n}\times\bar{H}^{inc}\left\{S_d^-,\bar{J}^{imp},\bar{M}^{imp}\right\} \qquad (2.9\text{-}2)$$

Quantity $\bar{E}_e^{scat}\left\{S_d^-,\bar{J}_s,\bar{M}_s\right\}$ is the field due to $\bar{J}_s$ and $\bar{M}_s$ in the free space region external ("e") to the object, evaluated in the limit as the observation point approaches the surface on S_d form the outside. Quantity $\bar{E}_d^{scat}\left\{S_d^-,\bar{J}_s,\bar{M}_s\right\}$ is the field due to $\bar{J}_s$ and $\bar{M}_s$ inside the dielectric object ("d"), but evaluated in the limit as the observation point approaches the surface on S_d from the inside. Similar comments apply to quantities $\bar{H}_e^{scat}\left\{S_d^-,\bar{J}_s,\bar{M}_s\right\}$ and $\bar{H}_d^{scat}\left\{S_d^+,\bar{J}_s,\bar{M}_s\right\}$.

If the moment method is used [UMAS86] to solve the above coupled integral equation model, a matrix equation of the form (2.7-3) is obtained, except that now the $[J]$ and $[M]$ are the column vectors of coefficients for the fictitious surface current densities rather than volume current densities. Symmetrisation can be done as in (2.8-6), and the characteristic mode eigenvalue problem written [CHAN77] in the same form as (2.8-7). As with the volume formulation of Section 2.8, No computed results (not even in [CHAN77]) have been published

[15] Poggio-Miller-Chang-Harrington-Wu-Tsai (PMCHWT), named after the authors whose work had independently used this integral equation.

for the characteristic mode currents and fields using this formulation. Such computations will be performed in this thesis and the related issues discussed.

2.10 THE SUB-STRUCTURE CHARACTERISTIC MODE CONCEPT

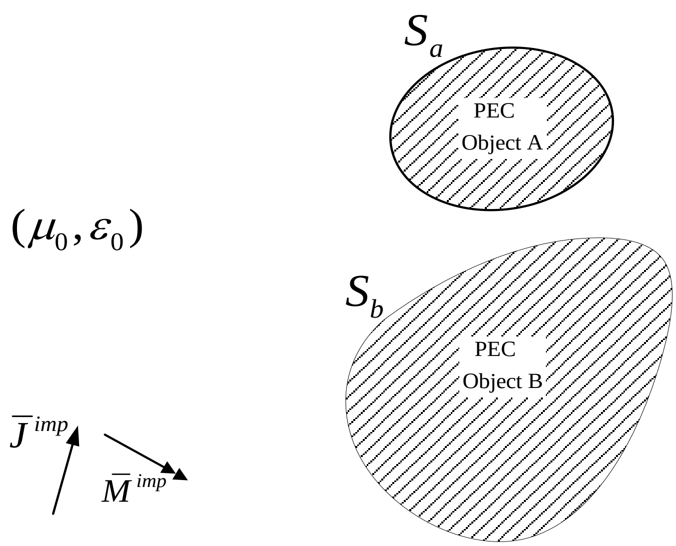

Figure 2.10-1: Two PEC Objects

Consider a PEC object that consists of two portions, modelled using an EFIE that is solved using the method of moments. Expansion and weighting functions will be distributed over the PEC surface in the usual manner. We consider the two portions to be Object A and Object B, with different expansion function subsets located on these two portions. The discrete form of the EFIE can then have its operator matrix [Z] partitioned such that it reads

$$\begin{bmatrix}[Z_{AA}] & [Z_{AB}]\\ [Z_{BA}] & [Z_{BB}]\end{bmatrix}\begin{bmatrix}[J_A]\\ [J_B]\end{bmatrix}=\begin{bmatrix}[V_A]\\ [V_B]\end{bmatrix} \tag{2.10-1}$$

This can of course be written as the two equations

$$[Z_{AA}][J_A]+[Z_{AB}][J_B]=[V_A] \tag{2.10-2}$$

and

$$[Z_{BA}][J_A]+[Z_{BB}][J_B]=[V_B] \tag{2.10-3}$$

It is assumed that the EFIE kernel was a free space Green's function $\mathbb{G}_{\text{free space}}$. It is easy to infer the meaning of each term in (2.10-1). The sub-matrices $[Z_{AA}]$ and $[Z_{BB}]$ are the impedance matrices for Object A and B when they are isolated from each other. Sub-matrices $[Z_{AB}]$ and $[Z_{BA}]$ are coupling matrices between the objects. The column vector $[J_A]$ contains the coefficients for the electric surface current density $\bar{J}_A$ on Object A, with a similar interpretation for $[J_B]$.

In the antenna context, where the excitation of the PEC object is localized, [ETHI12a] considered the problem where Object B is not fed, so that $[V_B]=0$. With $[V_B]=0$, expression (2.10-1) reduces to

$$\left\{[Z_{AA}]-[Z_{AB}][Z_{BB}]^{-1}[Z_{BA}]\right\}[J_A]=[V_A] \tag{2.10-4}$$

If we define

$$\left\{[Z_{AA}]-[Z_{AB}][Z_{BB}]^{-1}[Z_{BA}]\right\}=[Z_{SUB}] \tag{2.10-5}$$

the moment method matrix equation can be written as

$$[Z_{SUB}][J_A] = [V_A] \tag{2.10-6}$$

Equation (2.10-6) can be used to find the current distribution on Object A in the presence of Object B (subject to the excitation restrictions described). The current density on Object B can subsequently be found using

$$[J_B] = -[Z_{BB}]^{-1}[Z_{BA}][J_A] \tag{2.10-7}$$

In [ETHI12a] the matrix equation (2.10-6) is used to define a new set of CMs, which are referred to as sub-structure CMs, by solving the eigenvalue problem

$$[X_{SUB}][J_n] = \lambda_n [R_{SUB}][J_n] \tag{2.10-8}$$

These can be thought of as the CMs of Object A in the Object B, subject to the restriction that only those CMs that can be excited without any incident field on portion B are observable.

The example below further illustrates the above discussion. The strip dipole shown in Section 2.6.4 is considered as Object A whereas Object B is chosen to be a large PEC plate (40W x 5L) set below the strip with the spacing distance of 16.2 mm (0.1λ @ 1.855 GHz). Table 2.10-1 differentiates between the lowest CM resonance of the substructure and that of a strip dipole present in free space alone. Besides, the Table shows that the sub-structure concept filters out those CMs of Object B.

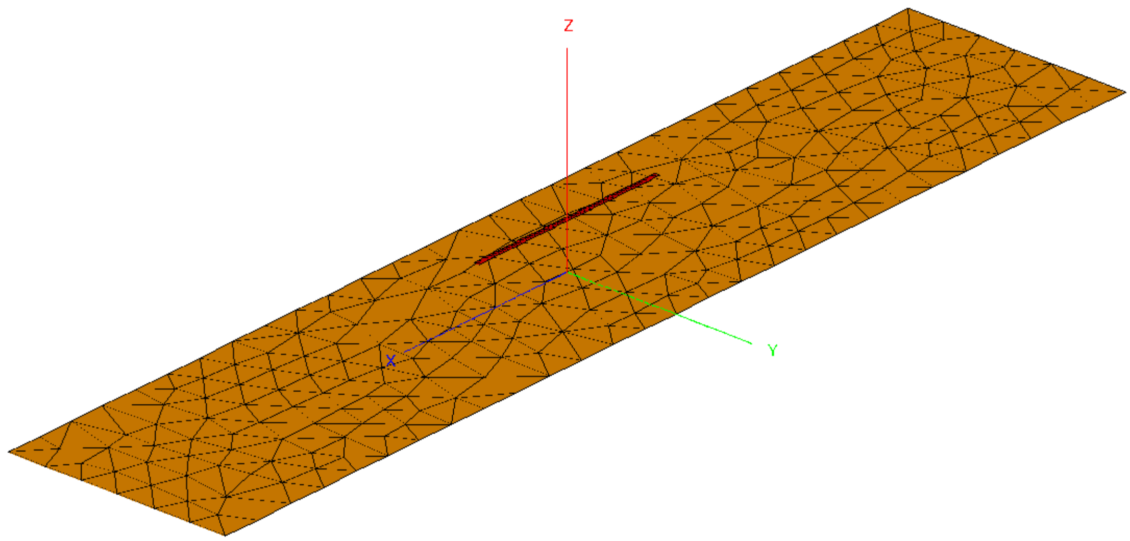

Figure 2.10-1: Strip dipole lies above a large finite-sized PEC plate apart of distance

Table 2.10-1: Frequency (GHz) at which CM eigenvalue is zero.

<table>
<tr><th>CM</th><th>Modes for Complete Structure</th><th>Sub-structure Modes for Object A</th><th>Modes for Object A (Isolated)</th></tr>
<tr><td>1</td><td>0.750</td><td>1.816</td><td>1.855</td></tr>
<tr><td>2</td><td>1.160</td><td colspan="2" rowspan="3">Resonances Higher Than 2 GHz</td></tr>
<tr><td>3</td><td>1.590</td></tr>
<tr><td>4</td><td>1.890</td></tr>
</table>

2.11 CONCLUDING COMMENTS

The fundamentals of characteristic mode analysis have been presented in this chapter. This will underpin everything that is discussed in the rest of this thesis. We have written things in a way that separates the definition of the characteristic mode concept from the methods used to compute them. Although integral equation methods are the most convenient for the computation of such modes, and the formulation via such integral equations very directly reveal the characteristic mode properties, they do not constitute the fundamental definition of the characteristic mode concept. This is not always made clear in the literature. Although computed characteristic mode results have been presented elsewhere for rectangular PEC plates and spheres in free space, we have shown results for these objects so as to be able to confirm the correctness of the way the thesis will do things by comparing such results to those obtained by other authors. Characteristic modes were also computed for the closed rectangular PEC box, and one with an aperture. Such cases have not been considered elsewhere; we have selected them to allow us to discuss such results in relation to natural modes (not the same as characteristic modes) in Chapter 3. Integral equation formulations for finding the characteristic modes of penetrable objects were reviewed in Sections 2.8 and 2.9; these are used in Chapter 5 to compute such modes for the first time. The mode-tracking of Section 2.5 is used throughout the thesis. The sub-structure characteristic mode idea introduced in Section 2.10 is discussed further in Chapter 4.

CHAPTER 3 The Relation of Characteristic Modes to the Exterior and Interior Natural Modes of PEC Objects

3.1 INTRODUCTION

As stated in Chapter 1, when the author of this thesis presented the paper [ALRO12], he was asked why natural modes could not be used instead. In order to properly answer this question, it has been necessary to examine the relation of natural modes to characteristic modes, since such a direct comparison does not appear to have been discussed elsewhere. In fact while many antenna engineers are familiar with the "resonant modes" of cavities, which are in fact interior natural modes, many are not familiar with the fact that exterior natural modes can be defined even for conducting objects. The reason is that such concepts are rarely needed in antenna work. The present chapter thus discusses the natural mode concept. Although relatively brief, we consider it to be more than a "mere" review of the type done for characteristic modes in Chapter 2, since much of the material is embedded in literature in a manner not directly accessible or attractive to those concerned with practical antenna design. The discussion will allow us to appreciate the difference between natural modes and characteristic modes.

3.2 FUNDAMENTAL DEFINITION OF NATURAL MODES

A natural mode of an object is one that can exist inside or outside the object, or both inside and outside, *in the absence of sources* (that is, with zero incident field). Its electromagnetic field satisfies Maxwell's equations and the physical boundary conditions dictated by the object. All physical objects have natural electromagnetic modes with which are associated resonant frequencies. Depending on the details of the structure these resonant frequencies may be real or complex; this will be discussed below. These resonant frequencies are found from a linear or non-linear eigenvalue problem.

We immediately note that No characteristic mode field satisfies, on its own, the physical boundary conditions dictated by the object. When an incident field $\bar{E}^{inc}(\bar{r})$ is specified, just the correct amount of each of the object's characteristic mode fields are generated (usually only a few of the modes have a significant complex amplitude) to give a scattered field $\bar{E}^{scat}(\bar{r})$, so that the total field $\bar{E}(\bar{r}) = \bar{E}^{inc}(\bar{r}) + \bar{E}^{scat}(\bar{r})$ satisfies the physical boundary conditions dictated by the object.

In what follows we wish to discuss the essence of the natural mode concepts and not be fettered by aspects that can be easily handled if they are included, but add details that obscure the understanding of the concepts we are trying to promote. Thus we assume that all materials are either perfect electric conductors or lossless penetrable media. In addition - and this is anyway the important case for all but problems in the bio-electromagnetics area - it is assumed that only homogeneous or piecewise homogeneous media are of interest.

3.3 DIFFERENTIAL EQUATION APPROACH FOR THE DETERMINATION OF NATURAL MODES - *PRELIMINARIES*

3.3.1 The Wave Equation

All electromagnetic fields must satisfy the source excited wave equation

$$\nabla \times \nabla \times \bar{E}(\bar{r}) - k^2 \bar{E}(\bar{r}) = -j\omega\mu \bar{J}^{imp}(\bar{r}) - \nabla \times \bar{M}^{imp}(\bar{r}) \qquad (3.3\text{-}1)$$

where $k^2 = \omega^2 \mu\varepsilon$, ω is the frequency, the properties of the material at point $\bar{r}$ are μ and ε, and $\bar{J}^{imp}(\bar{r})$ and $\bar{M}^{imp}(\bar{r})$ are the impressed sources. If there are No sources in the region where the electromagnetic field is desired then $\bar{J}^{imp}(\bar{r}) = 0$ and $\bar{M}^{imp}(\bar{r}) = 0$, and the fields must satisfy the source-free wave equation

$$\nabla \times \nabla \times \bar{E}(\bar{r}) - k^2 \bar{E}(\bar{r}) = 0 \qquad (3.3\text{-}2)$$

at all points in the region. We can recognize this as an eigenvalue problem by taking the second term over to the right hand side to obtain

$$\nabla \times \nabla \times \bar{E}(\bar{r}) = k^2 \bar{E}(\bar{r}) \qquad (3.3\text{-}3)$$

3.3.2 Spherical Vector Wave Functions

The general mathematical solution of the source-free vector wave equation in spherical coordinates [STRA 41] be written in terms of the so-called spherical vector wave functions, which are of two kinds, namely those TE to the radial direction (TE_r) and those TM to the radial direction (TM_r). Such wave functions can be outgoing, incoming, or of the standing wave type (essentially a combination of the other two types). Of course general solutions only become useful in particular circumstances when we apply appropriate physical boundary conditions. This will be done in the discussions to follow.

3.3.3 Material Objects of Interest

Fig.3.3-1 shows four three-dimensional objects. The first is a closed solid PEC object. The second is also a closed PEC object, but it is hollow, and would normally be called a cavity. The third is also has PEC walls, there are openings in the walls and so the object is not a closed one. Finally, the fourth object is a piece of penetrable material with the permittivity and permeability shown.

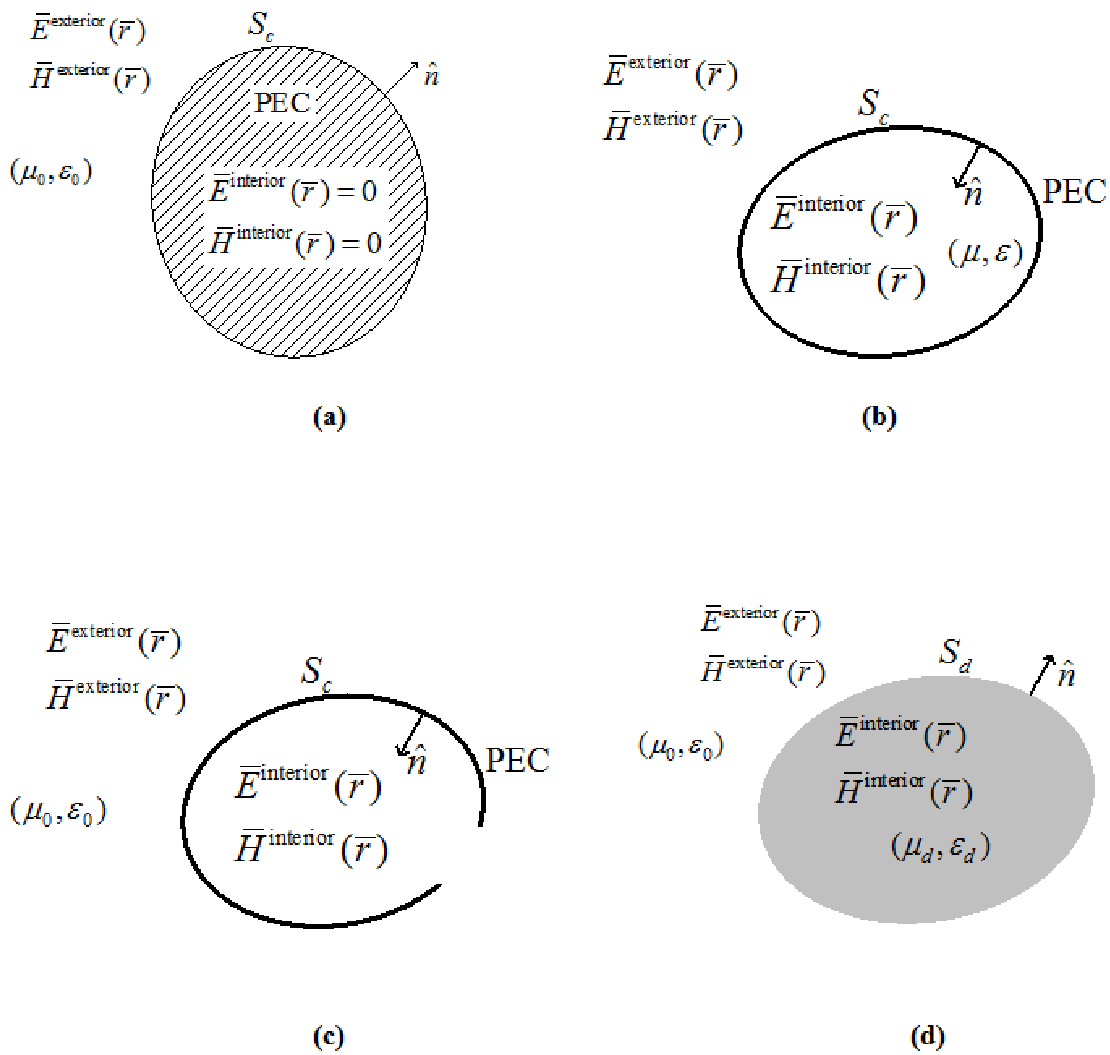

Figure 3.3-1: (a). Closed solid PEC object; (b). Closed hollow PEC object; (c). Hollow open PEC object; (d). Piece of penetrable material with the permittivity and permeability shown.

3.4 DIFFERENTIAL EQUATION APPROACH FOR THE DETERMINATION OF NATURAL MODES– INTERIOR MODES

3.4.1 The Basic Procedure

Consider the closed PEC objects shown in Fig.3.3-1 (a) and (b). Mere inspection tells us that (with or without sources) there will be No electromagnetic field interior to the surface S_c of the object in Fig.3.3-1(a). However, basic "cavity resonator" theory from microwave engineering tells us that there can be non-zero fields $\bar{E}(\bar{r})$ in the interior of the closed object in Fig.3.3-1(b) *in the absence of sources there*, but only at specific frequencies ω called the resonant frequencies of the cavity[1]. These are the interior natural mode frequencies of the closed object, and at each of these frequencies there is an associated electromagnetic field distribution $(\bar{E},\bar{H})$, called the interior natural mode fields. The interior natural modes are usually referred to as cavity modes. The solution of (3.3-2) subject to the boundary condition that $\hat{n}\times\bar{E}=0$ at points on S_c can be found in analytical form for rectangular cavities (boxes) [COLL 91], cylindrical cavities of circular cross-section [BLAD07] and spherical cavities [HANS02, EOM04, BALA89]. Numerical solutions for these interior natural modes of closed PEC objects are these days done relatively painlessly using the finite element method (FEM) approach[2]. In essence, the wave equation with zero excitation is discretized by the FEM into a matrix eigenvalue problem, and this is solved numerically to find the natural mode resonant frequencies and field distributions. Once the field distributions are known the usual boundary conditions can be used to find the associated natural mode current distributions on the object.

3.4.2 Spherical PEC Cavities

For reference in Section 3.5.2, rather than because it is of practical use, we remark that it can be shown that the interior natural mode resonant frequencies of a spherical cavity of radius *a* are as follows [BALA 89, pp.557-560] :

$$TE_r \qquad \omega_{NM}^{\text{int}}(m,n,p)=\frac{\xi_{np}}{a\sqrt{\mu_0\varepsilon_0}} \qquad \begin{array}{l} m=0,1,2,3,..........,n \\ n=1,2,3,.................. \\ p=1,2,3,................... \end{array} \tag{3.4-1}$$

where the quantities ξ_{np} are the roots of the spherical Bessel function, namely $\hat{J}_n(\xi_{np})=0$.

$$TM_r \qquad \omega_{NM}^{\text{int}}(m,n,p)=\frac{\xi'_{np}}{a\sqrt{\mu_0\varepsilon_0}} \qquad \begin{array}{l} m=0,1,2,3,..........,n \\ n=1,2,3,.................. \\ p=1,2,3,................... \end{array} \tag{3.4-2}$$

[1] Equivalently, only for certain values (that is eigenvalues) of $k^2=\omega^2\mu\varepsilon$.

[2] As is done, for instance, in the commercial code HFSS.

where the quantities ξ'_{np} are the roots of the derivative of the spherical Bessel function, namely $\hat{J}'_n(\xi_{np}) = 0$. Expressions for the interior natural mode fields associated with each resonant frequency, and the associated natural mode currents on the PEC sphere, can also be obtained to within an arbitrary constant.

In the case of a lossless medium inside the closed PEC object the eigenvalues k^2 are always real, and thus the resonant frequencies obtained from them are also real[3].

3.4.3 The Complete Story for a Simple Two-Dimensional PEC Case

We wish to indicate how the fields in a closed region, when there is a source placed in the region, can in fact be written as a summation of interior natural mode fields. Although this could be illustrated for the three-dimensional closed PEC objects whose interior natural mode fields are available in analytical form, such expressions tend to be cumbersome. Consideration of the two-dimensional cavity problem[4], shown in Fig.3.4-1, is able to reveal the essence of what needs to be shown without this notational baggage.

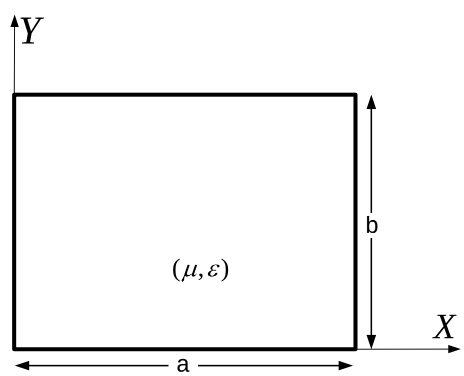

Figure 3.4-1: Cross-Section of Two-Dimensional Rectangular Cavity

The interior resonance frequencies of the two-dimensional cavity with field $E_z(x, y)$ can be found as the solution of the two-dimensional form of (3.3-2), namely

---

[3] We discuss what is meant by a complex frequency in Section 3.5.
[4] It should not be thought of as a waveguide, as there is No wave propagation along the z-axis.

$$\nabla_t^2 E_z(x,y) + k^2 E_z(x,y) = 0 \tag{3.4-3}$$

subject to the boundary condition that at all points on the PEC surface. This is an eigenvalue problem, which has non-zero solutions

$$E_z(x,y) = C_{mn} \sin\left(\frac{m\pi x}{a}\right) \sin\left(\frac{n\pi y}{b}\right) \tag{3.4-4}$$

but only at those values of $k^2 = k_{mn}^2$, where

$$k_{mn}^2 = (m\pi / a)^2 + (n\pi / b)^2 \tag{3.4-5}$$

Since $k^2 = \omega^2 \mu\varepsilon$, this implies that non-zero fields only exist in the cavity at the frequencies

$$\omega_{NM}^{\mathrm{int}}(m,n) = \frac{1}{\sqrt{\mu\varepsilon}} \sqrt{(m\pi / a)^2 + (n\pi / b)^2} \tag{3.4-6}$$

The theory of Green's functions (also referred to as "source-excited boundary value problems" in the literature) is able to use [EOM04, Chap.8] such natural modes to construct the Green's function for the problem as

$$G(x,y,x',y') = \frac{4}{ab} \sum_{m=0}^{\infty} \sum_{n=0}^{\infty} \frac{\sin\left(\frac{m\pi x}{a}\right) \sin\left(\frac{n\pi y}{b}\right) \sin\left(\frac{m\pi x'}{a}\right) \sin\left(\frac{n\pi y'}{b}\right)}{k_{mn}^2 - k^2} \tag{3.4-7}$$

This means that if we have a known impressed electric current density distribution $J_z^{imp}(x,y)$ inside the cavity then electric field can be determined using the superposition integral

$$E_z(x,y) = j\omega\mu \iint_{S'} J_z^{imp}(x',y') G(x,y,x',y') \, dS' \tag{3.4-8}$$

where S' is the cross-section of the two-dimensional impressed current density. Using (3.4-7) with (3.4-8) allows us to write

$$E_z(x,y) = \sum_{m=0}^{\infty}\sum_{n=0}^{\infty} A_{mn} \sin\left(\frac{m\pi x}{a}\right)\sin\left(\frac{n\pi y}{b}\right) \tag{3.4-9}$$

with

$$A_{mn} = \frac{j4\omega\mu_0 / ab}{(k_{mn}^2 - k^2)} \iint_{S'} J_z(x',y')\sin\left(\frac{m\pi x'}{a}\right)\sin\left(\frac{n\pi y'}{b}\right) dx'dy' \tag{3.4-10}$$

Expression (3.4-10) is an expansion of the actual field in the cavity, when there is a source at any frequency we wish, written in terms of the interior natural modes of the cavity.

We could write down similar results [TYRA69] from the solution of (3.4-3) for the two-dimensional circular cavity in Fig.3.4-2. Due to comments we wish to make later, suffice it to say that the interior natural mode resonant frequencies are

$$\omega_{NM}^{\text{int}}(m,n) = \frac{k_{mn}}{\sqrt{\mu\varepsilon}} \tag{3.4-11}$$

where the k_{mn} are the roots of the equation

$$J_m(k_{mn}a) = 0 \tag{3.4-12}$$

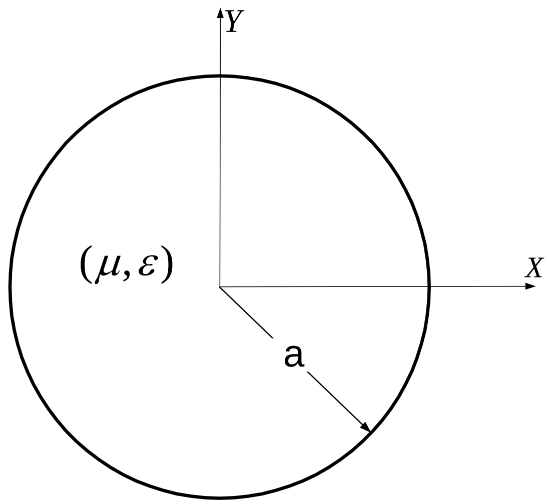

Figure 3.4-2: Two-Dimensional Circular Cavity

3.4.4 Interior Natural Modes of Open PEC Objects and Penetrable Objects

Now consider the open PEC object shown in Fig.3.3-1 (c), and the penetrable object in Fig.3.3-1(d). Neither of these objects possesses interior natural modes. Firstly, the open PEC object in Fig.3.3-1(c) has No interior that is disconnected from its exterior. Secondly, for the penetrable object in Fig.3.3-1(d) there is No practical situation where its fields could be completely confined to the penetrable material. Thirdly, the closed PEC objects in Fig.3.3-1(a) and (b) will have exterior natural modes in addition to the interior ones described above.

3.5 DIFFERENTIAL EQUATION APPROACH FOR THE DETERMINATION OF NATURAL MODES – *EXTERIOR MODES*

3.5.1 Problem Difficulties

The exterior natural mode problem[5] is different. In the case of the closed or open PEC objects, we must now find solutions to the eigenvalue problem (3.3-2) in the region outside the closed PEC object, subject to the physical boundary condition $\hat{n} \times \bar{E} = 0$ at all points on the walls of the object and subject to the radiation condition at infinity. In the case of the penetrable object we

[5] Also referred to as an open resonator problem. The topic is referred to as studying the free oscillations of objects.

have to find solutions to the eigenvalue problem (3.3-2) in the region inside and outside the object, subject to the physical boundary conditions of continuity of the tangential components of both $\bar{E}$ and $\bar{H}$ at all points on the surface of the object, and subject to the radiation condition at infinity.

This is not easily done numerically using the FEM approach. Commercial codes such as HFSS do not yet support such an eigenanalysis of open resonators (as opposed to the deterministic problem of the same object with impressed sources present). Very special considerations are required. As stated in Part B of Section 2.4, development of a means of using the FEM for the eigenanalysis of an open resonator is apparently under development [MAXI 12], [ZEKI 13], [KYRI 13], but mainly for two-dimensional structures, with the extension to 3-D structures on-going and having certain numerical difficulties. Although the above represents good work on a topic that has "vast research challenges" [ZEKI 13], the unfortunate thing is that the eigenvalue problem becomes a non-linear one. The latter is computationally very burdensome. At present the exterior natural modes of PEC or penetrable objects of general shape are found numerically using integral equation methods, as will be discussed in Section 3.5.

3.5.2 Known Analytical Solutions

The differential equation route for finding exterior natural modes can be used to obtain analytical solutions for a very limited number of objects. We write some of these down here in order to be able to interpret them, and hence something about exterior modes in general.

A. Two-Dimensional PEC Circular[6] Cylinder of Radius a

The exterior natural mode frequencies for the TM case can be found from the roots of the equation [CHO92]

$$H_m^{(2)}(k_{mn}a) = 0 \tag{3.5-1}$$

---

[6] Such solutions are also available for such cylinders of elliptical cross-section.

where $H_m^{(2)}(...)$ is the Hankel function. In the TE case they are the roots of the equation [CHO90, NASH92]

$$H_m^{(2)\prime}(k_{mn}a) = 0 \tag{3.5-2}$$

where the prime indicates differentiation with respect to the argument of the Hankel function. In [CHUA85] the natural mode frequencies are given as

$$s_{mn} = \frac{\xi_{mn}}{a\sqrt{\mu_0 \varepsilon_0}}$$

(3.5-3)

where the ξ_{mn} are the roots of the modified Bessel function, namely

$$K_m{}'(\xi_{mn}) = 0 \tag{3.5-4}$$

In [JONE64,pp.73] one finds that

$$K_\nu(jz) = -\frac{\pi}{2} j e^{-j\nu\pi/2} H_\nu^{(2)}(z) \tag{3.5-5}$$

and so the results from the two references are in fact the same.

B. PEC Sphere[7] of Radius a

It can be shown [STRA41, CHO92] that the exterior natural mode resonant frequencies of a spherical PEC object of radius *a* are

$$TE_r \qquad \hat{H}_m^{(2)}(ka) = 0 \tag{3.5-6}$$

and

$$TE_r \qquad \frac{d}{dr}\left\{ r\, \hat{H}_m^{(2)}(kr) \right\}\Bigg|_{r=a} = 0 \tag{3.5-7}$$

where $\hat{H}_m^{(2)}(...)$ is the spherical Hankel function.

---

[7] Such solutions are also available for spheroids.

C. Dielectric Sphere[8]

The natural modes of spherical dielectric resonators have been described in [GAST67].

3.5.3 Interpretation of the Analytical Solutions – Complex Frequencies

In order to obtain numerical values for the natural mode frequencies from the analytical results in Section 3.5.2, some root finding scheme has to be used to find the values k_{mn} of k that satisfy (3.5-1), (3.5-2), (3.5-6) and (3.5-7). What would be found is that these values are always complex[9], with $\mathrm{Re}\{k_{mn}\} > 0$ and $\mathrm{Im}\{k_{mn}\} > 0$, for the usual time dependence $e^{j\omega t}$. In order to understand the significance of a complex k_{mn}, we recall the s-domain variable $s = \sigma + j\omega$, and note that we can write

$$k_{mn} = \mathrm{Re}\{k_{mn}\} + j\,\mathrm{Im}\{k_{mn}\} = \underbrace{(\omega_{mn} - j\sigma_{mn})}_{\Omega_{mn}}\sqrt{\mu_0\varepsilon_0} = -j\underbrace{(\sigma_{mn} + j\omega_{mn})}_{s_{mn}}\sqrt{\mu_0\varepsilon_0} \tag{3.5-8}$$

through inspection of which we have

$$\omega_{mn} = \frac{\mathrm{Re}\{k_{mn}\}}{\sqrt{\mu_0\varepsilon_0}} \tag{3.5-9}$$

$$\sigma_{mn} = -\frac{\mathrm{Im}\{k_{mn}\}}{\sqrt{\mu_0\varepsilon_0}} \tag{3.5-10}$$

Some references refer to *s* as the complex frequency, while others call Ω the complex frequency (and ω as the "real frequency"), the two quantities being related via $s = j\Omega$. Examples of the exterior natural frequencies of a thin wire[10] are shown in Fig.3.5-1.

---

[8] In principle such solutions should also be possible for spheroidal shapes, although we are not aware of a specific reference that does this.
[9] Unlike the interior natural mode cases where such values are always real.
[10] Albeit found using the integral equation approach to be discussed in Section 3.6.

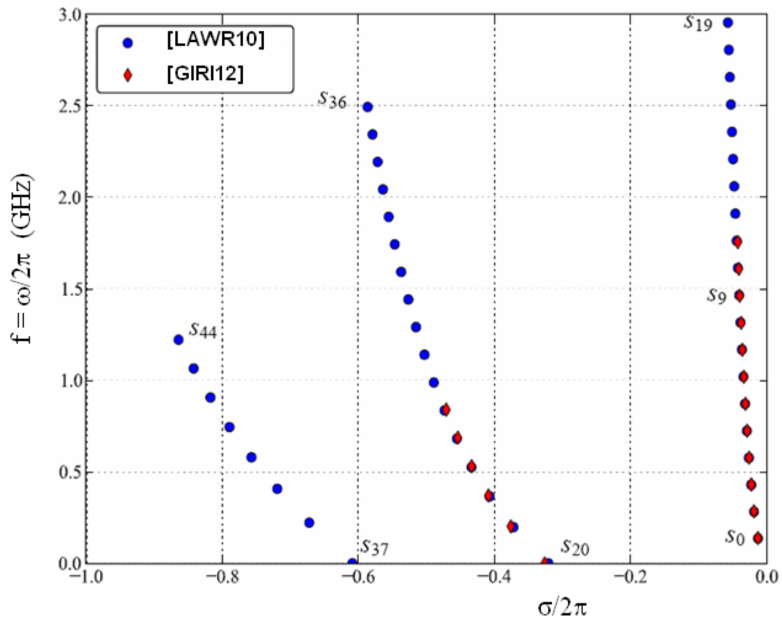

Figure 3.5-1: Computed Complex Natural Frequencies for Thin Straight Wire, of Length 1m and Radius 5mm (After [LAWR10]).

3.6 INTEGRAL EQUATION APPROACH FOR THE DETERMINATION OF NATURAL MODES - *EXTERIOR MODES*

3.6.1 Introductory Remarks

We saw in Section 3.4 that numerical solution (using the FEM, for example) of the appropriate differential equation is now an almost routine way of determining the interior natural modes (viz. frequencies, currents and fields) of closed objects. However, this approach has not yet reached the same point for exterior natural modes. Thus integral equation models are currently used instead, albeit not without difficulty.

3.6.2 Exterior Natural Mode Determination Using Integral Equations

We know from Part A of Section 2.3.2 that the EFIE can be used to model PEC objects. In most cases time-harmonic solutions of the EFIE are required. In order to use it to find the exterior natural modes it has to be changed to the s-domain. This can be done by replacing all ω quantities by *s/j*. Use of the method of moments then results in a matrix equation

$$[Z(s)][J(s)] = [V^{inc}(s)] \tag{3.6-1}$$

and the exterior natural modes are the non-trivial solutions of the equation

$$[Z(s)][J(s)] = [0] \tag{3.6-2}$$

These will occur at those complex frequencies for which

$$\det[Z(s)] = 0 \tag{3.6-3}$$

The exterior resonant frequencies found in this way can be shown to be intrinsic to the scattering object, and are thus independent of the specific integral equation used [DOLP80].

It has been pointed out [DOLP80] that the poles so determined are a union of two sets. One set consists of those values of *s* where the integral equation operator is not able to provide unique solutions to the problem at hand (only occurring for closed objects). This is called the "internal resonance problem" in computational electromagnetics [PETE97]. However, it does not necessarily represent a physical interior natural mode resonance of the object under investigation. If the CFIE of Section 2.3.5, which does not suffer from such "internal resonance problems", were to be applied to the same object to arrive at an equation such as (3.6-3), the same exterior natural mode resonances would be found but No interior resonances. Thus the "internal resonances" that may be detected are not necessarily intrinsic to the scatterer, since they depend on the integral equation operator formulation used.

Examples of applications of the EFIE to find the exterior natural modes of three-dimensional PEC objects have been provided for rectangular boxes [LONG94], spheres with a circular aperture [ROTH99], thin wires [MYER11, GIRI12], rectangular plates [SUN90], circular disks [KRIS84], rectangular cavity with an aperture [CHAU10] and several other rotationally symmetric objects (bodies of revolution) [VECH90].

As an additional comment, note that if we have an aperture in an otherwise closed PEC object [ROTH99, CHAU10] then rigorously speaking the object has No interior natural modes. In such cases it is possible to show that some exterior natural modes tend to specific interior modes (that exist when there is No aperture) as the aperture is made smaller and smaller. However, there are also exterior natural modes that are unrelated to any interior modes that are present when the aperture is closed.

3.6.3 Relationship Between Exterior Natural Mode Frequencies and Frequencies at Which the Characteristic Mode Eigenvalues are Zero[11]

The discrete generalized eigenvalue equation for characteristic modes was shown in Section 2.3.3 to be

$$[X][J_n] = \lambda_n [R][J_n] \tag{3.6-4}$$

This can be rewritten as

$$[R]^{-1}[X][J_n] = \lambda_n [J_n] \tag{3.6-5}$$

Mathematical identities may be used to show that the determinant of $[R]^{-1}[X]$ is

$$\det\left([R]^{-1}[X]\right) = \det\left([R]^{-1}\right)\det\left([X]\right) = \det\left([R]\right)^{-1}\det\left([X]\right) = \frac{\det\left([X]\right)}{\det\left([R]\right)} \tag{3.6-6}$$

Thus, if at least one eigenvalue λ_n is zero then $\det\left([X]\right) = 0$ or $\det\left([R]^{-1}\right) \to \infty$. There is only a slight chance that the determinant of [R] approaches infinity. It is more likely that the determinant of [X] must equal zero when any eigenvalue is zero. Since the condition number of a matrix is a measure of how singular it is, the closer its determinant is to zero the larger its condition number. Thus we can try to detect those frequencies at which at least one CM eigenvalue λ_n.

We used expression (3.4-12) to determine the interior natural frequencies of the 2-D circular cylinder; these are given in Table 3.6-1. Then expression (3.5-1) was used to find the complex exterior natural frequencies of the same cylinder; the real frequencies were determined from (3.5-9) and listed in Table 3.6-2.

---

[11] This was suggested by Dr. Jonathan Ethier, formerly with the University of Ottawa, and now with the Communications Research Centre of Industry Canada.

Table 3.6-1: Interior modes resonant frequencies in GHz for 2-D PEC circular cylinder of radius a = 150 mm using expression (3.4-12).

	n=1	n=2
m = 0	0.765 GHz	1.757 GHz
m = 1	1.219 GHz	2.233 GHz
m = 2	1.634 GHz	2.679 GHz
m = 3	2.030 GHz	3.107 GHz

Table 3.6-2: Exterior modes resonant frequencies in GHz for 2-D PEC circular cylinder of radius a = 150 mm using expression (3.5-1).

	n=1	n=2
m = 0	0.284 GHz	1.259 GHz
m = 1	0.699 GHz	1.728 GHz
m = 2	1.077 GHz	2.162 GHz
m = 3	1.440 GHz	2.577 GHz

Notice in Table 3.6-1 that the interior natural mode resonance frequencies are those at which the "internal resonance problem" (non-uniqueness of the EFIE solution) mentioned in Section 3.6.2, occurs. This is borne out by the plot of the condition number of the complete operator matrix plotted versus frequency in Fig.3.6-1. As also stated in Section 3.6.2, this is not really a reliable way of identifying the interior natural frequencies of an object, since a different integral equation (eg. CFIE) would not give the same results. And we should be reluctant about drawing physical conclusions from the EFIE at frequencies where we know its solution is non-unique. The frequencies where the EFIE has non-unique solutions just happen to coincide with those of the interior natural modes of the object.

A plot of $cond[X]$ versus frequency for the same circular cylinder is shown in Fig.3.6-2. The peaks in this condition number are found to coincide with the frequencies at which the CMs computed in Part B of Section 2.6-1 pass through zero. They are also the same as the real part of the exterior natural mode frequencies of this same cylinder given in Table 3.6-2. The same observations were found for the 2-D cylinder of rectangular cross-section discussed in Part A of

Section 2.6-1. It should of course be remembered that although examination of $cond[X]$ gives an indication of the real part of the exterior natural mode frequencies, it does not supply their imaginary parts, the latter being needed to completely define the particular natural modes.

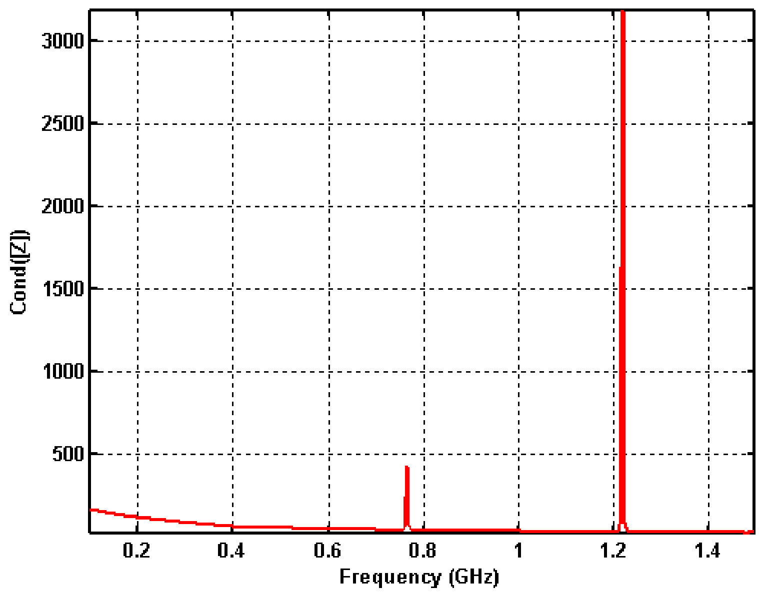

Figure 3.6-1: Condition number of the complete operator matrix [Z] for a 2-D PEC circular cylinder.

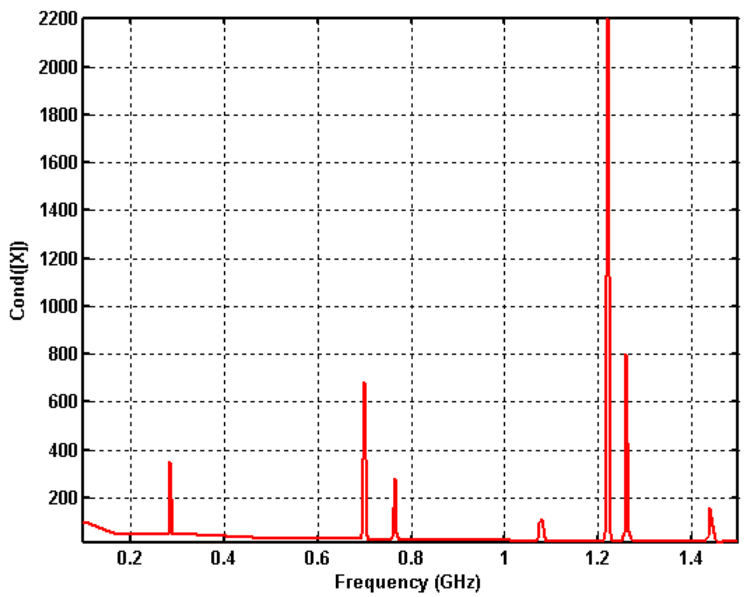

Figure 3.6-2: Condition number of [X] for a 2-D PEC circular cylinder.

3.6.4 Exterior Natural Modes of Penetrable Objects

It has been known at least as far back as 1939 that a penetrable object has exterior natural modes [RICH39]. Rigorously speaking, such objects do not have interior natural modes. If we wish to determine the natural modes of penetrable objects, the volume integral equation formulation of Section 2.8 or the surface integral equation formulation of Section 2.9 may be used to arrive at equations of the form (3.6-3). The surface integral equation formulation (specifically the PMCHWT one), was in [GLIS83] and [KAJF8, KAJF84] to determine the exterior natural modes of rotationally symmetric dielectric resonators. Both the complex resonant frequencies and the natural mode field distributions were computed. We have applied the FEKO code, both its volume integral equation option and its surface integral equation option, to find the exterior natural mode frequencies of dielectric objects, namely the puck [MONG94]. In the results shown below we have not found the complex frequencies, as needs to be done to obtain the complete picture of the natural modes [GLISS83], but just the real parts of the resonant frequencies, by detecting where the condition number of the matrix $[Z(\omega)]$ peaks, a suggested in [LIU04].

We elaborate more on the case with the example of a 3-D dielectric puck discussed in [MONG94]. More details on the FEKO models, as well as the computational resources needed, are given when we discuss the use of these same models to determine the characteristic modes of the same objects in Chapter 5. The condition number if the MOM operator matrix were computed using both SIE and VIE; Fig. 3.6-3 shows both condition numbers along with the red dashed vertical lines shown in the graph. These dashed lines lie at those frequencies at which the exterior natural mode resonates as given in Table 3.6-3. Both condition numbers peak roughly at the same frequencies (the real part of the resonant complex frequency of the natural mode) agreeing with the analysis discussed above. The reader should be aware that the operator matrix using VIE was computed using a coarse mesh since a finer mesh would require enormous resources for processing the computation; that might explain the cause of the discrepancy between both condition numbers.

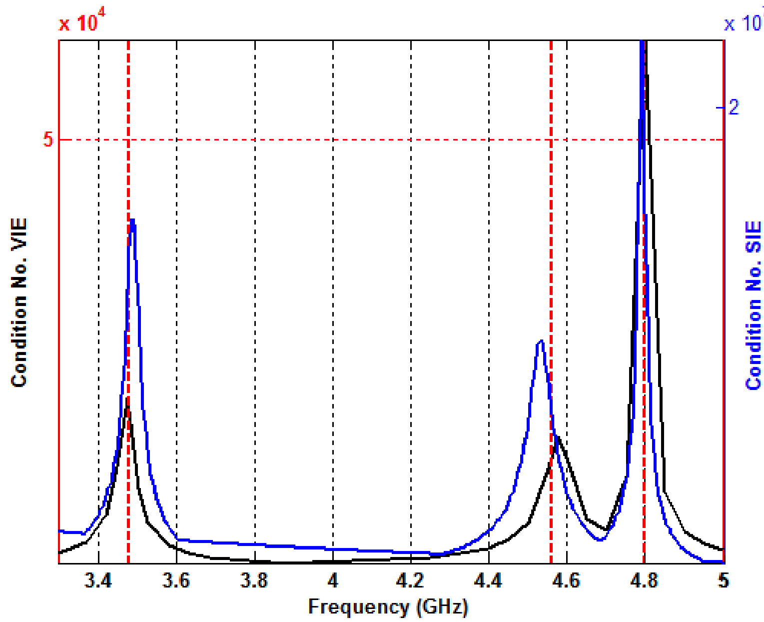

Figure 3.6-3: Condition number of the MoM operator matrix for a 3-D dielectric puck. (———) SIE , (———) VIE, and (— — —) real part of resonant frequency of natural modes.

Table 3.6-3: Natural modes resonances for the 3-D dielectric puck given in [MONG94]

Modes of an Isolated Cylindrical Dielectric Resonator. ε_d = 79.7, d=10.29mm, h=4.51mm	
Natural Mode	**Resonant Frequency (GHz)**
$TE_{01\delta}$	3.479
$HEM_{11\delta}$	4.560
$HEM_{12\delta}$	4.779

3.7 APPLICATIONS OF EXTERIOR NATURAL MODES

3.7.1 Dielectric Resonators

Dielectric resonators have been widely used in antenna design [PETO07], and are in No need of further discussion. In the present terminology, it is the exterior natural modes of the dielectric resonators that are used in such antennas.

3.7.2 Radar Target Identification

We imagine an object illuminated by an incident broadband wave. In the time domain it is found [BAUM76] that the scattered field response consists of an early time portion that lasts over a period dependent on the object size and a late time portion than can be expressed as the sum of sinusoids

$$h_{\text{late}}(t) \approx \sum_{q=1}^{Q} 2\left|R_q\right| e^{\sigma_q t} \cos(\omega_q t + \varphi_q) \tag{3.7-1}$$

The Laplace transform of (3.7-1) gives a "transfer function" that corresponds to the sum of pairs of complex conjugate poles in the complex frequency plane, namely (the singularity expansion)

$$H(s) \approx \sum_{q=1}^{Q} \left(\frac{R_q}{s - s_q} + \frac{R_q^*}{s - s_q^*} \right) \tag{3.7-2}$$

with $s_q = \sigma_q + j\omega_q$, quantity Q the total number of exterior natural modes of the object (the "target") used in the series, and R_q the residue of the natural pole s_q. The real part σ_q of s_q will be negative, and represents a damping. In the case of a lossless object this damping is due to radiation outside the object.

The exterior natural mode frequencies of an object are a property of the object. As stated in [BLAD07], if the frequency of the incident wave is swept the different natural modes will resonate successively, giving peaks in the scattered field that could serve to identify the object. In order to do this one must of course know the exterior natural mode frequencies of an object in order to be able to recognize it. It is not clear from the literature how far advanced such radars are at present. All papers on the topic that we have located, some of which have been referenced in Section 3.6, deal with finding the exterior natural modes of geometrically simple objects.

3.7.3 Use of Natural Modes to Represent Fields and Current Distributions on Broadband Antennas

There has recently been limited use [COLL09, LAWR10, LAWR12] of natural mode concepts to represent the terminal properties of broadband antennas in the time or frequency domains along the lines of expressions (3.7-1) or (3.7-2). But such use as an analysis tool is not the same as that using characteristic mode concept for antenna synthesis work such as [ETHI10c], where new characteristic modes have to be found each time the geometry is altered as part of the shaping process.

3.8 CONCLUDING REMARKS

An understanding of natural modes has been developed in this chapter. Although the work is not new, the perspective into which the topic has been put here has not been provided elsewhere. By doing this we have been able to indicate how natural modes are different from characteristic modes. Finding the natural modes (frequencies, fields, currents) of objects using integral equation methods is possible but computationally time-consuming. The reason is that the procedure becomes a non-linear eigenvalue problem, which involves the finding of the complex roots of a determinant of the moment method matrix. These matrices will be large if one wishes to have a suitable number of unknowns for accurate modeling of the object in question. The resulting computation time can be enormous, and cannot be unsupervised. Mathematical texts on numerical analysis always advise their readers to avoid determinant evaluation if at all possible. The computational difficulties that remain are evidenced by the fact that papers are still being published in archival journals on actual numerical values for PEC objects of simple shape, whereas finding the characteristic modes of PEC objects (albeit not penetrable objects) of some complexity is now relatively routine. Thus characteristic modes are at present more suitable for exterior problems of the type encountered in antenna work. The remainder of this thesis discusses characteristic modes only.

CHAPTER 4 Characteristic Modes for Restricted Incident Field Subsets

4.1 INTRODUCTION

Part of the research of the present thesis has been the careful consideration and interpretation of various characteristic mode conceptual details that have not enjoyed attention elsewhere. This chapter sets down on paper some of these deliberations. Section 4.2 is merely a statement of a purely mathematical result that will be of use in the discussion to follow. In particular it is used in Section 4.3 to reiterate that coupling between two PEC objects results in the characteristic mode sets of the combined object not being a simply union between that of the individual objects. This could be considered a somewhat obvious result, but is explicitly commented on for later reference in the rest of the chapter. Characteristic modes have been computed for objects in the presence of other objects (eg. infinite groundplanes) using modified Green’s functions that account for the presence of the additional objects. We discuss, in Section 4.4, the fact that these should strictly speaking be considered a different type of characteristic mode, which we have termed modified characteristic modes. The sub-structure characteristic mode concept is revisited in Section 4.5. We explain why a certain assumption made in earlier work need not be considered necessary. We also demonstrate that these modes are in fact the same as modified characteristic modes, with the difference being that they are formulated in a way that makes them of greater direct practical use than when viewed from a modified Green’s function approach explicitly. Section 4.6 is a short note that attempts to interpret how to attach some meaning to the idea of the characteristic modes of a body of infinite extent. This allows us to move seamlessly to what we have called restricted characteristic modes, which provides a framework in which to think about the characteristic modes of useful but idealized objects such as two-dimensional cylindrical objects and infinite periodic structures. In Section 4.8, the sub-structure characteristic mode concept to apply when the nearby object is not only a PEC object but a penetrable object as well[1]. Finally, it is shown that the set of characteristic modes for rotationally symmetric objects,

[1] But these are not the characteristic modes of penetrable objects. That will be the subject of Chapter 5.

when computed using so-called body-of-revolution (BOR) moment method formulations, is the union of the sets determined from each of the harmonic matrix equations separately. Some concluding remarks are made in Section 4.9.

4.2 SOME STATEMENTS FROM MATRIX ALGEBRA

If we have a square complex matrix [B] that has been partitioned into four square sub-matrices (which need not be of the same size) as

$$[H] = \begin{bmatrix} [H_{AA}] & [H_{AB}] \\ [H_{BA}] & [H_{BB}] \end{bmatrix} \tag{4.2-1}$$

then $\lambda\{[H]\}$ is not directly related to the spectra of any of the individual matrices. However, if $[H_{BA}] = [0]$, so that

$$[H] = \begin{bmatrix} [H_{AA}] & [H_{AB}] \\ [0] & [H_{BB}] \end{bmatrix} \tag{4.2-2}$$

Then [GOLU 96]

$$\lambda\{[H]\} = \lambda\{[H_{AA}]\} \cup \lambda\{[H_{BB}]\} \tag{4.2-3}$$

Obviously this is also true if, in addition to $[H_{BA}] = [0]$, we also have $[H_{AB}] = [0]$. We will use these results in later sections of this chapter.

4.3 ON THE CHARACTERISTIC MODES OF COUPLED PEC OBJECTS

Consider a PEC structure that is modeled using an EFIE that is solved using the method of moments. Expansion and weighting functions will be distributed over the PEC surface. We consider the object as consisting of two portions, Object A and Object B, with different expansion function subsets located on these two portions. The discrete form of the EFIE can then have its operator matrix [Z] partitioned such that it reads

$$\begin{bmatrix} [Z_{AA}] & [Z_{AB}] \\ [Z_{BA}] & [Z_{BB}] \end{bmatrix} \begin{bmatrix} [J_A] \\ [J_B] \end{bmatrix} = \begin{bmatrix} [V_A] \\ [V_B] \end{bmatrix} \qquad (4.3\text{-}1)$$

Using the mathematical facts quoted in Section 4.2, we can immediately state that, in general, the set of characteristic mode eigenvalues $\lambda_{\mathrm{CM}}\{[Z]\}$ of the complete object is not simply the union of the sets $\lambda_{\mathrm{CM}}\{[Z_{AA}]\}$ and $\lambda_{\mathrm{CM}}\{[Z_{BB}]\}$, the latter being the sets of characteristic mode eigenvalues of Objects A and B considered in isolation from each other. If there were No mutual coupling between Objects A and B, so that $[Z_{AB}]=[Z_{BA}]=[0]$, then (4.2-2) would indeed imply that

$$\lambda_{\mathrm{CM}}\{[Z]\} = \lambda_{\mathrm{CM}}\{[Z_{AA}]\} \cup \lambda_{\mathrm{CM}}\{[Z_{BB}]\} \qquad (4.3\text{-}2)$$

Such a situation would rarely occur in practice, unless the two objects are so widely separated that $[Z_{AB}]\approx[0]$ and $[Z_{BA}]\approx[0]$. In such a case, it then makes physical sense that the set of characteristic modes of the PEC object is simply the union of the sets of individual characteristic modes. In an electromagnetic system it would not be possible to have $[Z_{AB}]$ non-zero and yet have $[Z_{BA}]=[0]$ - so that the result (4.2-3) applies once more - unless some rather unusual non-reciprocal material configuration were to be used; this possibility is not pursued further here.

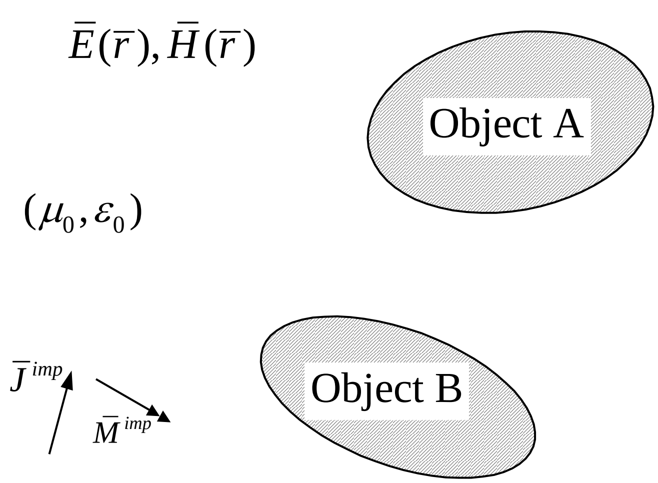

Figure 4.3-1: PEC Objects A and B

4.4 CHARACTERISTIC MODES COMPUTED USING INTEGRAL EQUATIONS WITH MODIFIED GREEN'S FUNCTION KERNELS

Consider the situation where there are two conducting objects as before, as illustrated in Fig.4.3-1. However, we suppose that we know the modified Green's function which can be used to determine the field in all of space for an arbitrary electric current density distribution in the presence of Object B. We will denote the appropriate modified Green's function by the symbol $\mathcal{G}_{\text{modified}}$. An EFIE to determine the scattering from the two coupled objects can be derived in terms of the surface current density $\bar{J}_A$ on Object A only, using the modified Green's function. This has the form

$$E_{\tan}^{scat}\left\{\bar{r}, \bar{J}_A, \mathcal{G}_{\text{modified}}\right\} = -E_{\tan}^{inc}\left\{\bar{r}, \bar{J}^{imp}, \bar{M}^{imp}, \mathcal{G}_{\text{modified}}\right\} \qquad \bar{r} \in S_A \tag{4.4-1}$$

where S_A is the surface of Object A. Application of the method of moments, with N expansion functions and N weighting functions placed on Object A then yields the matrix equation

$$\left[Z_{AA}^{\text{modified}}\right]\left[J_A\right] = \left[V_A^{\text{modified}}\right] \tag{4.4-2}$$

with

$$Z_{ij}^{\text{modified}} = \left\langle \bar{E}_j^{scat}\left\{\bar{r}, \bar{J}_j, \mathcal{G}_{\text{modified}}\right\}, \bar{W}_i\left(\bar{r}\right)\right\rangle \tag{4.4-3}$$

$$V_i^{\text{modified}} = \left\langle -\bar{E}^{inc}\left\{\bar{r}, \bar{J}^{imp}, \bar{M}^{imp}, \mathcal{G}_{\text{modified}}\right\}, \bar{W}_i\left(\bar{r}\right)\right\rangle \tag{4.4-4}$$

$$\left[J_A\right] = \left[I_1 \quad I_2 \quad \cdot \quad \cdot \quad \cdot \quad I_N\right]^T \tag{4.4-5}$$

and

$$\bar{J}_A\left(\bar{r}\right) = \sum_{j=1}^{N} I_j \bar{J}_j\left(\bar{r}\right) \tag{4.4-6}$$

Some discussion of the above terms is in order. The elements of $\left[V_A^{\text{modified}}\right]$ are not the same as they would have been if the free space Green's function had been used and the currents $\left[J_A\right]$ and $\left[J_B\right]$ had been unknowns. Once $\left[J_A\right]$ has been found, the same modified Green's function is used to find the field everywhere due to $\left[J_A\right]$ (it will be a scattered field). This scattered field is added to the incident field to find the total field, and this total field can be used in the boundary condition $\bar{J}_a = \hat{n}\times\bar{H}$ to determine the current density $\left[J_B\right]$ on Object B. If $\left[J_A\right]$ and $\left[J_B\right]$ are used with the free space Green's function the same total field would of course be found everywhere. This approach has been used (without explicitly stating it) in the following three references:

[ANGU98] – Microstrip patch on an infinitely large grounded dielectric slab.

[VANN12] – Conducting strips in a layered dielectric medium of infinite extent.

[GALL13] – Microstrip patch (with shorting pin) on an infinitely large grounded dielectric slab.

It is clear from Section 4.3 that the characteristic modes found in this way cannot be called *the* characteristic modes of the object mentioned. They could be referred to as its *modified characteristic modes*. Any object could have many different types of modified characteristic modes depending on which modified Green's function is used in the moment method formulation in a particular case.

4.5 REVISIT OF THE SUB-STRUCTURE CHARACTERISTIC MODE CONCEPT

The discussion of the sub-structure characteristic mode concept in Section 2.10 started with the assumption that there is No incident field on Object B, so that $\left[V_B\right]=0$. Suppose we do not make this assumption. We can use (2.10-3) to write

$$\left[J_B\right] = -\left[Z_{BB}\right]^{-1}\left[Z_{BA}\right]\left[J_A\right] + \left[Z_{BB}\right]^{-1}\left[V_B\right] \tag{4.5-1}$$

If this is then substituted into the upper part of (2.10-1), some elementary matrix algebra allows us to write it in the form

$$\underbrace{\left\{[Z_{AA}]-[Z_{AB}][Z_{BB}]^{-1}[Z_{BA}]\right\}}_{[Z_{SUB}]}[J_A]=[V_A]-[Z_{AB}]\left[Z_{BB}\right]^{-1}\left[V_B\right] \qquad (4.5\text{-}2)$$

where $[Z_{SUB}]$ is the same as it was in Section 2.10 and [ETHI 12a]. Expression (4.5-2) is a matrix equation for the unknown current density $\left[J_A\right]$ on Object A. The influence of Object B is contained in matrix $[Z_{SUB}]$. The excitation term has altered to one that depends on the illumination of both Object A and Object B.

Observe that both (4.5-2) and (4.4-2) are matrix forms of the EFIE for the unknown $\left[J_A\right]$ on Object A. Thus we conjecture that sub-structure characteristic modes, and modified characteristic modes, are one and the same thing. The sub-structure mode is effectively using a discrete form of the modified Green's function[2] for Object B, although this Green's function is not generated explicitly. It has not been possible to rigorously prove this analytically because the only modified Green's functions of interest in electromagnetics problems are for cases where Object B is of infinite extent, and it is not possible to obtain a matrix $\left[Z_{BB}\right]$ for such an object. The sub-structure approach thus makes the use of modified characteristic modes practical.

A numerical experiment serves to demonstrate the point. We consider the strip dipole of Section 2.6.4 to be Object A, and compute the following:

♦ The modified characteristic modes of Object A when Object B is completely accounted for via a modified Green's function.

♦ The sub-structure characteristic modes of Object A when Object B is a large but finite flat PEC groundplane of dimensions 5 L x 40 W.

♦ The sub-structure characteristic modes of Object A when Object B is a small finite flat PEC groundplane of dimensions 1.5L x 5 W.

It is clear that the sub-structure modes of Object A in the presence of the large groundplane are equivalent to those of the modified modes. This holds up to a certain order of characteristic mode only. However, if the finite groundplane is made larger, characteristic modes up to a higher order

---

[2] Numerically generated modified Green's functions have been explicitly generated by a few authors (eg.[GLIS80a]), albeit not in the characteristic mode context, but the use of such explicit numerical Green's functions is not widespread.

can be made to match each other. This demonstrates the equivalence of the sub-structure and modified characteristic mode concepts.

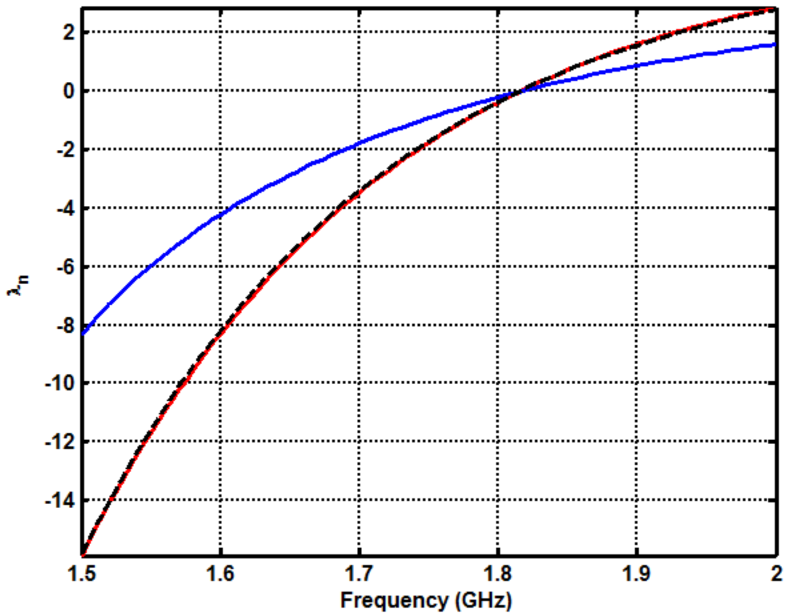

Figure 4.5-1: Plot of λ1 versus frequency for strip dipole above an infinite groundplane using appropriate modified Green's function (▬ ▬ ▬), of the sub-structure modes for a large finite groundplane (▬▬▬), and the sub-structure modes above a small groundplane (▬▬▬)

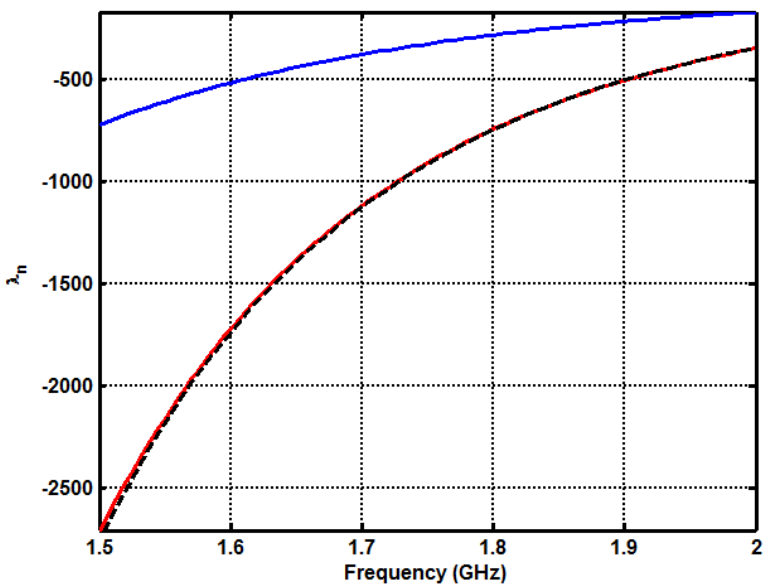

Figure 4.5-2: Plot of λ2 versus frequency for strip dipole above an infinite groundplane using appropriate modified Green's function (▬ ▬ ▬), of the sub-structure modes for a large finite groundplane (▬▬▬), and the sub-structure modes above a small groundplane (▬▬▬).

In order that the reader is able to reproduce these desired results, we remark that the computations were done using the FEKO code. The triangular mesh on the strip dipole was such that No triangle edge length was more than 2.15 mm (λ/70 at 2 GHz which is a very fine mesh) and that on the finite sized groundplane such that No triangle edge larger than 15 mm (λ/10 at 2 GHz which is an average mesh).

4.6 THE CHARACTERISTIC MODES OF INFINITELY LARGE PEC OBJECTS

Consider again the finite-sized PEC rectangular flat plate whose characteristic modes were determined in Section 2.10. In order to have an object whose size can be described by a single quantity (for reasons that will be clear below) we here further examine such a plate, using three different sizes. Fig.4.6-1 shows a plot of $\lambda_{\text{CM}}\{[Z]\}$ (magnitude in dB) versus frequency for different values of the dimension W. It is clear that as the plate size increases the $\lambda_{\text{CM}}\{[Z]\}$ start to bunch together. In the limit as $W \to \infty$ (in which case the plate becomes the proverbial infinite groundplane) the characteristic modes would all coalesce, and so it does not make sense to talk about the characteristic modes of an infinitely large object.

This raises the question as to the meaning of the characteristic modes of infinitely long PEC cylinders determined by other authors, and computed in Section 2.6.1 through 2.6.3. We believe that such results have not yet been properly interpreted. We cannot claim that the presence of an infinitely large object always makes the electromagnetics problem a two-dimensional one. We can see this by simply referring to the problem of a finite source radiating in the presence of an infinitely long PEC cylinder. This is a valid electromagnetics problem, and various manifestations of it have been published (albeit not in the characteristic mode context), in [CART 43] and [LUCK 51]. So this is a three-dimensional problem form an electromagnetics point of view. Yet we are not able to make sense of the characteristic modes of one of the objects involved. This has prompted us to introduce the idea of a restricted characteristic mode in Section 4.7.

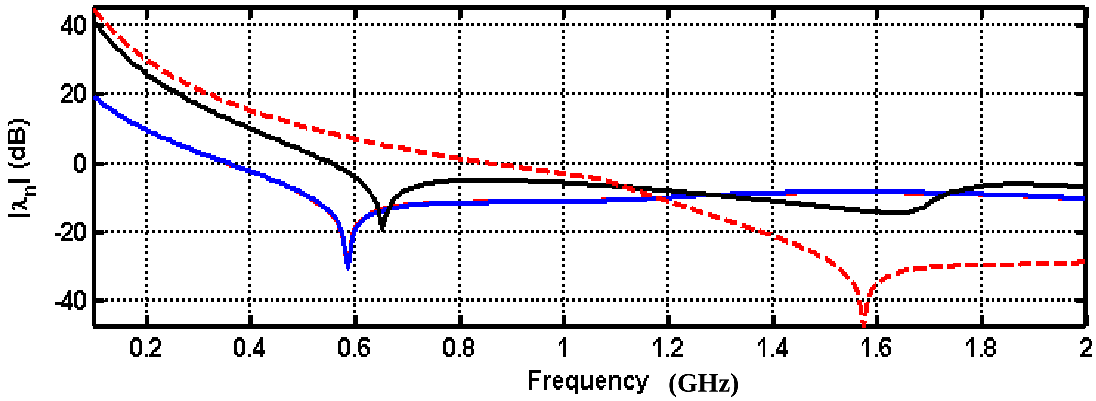

(a) W= λ and L= λ

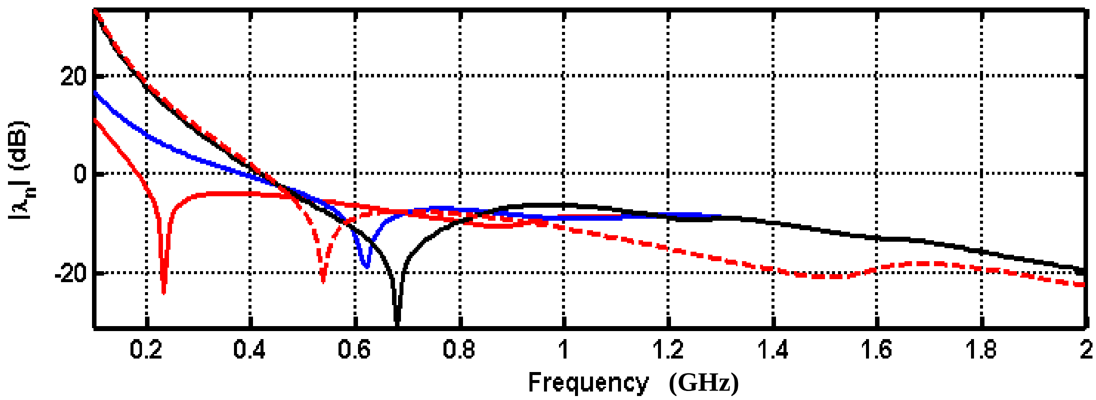

(b) W= 2λ and L= λ

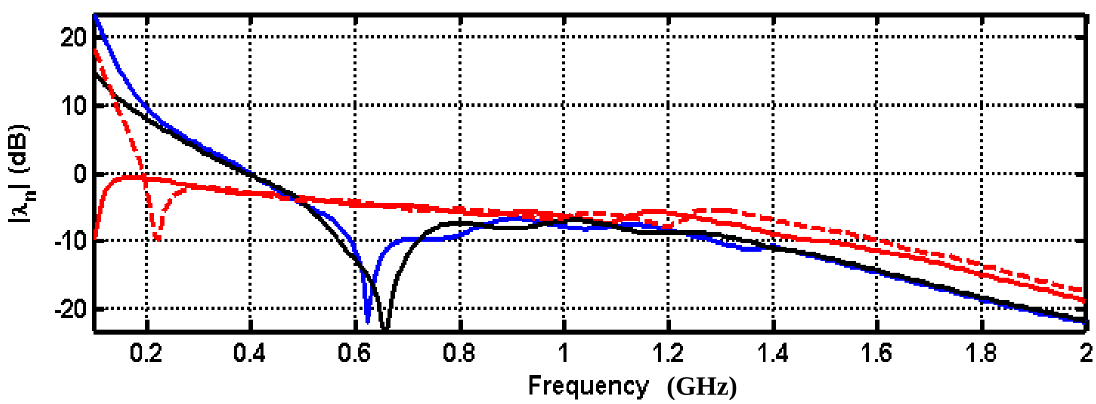

(c) W= 3λ and L= λ

Figure 4.6-1: Plots of various λ_n (only first four CMs shown) versus frequency for a rectangular PEC plate as the size of the plate increases. (——) λ_1, (——) λ_2, (——) λ_3, and (– – –) λ_4.

4.7 RESTRICTED CHARACTERISTIC MODES

Suppose we have an integral equation written in operator notation as

$$\mathcal{Z}\{\mathcal{J}\} = \mathcal{E}^{inc} \tag{4.7-1}$$

The range of the operator $\mathcal{Z}\{\cdots\}$ is the space of allowed incident field vectors $\mathcal{E}^{inc}$. Now suppose we have a projection operator $\mathcal{P}(\cdots)$ that restricts the range of $\mathcal{Z}\{\cdots\}$ to a subspace of the original range. In other words, if we were to take all possible elements $\mathcal{E}^{inc}$ of the range and allow $\mathcal{P}(\cdots)$ to operate on them, then the resulting set $\mathcal{P}(\mathcal{E}^{inc})$ would be a subspace of the original range of $\mathcal{Z}\{\cdots\}$. So let us apply to $\mathcal{P}(\cdots)$ to both sides of (1), to get

$$\mathcal{P}(\mathcal{Z}\{\mathcal{J}\}) = \mathcal{P}(\mathcal{E}^{inc}) \tag{4.7-2}$$

$\mathcal{P}(\mathcal{E}^{inc})$ is the restricted set of incident fields. However, we note that (4.7-2) is not the same integral equation as (4.7-1) in that we have a new operator $\mathcal{P}(\mathcal{Z}\{\cdots\})$. The characteristic modes of $\mathcal{Z}\{\cdots\}$ will not necessarily be the same as those of $\mathcal{P}(\mathcal{Z}\{\cdots\})$. We will refer to these as *restricted characteristic modes*. It is clear that restricted characteristic modes and modified/sub-structure characteristic modes are not the same thing.

This is what is actually being done when people talk about the characteristic modes of infinite cylinders. The set of possible incident fields is restricted to be normally incident plane waves. This alters the integral equation to a two-dimensional one, either one that is TE or TM to the axis of the cylinder, depending on the polarization one has in mind for the incident plane wave. It is this type of integral equation that was used to determine the characteristic modes of the two-dimensional cylindrical PEC objects in Sections 2.6.1 through 2.6.3, and the references provided there.

A similar situation arises when we wish to talk about the characteristic modes of an infinite periodic structure. Most readers will be familiar with moment method formulations of plane wave scattering of such problems. The fact that it is accepted that the incident field is always a plane wave (which may have normal or oblique incidence) allows the problem to be reduced to one of finding the equivalent current densities over just one cell of the infinite periodic structure.

Characteristic modes can be determined from the resulting matrix equation form of the integral equation, but clearly these are restricted characteristic modes since the form of the integral equation was only possible subject to the implicit constraints on the form of the incident field. One might be tempted to consider these to be modified characteristic modes since the integral equation for the infinite periodic structure can be viewed as using a non-free-space Green's function. However, it must be remembered that such Green's functions are not true modified Green's functions in that they can only be used under the assumption of the incident field being restricted to a plane wave.

4.8 EXTENDED APPLICATION OF THE SUB-STRUCTURE CHARACTERISTIC MODE CONCEPT

The sub-structure characteristic mode concept was introduced in [ETHI 12a], and reviewed in Section 2.10. It was applied to the case of two PEC objects in the vicinity of each other. This can be extended to the case of a PEC object close to a dielectric object. It is possible to derive a pair of coupled integral equations to describe electromagnetic scattering from such a composite structure that models the PEC object by surface current densities $\overline{J}_s$ and volume polarization current densities $\overline{J}_{\mathrm{v}}$ in the dielectric. Application of the moment method will as usual reduce this integral equation pair into a matrix equation of the same form as that in (2.3-3). However, we can write this in partitioned form as (2.10-1)

$$\begin{bmatrix} [Z_{\mathrm{ss}}] & [Z_{\mathrm{sv}}] \\ [Z_{\mathrm{vs}}] & [Z_{\mathrm{vv}}] \end{bmatrix} \begin{bmatrix} J_s \\ J_{\mathrm{v}} \end{bmatrix} = \begin{bmatrix} V^{inc} \end{bmatrix} \tag{4.8-1}$$

This in turn has the same form as (2.10-1). Thus, if we view the PEC body as Object A and the dielectric body as Object B, we can determine the sub-structure modes of Object A to be $\lambda_{\mathrm{CM}}\left\{[Z_{sub}]\right\}$ where

$$[Z_{SUB}] = \left\{[Z_{SS}] - [Z_{SV}][Z_{VV}]^{-1}[Z_{VS}]\right\} \tag{4.8-2}$$

As an example we consider the geometry shown in Figure 4.8-1. The strip dipole is the same as that discussed in Section 2.6.4. The dielectric block has a width (w) of 93.75mm, depth (a) of 20mm and height (b) of 40mm. Its relative permittivity is 6.9. The spacing between the strip dipole and the dielectric block is 1.8mm.

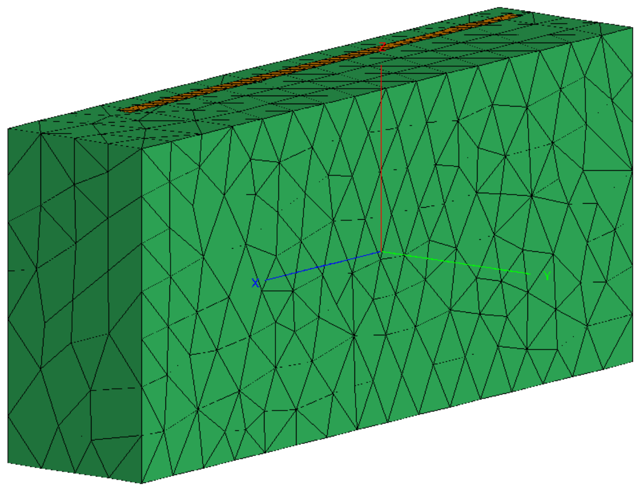

Figure 4.8-1: In FEKO, numerical model of a PEC strip dipole located above a dielectric block. The strip is parallel to the one face of the block.

The sub-structure CMs of the strip dipole with the presence of the dielectric block were computed from 1.5 to 2.3 GHz using expression (2.10-8). Compared to those eigenvalues of the strip dipole placed in free space discussed in Section 2.6.4, the general behavior of the eigenvalues evidently affected by the presence of the dielectric block which theoretically resonates at 2.1[3] GHz (close enough to the resonance of the dipole strip first resonance). A comparison between the two cases is shown in Fig. 4.8-2. Only those sub-structure CMs of object A were computed assuming that we have No interest in finding the substructure CMs of Object B (the dielectric block). To compare those CM resonances of the isolated strip in free space to the resonances of the sub-structure CMs, the resonance of the lowest sub-structure CM is at 1.557 GHz compared to 1.855 GHz for the resonance of the lowest CM of the isolated strip dipole in free space. This is evident that loading the strip lowered the resonant frequency of strip

[3] [PETO07,pp. 31] shows how you calculate this value

dipole, and it shows how effective the study of the substructure CM rather than the whole structure's (especially when it comes to the shape synthesis analysis).

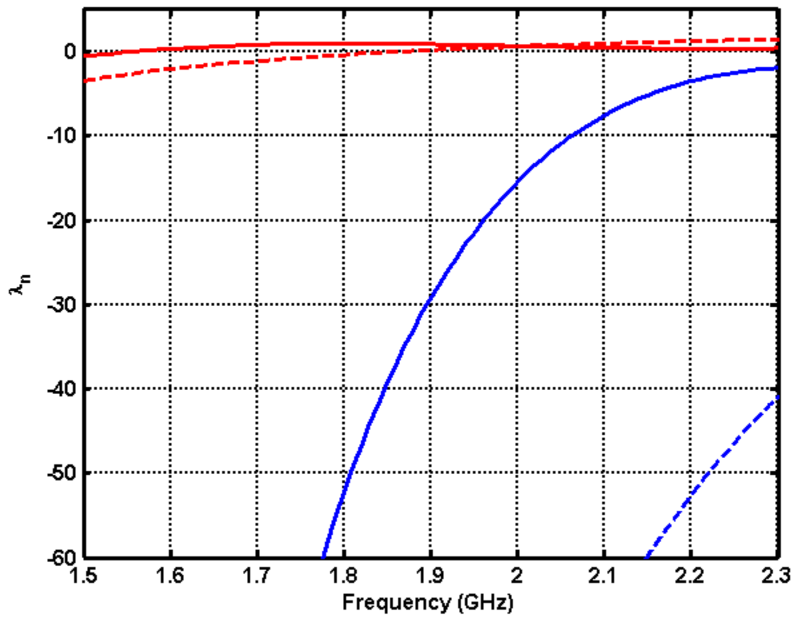

Figure 4.8-2: Eigenvalues of the two lowest sub-structure CMs of the strip dipole with the presence of the dielectric block. (——) λ_1, (——) λ_2. Eigenvalues of the two lowest CMs of the isolated strip dipole in free space. (— — —) λ_1, (— — —) λ_2.

The eigencurrents for those associated to Object B were found as discussed in Section 4.5; thus, the eigencurrents due to object A and B can be formed and exported to FEKO for modal current and field analysis. The surface currents on the strip and eigenfields of the lowest three substructure CMs were computed at the resonant frequency of the lowest CM of the isolated strip dipole. They were checked for their satisfaction of the orthogonality condition given through the evaluation of expressions (2.3-16) and (2.3-21): the results are given in Tables 4.8-1 and 4.8-2 respectively. The current distribution on the surface of the strip[4] and the radiation pattern of the substructure CMs are shown in Fig. 4.8-3. As expected, the substructure CM fields are not the same as those of the isolated strip dipole, discussed in Section 2.6-4.

[4] We are not really concerned with the polarization current in the dielectric block, assuming that we only have interest in performing shape synthesis on Object A (i.e. strip dipole)

Table 4.8-1: Expression (2.3-16) evaluated for the lowest three sub-structure CMs for the PEC strip dipole above the dielectric block.

m/n	1	2	3
1	-1.000	0.000	0.000
2	-0.002	-1.000	0.000
3	-0.020	0.000	-1.000

Table 4.8-2: Expression (2.3-21) evaluated for the lowest three sub-structure CMs for the PEC strip dipole above the dielectric block.

m/n	1	2	3
1	1.002+0.000i	0.005+0.015i	0.010-0.004i
2	0.005-0.015i	0.998+0.000i	-0.003-0.014i
3	0.010+0.004i	-0.003+0.014i	0.979+0.000i

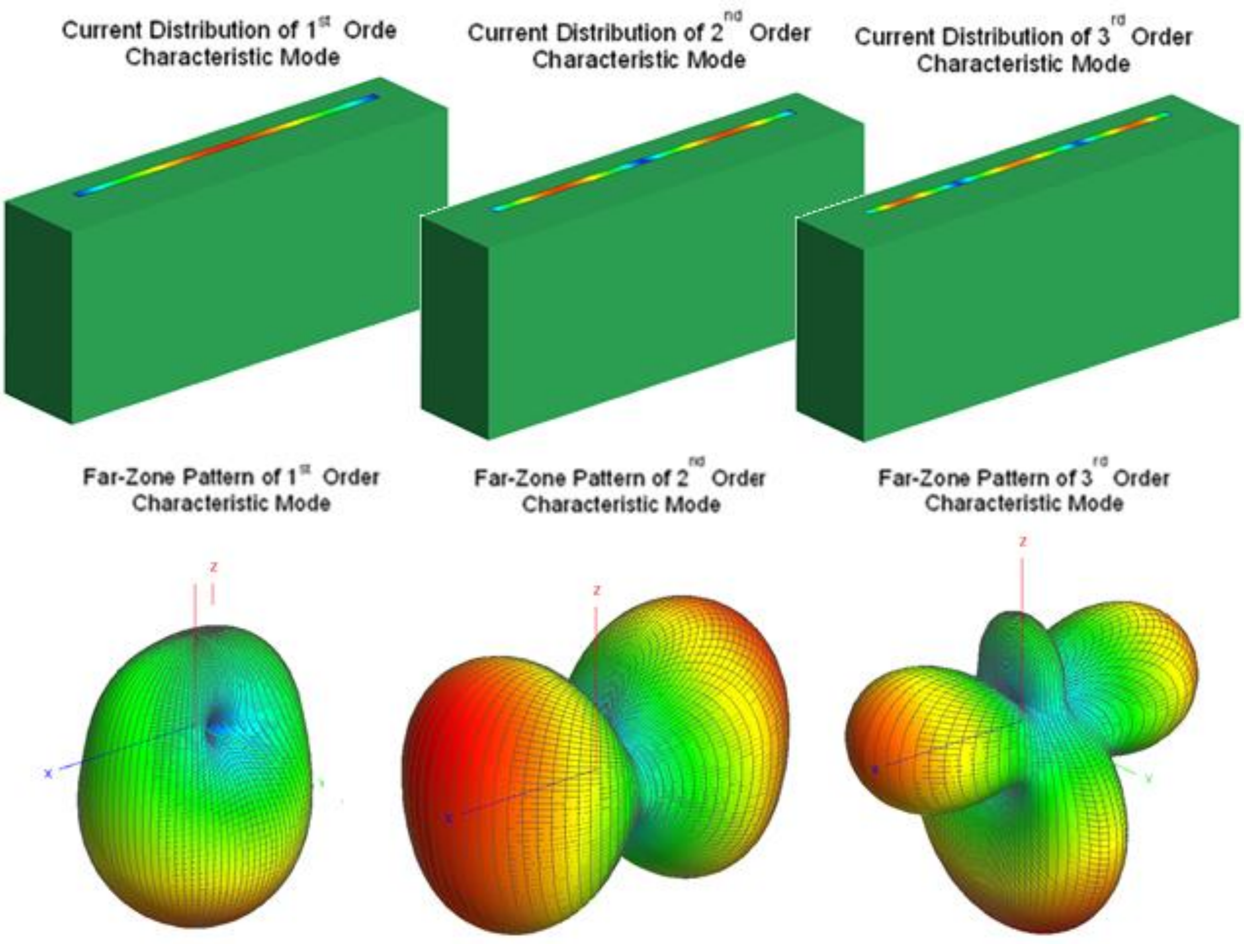

Figure 4.8-3: Current distribution and field radiation patterns of sub-structure CMs of strip dipole

4.9 CHARACTERISTIC MODES OBTAINED USING BODY-OF-REVOLUTION (BOR) FORMULATIONS

4.9.1 The Body-of-Revolution Concept

Integral equation formulations for scattering from a body-of-revolution, that implicitly account for the geometrical rotational symmetry of the object, are for obvious reasons known as body-of-revolution (BOR) methods. Detailed formulations can be found in [HARR69] and [GLIS 80b], for example. With reference to Fig.4.9-1, the current density on the BOR object can be written in terms of two components, namely $J_t(t,\phi)$ and $J_\phi(t,\phi)$. The ϕ-dependence is represented by complex Fourier series type expansion functions of the form $e^{-jp\phi}$ for integer p ranging from $-\infty$ through zero to $+\infty$. We will refer to these as the BOR harmonics. The t-dependence is represented by conventional expansion functions (eg. spatial "pulse" functions; overlapping triangular functions) which can be denoted by $f_q(t)$. The same is done for the ϕ-dependence and t-dependence of the weighting functions. The final discretized form of the EFIE is then an (in principle) an infinite set of uncoupled matrix equations, one matrix equation for each BOR harmonic. The matrix equations are uncoupled because of the selection of the complex Fourier series type expansion function to represent the ϕ-dependence. Each of the independent harmonic matrix equations has the form

$$\begin{bmatrix} [\hat{Z}_p^{tt}] & [\hat{Z}_p^{t\phi}] \\ [\hat{Z}_p^{\phi t}] & [\hat{Z}_p^{\phi\phi}] \end{bmatrix} \begin{bmatrix} [I_p^t] \\ [I_p^\phi] \end{bmatrix} = \begin{bmatrix} [V_p^t] \\ [V_p^\phi] \end{bmatrix} \qquad (4.9\text{-}1)$$

where the caret symbol does *not* indicate a unit vector. The elements of the column matrices $[I_p^t]$ and $[I_p^\phi]$ are the coefficients of the expansion functions associated with t-directed and ϕ-directed p-th BOR harmonic. The elements of the column matrices $[V_p^t]$ and $[V_p^\phi]$ are the coefficients of the excitation associated with t-directed and ϕ-directed p-th BOR harmonic; thus even the incident field is expanded in terms of such harmonics. We can write (4.9-1) this in the more compact form

$$\left[\hat{Z}_p\right]\left[\hat{I}_p\right]=\left[\hat{V}_p\right] \tag{4.9-2}$$

The complete matrix equation for the PEC object is[5]

$$\left[\begin{array}{c:c:c:c:c} [\hat{Z}_{-2}] & [0] & [0] & [0] & [0] \\ \hdashline [0] & [\hat{Z}_{-1}] & [0] & [0] & [0] \\ \hdashline [0] & [0] & [\hat{Z}_0] & [0] & [0] \\ \hdashline [0] & [0] & [0] & [\hat{Z}_1] & [0] \\ \hdashline [0] & [0] & [0] & [0] & [\hat{Z}_2] \end{array}\right]\left[\begin{array}{c} [\hat{I}_{-2}] \\ \hdashline [\hat{I}_{-1}] \\ \hdashline [\hat{I}_0] \\ \hdashline [\hat{I}_1] \\ \hdashline [\hat{I}_2] \end{array}\right]=\left[\begin{array}{c} [\hat{V}_{-2}] \\ \hdashline [\hat{V}_{-1}] \\ \hdashline [\hat{V}_0] \\ \hdashline [\hat{V}_1] \\ \hdashline [\hat{V}_2] \end{array}\right] \tag{4.9-3}$$

In order to compute characteristic mode using integral equation formulations it is necessary [HARR71b] that the expansion and weighting functions be real. The formulations [HARR69] and [GLIS 80b], that incorporate the complex Fourier series for the ϕ-dependence, are thus not directly suitable. We can instead [HARR71b, Sect.IV] use the real sets of expansion (and weighting functions)

$$\left\{\hat{t}\ f_q(t),\ \hat{t}\ f_q(t)\cos p\phi,\ \hat{\phi}\ f_q(t)\sin p\phi\right\} \tag{4.9-4}$$

and

$$\left\{\hat{\phi}\ f_q(t),\ \hat{t}\ f_q(t)\sin p\phi,\ -\hat{\phi}\ f_q(t)\cos p\phi\right\} \tag{4.9-5}$$

for p = 0, 1, 2, …….. (that is, only zero and positive integers), with both the above sets being needed. Fortunately, there exists a straightforward transformation between the above impedance matrix elements (with the “caret” symbol) for the case when the complex Fourier series is used, and those when the real Fourier series of (4.9-4) and (4.9-5) are used. This has been shown in [HARR71b] to be

$$[Z^{(0)}]=\begin{bmatrix} [Z_0^{tt}] & [0] \\ [0] & [Z_0^{\phi\phi}] \end{bmatrix}=\begin{bmatrix} [\hat{Z}_0^{tt}] & 0 \\ 0 & [\hat{Z}_0^{\phi\phi}] \end{bmatrix} \tag{4.9-6}$$

[5] For simplicity we show the matrix equation as if only the p = -2, -1, 0, 1, 2 BOR harmonics are needed. The number used may in practice be much larger.

and

$$[Z^{(p)}]=\begin{bmatrix}[Z_p^{tt}] & [Z_p^{t\phi}]\\ [Z_p^{\phi t}] & [Z_p^{\phi\phi}]\end{bmatrix}=\frac{1}{2}\begin{bmatrix}[\hat{Z}_p^{tt}] & -j[\hat{Z}_p^{t\phi}]\\ j[\hat{Z}_p^{\phi t}] & [\hat{Z}_p^{\phi\phi}]\end{bmatrix}\qquad \text{p = 1, 2, 3, ……….}$$

(4.9-7)

The quantities without the caret symbol are those applicable when the real expansion functions are used. The complete matrix equation for the PEC object is now[6]

$$\left[\begin{array}{c:c:c:c:c}
\begin{bmatrix}[Z_2^{tt}] & [Z_2^{t\phi}]\\ [Z_2^{\phi t}] & [Z_2^{\phi\phi}]\end{bmatrix} & \begin{bmatrix}[0] & [0]\\ [0] & [0]\end{bmatrix} & \begin{bmatrix}[0] & [0]\\ [0] & [0]\end{bmatrix} & \begin{bmatrix}[0] & [0]\\ [0] & [0]\end{bmatrix} & \begin{bmatrix}[0] & [0]\\ [0] & [0]\end{bmatrix}\\ \hdashline
\begin{bmatrix}[0] & [0]\\ [0] & [0]\end{bmatrix} & \begin{bmatrix}[Z_1^{tt}] & [Z_1^{t\phi}]\\ [Z_1^{\phi t}] & [Z_1^{\phi\phi}]\end{bmatrix} & \begin{bmatrix}[0] & [0]\\ [0] & [0]\end{bmatrix} & \begin{bmatrix}[0] & [0]\\ [0] & [0]\end{bmatrix} & \begin{bmatrix}[0] & [0]\\ [0] & [0]\end{bmatrix}\\ \hdashline
\begin{bmatrix}[0] & [0]\\ [0] & [0]\end{bmatrix} & \begin{bmatrix}[0] & [0]\\ [0] & [0]\end{bmatrix} & \begin{bmatrix}[Z_0^{tt}] & [0]\\ [0] & [Z_0^{\phi\phi}]\end{bmatrix} & \begin{bmatrix}[0] & [0]\\ [0] & [0]\end{bmatrix} & \begin{bmatrix}[0] & [0]\\ [0] & [0]\end{bmatrix}\\ \hdashline
\begin{bmatrix}[0] & [0]\\ [0] & [0]\end{bmatrix} & \begin{bmatrix}[0] & [0]\\ [0] & [0]\end{bmatrix} & \begin{bmatrix}[0] & [0]\\ [0] & [0]\end{bmatrix} & \begin{bmatrix}[Z_1^{tt}] & [Z_1^{t\phi}]\\ [Z_1^{\phi t}] & [Z_1^{\phi\phi}]\end{bmatrix} & \begin{bmatrix}[0] & [0]\\ [0] & [0]\end{bmatrix}\\ \hdashline
\begin{bmatrix}[0] & [0]\\ [0] & [0]\end{bmatrix} & \begin{bmatrix}[0] & [0]\\ [0] & [0]\end{bmatrix} & \begin{bmatrix}[0] & [0]\\ [0] & [0]\end{bmatrix} & \begin{bmatrix}[0] & [0]\\ [0] & [0]\end{bmatrix} & \begin{bmatrix}[Z_2^{tt}] & [Z_2^{t\phi}]\\ [Z_2^{\phi t}] & [Z_2^{\phi\phi}]\end{bmatrix}
\end{array}\right]
\left[\begin{array}{c}[I_2^a]\\ \hdashline [I_1^a]\\ \hdashline \begin{bmatrix}I_0^a\\ I_0^b\end{bmatrix}\\ \hdashline [I_1^b]\\ \hdashline [I_2^b]\end{array}\right]
=
\left[\begin{array}{c}[V_2^a]\\ \hdashline [V_1^a]\\ \hdashline \begin{bmatrix}V_0^a\\ V_0^b\end{bmatrix}\\ \hdashline [V_1^b]\\ \hdashline [V_2^b]\end{array}\right]$$

(4.9-8)

[6] The superscripts “a” and “b” are clarified in Section 4.9.2

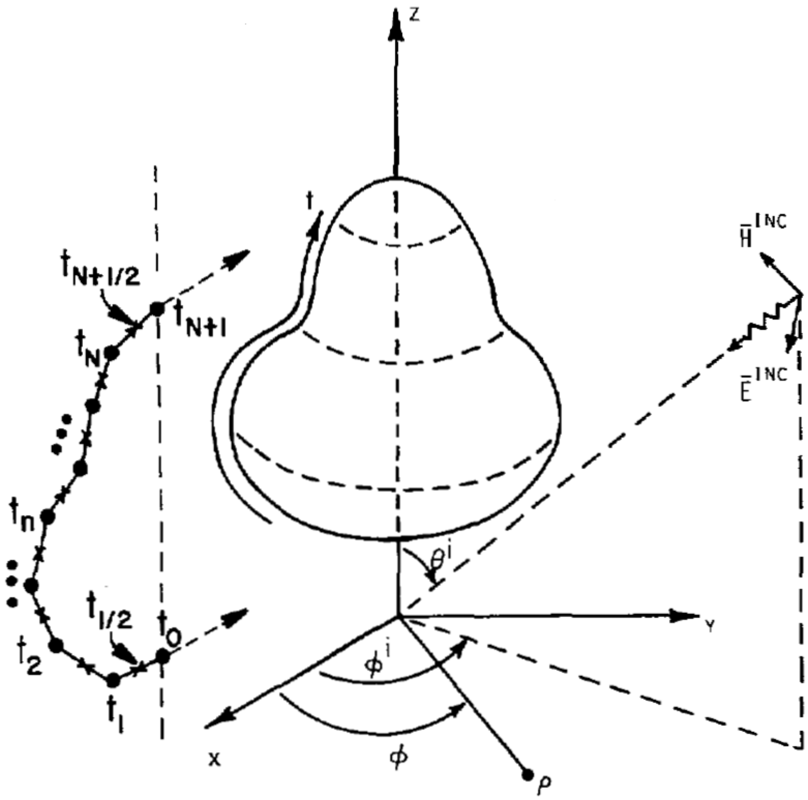

Figure 4.9-1: PEC body of revolution (After [GLIS80b]).

4.9.2 The Per-Harmonic Approach to Finding the Characteristic Modes of a Body-of-Revolution

In the interests of notational convenience we write the matrix equation (4.9-8) in the form

$$\begin{bmatrix} [Z^{(2)}] & [0] & [0] & [0] & [0] \\ [0] & [Z^{(1)}] & [0] & [0] & [0] \\ [0] & [0] & [Z^{(0)}] & [0] & [0] \\ [0] & [0] & [0] & [Z^{(1)}] & [0] \\ [0] & [0] & [0] & [0] & [Z^{(2)}] \end{bmatrix} \begin{bmatrix} [I_2^a] \\ [I_1^a] \\ \begin{bmatrix} I_0^a \\ I_0^b \end{bmatrix} \\ [I_1^b] \\ [I_2^b] \end{bmatrix} = \begin{bmatrix} [V_2^a] \\ [V_1^a] \\ \begin{bmatrix} V_0^a \\ V_0^b \end{bmatrix} \\ [V_1^b] \\ [V_2^b] \end{bmatrix} \qquad (4.9\text{-}9)$$

with the symbol $[Z^{(p)}]$ defined in (4.9-6) and (4.9-7). Note that the harmonic matrices $[Z^{(p)}]$, for $p \neq 0$, do indeed occur twice. Some explanation of the meaning of the terms in the excitation and solution vectors is in order. When the real expansion functions are used the incident field tangential to the BOR is expanded into orthogonal components of the form

$$\bar{E}_a^{inc} = \hat{t}\, E_t^{inc} \cos p\phi + \hat{\phi}\, E_\phi^{inc} \sin p\phi \tag{4.9-10}$$

and

$$\bar{E}_b^{inc} = \hat{t}\, E_t^{inc} \sin p\phi - \hat{\phi}\, E_\phi^{inc} \cos p\phi \tag{4.9-11}$$

This explains the use of the superscripts “a” and “b”.

If we split these harmonic matrices into their real and imaginary parts as $[Z^{(p)}] = [R^{(p)}] + j[X^{(p)}]$, then we can write the characteristic mode eigenvalue problem for the BOR object as

$$\begin{bmatrix} [X^{(2)}] & [0] & [0] & [0] & [0] \\ [0] & [X^{(1)}] & [0] & [0] & [0] \\ [0] & [0] & [X^{(0)}] & [0] & [0] \\ [0] & [0] & [0] & [X^{(1)}] & [0] \\ [0] & [0] & [0] & [0] & [X^{(2)}] \end{bmatrix} \begin{bmatrix} [I_2^a] \\ [I_1^a] \\ \begin{bmatrix} I_0^a \\ I_0^b \end{bmatrix} \\ [I_1^b] \\ [I_2^b] \end{bmatrix} = \lambda \begin{bmatrix} [R^{(2)}] & [0] & [0] & [0] & [0] \\ [0] & [R^{(1)}] & [0] & [0] & [0] \\ [0] & [0] & [R^{(0)}] & [0] & [0] \\ [0] & [0] & [0] & [R^{(1)}] & [0] \\ [0] & [0] & [0] & [0] & [R^{(2)}] \end{bmatrix} \begin{bmatrix} [I_2^a] \\ [I_1^a] \\ \begin{bmatrix} I_0^a \\ I_0^b \end{bmatrix} \\ [I_1^b] \\ [I_2^b] \end{bmatrix} \tag{4.9-12}$$

from which it follows that

$$\begin{bmatrix} [R^{(2)}] & [0] & [0] & [0] & [0] \\ [0] & [R^{(1)}] & [0] & [0] & [0] \\ [0] & [0] & [R^{(0)}] & [0] & [0] \\ [0] & [0] & [0] & [R^{(1)}] & [0] \\ [0] & [0] & [0] & [0] & [R^{(2)}] \end{bmatrix}^{-1} \begin{bmatrix} [X^{(2)}] & [0] & [0] & [0] & [0] \\ [0] & [X^{(1)}] & [0] & [0] & [0] \\ [0] & [0] & [X^{(0)}] & [0] & [0] \\ [0] & [0] & [0] & [X^{(1)}] & [0] \\ [0] & [0] & [0] & [0] & [X^{(2)}] \end{bmatrix} \begin{bmatrix} [I_2^a] \\ [I_1^a] \\ \begin{bmatrix} I_0^a \\ I_0^b \end{bmatrix} \\ [I_1^b] \\ [I_2^b] \end{bmatrix} = \lambda \begin{bmatrix} [I_2^a] \\ [I_1^a] \\ \begin{bmatrix} I_0^a \\ I_0^b \end{bmatrix} \\ [I_1^b] \\ [I_2^b] \end{bmatrix} \tag{4.9-13}$$

Since matrix

$$\begin{bmatrix} [R^{(2)}] & [0] & [0] & [0] & [0] \\ [0] & [R^{(1)}] & [0] & [0] & [0] \\ [0] & [0] & [R^{(0)}] & [0] & [0] \\ [0] & [0] & [0] & [R^{(1)}] & [0] \\ [0] & [0] & [0] & [0] & [R^{(2)}] \end{bmatrix} \qquad (4.9\text{-}14)$$

is block-diagonal, it follows that

$$\begin{bmatrix} [R^{(2)}] & [0] & [0] & [0] & [0] \\ [0] & [R^{(1)}] & [0] & [0] & [0] \\ [0] & [0] & [R^{(0)}] & [0] & [0] \\ [0] & [0] & [0] & [R^{(1)}] & [0] \\ [0] & [0] & [0] & [0] & [R^{(2)}] \end{bmatrix}^{-1} = \begin{bmatrix} [R^{(2)}]^{-1} & [0] & [0] & [0] & [0] \\ [0] & [R^{(1)}]^{-1} & [0] & [0] & [0] \\ [0] & [0] & [R^{(0)}]^{-1} & [0] & [0] \\ [0] & [0] & [0] & [R^{(1)}]^{-1} & [0] \\ [0] & [0] & [0] & [0] & [R^{(2)}]^{-1} \end{bmatrix}$$

(4.9-15)

and so (4.9-11) becomes

$$\begin{bmatrix} [R^{(2)}]^{-1} & [0] & [0] & [0] & [0] \\ [0] & [R^{(1)}]^{-1} & [0] & [0] & [0] \\ [0] & [0] & [R^{(0)}]^{-1} & [0] & [0] \\ [0] & [0] & [0] & [R^{(1)}]^{-1} & [0] \\ [0] & [0] & [0] & [0] & [R^{(2)}]^{-1} \end{bmatrix} \begin{bmatrix} [X^{(2)}] & [0] & [0] & [0] & [0] \\ [0] & [X^{(1)}] & [0] & [0] & [0] \\ [0] & [0] & [X^{(0)}] & [0] & [0] \\ [0] & [0] & [0] & [X^{(1)}] & [0] \\ [0] & [0] & [0] & [0] & [X^{(2)}] \end{bmatrix} \begin{bmatrix} [I_2^a] \\ [I_1^a] \\ \begin{bmatrix} I_0^a \\ I_0^b \end{bmatrix} \\ [I_1^b] \\ [I_2^b] \end{bmatrix} = \lambda \begin{bmatrix} [I_2^a] \\ [I_1^a] \\ \begin{bmatrix} I_0^a \\ I_0^b \end{bmatrix} \\ [I_1^b] \\ [I_2^b] \end{bmatrix}$$

(4.9-16)

Simple matrix multiplication reduces this to

$$\begin{bmatrix} [R^{(2)}]^{-1}[X^{(2)}] & [0] & [0] & [0] & [0] \\ [0] & [R^{(1)}]^{-1}[X^{(1)}] & [0] & [0] & [0] \\ [0] & [0] & [R^{(0)}]^{-1}[X^{(0)}] & [0] & [0] \\ [0] & [0] & [0] & [R^{(1)}]^{-1}[X^{(1)}] & [0] \\ [0] & [0] & [0] & [0] & [R^{(2)}]^{-1}[X^{(2)}] \end{bmatrix} \begin{bmatrix} [I_2^a] \\ [I_1^a] \\ \begin{bmatrix} I_0^a \\ I_0^b \end{bmatrix} \\ [I_1^b] \\ [I_2^b] \end{bmatrix} = \lambda \begin{bmatrix} [I_2^a] \\ [I_1^a] \\ \begin{bmatrix} I_0^a \\ I_0^b \end{bmatrix} \\ [I_1^b] \\ [I_2^b] \end{bmatrix}$$

(4.9-17)

If we use the result (4.2-3) on (4.9-15) it is clear that the spectrum of the matrix on the left hand side of (4.9-15) – these are the characteristic modes of the BOR – can be stated as

$$\lambda\left\{[R^{(2)}]^{-1}[X^{(2)}]\right\}\cup\lambda\left\{[R^{(1)}]^{-1}[X^{(1)}]\right\}\cup\lambda\left\{[R^{(0)}]^{-1}[X^{(0)}]\right\}\cup\lambda\left\{[R^{(1)}]^{-1}[X^{(1)}]\right\}\cup\lambda\left\{[R^{(2)}]^{-1}[X^{(2)}]\right\} \tag{4.9-18}$$

The eigenvalues associated with each p-th BOR harmonic for $p \neq 0$ occur twice (it has multiplicity of two). So we can write (4.9-16) symbolically as

$$\text{Set of } \lambda_{\mathrm{CM}} \text{ for a BOR } = \text{ Set } \lambda\left\{[R^{(p)}]^{-1}[X^{(p)}]\right\}_{p=0,1,2,3,.......} \tag{4.9-19}$$

remembering that all eigenvalues so-obtained occur twice for $p \neq 0$.

In [HARR71b] the characteristic modes were computed using the matrix equation for each individual BOR harmonic. However, it was not shown there that doing this in fact gives us the actual complete set of characteristic modes of the BOR. This fact has been proven here, and will be demonstrated numerically below.

4.9.3 Some Computational Results for the Characteristic Modes of PEC Bodies-of-Revolution Determined on a Per-Harmonic Basis

In Section 2.6.4, we considered the CMs of a PEC sphere and a PEC cylinder, without any special recognition of the fact that these are BOR objects. Here we wish to use a BOR formulation to find the CMs of these same objects, and to compare them to what we obtained Section 2.6.4. We have used the PEC version of the code DBR [GLIS 80b][7].

A PEC Sphere

The same sphere studied in Section 2.6.4 is analyzed using the BOR formulation, and an attempt is made to make an association between those CMs presented there and these computed from the individual BOR harmonics. In theory, the number of BOR harmonics is infinite; however, few harmonics may provide a good approximation for the solution. Fig.

[7] This was made available to us by Dr. Allen Glisson, Department of Electrical Engineering, University of Mississippi, University. MS 38677, USA.

4.9-2 shows the lowest ten CM eigenvalues of the zeroth BOR harmonic: most of them are comparable to those eigenvalues shown in Fig. 2.6-10. Figure 4.9-3 is a plot of the same eigenvalues except the modulus in dB was taken in consideration to closely examine the higher modes and easily spot the resonance. Similarly, the CM eigenvalues corresponding to the 1st BOR harmonic were calculated as well, as shown in figures 4.9-4 and 4.9-5. The CM eigenvalues corresponding to zeroth and first BOR harmonic resembles those eigenvalues computed in Part A Section 2.6.4. The third CM of both harmonics is found to resonate at 4.47 GHz at which the CM eigenvalue computed using EFIE in FEKO, resonate. And actually, both BOR harmonics has resulted in the same eigenvalues, which can be shown in Table 4.9-1. A comparison between the eigenvalues computed for the first three harmonics and those computed previously in Section 2.6.4 are given in the Table as well. The CMs that were computed using the matrix equation for zeroth, first, and second BOR harmonics are found to be subsets of the characteristic modes found in Section 2.6.4. The association is made using different font colours; for instance, the eigenvalue -1.082 of zeroth BOR harmonic can be associated to -1.085 (the one previously calculated using FEKO). And due to multiplicity mentioned earlier in this section, the eigenvalue -1.082 corresponding to the first harmonic is associated to -1.086 and -1.088. The reader is reminded that the multiplicity should be taken into account for the harmonics other than the zeroth order. The degenerate eigenvalues are found to be distributed between the BOR harmonics. For example, the eigenvalue, -11.2, appears five times and can be associated to -11.00 in the zeroth harmonic, two of -11.00 in the harmonic first, and two of -11.00 in the second harmonic. So, the characteristic modes of the individual BOR harmonic are the subset of the complete set of entire body's characteristic modes.

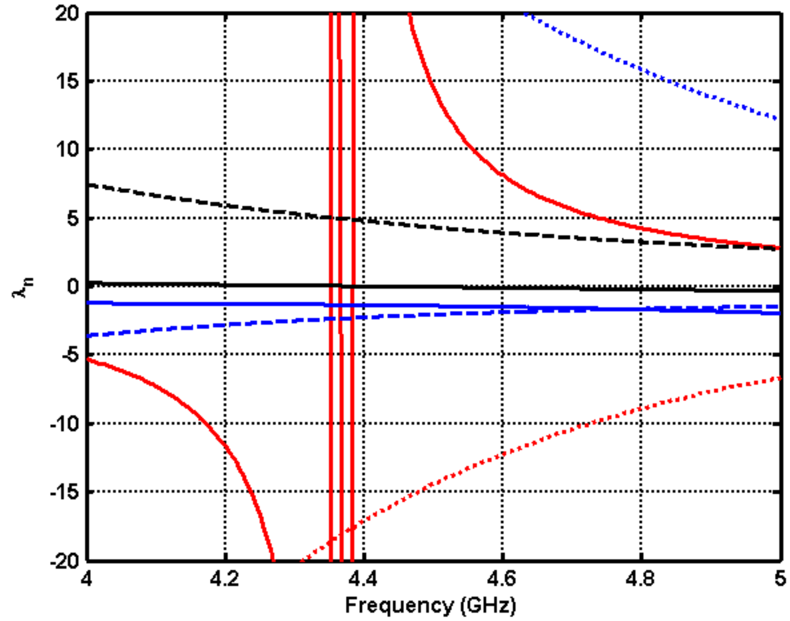

Figure 4.9-2: Eigenvalues of the ten lowest CMs of the BOR zero harmonic of the PEC sphere

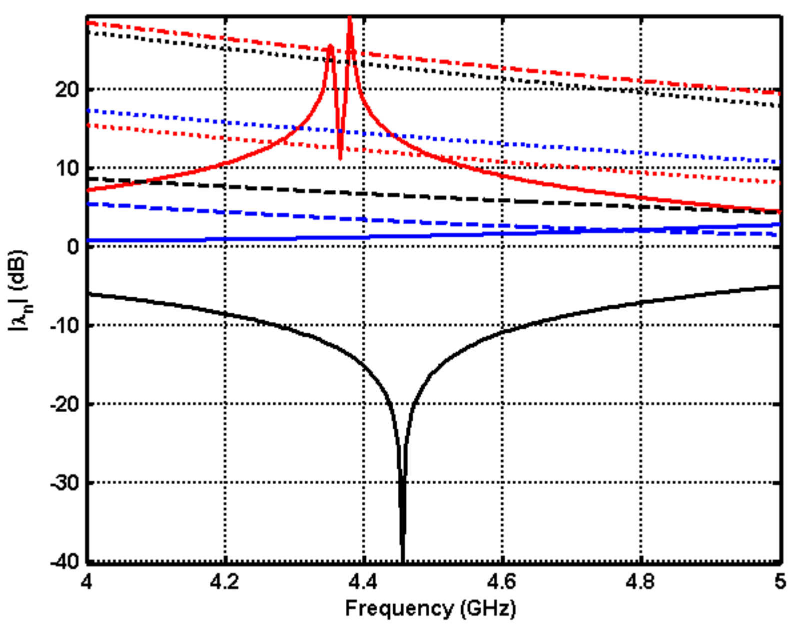

Figure 4.9-3: Eigenvalues (magnitude in dB) of the ten lowest CMs of the BOR zero harmonic of the PEC sphere

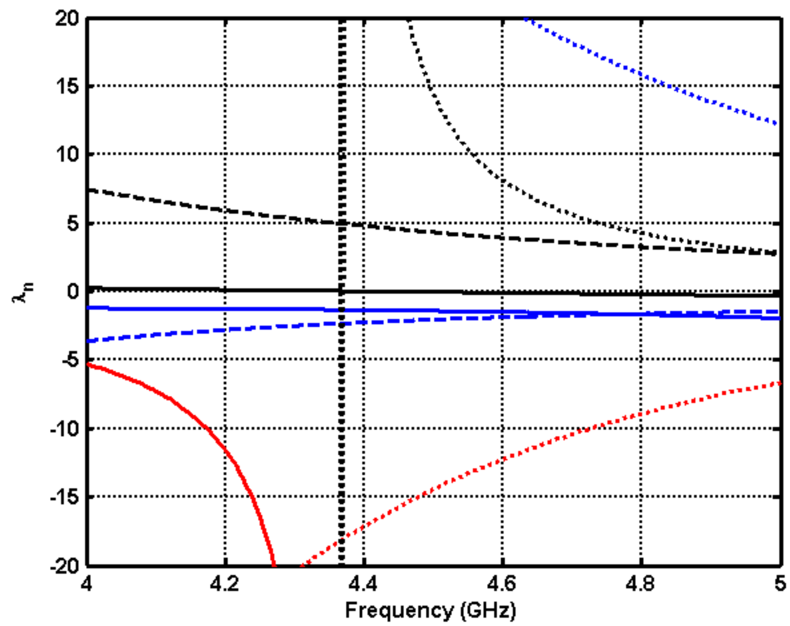

Figure 4.9-4: Eigenvalues of the ten lowest CMs of the BOR 1st harmonic of the PEC sphere

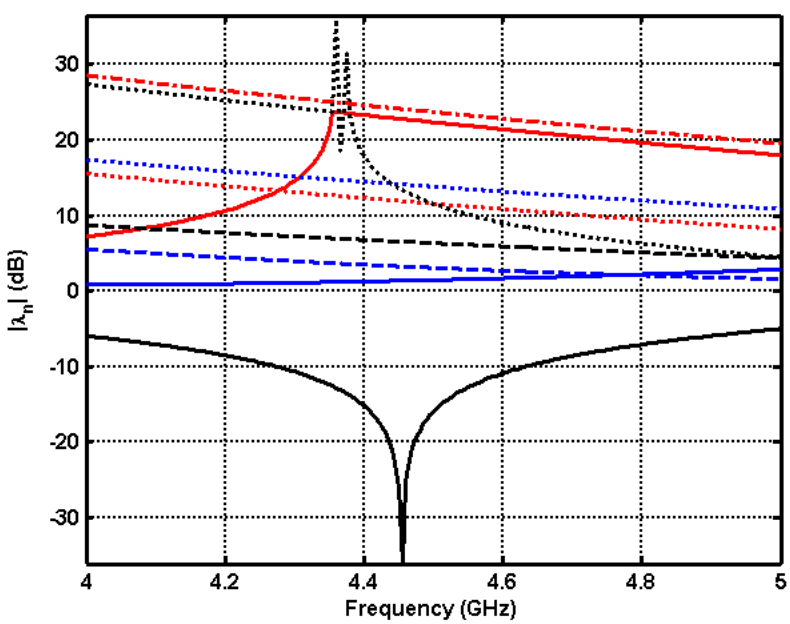

Figure 4.9-5: Eigenvalues (magnitude in dB) of the ten lowest CMs of the BOR 1st harmonic of the PEC sphere

Table 4.9-1: Comparison between CM eigenvalues computed in FEKO and DBR codes at 2 GHz – PEC sphere

	Using FEKO (Section 2.6.4)	Using DBR code Zeroth BOR Harmonic	Using DBR code First BOR Harmonic	Using DBR code Second BOR Harmonic
λn	-1.085	-1.082	-1.082	-11.008
	-1.086	2.674	2.674	21.609
	-1.088	-11.002	-11.001	-284.675
	2.700	21.610	21.613	411.786
	2.701	-284.344	-284.377	-11882.441
	2.701	**Higher Modes are not considered**		
	-11.214			
	-11.224			
	-11.233			
	-11.238			
	-11.249			
	21.993			
	22.000			
	22.012			
	22.012			
	22.015			
	-292.521			
	-292.865			
	-292.958			
	-293.129			
	-293.343			
	-293.637			
	-293.922			

B PEC Open-ended Cylinder

Here, an open-ended cylinder is considered as a rotationally symmetric structure. It is necessary to inquire further numerical results to confirm our observation made on the sphere in Part A in this section. Thus, the CMs of the individual harmonics were computed to show that these CMs are merely subsets of the complete set of characteristic modes found in Part E in Section 2.6-4. Fig. 4.9-6 through 4.9-9 shows the eigenvalues of the CMs and their magnitude (in dB) for both zeroth and first BOR harmonics. Not all the CMs are degenerate unlike the case with the sphere; the first CM of the zeroth BOR harmonic does not exist for that 1st BOR harmonic as an example. This CM resonates at 1.73 GHz which agrees with that resonant frequency found in Section 2.6-4. An example of the association is that the eigenvalues of the degenerate CMs, -36.56 and -36.83, found in Section 2.6-4, can be associated to the double eigenvalue (multiplicity), -34.31. The rest of the eigenvalues can be associated in the same manner, and similar argument found in Part A can be made here too.

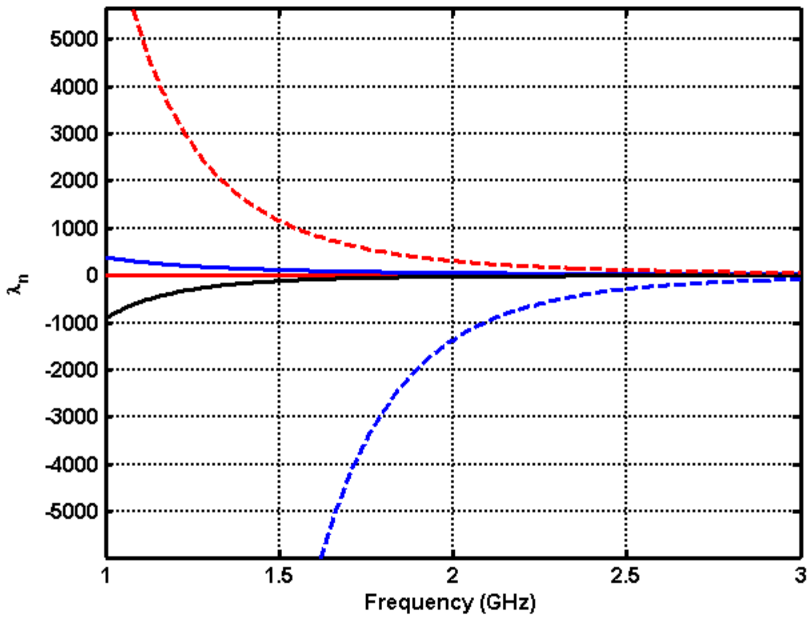

Figure 4.9-6: Eigenvalues of the lowest five CMs of the BOR 0^{th} harmonic for the PEC open-ended cylinder

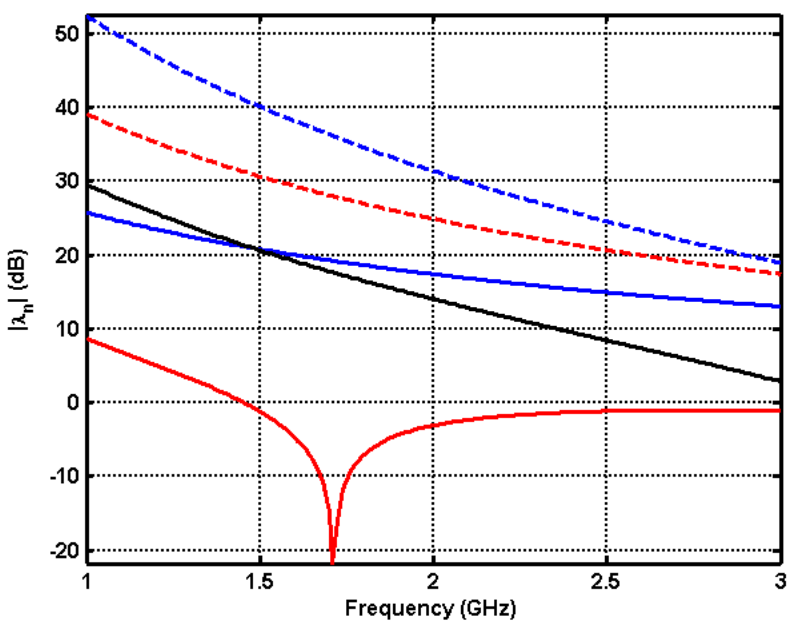

Figure 4.9-7: Eigenvalues (magnitude in dB) of the lowest five CMs of the BOR 0^{th} harmonic for the PEC open-ended cylinder

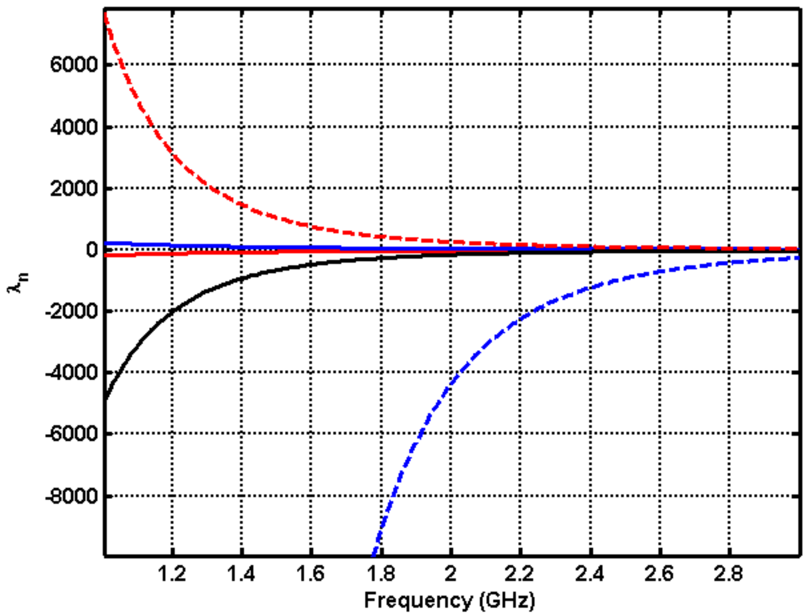

Figure 4.9-8: Eigenvalues of the five lowest CMs of the BOR 1st harmonic for the open-ended PEC cylinder.

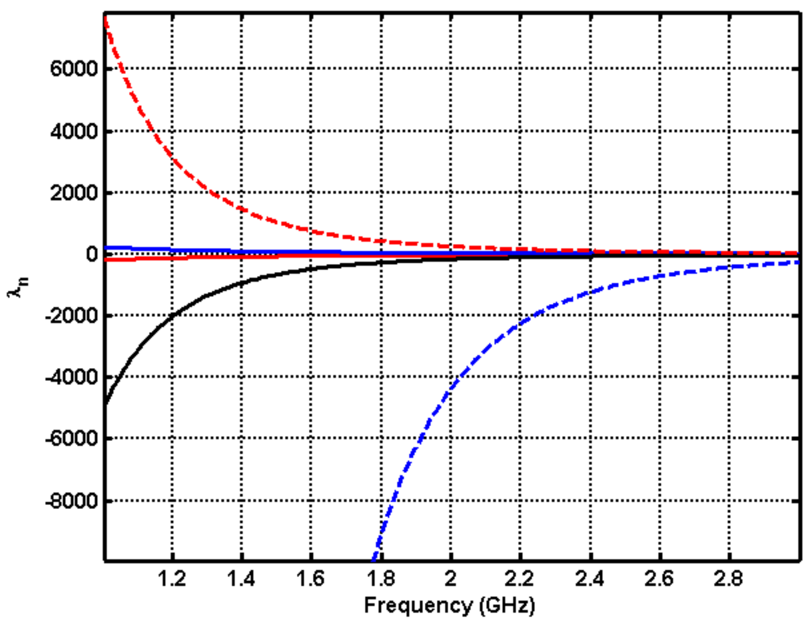

Figure 4.9-9: Eigenvalues (magnitude in dB) of the lowest five CMs of the BOR 1st harmonic of the PEC open-ended cylinder

Table 4.9-2: Comparison between CM eigenvalues computed in FEKO and DBR code at 2 GHz for the open-ended PEC cylinder.

	Using FEKO (Section 2.6.4)	Using DBR code Zeroth BOR Harmonic	Using DBR code First BOR Harmonic
λ_n	0.488	0.493	-34.313
	-27.099	-25.348	41.752
	-36.561	55.118	-161.440
	-36.827	309.135	254.247
	45.692	**Higher Modes are not considered**	
	59.572		
	-175.716		
	-176.038		
	294.202		
	296.988		
	341.064		

4.10 CONCLUDING REMARKS

The new contributions and clarifications offered in this chapter are as follows:

(a). We have confirmed that characteristic modes found from integral equation formulations which incorporate modified Green's functions should be considered different from those that use the free space Green's function. We have termed the former "modified characteristic modes".

(b). We have shown that previously-defined sub-structure modes are in fact the same as modified characteristic modes. The advantage of the sub-structure mode approach is that the modified Green's functions need not be known explicitly; formulations using the free space Green's function are used and matrix manipulation employed to arrive at a characteristic mode eigenvalue problem that effectively incorporates the desired modified Green's function. This is of practical importance since modified Green's functions are known only for a restricted number of cases of use in antenna work, usually when one part of a problem geometry is infinite (eg. infinitely large groundplane; infinitely large dielectric layers).

(c). We have demonstrated that the sub-structure characteristic mode concept extends to problems involving both conducting (PEC) and dielectric objects, with the PEC portion modeled by conduction surface current densities and the dielectric by volume electric polarization current densities. It has also been argued and shown that sub-structure modes are true characteristic modes in the sense that they possess both current and far-field orthogonality.

(d). We have introduced the idea of "restricted characteristic modes" to allow placement, in the general characteristic mode context, of the characteristic modes of certain idealized infinitely large structures. The latter objects are useful since the associated characteristic modes can be found from simplified (eg. two-dimensional) integral equations. These are useful for numerical experimentation on the determination of characteristic modes.

(e). We have shown that to find all the characteristic modes of a body-of-revolution (BOR) it is in fact sufficient to perform characteristic mode analyses on the operator matrices of the individual BOR harmonics. This has important implications for future antenna shape synthesis work involving dielectric radiators, as will be noted in Chapter 5.

Equally important are some findings related to numerical aspects of the characteristic mode problem:

(f). If one wishes to determine the characteristic mode eigenvalues, eigencurrents and eigenfields with some accuracy, then one has to be "numerically careful" at all stages". We have confirmed that the method of moments is a most suitable way of doing this. However, many approximations made in its implementation for specific classes of problem, that might be satisfactory for deterministic problems, might not be good enough for eigenvalue problems of the characteristic mode kind. Fortunately, the increased speed of computation, the continuing development of more precise numerical operations related to the generation of moment method matrices (eg. customized integration schemes for very accurate evaluation troublesome integrals with peaked integrands), the use of higher-order expansion functions, and the ability to have more truly Galerkin approaches, will make this possible. Commercial codes are starting to incorporate such improvements and so will be useable for characteristic mode analysis, at least those that allow access to individual matrices

CHAPTER 5 Determination of the Characteristic Modes of Penetrable Objects

5.1 PRELIMINARY REMARKS

It will have been clear from Chapter 2 that great progress has been made by many authors in studying the CMs of perfectly-conducting objects. However, it was indicated in Sections 2.8 and 2.9 that, while formulations for the CMs of penetrable objects appeared soon after those for PEC objects, actual numerical results (eigenvalues, eigencurrents and eigenfields) for the characteristic modes of penetrable objects found using these formulations have not yet been published in the open literature, indeed not even in the seminal publication [HARR85]. We also mentioned in Section 2.8 that in oral conference presentations and discussions by others it has from time to time been stated that the determination of the CMs of penetrable objects is difficult, but without further comments as to why this is so. In this chapter we successfully tackle such computation of the CMs of penetrable objects, apparently for the first time.

Section 5.2 does so using the volume integral equation formulation. We first perform such computations for a 2-D penetrable cylinder using a moment method code 2DPBV developed specifically for this purpose as part of the work of this thesis. It was important for this research to have complete access to such a code in order to build up confidence in the use of volume formulations from first principles. This is followed by the computation of the CMs for 3-D penetrable objects using the volume formulation implemented in the commercial code *FEKO*. It is important to be aware of the fact that FEKO does not have a capability to compute the CMs of penetrable objects. We merely use it as a means of modelling the geometry and providing the moment method matrix. The matrix transformations and eigenanalysis needed for determining the CMs are done separate from FEKO. The CM currents so determined are then fed back to FEKO in order to compute the far-zone CM fields. These are then transferred from FEKO and used by a customized code to check the orthogonality of the far-zone CM fields.

Section 5.3 follows much the same route as Section 5.2, except that surface integral equation formulations are used, first using for a 2-D penetrable cylinder using a moment method code 2DPBS developed specifically for this purpose, and then for 3-D objects utilizing FEKO.

Unless otherwise stated for some special purpose, a fine segmentation is used to ensure accuracy of the computation for both 2-D or 3-D objects. The segmentation must be sufficiently fine to resolve the geometry and properly represent the spatial variation. In all cases, we assume an object is placed in a free-space environment ($\varepsilon_e = \varepsilon_o$ and $\mu_e = \mu_o$). Additionally, we assume objects are either homogenous dielectric objects with permittivity ε_d, homogenous magnetic objects with permeability μ_d, or homogeneous magneto-dielectric objects with properties ε_d and μ_d. Finally, only a transverse magnetic (TM) current formulation will be only considered for the 2-D objects, and the axis of the 2-D objects is assumed to be parallel to the z axis for all the cases.

5.2 THE DETERMINATION OF CHARACTERISTIC MODES USING VOLUME INTEGRAL EQUATION FORMULATIONS

In this section, we discuss the theory of characteristic modes for dielectric bodies, magnetic bodies, and magneto-dielectric bodies, using the volume integral equation (VIE) formulation, which was referred to in general terms in Section 2.8. We shall consider only loss-free material, for the same reasons as mentioned in Section 3.2.

Section 5.2.1 specializes the general integral-equation / moment method formulation of Section 2.8 to the 2-D TM_z case. This is used in Section 5.2.2 to find the CMs of such objects, specifically dielectric $(\varepsilon_d \neq \varepsilon_0, \mu_d = \mu_0)$ cylinders of circular and rectangular cross-section.

Section 5.2.3 describes the computation of the CMs of the following 3-D objects :

- Finite length, cylindrical dielectric object with $\varepsilon_d = 79.7\varepsilon_0$ and $\mu_d = \mu_0$.
- Notched rectangular dielectric object with $\varepsilon_d = 37.84\varepsilon_0$ and $\mu_d = \mu_0$.
- Finite length, cylindrical magnetic object with $\varepsilon_d = \varepsilon_0$ and $\mu_d = 79.7\mu_0$.
- Finite length, cylindrical magneto-dielectric objects with $\varepsilon_d = 79.7\varepsilon_0$ and different permeability values $\mu_d = 2\mu_0$, $\mu_d = 15\mu_0$ and $\mu_d = 30\mu_0$ in succession.

5.2.1 Two-Dimensional Volume Integral Equation Formulation for a Dielectric Object

Analyzing a 2-D scattering object will serve as a first in the examination of the computation of the characteristic modes for dielectric objects. We consider only the TM_z case, as done for PEC objects in Section 2.6-1. We consider the case of a lossless non-magnetic dielectric material structure whose permittivity is greater than that of free-space but whose permeability is equal to that of free space. As discussed in Section 2.8, everything can be described in terms of an equivalent volume electric current density only, and so only the single integral equation (2.8-1) is needed. For the 2-D TM_z case being considered the equivalent electric current density is entirely z-directed, and so the scattered electric field due to the this current density can be written as

$$E_z^s\{\bar{\rho},\bar{J}_{eq}\} = -j\omega A(\bar{\rho}) = -j\omega\left[\frac{\mu_e}{4j}\iint_{S_d} J_z(\bar{\rho}')H_o^{(2)}\left(k\left|\bar{\rho}-\bar{\rho}'\right|\right)dS'\right] \qquad (5.2\text{-}1)$$

where S_d is the cross-section of the cylindrical object. Integral equation (2.8-1) then simplifies to the VIE integral equation [PETE97]

$$\frac{J_z(\bar{\rho})}{j\omega\left(\varepsilon_d-\varepsilon_e\right)} + \frac{\omega\mu_e}{4}\iint_{S_d} J_z(\bar{\rho}')H_o^{(2)}\left(k\left|\bar{\rho}-\bar{\rho}'\right|\right)dS' = E_z^i(\bar{\rho}) \qquad (5.2\text{-}2)$$

In order to apply the method of moments to find a numerical solution of (5.2-2), we segment the cross-section S_d of the cylindrical object (in the xy-plane) into N rectangular elements of size Δx by Δy. Pulse functions are used as expansion functions to represent the unknown volume equivalent current density J_z. The weighting functions will be delta functions located at the centre of each element. Application of the method of moments to (5.2-2) using these expansion and weighting functions reduces it to its discretized form represented by the usual matrix equation

$$[Z][I]=[V] \qquad (5.2\text{-}3)$$

where [Z] is the operator matrix (impedance matrix), [V] is the excitation vector, and $[I]=[I_1 \quad I_2 \quad \cdot \quad \cdot \quad \cdot \quad I_N]^T$ are the unknown coefficients that give the desired volume equivalent current density as

$$J_z\left(\bar{\rho}\right)=\sum_{n=1}^{N} I_n J_{zn}\left(\bar{\rho}\right) \tag{5.2-4}$$

Detailed expressions for the terms of the operator matrix [Z] and excitation vector [V] are presented in Appendix IV. The linear operator [Z] (impedance matrix) is symmetric. Thus, the theory of characteristic modes for dielectric objects using this formulation can follow the same arguments as those for PEC objects in Chapter 2. Therefore the eigenvalue equation for finding the CMs is (2.3-45), and the orthogonality relationships (2.3-38), (2.3-39), (2.3-40) and (2.3-21) must follow.

5.2.2 Numerical Experiments on the Characteristic Modes of Two-Dimensional Homogeneous Dielectric Objects

We next apply the formulation of Section 5.2.1 to find the CMs of 2-D homogeneous dielectric cylinders of circular and rectangular cross-section. The CMs of infinitely long cylinders are more of theoretical than practical interest, the interpretation of this type of CM being suggested in Section 4.7. However, a study of the CM eigenvalues of such objects, specifically the lower order CMs (their resonance frequencies, modal significance, modal volume current densities, and associated modal fields) will allow us to check that the orthogonality conditions hold, this being essential for a proper study of the CMs of 2-D dielectric objects[1].

We first consider a *dielectric circular cylinder* for which the permittivity is equal to $4\varepsilon_o$ and radius is equal to roughly 60 mm (0.1 λ_0 fixed at 500 MHz). The eigenvalues of the first five CMs are shown in Fig.5.2-1 over the frequency range 100 to 1500 MHz. All these CMs are capacitive at frequencies below the first resonance, but become inductive after resonance. Several curves overlap each other, which is indicative of the degeneracy caused by the rotational symmetry of the object. Fig.5.2-2 can be used to appreciate where the resonances occur, and this information is summarized in Table 5.2-1. The suspected mode degeneracies are confirmed by the repeated resonance frequencies in Table 5.2-1. The symmetry of some modal current distributions[2] is shown in Fig.5.2-3, and their corresponding far-zone fields are shown in Fig.5.2-4. The field patterns associated with the first and second CMs are alike, except for the direction

---

[1] No such results have been given in the literature even for such 2-D dielectric objects.
[2] Obtained using (5.2-4).

in which the maxima occur, due to their degeneracy. The same holds for the fourth and fifth CMs. The third mode radiates omni-directionally. The absolute orientation of the current density and their corresponding eigenfields is arbitrary; only relative orientations matter. In order to have a more detailed validation of the numerical data the current and field orthogonality was checked over the frequency range shown in the plots. Specifically, the CM eigenvalues, and the results for the orthogonality check at 1.2 GHz, are shown Tables 5.2-3 and 5.2-4. This shows that we have indeed found CMs for a 2-D dielectric object.

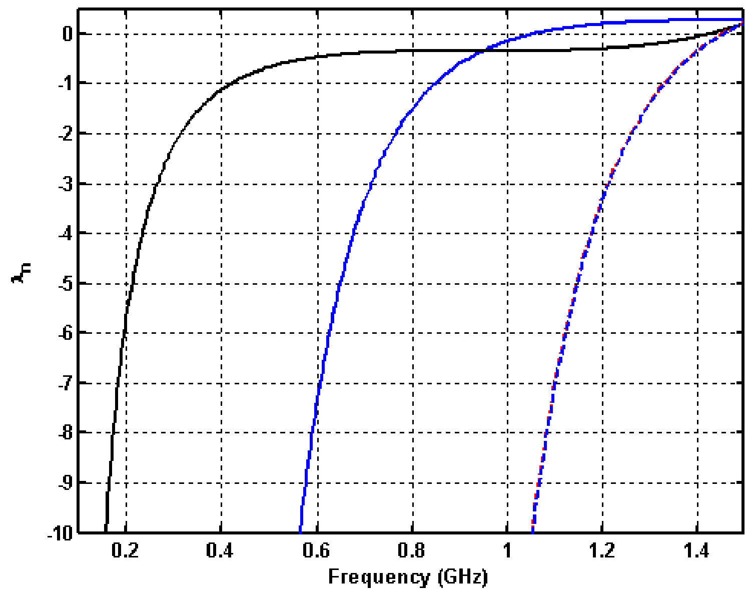

Figure 5.2-1: Eigenvalues of the first five CMs for the 2-D circular cylinder. (———) λ_1, (———) λ_2, (———) λ_3, (— — —) λ_4, (— — —) λ_5.

Table 5.2-1 Frequency of resonance of the first five CMs for a 2-D dielectric circular cylinder

Characteristic Mode Index	Resonant Frequency (GHz)
1	1.056
2	1.056
3	1.428
4	1.456
5	1.456

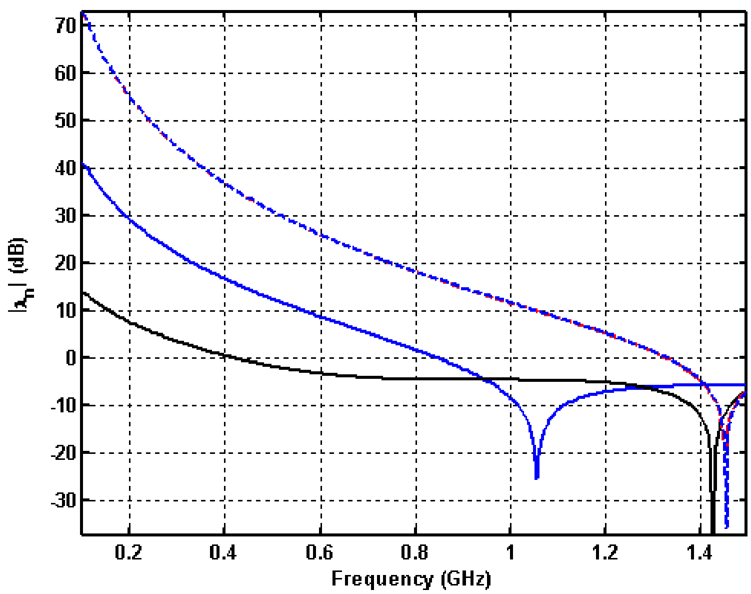

Figure: 5.2-2 Eigenvalues' magnitude (dB) of the first five CMs for the 2-D circular cylinder. (——) λ_1, (——) λ_2, (——) λ_3, (– – –) λ_4, (– – –) λ_5.

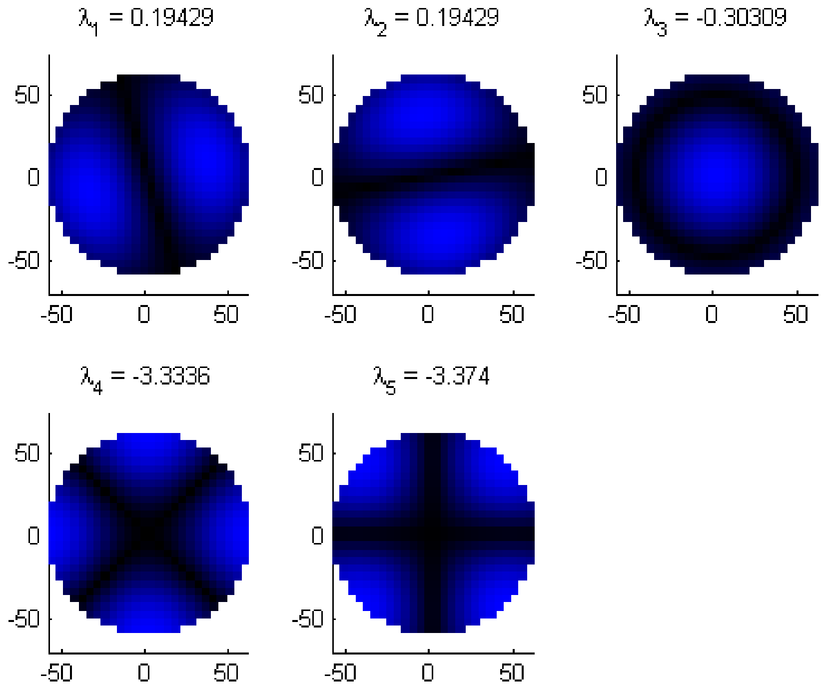

Figure 5.2-3: Modal current distributions of the first five CMs of the 2-D circular dielectric cylinder.

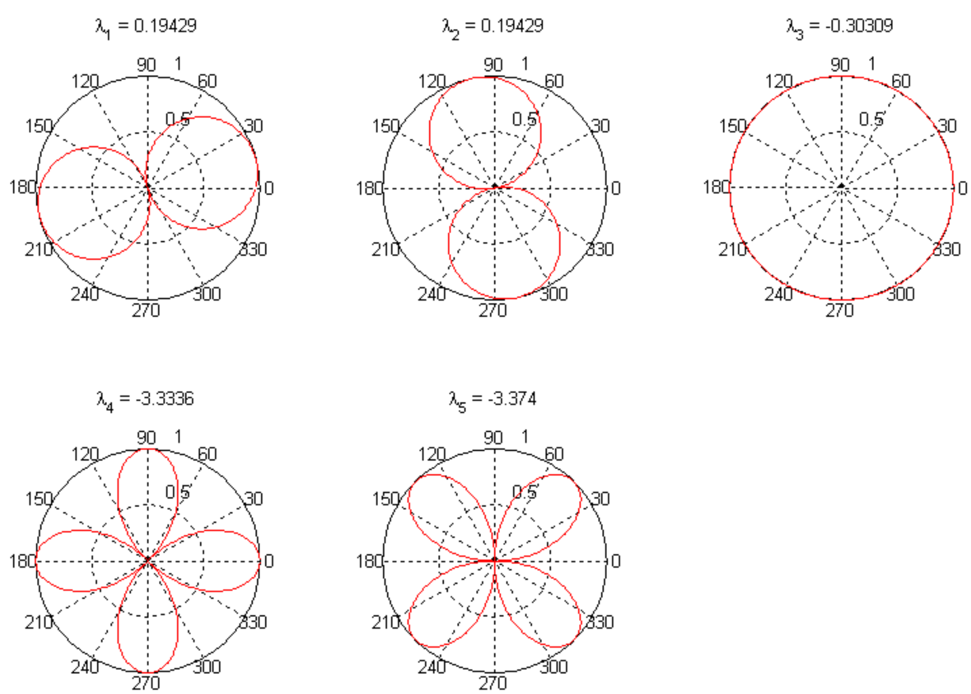

Figure 5.2-4: Normalized eigenfields (and associated eigenvalues) of the first five CMs - 2-D circular cylinder.

Table 5.2-2 Eigenvalues computed at 1.2 GHz for the 2-D circular dielectric cylinder

CM#	λ
1	**0.194**
2	**0.194**
3	**-0.303**
4	**-3.334**
5	**-3.374**

Table 5.2-3: Expression (2.2-46) evaluation at 1.2 GHz for the 2-D circular dielectric cylinder

m/n	1	2	3	4	5
1	1.000	0.099	0.000	0.000	0.000
2	0.099	1.000	0.000	0.000	0.000
3	0.000	0.000	1.000	0.000	0.000
4	0.000	0.000	0.000	1.000	0.000
5	0.000	0.000	0.000	0.000	1.000

Table 5.2-4: Expression (2.3-21) evaluation at 1.2 GHz using 361 integration points in the φ-direction for the 2-D circular dielectric cylinder.

m/n	1	2	3	4	5
1	0.994+0.000i	0.099-0.000i	0.000-0.004i	-0.000+0.005i	0.000-0.000i
2	0.099+0.000i	0.999+0.000i	0.000+0.001i	-0.000-0.001i	0.000+0.000i
3	0.000+0.004i	0.000-0.001i	0.996+0.000i	0.004-0.000i	0.000+0.000i
4	-0.000-0.005i	-0.000+0.001i	0.004+0.000i	0.993+0.000i	-0.000+0.000i
5	0.000+0.000i	0.000-0.000i	0.000-0.000i	-0.000-0.000i	0.999+0.000i

Note that coupling terms associated to that CMs pair 1-2 suffers from numerical inaccuracies because of degeneracy, discussed in Section 2.3.4.

We next consider a *dielectric rectangular cylinder* of permittivity $9.8\varepsilon_o$. The dimensions are 150 by 450 mm (0.25 λ x 0.75 λ at 500 MHz). The CMs were computed between 100 and 300 MHz, within which frequency range two resonances were detected, as shown in Fig.5.2-6. The vertical scale has been chosen to properly show the behavior of the first three modes. The 5th CM does not appear because of its large eigenvalue, but is visible when the logarithmic scale is again used in Fig.5.2-7. All these CMs are capacitive below the first resonance. The modal currents were verified to be orthogonal at all frequency points by (2.3-38) through (2.3-41). The modal far-zone fields of the first five CMs were computed at 500 MHz and are shown in Fig.5.2-8. These eigenfields were indeed found to be orthogonal by (2.3-21). Unlike the circular cylinder case, the CMs of the rectangular do not exhibit degeneracies, due to the absence of rotational symmetries.

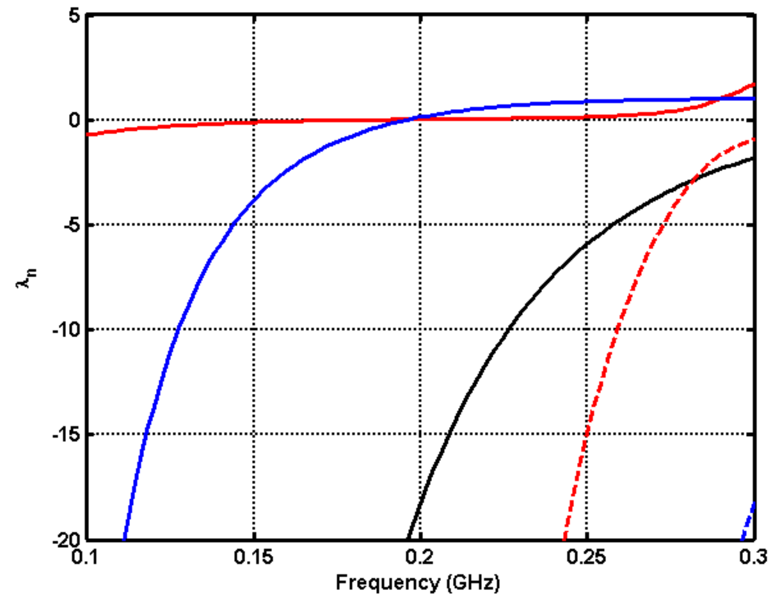

Figure 5.2-5: Eigenvalues of the first five CMs for the 2-D rectangular cylinder. (——) λ_1, (——) λ_2, (——) λ_3, (– – –) λ_4, (– – –) λ_5.

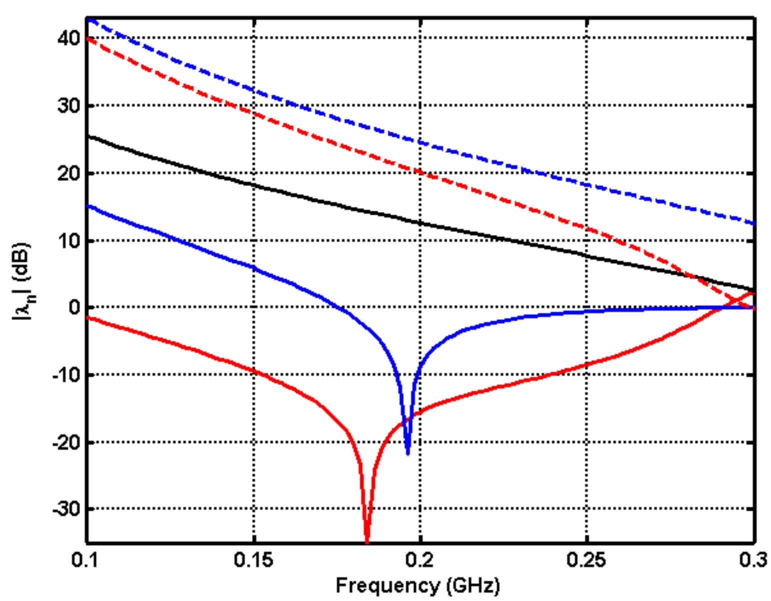

Figure 5.2-6: Eigenvalues' magnitude (dB) of the first five CMs for the 2-D rectangular cylinder. (——) λ_1, (——) λ_2, (——) λ_3, (– – –) λ_4, (– – –) λ_5.

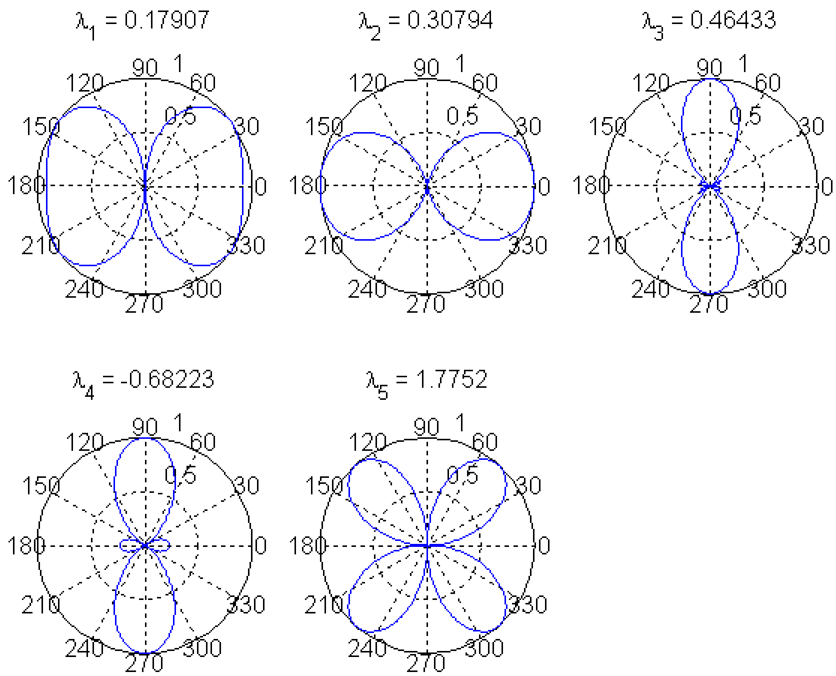

Figure 5.2-7 Normalized far-zone eigenfields (and associated eigenvalues) of the first five CMs of the 2-D rectangular cylinder at 500 MHz

5.2.3 Numerical Experiments on the Characteristic Modes of Three-Dimensional Penetrable Objects Using Volume Integral Equation Models

We next move to the discussion of the CMs of three-dimensional objects using a volume integral equation formulation. All cases are simulated in FEKO, utilizing it in the same manner as done for PEC objects, as importantly clarified in the second paragraph of Section 5.1. In essence the code FEKO simultaneously solves the pair of coupled integral equations (2.8-1) and (2.8-2) for magneto-dielectric objects, or either (2.8-1) or (2.8-2) if the object is a dielectric or magnetic object, respectively. It meshes the 3-D object into tetrahedra, in which are placed sophisticated expansion and weighting functions. Application of the method of moments then results in a matrix equation of the form (2.8-3). If a Galerkin approach is used for the method of moments, as should strictly be the case for finding CMs, the operator sub-matrices [Z], [D], [C] and [Y] would all be individually symmetric, and [C] would be equal to minus [D]. However, the use of true Galerkin methods is not necessary for deterministic problems[3] and adds additional computational burden on an already computer-time-consuming process. Thus commercial codes such as FEKO usually do not use true Galerkin methods. Fortunately the individual sub-matrices are nearly symmetric matrix if a sufficiently fines mesh (large number of elements) is used. Although briefly discussed in Section 2.8, some further details on the CM formulation that starts from (2.8-3) is required to actually apply it; this is taken from [HARR72a]. Recall from Section 2.8 that the discretization of the volume integral equation using the method of moments leads to the matrix equation (2.8-3). However, the operator matrix in (2.8-3) is not symmetric. But the formulation for finding CMs of lossless objects using integral equation approaches is based on the premise that the operator matrix is symmetric. It is therefore necessary to symmetrize the operator matrix in (2.8-3) in some way. This is done by a relatively straightforward transformation process [HARR72a] that converts the matrix equation into the form (2.8-6), which we rewrite here as

$$\begin{bmatrix} [Z] & [-\mathrm{j}C] \\ [-\mathrm{j}C] & [Y] \end{bmatrix} \begin{bmatrix} [J] \\ [\mathrm{j}M] \end{bmatrix} = \begin{bmatrix} [\mathrm{E}^i] \\ [\mathrm{j}H^i] \end{bmatrix} \tag{5.2-5}$$

The operator matrix in equation (5.2-5) will be called [T], and the CM eigenvalue equation for 3-D magneto-dielectric objects using the two kinds of volume current densities become [CHAN72]

$$\mathrm{Im}\{[T]\}[f]_n = \lambda_n \mathrm{Re}\{[T]\}[f]_n \tag{5.2-6}$$

where

$$[f]_n = \begin{bmatrix} [J] \\ [\mathrm{j}M] \end{bmatrix}_n \tag{5.2-7}$$

is the vector of eigencurrents, and λ_n the corresponding eigenvalues. If the characteristic mode currents are normalized in a manner similar to that done for PEC objects in Section 2.3.2, we can generalize the eigencurrent orthogonality relationships [HARR72a], which in matrix form are

[3] That is, non-eigenvalue problems.

$$[f_m]^T[T_1][f_n]=\delta_{mn} \tag{5.2-7a}$$

$$[f_m]^T[T_2][f_n]=\lambda_n\delta_{mn} \tag{5.2-7b}$$

$$[f_m]^T[T][f_n]=(1+j\lambda_n)\delta_{mn} \tag{5.2-7c}$$

where $[T]=[T_1]+j[T_2]$. Using the above relationships and the electromagnetic reciprocity theorem the far-zone eigenfields can be shown [HARR72a] to be orthogonal as well and to satisfy (2.3-21). Although not explicitly stated in [HARR72a], it is important to remember that the physical fields $(\bar{E}_n,\bar{H}_n)$ are those due to $(\bar{J}_n,\bar{M}_n)$ and not $(\bar{J}_n,\mathrm{j}\bar{M}_n)$, and these are the fields that are orthogonal in the far-zone.

We next compute, for the first time, CM eigenvalues, eigencurrents, and eigenfields for 3-D penetrable objects. Two different widely used objects will be considered, namely the finite cylindrical dielectric object (CDR) shown in Fig.5.2-9 and the notched rectangular dielectric object (RDR) shown in Fig.5.2-18.

On a technical point, we note that the FEKO license available for this work does not limit the amount of memory that can be used. Thus we were able to take advantage of the complete 64 GBytes of memory accessible on the computer used. Although the computer has two CPUs, one is not able to execute FEKO simulations in parallel when one wishes to export the moment method operator matrix from FEKO to the MATLAB environment for eigenanalysis. We have used a parallel version of MATLAB to perform eigenanalyses at different frequencies in parallel. The eigenanalysis at each frequency is a very lengthy process with the huge operator matrix sizes needed here, as will be mentioned below.

A Cylindrical Dielectric Resonator

The natural mode frequencies of a CDR were computed using integral equation approaches[4] in Section 3.6.4. The same integral equation model is used here to find the CMs of the same object, whose FEKO model is shown in Fig.5.2-9 with $\varepsilon_d = 79.7\varepsilon_0$, diameter d = 10.29mm and

---

[4] Both volume and surface integral equation approaches were used in Section 3.6.4, and shown to give similar results. Here we use the volume integral equation model to find the characteristic modes. The surface integral equation approach is sued for the latter purpose in Section 5.3.

height h = 4.51mm. In other words, the CDR was modelled in FEKO using the volume integral equation capability, the moment method operator matrix was exported to the MATLAB environment and equation (5.2-6) solved to obtain the CM eigenvalues and eigencurrents, and these eigencurrents were ported back to FEKO to find the far-zone fields of each CM.

The number tetrahedral elements used in the problem was 4478, which means that the largest tetrahedral edge length is roughly $\lambda_0/7$ at 4.8 GHz (the highest frequency in the range we will be considering). The moment method matrix size is 9431 x 9431 for this mesh, which is considered by FEKO to be a coarse one. A fine mesh, which would give a maximum tetrahedral edge length of $\lambda/16$, would require 56781 tetrahedra and a correspondingly large moment method matrix. Single-frequency computations for this fine mesh would be feasible (albeit lengthy) in FEKO, and the moment method matrix could be exported to the Matlab environment. The computation time for a frequency sweep simply increases by a multiplicative factor equal to the number of frequency samples (eg. 41 samples in the range 3.3GHz to 4.8 GHz). However, the eigenanalysis of such large matrices would be prohibitive. So the computation is a cumbersome one for penetrable objects using the volume formulation, especially when CMs are desired close to their resonances (which would be the case in antenna work)..

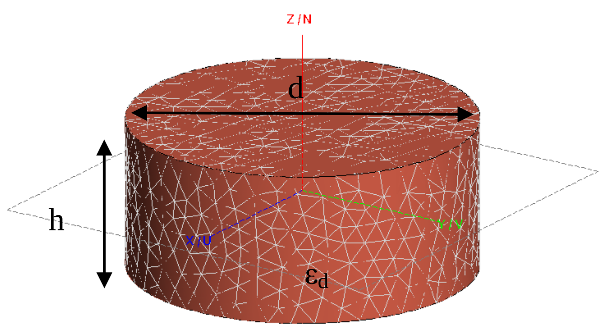

Figure 5.2-8: Three-dimensional cylindrical geometry (CDR) modelled in FEKO, showing the faces of the tetrahedral that lie on the surface of the CDR.

Figure 5.2-10 shows the computed eigenvalues for the first four CMs in the frequency range shown. At lower frequencies all four CMs shown start out as capacitive, then pass through resonance, and thereafter become inductive. As expected due to the rotational symmetry of the object, some CMs are degenerate. This is clarified by the repeated eigenvalues given in Table

5.2-5. The CMs resonate at the same frequencies as the natural modes for the identical CDR considered in Section 3.6.4. This is shown in Table 5.2-6, where the agreement between the two sets of frequencies is within 4%.

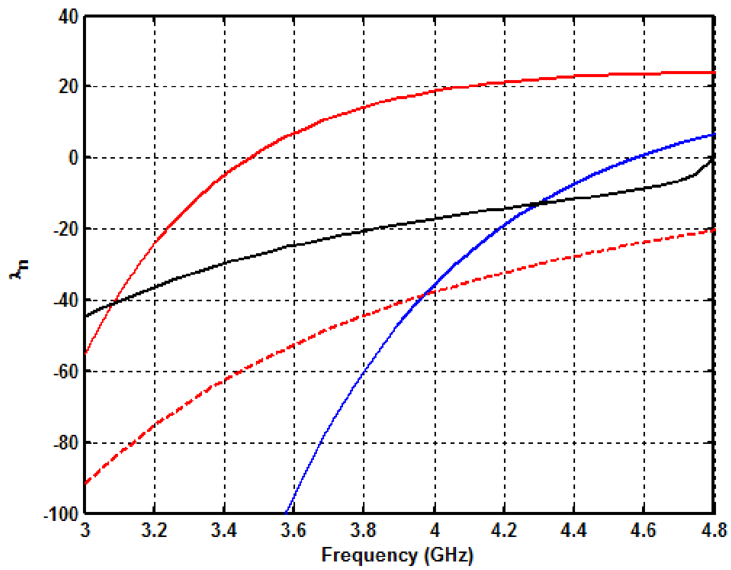

Figure 5.2-9: Eigenvalues of the first four CMs for the 3-D circular cylinder. (——) λ_1, (——) λ_2, (——) λ_3, and (– – –) λ_4.

Table 5.2-5 Computed CM eigenvalues at 3.474 GHz for the CDR in Fig.5.2-9

CM#	λ_n
1	0.0191
2	-27.8
3	-27.8
4	-58.7
5	-126.0

Table 5.2-6 : Real Resonant Frequencies of the Natural Modes, and Resonant Frequencies of the Characteristic Modes, of an Isolated Finite Cylindrical Dielectric Object with permittivity $\varepsilon_d = 79.7\varepsilon_0$, permeability $\mu_d = \mu_0$, diameter d = 10.29mm, and height h = 4.51mm

Natural Mode	Measured Natural Mode Real Resonant Frequency (GHz) [MONG94]	Characteristic Mode	Characteristic Mode Resonant Frequency (GHz)
$TE_{01\delta}$	3.479	1	3.470
$HEM_{11\delta}$	4.560	2	4.571
$HEM_{12\delta}$	4.779	3	4.799

The corresponding CM eigencurrents were checked to satisfy the orthogonality relationships (5.2-7) at all frequency samples, for which the results in Table 5.2-7 are an example. The negative sign is a result of FEKO placing a minus sign in front of the operator matrix of the solution, instead of having it in front of the excitation vector. This could be "corrected" by simply placing a negative sign in front of the operator matrix obtained from FEKO, but is not necessary.

The far-zone eigenfields due to each of these eigencurrents were computed by feeding the current vectors back to FEKO and requesting the far-zone fields; these were shown[5] to satisfy the field orthogonality (2.3-21) at all frequencies[6]. Illustrative numerical results are shown in Table 5.2-8. The distribution of the electric and magnetic eigenfields in the near-zone (including inside the dielectric object itself) was also examined and compared to those results of the field distributions of the natural modes of the CDR from [KAJF83, KAJF84]. In the horizontal cross-sectional view (half way up from the base of the CDR) shown in Fig.5.2-12, the electric field of the first CM was calculated at multiple points and plotted as shown in Fig.5.2-13. It is clear that the field intensity variation follows that of the $TE_{01\delta}$ natural mode given in [KAJF83, KAJF84] and reproduced here as Fig.5.2-14. The magnetic field intensity in the meridian plane indicated in Fig.5.2-15 was also computed for this first CM and is provided in Fig.5.2-16, and again its similarity to that of the $TE_{01\delta}$ natural mode in the same plane and shown Fig.5.2-17 is obvious. The far-zone eigenfield patterns for the first three CMs are shown in Fig.5.2-11, having been obtained using the CM currents resulting from the eigenanalysis.

It is tempting to assert that the field distributions of the natural modes are identical to those of the characteristic modes because of the similarities mentioned above. However, as stated in Section 2.3, a natural mode of the object is one that exists with zero incident field. Its electromagnetic field satisfies Maxwell's equations and the physical boundary conditions dictated by the object. On the other hand, we know from Section 2.3 that No characteristic mode field satisfies, on its own, the physical boundary conditions dictated by the object, but needs an incident field to do so. Thus in general natural mode fields and characteristic mode fields will not

[5] We remind the reader that, a stated earlier, all integrals (2.3-21) were evaluated using the method of [DICH97] for the m = n case, and the numerical approximation (2.6-13) for the other cases.
[6] We will see in Section 5.3 why it is important always to check the orthogonality of the far-zone fields.

be exactly identical everywhere, even though it appears that the real part of the natural mode frequencies are equal to the frequencies at which the CMs are resonant.

Table 5.2-7 Numerical values of (5.2-7a) at 1.2 GHz for the CDR of Fig.5.2-9

m/n	1	2	3	4	5
1	-1.000	0.000	0.000	0.000	0.000
2	0.000	-1.000	0.008	0.000	0.000
3	0.000	0.008	-1.000	0.000	0.000
4	0.000	0.000	0.000	-1.000	0.000
5	0.000	0.000	0.000	0.000	-1.000

Note that coupling terms associated to that CMs pair 2-3 suffers from numerical inaccuracies because of the degeneracy, discussed in Section 2.3.4.

Table 5.2-8 Numerical values of (2.3-21) at 3.474 GHz for the CDR of Fig.5.2-9, using 101 integration points in theta direction and 126 points in phi direction.

m/n	1	2	3	4	5
1	0.988+0.000i	-0.000+0.002i	0.000+0.009i	-0.000-0.000i	0.000-0.000i
2	-0.000-0.002i	0.988+0.000i	-0.006-0.000i	-0.000-0.000i	0.000-0.000i
3	0.000-0.009i	-0.006+0.000i	0.988+0.000i	-0.000-0.000i	-0.000+0.000i
4	-0.000+0.000i	-0.000+0.000i	-0.000+0.000i	0.988+0.000i	-0.000-0.008i
5	0.000+0.000i	0.000+0.000i	-0.000-0.000i	-0.000+0.008i	0.988+0.000i

Similarly, the coupling terms associated to that CMs pair 2-3 suffers from numerical inaccuracies because of the degeneracy, discussed in Section 2.3.4.

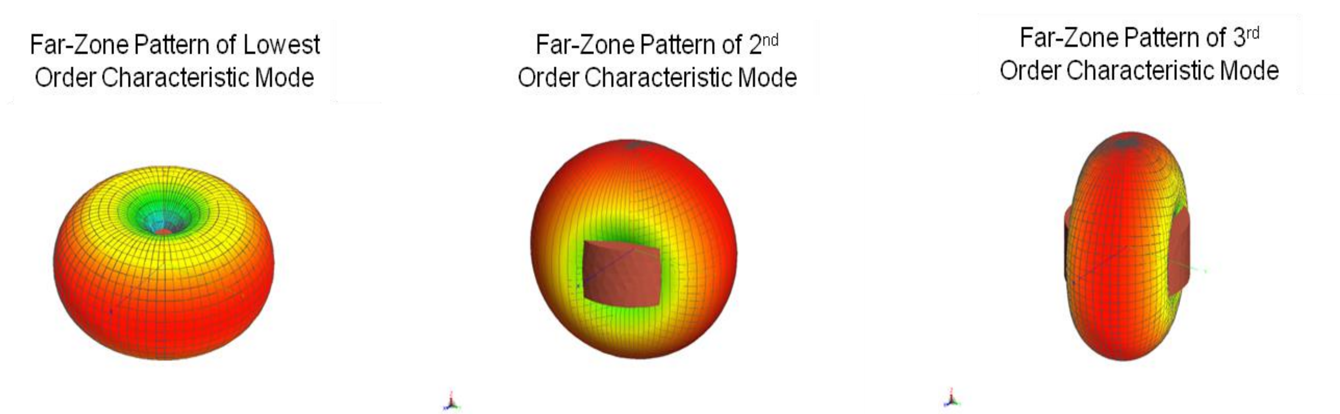

Figure 5.2-10: Normalized far-zone eigenfield distributions of the first three CMs of the CDR.

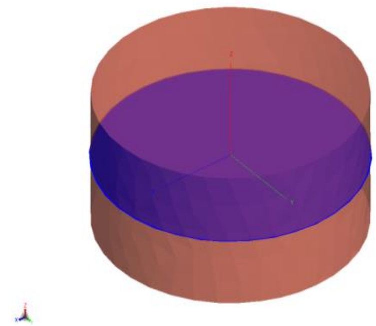

Figure 5.2-11: Horizontal cut in the equatorial plane of the CDR.

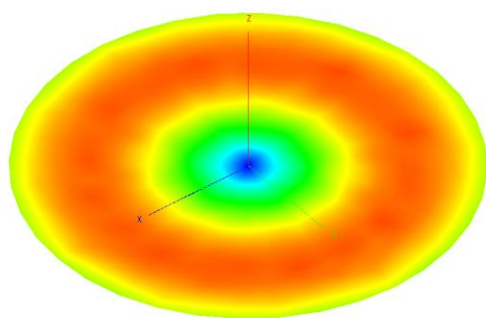

Figure 5.2-12: Electric field intensity of the first CM of the CDR in the horizontal cut of Fig.5.2-11, obtained using FEKO.

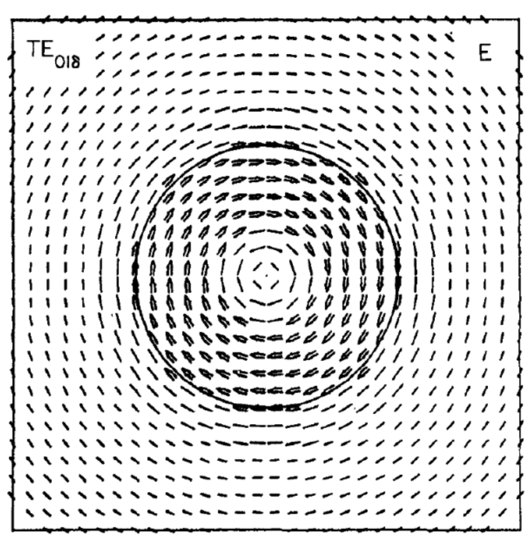

Figure 5.2-13: Electric field intensity calculated in [KAJF84]

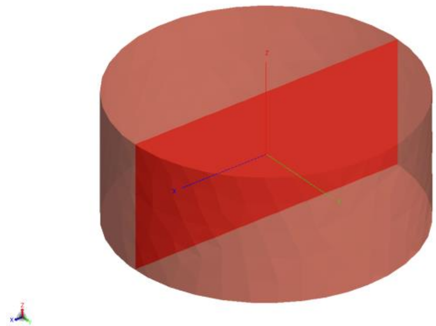

Figure 5.2-14: Vertical cut in the meridian plane of the CDR.

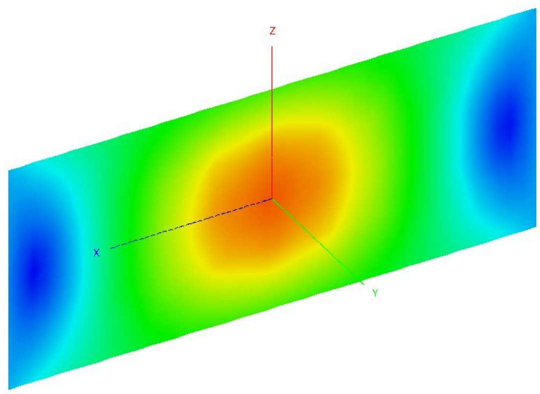

Figure 5.2-15 Magnetic field intensity of the first CM of the CDR in the vertical cut of Fig.5.2-14, obtained using FEKO.

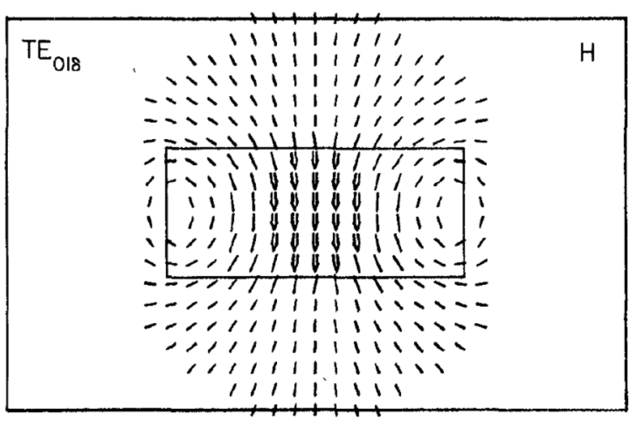

Figure 5.2-16 Magnetic field intensity calculated in [KAJF84].

B Rectangular Dielectric Resonator with a Notch

The fact that they provide designers with two degrees of freedom, namely the length-to-height ratio and the length-to-width ratio, has made rectangular dielectric resonators (RDR) popular shapes to use [PETO07]. The additional degree of freedom compared to the CDR (diameter-to-height ratio) gives extra flexibility. The introduction of a notch the RDR apparently reduces the effective permittivity, which decreases the Q-factor, and so the impedance bandwidth is enhanced [LIU01]. We here compute the CMs of the notched RDR as an example of such a calculation for a somewhat irregularly shaped object without any rotational symmetry such as the CDR. Figure 5.2-18 shows top and perspective views of the RDR, whose specifications are those found in [LIU01,Sect.V], namely permittivity $\varepsilon_d = 37.84\varepsilon_0$, permeability $\mu_d = \mu_0$, and dimensions $a = b = 8.77$mm, $a_n = b_n = 2$mm. The notch is present in the centre of y-z plane.

The CMs are computed using the same steps as for the CDR object. The RDR was analysed in [LIU07] using a volume integral equation model (albeit not via the FEKO code) to find the natural mode frequencies by identifying peaks in the condition number of the moment method matrix, as was done in Section 3.6.4. We have here used the same number of tetrahedral expansion functions as was done in [LIU07] for the same sized RDR. This means that there were 2184 tetrahedral elements (giving a maximum tetrahedral edge length of roughly $\lambda/6.4$ at 6.4GHz), which is considered to by the FEKO code to be a coarse mesh. The eigenvalues of the first four CMs are depicted in Fig.5.2-19 as a function of frequency. An alternative perspective is given by their modal significance plotted Fig.5.2-20, which shows that the first CM dominates the rest over the frequency range shown. The lowest natural mode frequency [LIU07] and resonance frequency of the first CM computed here are compared in Table 5.2-9. The two values are within 0.1% of each, and are considered identical.

It was confirmed that the eigencurrents satisfied the orthogonality relationships (5.2-7) at all frequencies considered, and that the eigenfields due to these eigencurrents are orthogonal because they satisfy (2.3-21). The related data is that in Table 5.2-10 and Table 5.2-11, respectively. The electromagnetic field distributions on certain cuts within the RDR itself are shown in Fig.5.2-21, and the far-zone CM field patterns are plotted in Fig.5.2-22, for the first three CMs at the resonance frequency of the first CM (that is, 6.177 GHz).

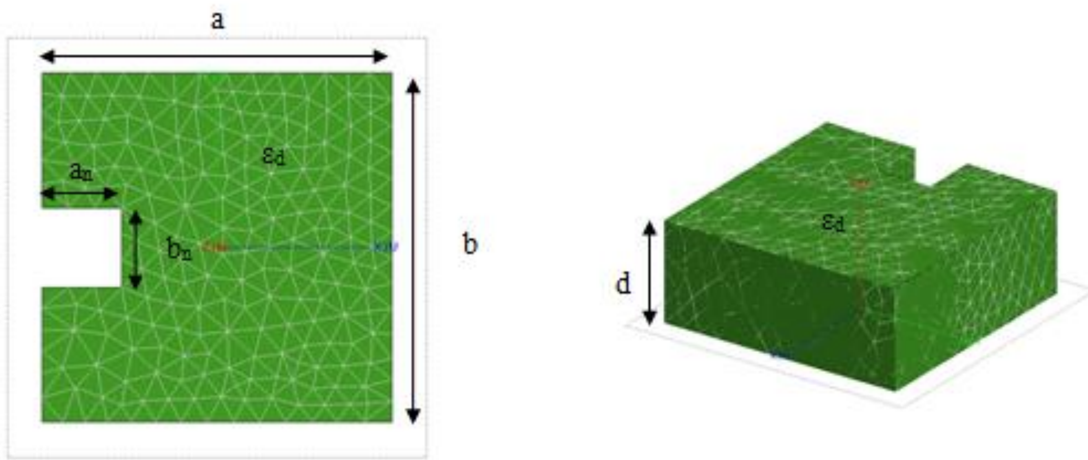

Figure 5.2-17: Notched rectangular dielectric resonator (RDR) modelled using FEKO.

Table 5.2-9: Real Resonant Frequencies of the Natural Modes, and Resonant Frequencies of the Characteristic Modes, of an Isolated Notched Rectangular Dielectric Object (RDR) with permittivity ε_d = 37.84ε_0, permeability $\mu_d = \mu_0$, and dimensions a = b = 8.77mm, a_n = 2mm and b_n = 2mm.

Natural Mode Designation	Natural Mode Resonant Frequency (GHz) [LIU07]	Characteristic Mode	Computed Characteristic Mode Resonant Frequency (GHz)
1	6.184	1	6.177

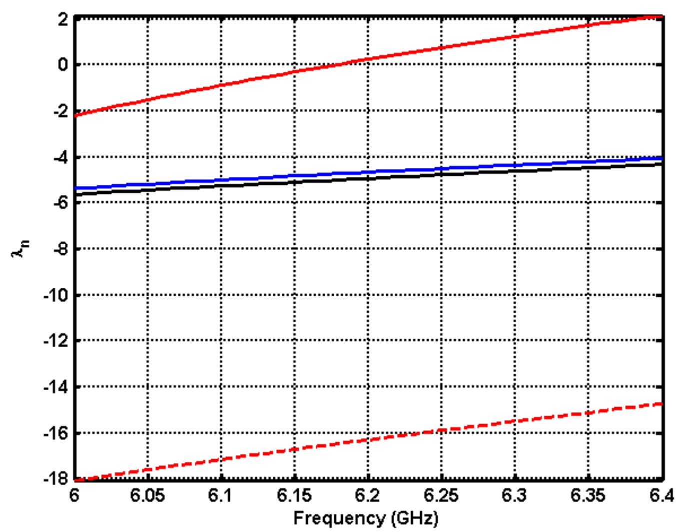

Figure 5.2-18: Eigenvalues of the first four CMs -3-D RDRA with notch. (——) λ_1, (——) λ_2, (——) λ_3, (– – –) λ_4.

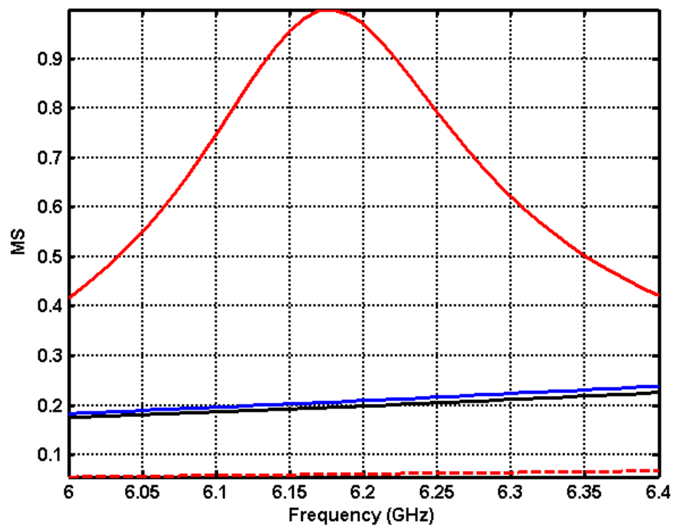

Figure 5.2-19: Modal significance of the first four CMs- 3-D RDRA with notch. (———) λ_1, (———) λ_2, (———) λ_3, (— — —) λ_4.

Table 5.2-10: Numerical values of (5.2-7a) at 6.177 GHz for the RDR of Fig.5.2-18

m/n	1	2	3	4	5
1	-1.000	0.000	0.000	0.000	0.000
2	0.000	-1.000	0.000	0.000	0.000
3	0.000	0.000	-1.000	0.000	0.000
4	0.000	0.000	0.000	-1.000	0.000
5	0.000	0.000	0.000	0.000	-1.000

Table 5.2-11: Numerical values of (2.3-21) at 6.177GHz for the RDR of Fig.5.2-18, using 101 integration points in the theta direction and 126 points in the phi direction.

m/n	1	2	3	4	5
1	0.974+0.000i	-0.000+0.009i	-0.000+0.000i	0.000-0.000i	0.000+0.000i
2	-0.000-0.009i	0.974+0.000i	0.000+0.000i	0.000-0.000i	-0.000+0.000i
3	-0.000-0.000i	0.000-0.000i	0.974+0.000i	0.000+0.000i	-0.000+0.000i
4	0.000+0.000i	0.000+0.000i	0.000-0.000i	0.974+0.000i	0.000+0.010i
5	0.000-0.000i	-0.000-0.000i	-0.000-0.000i	0.000-0.010i	0.974+0.000i

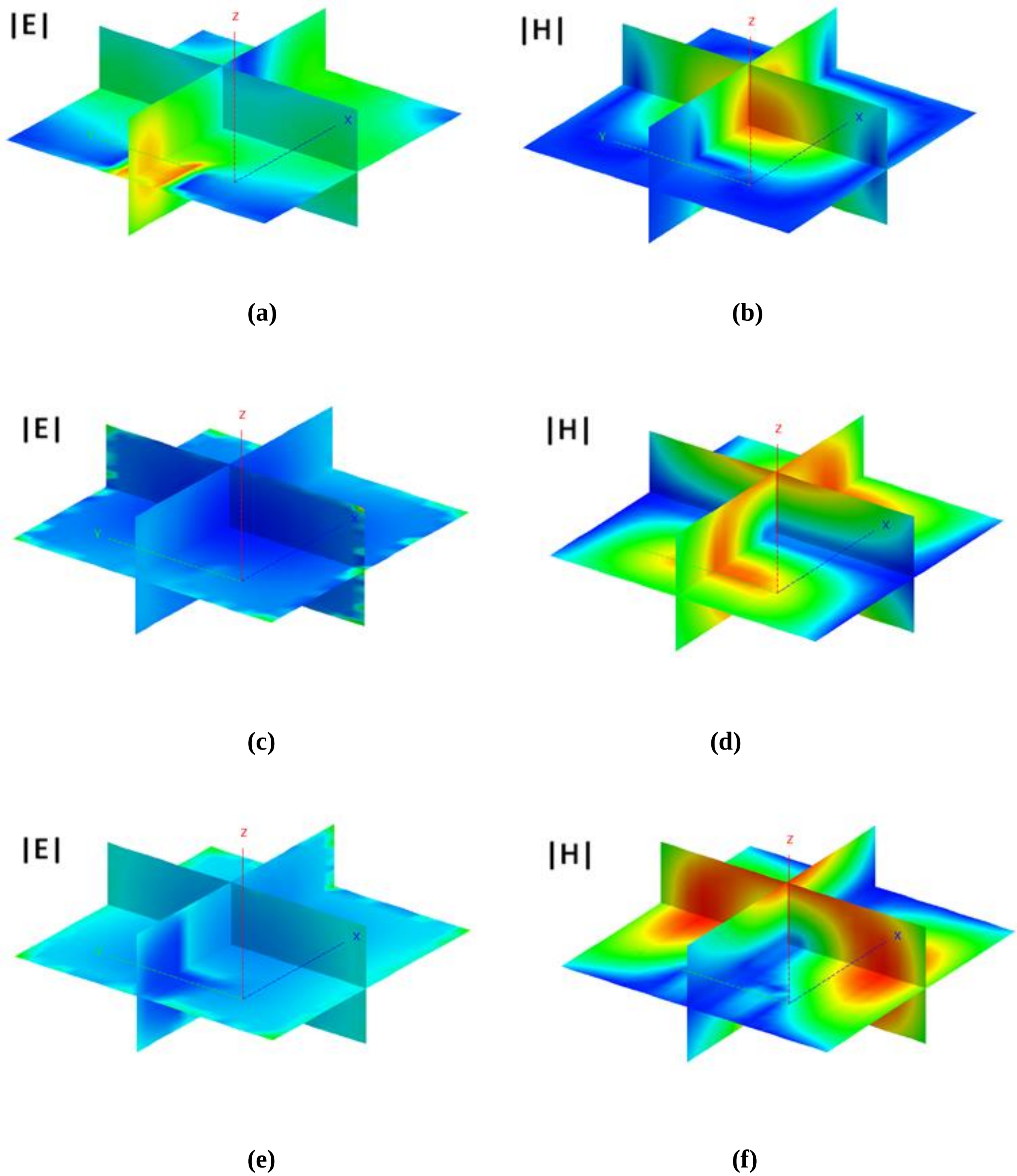

Figure 5.2-20: (a) Electric field, and (b) magnetic fields, of the 1st CM in selected cuts of the notched RDR. Views (c) and (d) apply similarly to the 2nd CM, while (e) and (f) apply to the 3rd CM. All fields are at a frequency of 6.177 GHz, which is the resonance frequency of the 1st CM.

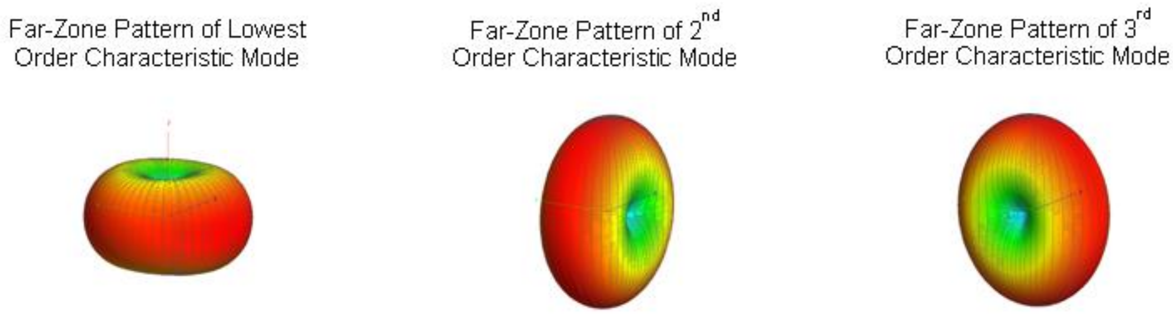

Figure 5.2-21: Normalized far-zone eigenfields of the first three CMs of the notched RDR.

C Magnetic Resonator

We here reconsider the same size CDR from Part A, except that now object with $\varepsilon_d = \varepsilon_0$ and $\mu_d = 79.7\mu_0$. It will thus be referred to as the magnetic-CDR[7]. This was modelled in precisely the same way as for the dielectric-CDR in Part A; the material properties were simply "switched" as indicated above. The eigenvalues of the first five modes are identical to those in Table 5.2-5 for the dielectric-CDR. The current and field orthogonality conditions are satisfied at all frequencies, as shown via Tables 5.2-12 and 5.2-13 for the specific case of 3.474 GHz. The far-zone field patterns of the first three CMs are shown in Fig.5.2-23; they are identical to those of the dielectric-CDR in Fig.5.-17, except that the polarization is rotated by 90°, as expected.

Table 5.2-12: Numerical values of (5.2-7a) at 3.474 GHz for the magnetic-CDR.

m/n	1	2	3	4	5
1	-1.000	0.000	0.000	0.000	0.000
2	0.000	-1.000	0.008	0.000	0.000
3	0.000	0.008	-1.000	0.000	0.000
4	0.000	0.000	0.000	-1.000	0.000
5	0.000	0.000	0.000	0.000	-1.000

Note that the coupling terms associated to that CMs pair 2-3 suffers from numerical inaccuracies because of the degeneracy, discussed in Section 2.3.4.

[7] We will refer to it as a "CDR" simply to identify it as the same cylindrical object form Part A, except that here in Part C it will be comprised of magnetic (and not dielectric) material, and in Part D will be comprised of magneto-dielectric material.

Table 5.2-13: Numerical values of (2.3-21) at 3.474GHz for the magnetic-CDR, using 101 integration points in the theta direction and 126 points in the phi direction.

m/n	1	2	3	4	5
1	0.988+0.000i	-0.000+0.002i	0.000+0.009i	-0.000-0.000i	0.000-0.000i
2	-0.000-0.002i	0.988+0.000i	-0.006-0.000i	-0.000-0.000i	0.000-0.000i
3	0.000-0.009i	-0.006+0.000i	0.988+0.000i	-0.000-0.000i	-0.000+0.000i
4	-0.000+0.000i	-0.000+0.000i	-0.000+0.000i	0.988+0.000i	-0.000-0.008i
5	0.000+0.000i	0.000+0.000i	-0.000-0.000i	-0.000+0.008i	0.988+0.000i

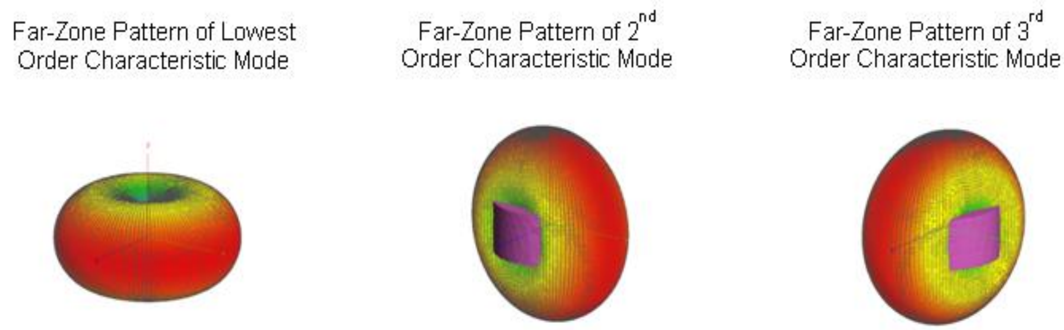

Figure 5.2-22: Normalized far-zone eigenfield patterns of the first three CMs computed at 3.474 GHz for the magnetic-CDR

D Cylindrical Magneto-Dielectric Resonator

The calculation of eigenvalues and eigencurrents was done for a magneto-dielectric CDR with $\varepsilon_d = 79.7\varepsilon_0$ and μ_d equal (in succession) to three different values. In this case, there are both electric and magnetic volume current densities, as explained in Section 2.8. This means that even for the same number of tetrahedra, the matrix size is double that for the same object when it is purely dieletric or purely magnetic. Thus CM analysis of a magneto-dielectric CDR in the vicinity of the resonance of the first CM becomes computationally burdensome. So in order to determine whether the volume integral equation does allow correct determination of CMs when an object has both its permittivity and permeability different from that of free space, we consider the magneto-dielectric CDR at a frequency (500 MHz) below resonance where the object is electrically smaller and the number of unknowns needed for a reliable computation can be handled. The number of tetrahedral elements used was 960 at that frequency. Table 5.2-14 shows the CM eigenvalues computed at 500 MHz; all are large because of the fact that No CMs are close to resonance at 500 MHz. Tables 5.2-15 through 5.2-20 show that the eigencurrents and far-zone eigenfields satisfy all the orthogonality requirements. The values of the field orthogonality integral for the m = n cases should of course be unity (they are normalized to radiate one Watt), but are substantially lower in some cases. This is attributed to numerical inaccuracies associated with the computation of such large eigenvalues (due to the object being far from resonance).

It is clear that use of volume integral equations places a serious computational burden on the CM analysis problem that might be prohibitive if we wish to use eventually it as a means of performing the shape synthesis of antennas made of penetrable material. An alternative means for the computation of the CMs such objects is the surface integral equation approach. This is the subject of the next section. Further remarks on the use of volume formulations, and its comparison to the use of surface formulations, for CM computation will be provided in Section 5.4, which concludes the chapter.

Table 5.2-14: Eigenvalues of the first five CMs of the magneto-dielectric CDR, at 500MHz, for $\varepsilon_d = 37.84\varepsilon_0$ and different values of μ_d.

CM Designation	CM Eigenvalues		
	$\mu_d/\mu_0 = 2$	$\mu_d/\mu_0 = 15$	$\mu_d/\mu_0 = 30$
1	-1.21E+04	-1.06E+04	-1.03E+04
2	-1.21E+04	-1.06E+04	-1.03E+04
3	-2.37E+04	-1.30E+04	-1.10E+04
4	-5.84E+04	-1.30E+04	-1.10E+04
5	-5.85E+04	-2.06E+04	-2.00E+04

Table 5.2-15: Numerical values of (5.2-7a) at 500 MHz for the magneto-dielectric CDR with $\varepsilon_d = 37.84\varepsilon_0$ and $\mu_d = 2\mu_0$.

m/n	1	2	3	4	5
1	-1.000	0.075	0.000	0.000	0.000
2	0.075	-1.000	0.000	0.000	0.000
3	0.000	0.000	-1.000	0.000	0.000
4	0.000	0.000	0.000	-1.000	0.014
5	0.000	0.000	0.000	0.014	-1.000

Table 5.2-16: Numerical values of (2.3-21) at 500 MHz for the magneto-dielectric CDR with $\varepsilon_d = 79.7\varepsilon_0$ and different values of $\mu_d = 2\mu_0$, using 101 integration points in theta direction and 126 points in the phi direction.

m/n	1	2	3	4	5
1	0.987+0.000i	-0.070-0.000i	0.000-0.000i	0.000+0.000i	0.000+0.000i
2	-0.070+0.000i	0.987+0.000i	-0.000-0.000i	0.000+0.000i	0.000-0.000i
3	0.000+0.000i	-0.000+0.000i	0.987+0.000i	-0.000-0.002i	0.000-0.006i
4	0.000-0.000i	0.000-0.000i	-0.000+0.002i	0.502+0.000i	-0.006-0.000i
5	0.000-0.000i	0.000+0.000i	0.000+0.006i	-0.006+0.000i	0.501+0.000i

Table 5.2-17: Numerical values of (5.2-7a) at 500 MHz for the magneto-dielectric CDR with $\varepsilon_d = 79.7\varepsilon_0$ and $\mu_d = 15\mu_0$.

m/n	1	2	3	4	5
1	-1.000	0.017	0.000	0.000	0.000
2	0.017	-1.000	0.000	0.000	0.000
3	0.000	0.000	-1.000	-0.010	0.000
4	0.000	0.000	-0.010	-1.000	0.000
5	0.000	0.000	0.000	0.000	-1.000

Table 5.2-18: Numerical values of (2.3-21) at 500 MHz for the magneto-dielectric CDR with $\varepsilon_d = 79.7\varepsilon_0$ and $\mu_d = 15\mu_0$, using 101 integration points in theta direction and 126 points in the phi direction.

m/n	1	2	3	4	5
1	0.987+0.000i	-0.014-0.000i	-0.000-0.000i	0.000+0.000i	0.000+0.000i
2	-0.014+0.000i	0.987+0.000i	0.000+0.000i	-0.000+0.000i	0.000+0.000i
3	-0.000+0.000i	0.000-0.000i	0.934+0.000i	0.006+0.000i	-0.000+0.008i
4	0.000-0.000i	-0.000-0.000i	0.006-0.000i	0.934+0.000i	0.000-0.004i
5	0.000-0.000i	0.000-0.000i	-0.000-0.008i	0.000+0.004i	0.987+0.000i

Table 5.2-19: Numerical values of (5.2-7a) at 500 MHz for the magneto-dielectric CDR with $\varepsilon_d = 79.7\varepsilon_0$ and $\mu_d = 30\mu_0$.

m/n	1	2	3	4	5
1	-1.000	0.000	0.000	0.000	0.000
2	0.000	-1.000	0.000	0.000	0.000
3	0.000	0.000	-1.000	0.000	0.000
4	0.000	0.000	0.000	-1.000	0.000
5	0.000	0.000	0.000	0.000	-1.000

Table 5.2-20: Numerical values of (2.3-21) at 500 MHz for the magneto-dielectric CDR with $\varepsilon_d = 79.7\varepsilon_0$ and $\mu_d = 30\mu_0$, using 101 integration points in theta direction and 126 points in the phi direction.

m/n	1	2	3	4	5
1	0.987+0.000i	0.000+0.000i	0.000+0.000i	-0.000+0.000i	0.000+0.000i
2	0.000-0.000i	0.987+0.000i	0.000-0.000i	-0.000+0.000i	0.000-0.000i
3	0.000-0.000i	0.000+0.000i	0.967+0.000i	0.005+0.000i	-0.000-0.005i
4	-0.000-0.000i	-0.000-0.000i	0.005-0.000i	0.967+0.000i	-0.000+0.008i
5	0.000-0.000i	0.000+0.000i	-0.000+0.005i	-0.000-0.008i	0.987+0.000i

5.3 THE DETERMINATION OF THE CHARACTERISTIC MODES USING SURFACE INTEGRAL EQUATION FORMULATIONS

The coupled surface integral equations introduced in Section 2.9 can be used to model penetrable bodies using equivalent surface current densities $\bar{J}_s$ and $\bar{M}_s$ as the unknowns. In this formulation there are always both electric and magnetic surface current densities, whether the object is a dielectric, magnetic or magneto-dielectric one. One huge advantage of the surface formulation over the volume formulation utilized in Section 5.2 is that number of unknowns required to solve the problem is drastically reduced, since expansion functions are only needed on the surface of the penetrable object. Application of the method of moments to the PMCHWT surface integral equation mentioned in Section 2.9 results in a matrix equation that can be rewritten in the symmetrized form (5.2-5). The characteristic mode eigenvalue equation is then that in (5.2-6), where the equivalent current $[f]_n$ in (5.2-7) now represents the equivalent surface current densities[8]. The characteristic modes so found then satisfy the orthogonality requirements (5.2-7) and (2.3-21).

Section 5.3.1 specializes the PMCHWT surface integral equation / moment method formulation of Section 2.8 to the 2-D TM_z case. This is used in Section 5.3.2 to find the CMs of such objects, specifically dielectric $(\varepsilon_d \neq \varepsilon_0, \mu_d = \mu_0)$ cylinders of circular and rectangular cross-section. Section 5.3.3 discusses why alternative surface formulations are not easily used for CM determination. Finally, Section 5.3.4 describes the computation of the CMs of the notched rectangular dielectric object (RDR of the same dimensions as in Section 5.2.3) with $\varepsilon_d = 37.84\varepsilon_0$ and $\mu_d = \mu_0$. We will see that some careful thought is needed when using the surface formulation to find characteristic modes.

5.3.1 Two-Dimensional Surface Integral Equation Formulations for a Dielectric Object

Customization of the coupled integral equations for the PMCHWT formulation of Section 2.9 to the 2-D TMz problem, and the application of the method of moments for its numerical solution, is discussed here. The derivation of implementable expressions for the various matrix terms, is described in Appendix III. We begin with the integral equation pair (2.9-1) and (2.9-2). These can be written as

$$\mathcal{L}_{\mathrm{EJ}}^{\mathrm{e}}\left\{S_d^-,\bar{J}_s\right\}+\mathcal{L}_{\mathrm{EM}}^{\mathrm{e}}\left\{S_d^-,\bar{M}_s\right\}+\mathcal{L}_{\mathrm{EJ}}^{d}\left\{S_d^+,\bar{J}_s\right\}+\mathcal{L}_{\mathrm{EM}}^{d}\left\{S_d^+,\bar{M}_s\right\}=\bar{E}_{\tan}^{inc}(S_d^-) \qquad (5.3\text{-}1)$$

and

$$\mathcal{L}_{\mathrm{HJ}}^{\mathrm{e}}\left\{S_d^-,\bar{J}_s\right\}+\mathcal{L}_{\mathrm{HM}}^{\mathrm{e}}\left\{S_d^-,\bar{M}_s\right\}+\mathcal{L}_{\mathrm{HJ}}^{\mathrm{d}}\left\{S_d^+,\bar{J}_s\right\}+\mathcal{L}_{\mathrm{HM}}^{\mathrm{d}}\left\{S_d^+,\bar{M}_s\right\}=\bar{H}_{\tan}^{inc}(S_d^-) \qquad (5.3\text{-}2)$$

[8]Instead of the physical volume current densities used in Section 5.2.

where, by comparison of (2.9-1) and (2.9-2) with (5.3-1) and (5.3-2) it is clear that

$$\hat{n}\times\bar{E}_{e}^{scat}\left\{S_{d}^{-},\bar{J}_{s},\bar{M}_{s}\right\}=\mathcal{L}_{\mathrm{EJ}}^{\mathrm{e}}\left\{S_{d}^{-},\bar{J}_{s}\right\}+\mathcal{L}_{\mathrm{EM}}^{\mathrm{e}}\left\{S_{d}^{-},\bar{M}_{s}\right\} \tag{5.3-3}$$

$$\hat{n}\times\bar{E}_{d}^{scat}\left\{S_{d}^{+},\bar{J}_{s},\bar{M}_{s}\right\}=\mathcal{L}_{\mathrm{EJ}}^{d}\left\{S_{d}^{+},\bar{J}_{s}\right\}+\mathcal{L}_{\mathrm{EM}}^{d}\left\{S_{d}^{+},\bar{M}_{s}\right\} \tag{5.3-4}$$

$$\hat{n}\times\bar{H}_{e}^{scat}\left\{S_{d}^{-},\bar{J}_{s},\bar{M}_{s}\right\}=\mathcal{L}_{\mathrm{HJ}}^{\mathrm{e}}\left\{S_{d}^{-},\bar{J}_{s}\right\}+\mathcal{L}_{\mathrm{HM}}^{\mathrm{e}}\left\{S_{d}^{-},\bar{M}_{s}\right\} \tag{5.3-5}$$

$$\hat{n}\times\bar{H}_{d}^{scat}\left\{S_{d}^{+},\bar{J}_{s},\bar{M}_{s}\right\}=\mathcal{L}_{\mathrm{HJ}}^{\mathrm{d}}\left\{S_{d}^{+},\bar{J}_{s}\right\}+\mathcal{L}_{\mathrm{HM}}^{\mathrm{d}}\left\{S_{d}^{+},\bar{M}_{s}\right\} \tag{5.3-6}$$

$$-\hat{n}\times\bar{E}^{inc}\left\{S_{d}^{-},\bar{J}^{imp},\bar{M}^{imp}\right\}=\bar{E}_{\tan}^{inc}(S_{d}^{-}) \tag{5.3-7}$$

and

$$-\hat{n}\times\bar{H}^{inc}\left\{S_{d}^{-},\bar{J}^{imp},\bar{M}^{imp}\right\}=\bar{H}_{\tan}^{inc}(S_{d}^{-}) \tag{5.3-8}$$

In other words, $\mathcal{L}_{\mathrm{EJ}}^{\mathrm{e}}\left\{S,\bar{J}_{s}\right\}$ gives $\hat{n}\times\bar{E}$ at points $\bar{r}$ on any surface S due to an electric current density $\bar{J}_{s}$ on the surface radiating in an unbounded medium with properties $(\mu_{e},\varepsilon_{e})$. Operator $\mathcal{L}_{\mathrm{HJ}}^{d}\left\{S,\bar{J}_{s}\right\}$ gives $\hat{n}\times\bar{H}$ at points $\bar{r}$ on surface S due to an electric current density when $\bar{J}_{s}$ radiating in an unbounded medium with properties $(\mu_{d},\varepsilon_{d})$ and similarly for the other operators. We use the same expansion functions $\bar{f}_{n}(\bar{\rho})$ for both equivalent surface currents $\bar{J}_{s}$ and $\bar{M}_{s}$, so that

$$\bar{J}_{s}=\sum_{n=1}^{N}a_{n}\bar{f}_{n}(\bar{\rho}) \qquad \bar{\rho}\in S_{d} \tag{5.3-9}$$

and

$$\bar{M}_{s}=\sum_{n=1}^{N}b_{n}\bar{f}_{n}(\bar{\rho}) \qquad \bar{\rho}\in S_{d} \tag{5.3-10}$$

where a_n and b_n are the unknown coefficients for the current densities, and N is the total number of expansion functions used. The 2-D contour is divided into N segments. In particular, we choose pulse expansion function

$$\bar{f}_n(\bar{\rho}) = P_n(\bar{\rho}) = \begin{cases} 1 & \bar{\rho} \in [\rho_n^{(1)}, \rho_n^{(1)}] \\ 0 & \bar{\rho} \notin [\rho_n^{(1)}, \rho_n^{(1)}] \end{cases} \tag{5.3-11}$$

over the n-th segment, and delta weighting function

$$\bar{W}_m(\bar{\rho}) = \delta(\rho_m - \rho') \tag{5.3-12}$$

over the m-th segment. The usual procedure of applying the method of moments to the coupled integral equations (5.3-1) and (5.3-2) leads to the matrix equation

$$\begin{bmatrix} [Z] & [D] \\ [C] & [Y] \end{bmatrix} \begin{bmatrix} [I_f] \\ [V_f] \end{bmatrix} = \begin{bmatrix} [V_g] \\ [I_g] \end{bmatrix} \tag{5.3-13}$$

This represents a set of 2N equations in the 2N unknowns $a_1, a_2, ...a_N, b_1, b_2, ...b_N$. Detailed implementable expressions for the various matrix terms in (5.3-13) are provided in Appendix III. The moment method matrix in (5.3-13) possesses the properties that allow it to be written in the symmetrized form (5.2-5) so that it can be used for finding the CMs of the penetrable cylinder. A computer code *2DPBS* was developed based on this formulation, and is used in Section 5.3.2 to determine the CMs of 2-D penetrable objects.

5.3.2 Determination of the Characteristic Modes of 2-D Penetrable Objects Using the PMCHWT Surface Integral Equation Formulation

The code *2DPBS* is next used to determine the CMs of 2-D dielectric cylinders of circular and rectangular cross-section of the same dimensions as in Section 5.2.2, over the same frequency range as done there.

Considering the 2-D dielectric circular cylinder first, the eigenvalues of the first five tentative[9] CMs are shown in Fig.5.3-1, and in magnitude form in Fig.5.3-2. Before commenting further on these two plots, we draw the reader's attention Table 5.3-1, which shows the eigenvalues (at 1.2 GHz) of the above five CMs plus an additional five. The left-most column in Table 5.3-1 shows the tentative CM designations. We next evaluated the current orthogonality relations (5.2-7) and the far-zone field orthogonality expression (2.3-21). Tables 5.3-2 and 5.3-3 reveal the results of the orthogonality computations for the first five tentative CMs. We indicate in Table 5.3-1 which of these tentative CMs satisfy the two orthogonality requirements. Some of the modes do not completely satisfy the field orthogonality requirement[10], are therefore deemed non-physical, and the physical CMs are renumbered as in the right-most column in Table 5.3-1. The five CMs that have been retained as physical modes (as opposed to false non-physical ones) are in fact the first five CMs for the same object obtained using the volume integral equation formulation in Section 5.2.2, where No non-physical modes were obtruded. The reason for the appearance of the non-zero quantity "0.310" in Table 5.3-3 is that physical CM pair 1-2 is degenerate due to the rotational symmetry of the circular cylinder. Returning to Fig.5.3-1, we note that the tentative CMs whose eigenvalues are positive ("inductive") at frequencies lower than their resonance are the two of the five shown that turn out to be non-physical. Finally, far-zone eigenfield patterns of all ten tentative CMs are shown in Fig.5.3-3, but only those shown with their eigenvalues underlined in blue are physical CMs. Direct comparison of the first three physical CMs obtained using the present surface formulation, and those find from the volume formulation in Section 5.2.2, is provided in Fig.5.3-4.

---

[9] The reason for the use of the word *tentative* will become clear shortly.
[10] In particular, the m=n terms.

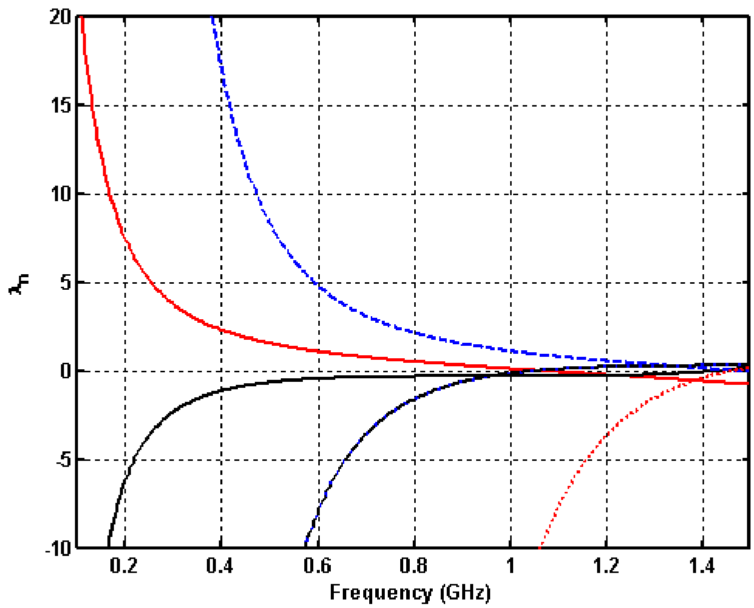

Figure 5.3-1: Eigenvalues of the first five tentative CMs of the 2-D dielectric circular cylinder.

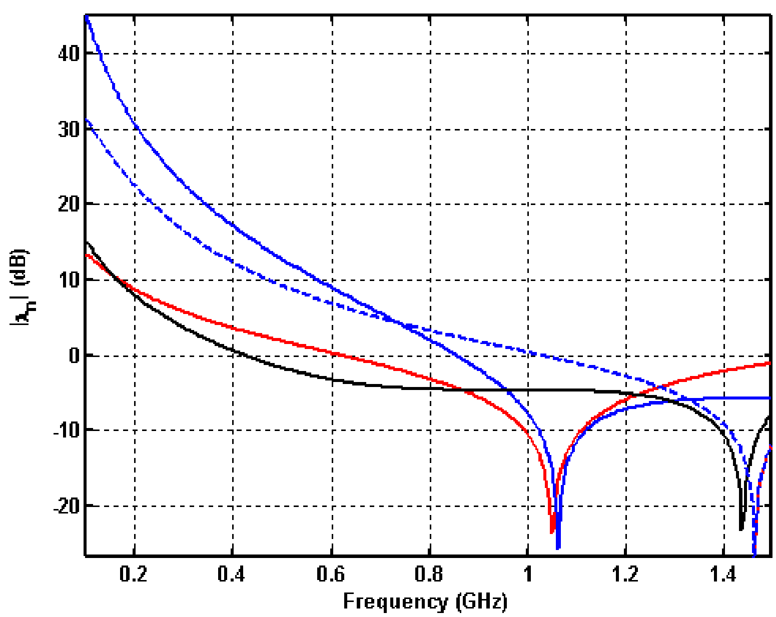

Figure 5.3-2: Eigenvalue magnitudes of the first five tentative CMs of the 2-D dielectric circular cylinder.

Table 5.3-1: Eigenvalues of the tentative first ten CMs computed at 1.2 GHz.

Tentative CM Designations (Prior to Orthogonality Checking)	λ_n	Satisfies Current Orthogonality Relations (5.2-7)?	Satisfies Field Orthogonality Relation (2.3-21)?	Final CM Designations (After Orthogonality Checking)
1	0.196	Yes	Yes	1
2	0.196	Yes	Yes	2
3	-0.250	Yes	No	Non-Physical
4	-0.311	Yes	Yes	3
5	0.532	Yes	No	Non-Physical
6	0.532	Yes	No	Non-Physical
7	2.038	Yes	No	Non-Physical
8	2.038	Yes	No	Non-Physical
9	-3.648	Yes	Yes	4
10	-3.648	Yes	Yes	5

Table 5.3-2 Numerical values of (5.2-7a) at 1.2 GHz for the first five tentative CMs of the 2-D dielectric circular cylinder.

m/n	1	2	3	4	5
1	-1.000	-0.310	0.000	0.000	0.024
2	-0.310	-1.000	0.000	0.000	0.008
3	0.000	0.000	-1.000	-0.150	0.000
4	0.000	0.000	-0.150	-1.000	0.000
5	0.024	0.008	0.000	0.000	-1.000

Table 5.3-3 Numerical values of (2.3-21) at 1.2 GHz for the first five tentitive CMs of the 2-D dielectric circular cylinder. The integrations used 361 integration points in the φ-direction.

m/n	1	2	3	4	5
1	0.999+0.000i	0.310-0.000i	0.000+0.000i	0.000+0.000i	-0.007+0.000i
2	0.310+0.000i	0.999+0.000i	0.000+0.000i	0.000+0.000i	-0.002-0.000i
3	0.000-0.000i	0.000-0.000i	0.001+0.000i	0.027-0.000i	-0.000+0.000i
4	0.000-0.000i	0.000-0.000i	0.027+0.000i	0.984+0.000i	0.000+0.000i
5	-0.007-0.000i	-0.002+0.000i	-0.000-0.000i	0.000-0.000i	0.000+0.000i

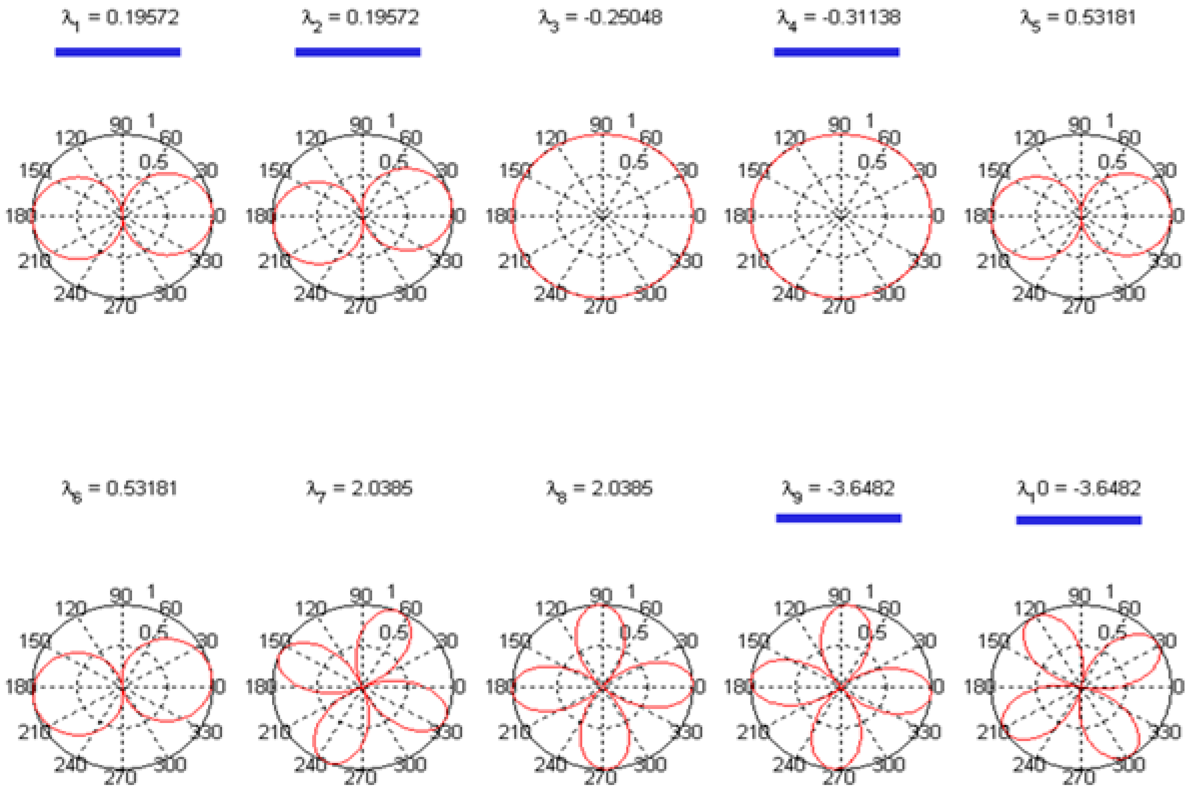

Figure 5.3-3: Normalized far-zone eigenfield patterns of the first ten tentative CMs of the 2-D dielectric circular cylinder, along with the eigenvalue of each, at 1.2 GHz. Not all are physical CMs. The blue bars underline the physical CMs.

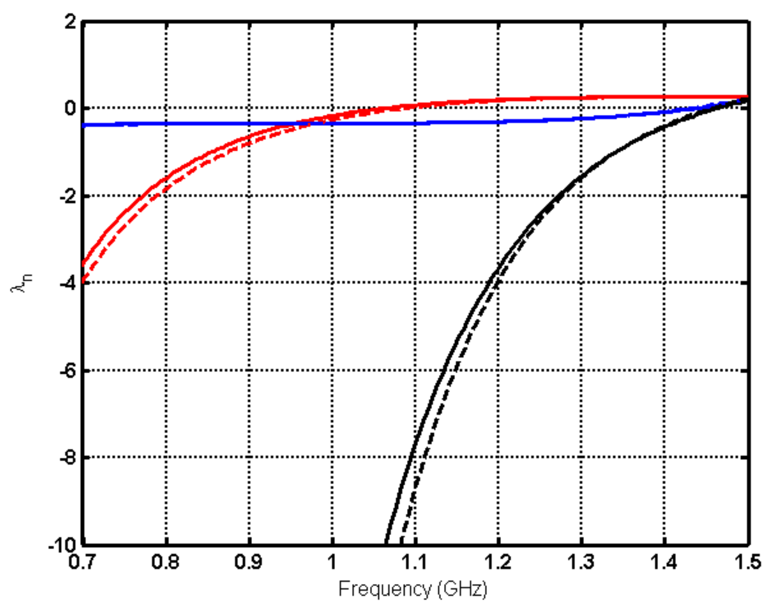

Figure 5.3-4: Comparison between CM eigenvalues computed using the surface formulation (solid lines) and volume formulation (dashed lines). Colour coding is (——) λ_1, (——) λ_2, and (——) λ_3.

As done in Section 5.2.2, we next consider a 2-D object of rectangular cross-section and use the PMCHWT formulation of code *2DPBS* to determine its CMs. Once again there were modes that did not completely satisfy the field orthogonality condition (2.3-21), and so were discarded as non-physical. These non-physical modes were again those that were inductive at frequencies lower than their resonance. The far-zone eigenfields of the first five physical CMs are plotted in Fig.5.3-5, and the eigenvalues of the first three physical CMs in Fig.5.3-6.

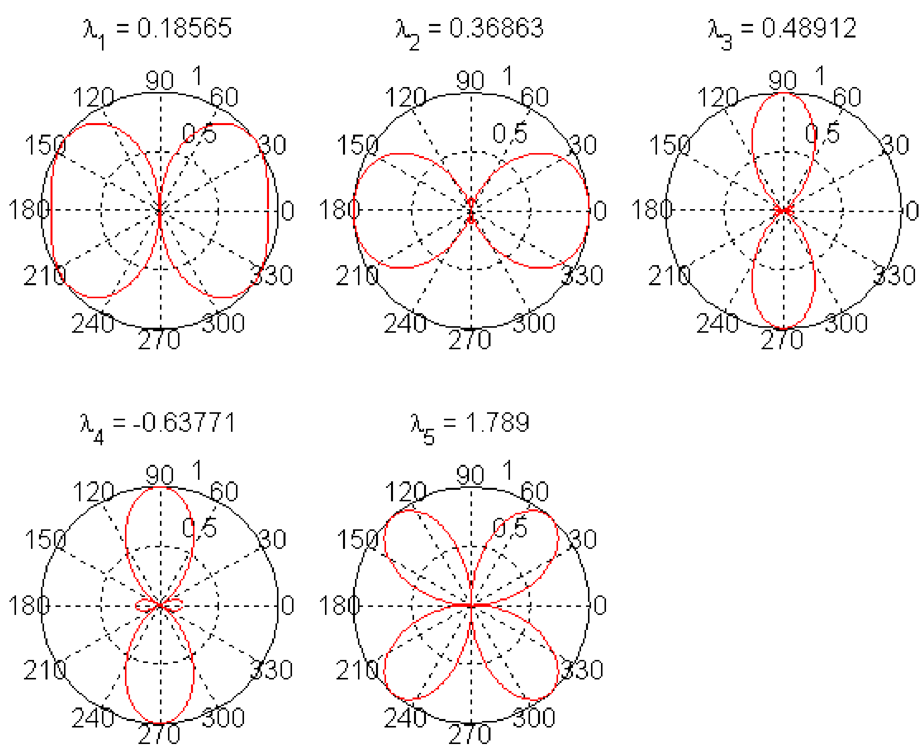

Figure 5.3-5 Normalized far-zone eigenfields of the physical CMs computed using the surface integral equation approach, at 500 MHz.

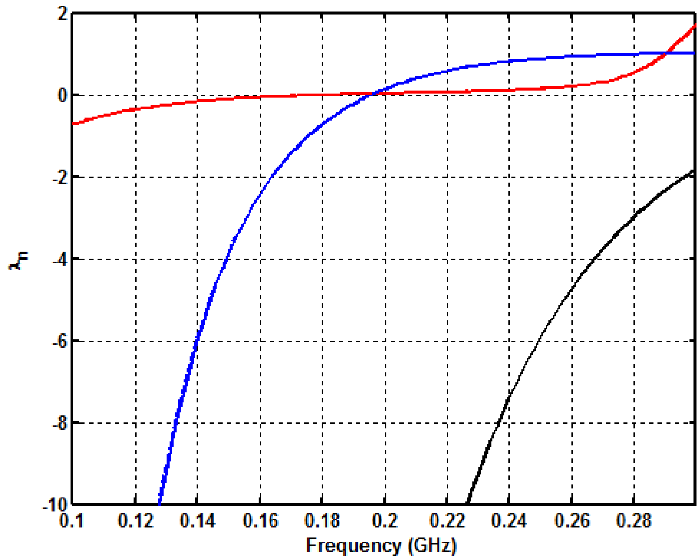

Figure 5.3-6: Comparison between eigenvalues computed using the surface formulation (solid line) and volume formulation (dashed line, not visible because it coincides with the solid one).

5.3.3 On the Possibility of Using Alternative Surface Integral Equation Formulations

We mentioned in Section 2.9 that there are very many surface integral equation formulations that can be derived. The preferred formulation, namely that called PMCHWT, was used in Sections 5.3.1 and 5.3.2, and will be used in Section 5.3.4 for three-dimensional objects. As part of the research for this thesis it was decided to investigate whether alternative surface formulations might not produce the non-physical modes mentioned in the previous section. We thought that this perhaps occurred due to the fact that both types of current density are present. It was therefore decided to study a 2-D TM_z formulation for scattering from penetrable objects that involved electric surface current densities only. The proposed formulation is extracted from [YUAN87,Sec.III]. Some minor modifications were needed. The object is modelled in terms of two electric surface current densities, one ”internal” and one “external”. Application of the boundary conditions leads [YUAN87], in the notation of Section 5.3.1, to the coupled integral equations

$$\mathcal{L}_{\mathrm{EJ}}^{\mathrm{e}}\left\{S_d^-,\bar{J}^{ext}\right\}+\mathcal{L}_{\mathrm{EJ}}^{\mathrm{e}}\left\{S_d^-,\bar{J}^{\mathrm{int}}\right\}+\mathcal{L}_{\mathrm{EJ}}^{d}\left\{S_d^+,\bar{J}^{ext}\right\}+\mathcal{L}_{\mathrm{EJ}}^{d}\left\{S_d^+,\bar{J}^{\mathrm{int}}\right\}=\bar{E}_{\tan}^{inc}(S_d^-) \qquad (5.3\text{-}14)$$

$$\mathcal{L}_{\mathrm{HJ}}^{\mathrm{e}}\left\{S_d^-,\bar{J}^{ext}\right\}+\mathcal{L}_{\mathrm{HJ}}^{\mathrm{e}}\left\{S_d^-,\bar{J}^{\mathrm{int}}\right\}+\mathcal{L}_{\mathrm{HJ}}^{\mathrm{d}}\left\{S_d^+,\bar{J}^{ext}\right\}+\mathcal{L}_{\mathrm{HJ}}^{\mathrm{d}}\left\{S_d^+,\bar{J}^{\mathrm{int}}\right\}=\bar{H}_{\tan}^{inc}(S_d^-) \qquad (5.3\text{-}15)$$

where,

$$\mathcal{L}_{\mathrm{EJ}}^{\mathrm{e}}\left\{S_d^-,\bar{J}^{ext}\right\}+\mathcal{L}_{\mathrm{EJ}}^{\mathrm{e}}\left\{S_d^-,\bar{J}^{\mathrm{int}}\right\}=\hat{n}\times\bar{E}_e^{scat}\left\{S_d^-,\bar{J}^{ext},\bar{J}^{\mathrm{int}}\right\} \qquad (5.3\text{-}16)$$

$$\mathcal{L}_{\mathrm{EJ}}^{d}\left\{S_d^+,\bar{J}^{ext}\right\}+\mathcal{L}_{\mathrm{EJ}}^{d}\left\{S_d^+,\bar{J}^{\mathrm{int}}\right\}=\hat{n}\times\bar{E}_d^{scat}\left\{S_d^+,\bar{J}^{ext},\bar{J}^{\mathrm{int}}\right\} \qquad (5.3\text{-}17)$$

$$\mathcal{L}_{\mathrm{HJ}}^{\mathrm{e}}\left\{S_d^-,\bar{J}^{ext}\right\}+\mathcal{L}_{\mathrm{HJ}}^{\mathrm{e}}\left\{S_d^-,\bar{J}^{\mathrm{int}}\right\}=\hat{n}\times\bar{H}_e^{scat}\left\{S_d^-,\bar{J}^{ext},\bar{J}^{\mathrm{int}}\right\} \qquad (5.3\text{-}18)$$

and

$$\mathcal{L}_{\mathrm{HJ}}^{\mathrm{d}}\left\{S_d^+,\bar{J}^{ext}\right\}+\mathcal{L}_{\mathrm{HM}}^{\mathrm{d}}\left\{S_d^+,\bar{J}^{\mathrm{int}}\right\}=\hat{n}\times\bar{H}_d^{scat}\left\{S_d^+,\bar{J}^{ext},\bar{J}^{\mathrm{int}}\right\} \qquad (5.3\text{-}19)$$

Using pulse expansion functions and delta weighting functions as was done in Section 5.3.1, the moment method one is able to derive matrix equation

$$\begin{bmatrix}\left[Z^{\mathrm{int}}\right] & \left[Z^{ext}\right]\\ \left[Y^{\mathrm{int}}\right] & \left[Y^{ext}\right]\end{bmatrix}\begin{bmatrix}\left[I^{\mathrm{int}}\right]\\ \left[-I^{ext}\right]\end{bmatrix}=\begin{bmatrix}\left[V^{i}\right]\\ \left[I^{i}\right]\end{bmatrix} \qquad (5.3\text{-}20)$$

with

$$V_m^i=\left\langle\bar{W}_m,\bar{E}^i(S_d^-)\right\rangle \qquad (5.3\text{-}21)$$

$$I_m^i=\left\langle\bar{W}_m,\hat{\mathrm{n}}\mathrm{x}\,\bar{H}^i(S_d^-)\right\rangle \qquad (5.3\text{-}22)$$

$$Z_{mn}^{\mathrm{int}}=\left\langle\bar{W}_m,\hat{n}\times\bar{E}_e^{scat}\left\{S_d^-,\bar{J}^{ext},\bar{J}^{\mathrm{int}}\right\}\right\rangle \qquad (5.3\text{-}23)$$

and

$$V^i=\left\langle\bar{W}_m,\bar{E}^i(S_d^-)\right\rangle \qquad (5.3\text{-}24)$$

Detailed expressions that can be used for the numerical evaluation of the above matrix terms are given in Appendix III. A computer code *2DPBJ* was developed based on this formulation and validated by finding the scattered field for given incident fields. Unfortunately, even though the individual sub-matrices are symmetric, the complete operator matrix is asymmetric (as for the PMCHWT case) but cannot be symmetrized in the manner of (5.2-5), whereas the PMCHWT formulation can. It, and several other possible alternative surface formulations, thus appear to be inappropriate for characteristic mode work.

5.3.4 Numerical Experiments on the Characteristic Modes of Three-Dimensional Penetrable Objects

We next move to the discussion of the CMs of three-dimensional objects using a PMCHWT surface integral equation formulation. All cases are simulated in FEKO, utilizing it in the same manner as done for PEC objects, as importantly clarified in the second paragraph of Section 5.1. In essence the code FEKO simultaneously solves the pair of coupled integral equations (2.9-1) and (2.9-2) whether for magneto-dielectric, solely dielectric, or solely magnetic objects. It meshes the surface of the 3-D object into triangles, in which are placed sophisticated expansion and weighting functions. Application of the method of moments then results in a matrix equation of the form (2.8-3). The CMs are then found as described in the first paragraph of this Section 5.3.

We computed the CMs for the notched rectangular dielectric resonator (RDR) discussed in Section 5.2.3. A total of 1470 expansion functions (490 triangles) were used at all frequency samples in the range 6.0 GHz to 6.4 GHz. The CMs were all initially considered tentative, and the values of the current and field orthogonality expressions were examined. Those CMs that satisfy the far-zone field orthogonality requirements were retained as physical CMs, and the remainder discarded[11]. Their behaviour is presented in Fig.5.3-7 and 5.3-8, and their orthogonality satisfaction in Tables 5.3-4 and 5.3-5. Plots of the far-zone eigenfields are given in Fig.5.3-9, and are seen to be the same as those found for the identical notched RDR in Part B of Section 5.2.3 using the volume formulation. A comparison of the first three physical CMs found using the volume and surface formulations is provided in Fig.5.3-10. We conjecture that the difference is due to the fact that the volume formulation was only able to use a coarse mesh (for

[11] These non-physical modes were again those that were inductive at frequencies lower than their resonance, but we are not able to make generalizations.

computational reasons given in Section 5.2.3) whereas the surface formulation is easily able to use a much finer mesh.

The equivalent surface currents are not actual physical current densities in the manner that surface conduction currents on PEC objects, or the volume currents in penetrable objects, are. When using CMs in antenna design physical currents are needed to determine where to place feeds in order to excite the desired CMs. When the surface formulation is used, the equivalent surface current densities can be used to compute the fields inside the penetrable object itself. This is shown in Fig.5.3-11 for the notched RDR under discussion. Inspection of Fig.5.3-11, and the plots in Fig.5.2-21 (a) and (b) obtained from the volume formulation, shows that these field distributions are the same. We can use these fields inside the object itself to determine the actual volume polarization currents using

$$\bar{J}_{eq}(\bar{r}) = j\omega\{\varepsilon_d - \varepsilon_o\}\bar{E}(\bar{r}) \qquad \bar{r} \in V_d \tag{5.3-25}$$

and

$$\bar{M}_{eq}(\bar{r}) = j\omega\{\mu_d - \mu_o\}\bar{H}(\bar{r}) \qquad \bar{r} \in V_d \tag{5.3-26}$$

where V_d is the volume occupied by the penetrable object.

Table 5.3-4: Numerical value of (5.2-7a) at 6.12 GHz for the first five physical CMs of the notched RDR with $\varepsilon_d = 37.84\varepsilon_0$ and $\mu_d = \mu_0$

m/n	1	2	3	4	5
1	-1.000	0.000	0.000	0.000	0.000
2	0.000	-1.000	0.000	0.000	0.000
3	0.000	0.000	-1.000	0.000	0.000
4	0.000	0.000	0.000	-1.000	0.000
5	0.000	0.000	0.000	0.000	-1.000

Table 5.3-5 : Numerical value of (2.3-21) at 6.12 GHz for the first five physical CMs of the notched RDR with $\varepsilon_d = 37.84\varepsilon_0$ and $\mu_d = \mu_0$, using 101 integration points in the θ-direction and 126 points in the φ-direction.

m/n	1	2	3	4	5
1	0.974+0.000i	-0.001-0.009i	0.000+0.000i	-0.000-0.000i	0.000+0.000i
2	-0.001+0.009i	1.000+0.000i	-0.000+0.000i	-0.000-0.000i	0.000+0.000i
3	0.000-0.000i	-0.000-0.000i	0.999+0.000i	-0.000+0.000i	0.000-0.000i
4	-0.000+0.000i	-0.000+0.000i	-0.000-0.000i	0.998+0.000i	0.001+0.010i
5	0.000-0.000i	0.000-0.000i	0.000+0.000i	0.001-0.010i	0.988+0.000i

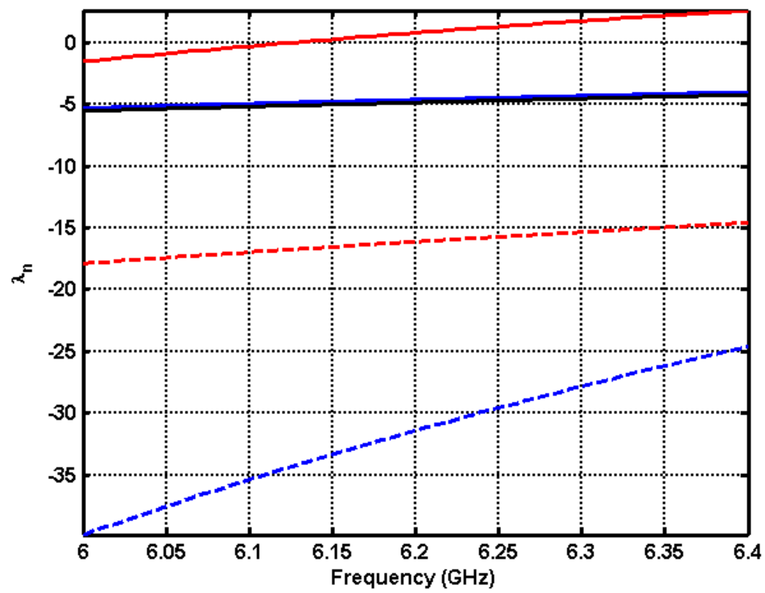

Figure 5.3-7: Eigenvalues of the first five physical CMs of the notched RDR with $\varepsilon_d = 37.84\varepsilon_0$ and $\mu_d = \mu_0$. Colour coding is (——) λ_1, (——) λ_2, (——) λ_3, (– – –) λ_4, (– – –) λ_5.

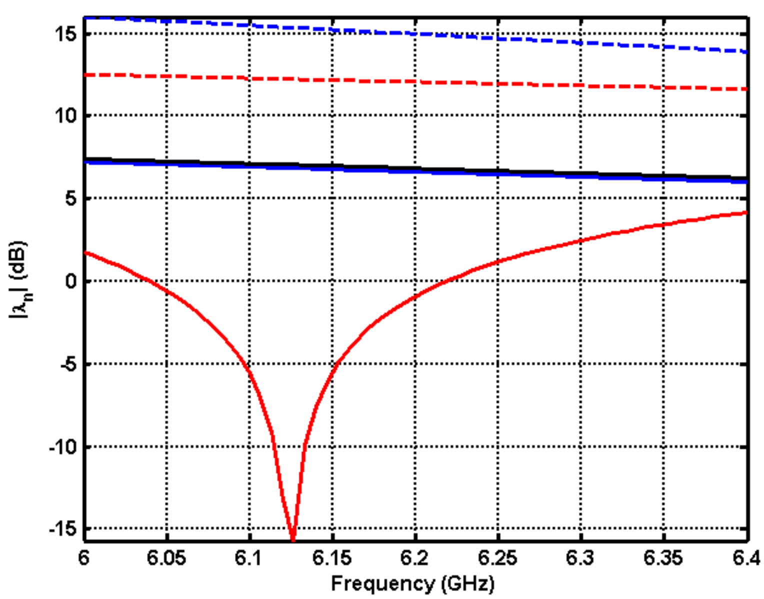

Figure 5.3-8: Eigenvalue magnitude (in dB) of the first five physical CMs of the notched RDR with $\varepsilon_d = 37.84\varepsilon_0$ and $\mu_d = \mu_0$. Colour coding is (——)λ_1, (——) λ_2, (——) λ_3, (– – –) λ_4, (– – –)λ_5

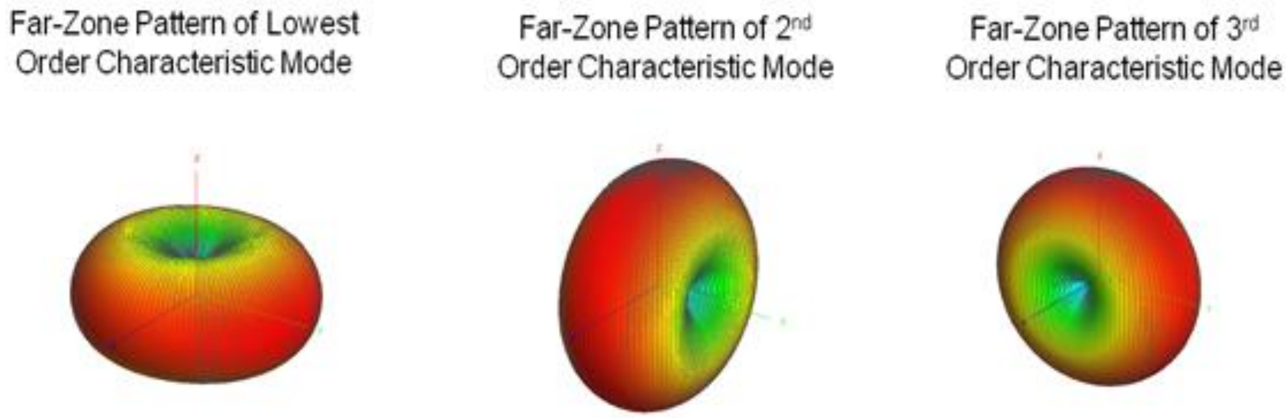

Figure 5.3-9: Far-zone patterns of the first three physical CMs at 6.12 GHz CMs of the notched RDR.

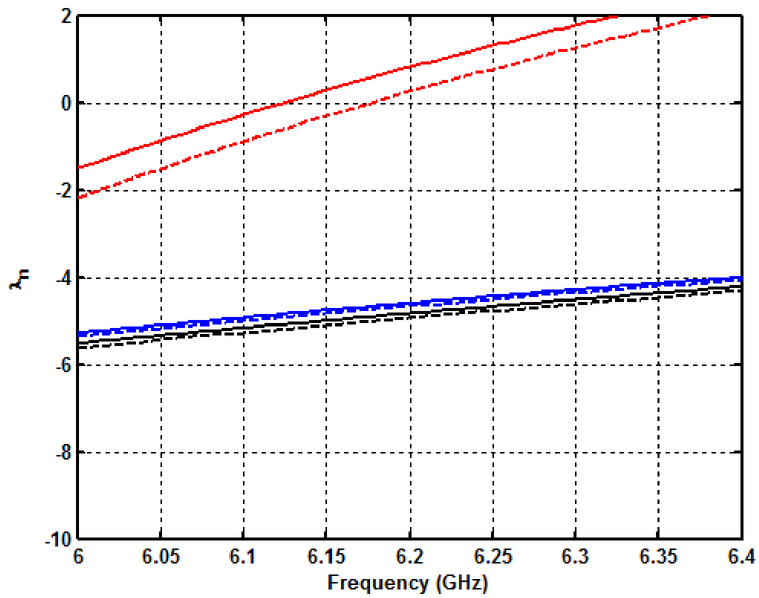

Figure 5.3-10: Comparison between the eigenvalues of the first three CMs of the notched RDR computed using the surface (solid line) and volume (dashed line) formulations.

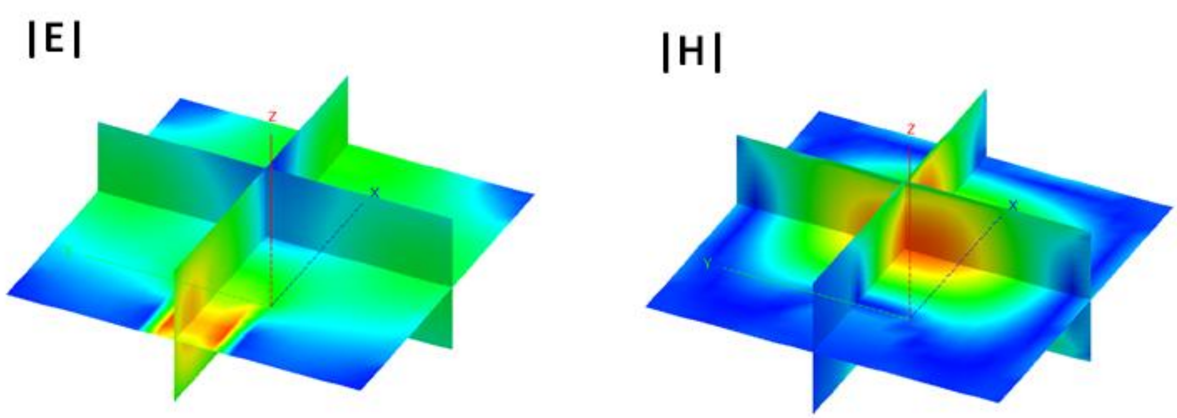

Figure 5.3-11: (a) Electric field, and (b) magnetic field, of the 1st CM in selected cuts of the notched RDR at 6.177 GHz using the PMCHWT surface integral equation formulation.

5.4 CONCLUDING REMARKS

A number of contributions have been presented in this chapter:

(a). We have demonstrated the actual computation of the characteristic mode eigenvalues, eigencurrents and eigenfields of penetrable objects for the first time. The use of both volume integral equation and surface integral equation formulations has been demonstrated.

(b). The volume integral equation approach has been shown to have what might prove, in antenna shape synthesis work, to be an excessive computational burden. Special computational resources are needed for performing the CM analysis of 3-D penetrable objects. The amount of memory, and the processing speed, needs to be high because of the massive mesh (and hence moment method matrix) sizes required. It would be wrong to think that, if one wishes to use characteristic mode analysis in antenna design (where many repeated characteristic mode analyses would be needed) that an ordinary personal computer would be sufficient. In the present work, a DELL workstation ("server") that has dual Intel(R) Xeon(R) CPUs (ES-2687W @ 3.10 GHz) and memory capacity of 64 GB has been used. Besides, a parallel processing license for both MATLAB and FEKO were available to us. In spite of this, the fine mesh that we would have desired for use in the volume integral equation approach was elusive.

(c). Many dielectric antennas are rotationally symmetric. We have shown in Section 4.9 that a BOR approach can be used to find the set of CMs of an object by finding the subsets associated with the BOR harmonics. The matrix equations for each of the BOR harmonics are small compared to the complete matrix equations of volume formulations that do not use a BOR viewpoint, and can be dealt with in parallel. Such BOR formulations of the volume integral equation have been published [KUCH00a, KUCH00b], albeit not in the context of characteristic modes. This would be useful in antenna shaping using CMs computed via volume formulations.

(d). We have shown that surface integral equation formulation does not possess the same computational burden, and so can be used with fine accurate meshing with relatively modest computational resources. This is of practical importance since the eventual aim of the characteristic mode analysis of penetrable objects is the shape synthesis of antennas made of such material, in the manner of [ETHI10c].

(e). We have revealed that the desirable surface integral equation formulation obtrudes CMs that are non-physical, but these can be identified and removed through far-zone field orthogonality checks. The development of such a check was made possible by the availability of the CM results from the volume formulation (which does not obtrude non-physical results). We have indicated how the actual volume polarization current densities can be easily obtained from the equivalent surface current densities.

(f). It was stated in Section 1.3 at the very start of the thesis that the "collective wisdom" (perhaps untried) considered the determination of the CMs of penetrable objects to be difficult. The computational burden of volume formulations, and the non-physical modes from surface formulations, would certainly lead to such a conclusion if only the one or the other method were to be tried. Fortunately, by examining both approaches, we have been able to show how the surface formulation can be used without confusion.

CHAPTER 6 General Conclusions

This thesis has made *three principal contributions*, which are as follows:

- In Chapter 5, we have actually computed the characteristic mode eigenvalues, eigencurrents and eigenfields of penetrable objects for what appears to be the first time. This has allowed us to validate the theory for these objects using both the volume and surface integral equation formulation. This opens the way for the use of characteristic mode theory in the shape synthesis of antennas made of penetrable material whose polarization current densities constitute the main radiating mechanism of the antenna, without having to select the feed type and location prior to shaping. This has only been done for conducting antennas up to now.

- Chapter 4 extended the sub-structure characteristic mode concept to problems involving both perfectly conducting (PEC) *and* penetrable material, with the PEC portion modelled by conduction surface current densities and the dielectric by volume electric polarization current densities. This will allow one to perform antenna shape synthesis on printed conducting antennas where the conduction currents are the main radiating mechanism, and the intention is to shape only the conducting portions of the antenna and not the dielectric substrate. Sub-structure modes have here been shown to be true characteristic modes in the sense that they possess both current and far-field orthogonality. This follows from the fact that we have shown that sub-structure modes can be viewed as characteristic modes that implicitly use modified Green's functions, but without such Green's functions being needed explicitly. This makes the concept really practical, since the desired Green's functions are not known explicitly in most cases.

- Also in Chapter 4, we have carefully interpreted various characteristic mode conceptual details, including the idea of modified characteristic modes and restricted characteristic modes. We have also shown why, in order to find the complete set of characteristic modes of a BOR object, it is sufficient to find the characteristic modes of the individual BOR harmonics.

Although *minor contributions* as far as the thesis is concerned, we have:

- In Chapter 3 collated and clarified the concept of a natural mode, and its differences to characteristic modes, using definitions and numerical results.

- In Chapter 2 presented a unifying summary of the theory of characteristic modes of both perfectly electrical conducting and penetrable objects.

Such reviews do not appear to be available elsewhere in one place.

There remain some issues related to characteristic modes whose investigation in *future work* are needed in order to be able to use them to perform the shape synthesis of dielectric antennas :

- Given a particular excitation (incident field) on an object, characteristic mode theory allows the easy computation of the excitation coefficients of the individual characteristic modes of the object actually excited. This is currently used in the shape synthesis of conducting antennas, and leads to practical feeding mechanisms. The details of how to do this, in practice, for antennas made of penetrable material needs to be examined and verified experimentally.

- A quantitative survey of the accuracy and computational-efficiency of various algorithms available for matrix eigenanalysis needs to be done.

- In spite of the success achieved in the work of the thesis, the impact of numerically-induced asymmetries in the constituent matrices of the discretized operator matrix (found using the method of moments), on the validity of the resulting characteristic mode eigenvalues and eigencurrents of a lossless object, should be investigated.

- The characteristic mode theory examined in this thesis for lossless penetrable materials should be extended to lossy objects.

- Although we have shown how to easily select the physical characteristic modes from the output of the eigenanalysis of the discretized operator of the surface integral equation formulation for penetrable objects, further investigation to determine the numerical reason for the appearance of (albeit easily rejected) non-physical modes in the first place.
- Many antennas are made of both conducting and penetrable material, where both the conduction currents and the polarization currents are equally important radiating mechanisms. The study of the characteristic modes (as opposed to sub-structure modes) of composite objects is necessary in order to be able to apply characteristic mode theory to the shape synthesis of such antennas is needed.

APPENDIX I

Integral Equation Models for Two-Dimensional PEC Cylinders of Circular Cross-Section

I.1 EFIE - TM CASE

We begin the derivation by stating the governing integral equation for TMz scattering from an infinite PEC cylinder of circular cross-section and radius a as

$$\frac{\eta k}{4}\int_0^{2\pi} J_z(\phi') H_o^{(2)}\left(k\left|\overline{\rho}-\overline{\rho'}\right|\right) a\, d\phi' = E_z^{inc}(\phi) \tag{AI-1}$$

where $\overline{\rho} = a\hat{\rho}$ and $\overline{\rho'} = a\hat{\rho}'$, with the unprimed coordinates referring to observation points anywhere on the cylinder and the primed coordinates referring to source locations on the same cylinder. We first note that, by the addition theorem, the Hankel function with the argument $k\left|\overline{\rho}-\overline{\rho'}\right|$ can be written in the form

$$H_o^{(2)}\left(k\left|\overline{\rho}-\overline{\rho'}\right|\right) = \sum_{q=-\infty}^{\infty} J_q(k\rho) H_q^{(2)}(k\rho') e^{jq(\phi-\phi')} \tag{AI-2}$$

and so with $\overline{\rho} = a\hat{\rho}$ and $\overline{\rho'} = a\hat{\rho}'$ we have

$$H_o^{(2)}\left(k\left|\overline{\rho}-\overline{\rho'}\right|\right) = \sum_{q=-\infty}^{\infty} J_q(ka) H_q^{(2)}(ka) e^{jq(\phi-\phi')} \tag{AI-3}$$

We want to select sets of expansion functions and weighting functions that are orthogonal with respect to the symmetric product over cylinder surface. Thus we expand the arbitrary current $J_z(\phi)$ using the expansion functions $e^{jn\phi}$, so that

$$J_z(\phi) = \sum_{n=-\infty}^{\infty} I_n e^{jn\phi} \tag{AI-4}$$

In order to maintain a Galerkin method to our approach (ensuring a symmetric discretized version of the impedance operator) we select weighting functions equal to the complex conjugate of the expansion functions, namely

$$W_m(\phi) = e^{-jm\phi} \tag{AI-5}$$

Substituting the convenient expression for the Hankel function into the integral equation, as well as representing the unknown current as the summation of expansion functions, reduces the EFIE to

$$\frac{\eta ka}{4}\int_0^{2\pi}\left\{\sum_{n=-\infty}^{\infty} I_n e^{jn\phi'}\right\}\left\{\sum_{q=-\infty}^{\infty} J_q(ka) H_q^{(2)}(ka) e^{jq(\phi-\phi')}\right\} d\phi' = E_z^{inc}(\phi) \tag{AI-6}$$

Rearranging, we find we can write this expression in a simpler form

$$\frac{\eta ka}{4}\sum_{n=-\infty}^{\infty} I_n \left\{\sum_{q=-\infty}^{\infty} J_q(ka) H_q^{(2)}(ka) e^{jq\phi}\int_0^{2\pi} e^{j(n-q)\phi'} d\phi'\right\} = E_z^{inc}(\phi) \tag{AI-7}$$

Note the integral

$$\int_0^{2\pi} e^{j(n-q)\phi'} d\phi' = \begin{cases} 2\pi & n = q \\ 0 & n \neq q \end{cases} \tag{AI-8}$$

and so (AI-7) simplifies to

$$\frac{\eta ka}{4}\sum_{n=-\infty}^{\infty} I_n J_n(ka) H_n^{(2)}(ka) 2\pi e^{jn\phi} = E_z^{inc}(\phi) \tag{AI-9}$$

We now take the symmetric product of both sides of the integral equation with respect to the weighting functions

$$\left\langle W_m(\phi), \frac{\eta ka}{4}\sum_{n=-\infty}^{\infty} I_n J_n(ka) H_n^{(2)}(ka) 2\pi e^{jn\phi}\right\rangle = \left\langle W_m(\phi), E_z^{inc}(\phi)\right\rangle \qquad \text{(AI-10)}$$

where the symmetric product is defined over the surface of the cylinder as

$$\left\langle f(\phi), g(\phi)\right\rangle = \int_0^{2\pi} f(\phi) g(\phi)\, a\, d\phi \qquad \text{(AI-11)}$$

So (AI-10) is

$$\int_0^{2\pi} W_m(\phi)\frac{\eta ka}{4}\sum_{n=-\infty}^{\infty} I_n J_n(ka) H_n^{(2)}(ka) 2\pi e^{jn\phi} d\phi = \int_0^{2\pi} W_m(\phi) E_z^{inc}(\phi) a\, d\phi \qquad \text{(AI-12)}$$

Substituting the expressions for the weighting functions gives

$$\int_0^{2\pi} \frac{\eta ka}{4}\sum_{n=-\infty}^{\infty} I_n J_n(ka) H_n^{(2)}(ka) 2\pi e^{j(n-m)\phi} d\phi = \int_0^{2\pi} E_z^{inc}(\phi) e^{-jm\phi}\, a d\phi \qquad \text{(AI-13)}$$

Simplifying further gives us

$$\sum_{n=-\infty}^{\infty} I_n \frac{\eta\pi ka}{2} J_n(ka) H_n^{(2)}(ka)\left\{\int_0^{2\pi} e^{j(n-m)\phi} d\phi\right\} = a\int_0^{2\pi} E_z^{inc}(\phi) e^{-jm\phi} d\phi \qquad \text{(AI-14)}$$

where we denote the discretized impedance operator terms by Z_{mn}, and the excitation vector term by V_m, with

$$Z_{mn} = \frac{\eta\pi ka}{2} J_n(ka) H_n^{(2)}(ka)\left\{\int_0^{2\pi} e^{j(n-m)\phi} d\phi\right\} = \begin{matrix} \eta\pi^2 ka J_n(ka) H_n^{(2)}(ka) & m = n \\ 0 & m \neq n \end{matrix} \qquad \text{(AI-15)}$$

and

$$V_m = a \int_0^{2\pi} E_z^{inc}(\phi) e^{-jm\phi} d\phi \quad \text{(AI-16)}$$

thus obtaining the matrix form

$$\sum_{n=-\infty}^{\infty} I_n Z_{mn} = V_m \quad \text{(AI-17)}$$

We observe that the impedance operator [Z] has been diagonalized. The Hankel function is related to Bessel and Neumann functions via the relationship

$$H_n^{(2)}(ka) = J_n(ka) - jY_n(ka) \quad \text{(AI-18)}$$

This allows us to write the real and imaginary parts of the impedance operator as

$$R_{mn} = \begin{cases} \eta\pi^2 ka J_n^2(ka) & m = n \\ 0 & m \neq n \end{cases} \quad \text{(AI-19a)}$$

and

$$X_{mn} = \begin{cases} -\eta\pi^2 ka J_n(ka) Y_n(ka) & m = n \\ 0 & m \neq n \end{cases} \quad \text{(AI-19b)}$$

The CM matrix eigenvalue problem is [HARR71]

$$[X][J] = \lambda [R][J] \quad \text{(AI-20)}$$

This can be rewritten as

$$[R]^{-1}[X][J]=\lambda[J] \qquad \text{(AI-21)}$$

unless $[R]^{-1}$ is not defined. Since [R] and [X] are diagonal matrices, we can write the eigenvalues as

$$\lambda_n = \frac{X_{nn}}{R_{nn}} \qquad R_{nn} \neq 0 \qquad \text{(AI-22)}$$

Using (AI-19) and (AI-22) we can write this as

$$\lambda_n = \frac{X_{nn}}{R_{nn}} = \frac{-\eta\pi^2 ka J_n(ka) Y_n(ka)}{\eta\pi^2 ka J_n^2(ka)} = -\frac{Y_n(ka)}{J_n(ka)} \qquad \text{(AI-23)}$$

Thus characteristic mode eigenvalues for an infinite PEC cylinder, for the TMz case, are

$$\lambda_n = -\frac{Y_n(ka)}{J_n(ka)} \qquad J_n(ka) \neq 0 \qquad \text{(AI-24)}$$

Notice that the index of the eigenvalue can be both negative and zero, as evident from the linear operator equation (AI-24). Given the symmetry of Bessel functions of the first and second kind, namely $J_{-n}(x)=(-1)^n J_n(x)$ and $Y_{-n}(x)=(-1)^n Y_n(x)$, the eigenvalue for index n is the same as the eigenvalue at index -n. Moreover, the eigenvalue does indeed exist at index n = 0.

I.2 MFIE - TM CASE

In the case of the circular cylinder of radius *a* the MFIE reduces to [WILT82]

$$J_z(\phi)+\lim_{\rho\to a}\left[\frac{a}{4j}\int_0^{2\pi} J_z(\phi')\frac{\partial}{\partial\rho}\left\{H_0^{(2)}\left(k\left|\bar{\rho}-\bar{\rho}'\right|\right)\right\}d\phi'\right]=H_\phi^{inc} \qquad \text{(AI-25)}$$

We have [WILT82]

$$\lim_{\rho\to a}\left[\frac{\partial}{\partial\rho}\left\{H_0^{(2)}\left(k\left|\bar{\rho}-\bar{\rho}'\right|\right)\right\}\right]=k\sum_{q=-\infty}^{\infty}J_n(ka)\,H_n^{(2)\prime}(ka)\,e^{jq(\phi-\phi')} \qquad \text{(AI-26)}$$

where the prime on the Hankel function, indicating differentiation with respect to its argument, should be noted. If we use entire domain expansion functions $e^{jn\phi}$ for the unknown current density $J_z(\phi)$, and weighting functions $e^{-jm\phi}$, then the MFIE operator discretizes to

$$\mathcal{L}_{mn}^{\mathrm{MFIE}}=\begin{cases}1+\dfrac{\pi ka}{2j}J_n(ka)H_n^{(2)\prime}(ka) & m=n\\ 0 & m\neq n\end{cases} \qquad \text{(AI-27)}$$

Following [NALB82] we write

$$\mathcal{L}_{mn}^{\mathrm{MFIE}}=U_{mn}-T_{mn} \qquad \text{(AI-28)}$$

where

$$T_{mn}=\begin{cases}-\dfrac{\pi ka}{2j}J_n(ka)H_n^{(2)\prime}(ka) & m=n\\ 0 & m\neq n\end{cases} \qquad \text{(AI-29)}$$

and

$$U_{mn} = \begin{cases} 1 & m = n \\ 0 & m \neq n \end{cases} \tag{AI-30}$$

The matrix eigenvalue problem for the characteristic modes is then [NALB82]

$$\{[U] - \mathrm{Re}[T]\}[J_{zn}] = \lambda_n \{\mathrm{Im}[T]\}[J_{zn}] \tag{AI-31}$$

Since all matrices are diagonal, we can write

$$\lambda_n = \frac{U_{nn} - \mathrm{Re}\{T_{nn}\}}{\mathrm{Im}\{T_{nn}\}} \tag{AI-32}$$

From (AI-29), and the fact that by definition $H_n^{(2)\prime}(ka) = J_n{}'(ka) - jY_n{}'(ka)$, we have

$$\mathrm{Re}\{T_{nn}\} = \frac{\pi ka}{2} J_n(ka) Y_n'(ka) \tag{AI-33}$$

and

$$\mathrm{Im}\{T_{nn}\} = \frac{\pi ka}{2} J_n(ka) J_n{}'(ka) \tag{AI-34}$$

Using (AI-33) and (AI-34) in (AI-32) gives

$$\lambda_n = \frac{1 - \dfrac{\pi ka}{2} J_n(ka) Y_n'(ka)}{\dfrac{\pi ka}{2} J_n(ka) J_n{}'(ka)} \tag{AI-35}$$

except when except when $J_n'(ka)$ and J_n (ka) are zero. We can rearrange the Wronskian $J_n(\xi)Y_n'(\xi) - Y_n(\xi)J_n'(\xi) = 2\pi/\xi$ into the form

$$J_n(\xi)Y_n'(\xi) = \frac{2\pi}{\xi} + Y_n(\xi)J_n'(\xi) \qquad \text{(AI-36)}$$

Substitution of (AI-36) into (AI-35) reduces the latter expression to

$$\lambda_n = -\frac{\frac{\pi ka}{2} Y_n(ka)J_n'(ka)}{\frac{\pi ka}{2} J_n(ka)J_n'(ka)} = -\frac{Y_n(ka)}{J_n(ka)} \qquad \text{(AI-37)}$$

except when $J_n'(ka)$ and J_n (ka) are zero.. This is the same expression as that found using the EFIE formulation and using "the recipe" of [HARR71].

If we had blindly used the recipe, given in [HARR71] for finding the CM eigenvalues using the EFIE, with the MFIE, we would have used

$$\lambda_n = \frac{\mathrm{Im}\{\boldsymbol{\mathcal{L}}_{nn}^{\mathrm{MFIE}}\}}{\mathrm{Re}\{\boldsymbol{\mathcal{L}}_{nn}^{\mathrm{MFIE}}\}} = \frac{\mathrm{Im}\{U_{nn} - T_{nn}\}}{\mathrm{Re}\{U_{nn} - T_{nn}\}} = \frac{\frac{\pi ka}{2} J_n(ka)J_n'(ka)}{1 - \frac{\pi ka}{2} J_n(ka)Y_n'(ka)} \qquad \text{(AI-38)}$$

Use of (AI-36) in the denominator of (AI-38) reduces the latter to

$$\lambda_n = \frac{\frac{\pi ka}{2} J_n(ka)J_n'(ka)}{1 - \frac{\pi ka}{2} J_n(ka)Y_n'(ka)} = \frac{\frac{\pi ka}{2} J_n(ka)J_n'(ka)}{\frac{\pi ka}{2} Y_n(ka)J_n'(ka)} = \frac{J_n(ka)}{Y_n(ka)} \qquad \text{(AI-39)}$$

which is not the correct CM eigenvalue.

APPENDIX II

Integral Equation Models for Two-Dimensional PEC Cylinders of Arbitrary Cross-Section – TM Case

II.1 INTEGRAL EQUATION AND A GENERAL MOMENT METHOD FROMULATION

This has been presented in Section 2.6-1.

II.2 EXPRESSIONS FOR THE MOMENT METHOD OPERATOR MATRIX TERMS AND FORCING VECTOR TERMS

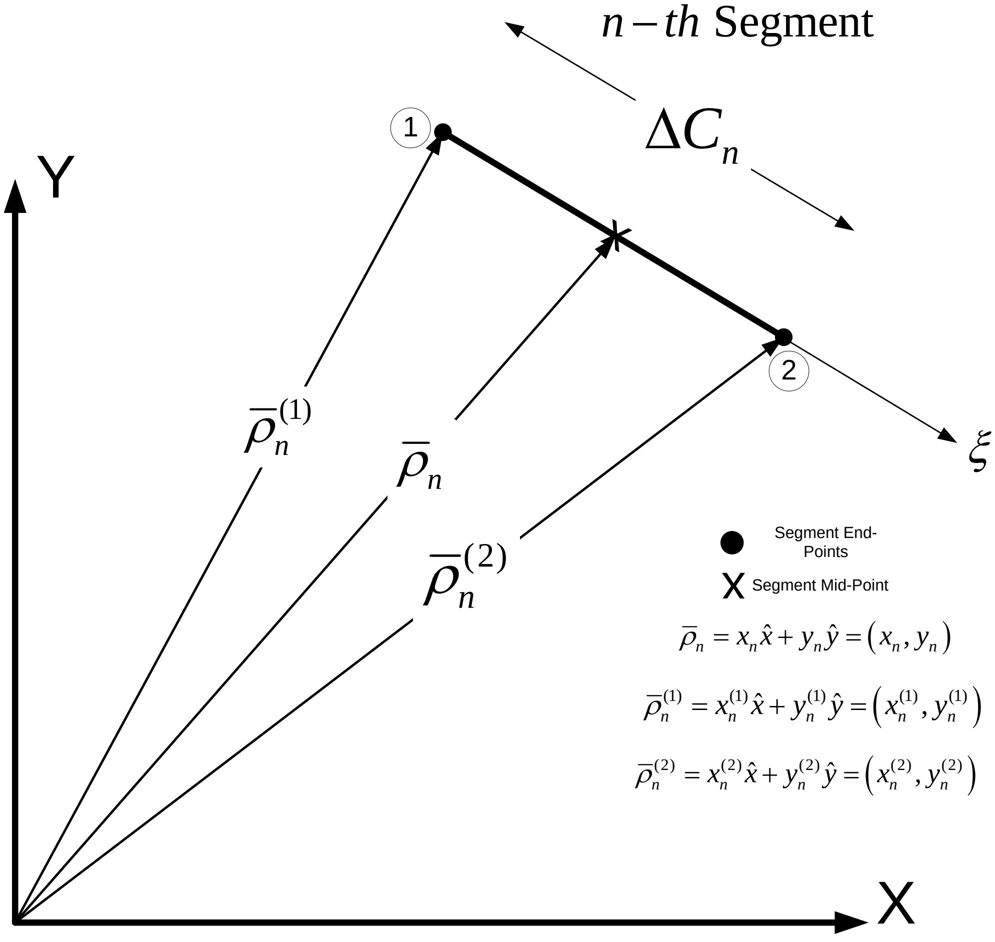

If pulse expansion functions and delta weighting functions are used, the detailed expression for the excitation vector terms is

$$V_m = \left\langle -E_z^{inc}\left(\bar{\rho}\right), W_{zm}\left(\bar{\rho}\right)\right\rangle = \left\langle -E_z^{inc}\left(\bar{\rho}\right), \delta\left(\bar{\rho}-\bar{\rho}_m\right)\right\rangle \tag{AII-1}$$

Use of the definition of the symmetric product therefore gives

$$V_m = -\int_{C_c} E_z^{inc}\left(\bar{\rho}\right)\delta\left(\bar{\rho}-\bar{\rho}_m\right)dC = -E_z^{inc}\left(\bar{\rho}_m\right) \tag{AII-2}$$

The field of an incident TM plane wave can be written as

$$E_z^{inc}\left(\bar{\rho}\right) = A_0 e^{-jk_0\left(-x_m\cos\phi_{inc}+y_m\sin\phi_{inc}\right)} \tag{AII-3}$$

and hence for such an incident field

$$V_m = -E_z^{inc}\left(\bar{\rho}_m\right) = -A_0 e^{-jk_0\left(-x_m\cos\phi_{inc}+y_m\sin\phi_{inc}\right)} \tag{AII-4}$$

Note that the excitation vector whose elements are given by (AII-4) will only be used to validate the code for this scattering problem. No excitation vector is needed in the eigenanalysis that gives us the characteristic modes.

The expression for the operator matrix terms is

$$Z_{mn} = \left\langle -j\omega A_{zn}\left(\bar{\rho}\right), W_{zm}\left(\bar{\rho}\right)\right\rangle = \left\langle -j\omega A_{zn}\left(\bar{\rho}\right), \delta\left(\bar{\rho}-\bar{\rho}_m\right)\right\rangle \tag{AII-5}$$

Therefore, (AII-5) becomes as follow

$$Z_{mn} = -j\omega A_{zn}\left(\bar{\rho}_m\right) = -\frac{\omega\mu}{4}\int_{C_c} P_n\left(\bar{\rho}'\right)H_0^{(2)}\left(k\left|\bar{\rho}_m-\bar{\rho}'\right|\right)dC' = -\frac{\omega\mu}{4}\int_{\Delta C_n} H_0^{(2)}\left(k\left|\bar{\rho}_m-\bar{\rho}'\right|\right)dC'$$

(AII-6)

where $P_n\left(\bar{\rho}'\right)$ is the pulse function. Gauss-Legendre quadrature can be used to evaluate (AII-6) for the off-diagonal terms ($m \neq n$). However, for the diagonal terms, the small argument form of the Hankel function can be used to find [VOLA11]

$$Z_{mm} = \frac{\eta k \Delta C_m}{4}\left[1 - j\frac{2}{\pi}\ln\left(\frac{\gamma k \Delta C_m}{4e}\right)\right] \qquad \text{(AII-8)}$$

where

$$\gamma = 1.781072416$$

$$k = \omega\sqrt{\mu_0 \varepsilon_0}$$

$$\eta = \sqrt{\mu / \varepsilon}$$

$$\Delta C_m = \sqrt{\left(x_m^{(2)} - x_m^{(1)}\right)^2 + \left(y_m^{(2)} - y_m^{(1)}\right)^2}$$

II.3 EXPRESSIONS FOR THE FIELD IN THE FAR-ZONE OF THE STRUCTURE

It is simpler to use the far-zone forms of the Green’s function to compute the far-zone fields. The scattered electric field due to the electric current density is given by

$$E_z^{scat}(\varphi) = -\frac{k\eta}{4}\sum_{n=1}^{N}\Delta C_n\, I_n\, e^{jkx_n^{(1)}\cos\phi} e^{jky_n^{(1)}\sin\phi}\int_{C'} e^{jk\{x'\cos\phi + y'\sin\phi\}}dC' \qquad \text{(AII-9)}$$

where N is the number expansion functions used.

II.4 CODE 2DCB

The above expressions have been implemented in MATLAB as code 2DCB (2-D Conducting Body)

APPENDIX III

Surface Integral Equation Models for Two-Dimensional Penetrable Cylinders of Arbitrary Cross-Section

III.1 *PMCHWT* FORMULATION

The matrix equation shown in (5.3-11) breaks down into the following

$$\left[V_g\right]=\begin{bmatrix}\left\langle \bar{W}_1,\bar{E}_{\tan}^{inc}(S_d^-)\right\rangle \\ \left\langle \bar{W}_2,\bar{E}_{\tan}^{inc}(S_d^-)\right\rangle \\ \vdots \\ \left\langle \bar{W}_m,\bar{E}_{\tan}^{inc}(S_d^-)\right\rangle \\ \vdots \\ \left\langle \bar{W}_N,\bar{E}_{\tan}^{inc}(S_d^-)\right\rangle\end{bmatrix} \qquad \left[I_g\right]=\begin{bmatrix}\left\langle \bar{W}_1,\bar{H}_{\tan}^{inc}(S_d^-)\right\rangle \\ \left\langle \bar{W}_2,\bar{H}_{\tan}^{inc}(S_d^-)\right\rangle \\ \vdots \\ \left\langle \bar{W}_m,\bar{H}_{\tan}^{inc}(S_d^-)\right\rangle \\ \vdots \\ \left\langle \bar{W}_N,\bar{H}_{\tan}^{inc}(S_d^-)\right\rangle\end{bmatrix} \tag{AIII-1}$$

$$\left[I_f\right]=\begin{bmatrix}a_1 \\ a_2 \\ \vdots \\ a_N\end{bmatrix} \qquad \left[V_f\right]=\begin{bmatrix}b_1 \\ b_2 \\ \vdots \\ b_N\end{bmatrix} \tag{AIII-2}$$

The operator matrix components are as follows

- Coupling between the expansion functions representing the $\bar{J}_s$.
-

$$Z_{mn}=\left\langle \bar{W}_m,\mathcal{L}_{\mathrm{EJ}}^{\mathrm{e}}\left\{S_d^-,\bar{f}_n\right\}\right\rangle+\left\langle \bar{W}_m,\mathcal{L}_{\mathrm{EJ}}^{d}\left\{S_d^+,\bar{f}_n\right\}\right\rangle \tag{AIII-3}$$

- Coupling between the expansion functions for $\bar{J}_s$ and $\bar{M}_s$.

$$C_{mn} = \left\langle \bar{W}_m, \mathcal{L}^{e}_{\text{HJ}}\left\{S_d^-, \bar{f}_n\right\} + \mathcal{L}^{d}_{\text{HJ}}\left\{S_d^+, \bar{f}_n\right\}\right\rangle \tag{AIII-4}$$

$$D_{mn} = \left\langle \bar{W}_m, \mathcal{L}^{e}_{\text{EM}}\left\{S_d^-, \bar{f}_n\right\} + \mathcal{L}^{d}_{\text{EM}}\left\{S_d^+, \bar{f}_n\right\}\right\rangle \tag{AIII-5}$$

It can be shown that $C_{mn} = -D_{mn}$.

- Coupling between the expansion functions representing the $\bar{M}_s$.

$$Y_{mn} = \left\langle \bar{W}_m, \mathcal{L}^{e}_{\text{HM}}\left\{S_d^-, \bar{f}_n\right\}\right\rangle + \left\langle \bar{W}_m, \mathcal{L}^{d}_{\text{HM}}\left\{S_d^+, \bar{f}_n\right\}\right\rangle \tag{AIII-6}$$

It can be shown that $Y^e_{mn} = Z^e_{mn} / \eta_e^2$ and $Y^d_{mn} = Z^d_{mn} / \eta_d^2$, due to duality.

The sub matrices Z_{mn}, C_{mn}, D_{mn} and Y_{mn} have been constructed through careful examination of certain terms $\hat{A}_{mn}$, $\hat{B}_{mn}$, $\hat{C}_{mn}$ and $\hat{D}_{mn}$ given in [GOGG90].

III.1.1 Moment Method Operator Matrix Terms

Each of the sub-matrices $[Z]$, $[Y]$, $[C]$ and $[D]$ is an N x N matrix. Since we are using the PMCHWT formulation discussed in Section 2.9, α = β = 1 should be used in all the expressions below.

$$Z_{mn} = \hat{B}^{ext}_{mn} + \alpha \hat{B}^{\text{int}}_{mn} \tag{AIII-7}$$

$$\hat{B}_{mn}^{ext} = \begin{cases} -\dfrac{k\eta\Delta C_n}{4}\left[1 - j\dfrac{2}{\pi}\ln\left(\dfrac{\gamma k\Delta C_n}{4e}\right)\right] & m = n \\ -\dfrac{k\eta\Delta C_n}{4}\displaystyle\int_{C_n} H_0^{(2)}\left(k\ \Delta\rho_{mn}\right)dC' & m \neq n \end{cases} \qquad \text{(AIII-8)}$$

$$\hat{B}_{mn}^{\text{int}} = \begin{cases} -\dfrac{k_d\eta_d\Delta C_n}{4}\left[1 - j\dfrac{2}{\pi}\ln\left(\dfrac{\gamma k_d\Delta C_n}{4e}\right)\right] & m = n \\ -\dfrac{k_d\eta_d\Delta C_n}{4}\displaystyle\int_{C_{n'}} H_0^{(2)}\left(k_d\Delta\rho_{mn}\right)dC' & m \neq n \end{cases} \qquad \text{(AIII-9)}$$

where

$$\gamma = 1.781072416$$

$$k = \omega\sqrt{\mu_0\varepsilon_0}$$

$$k_d = \omega\sqrt{\mu_d\varepsilon_d}$$

$$\eta = \sqrt{\mu_o / \varepsilon_o}$$

$$\eta_d = \sqrt{\mu_d / \varepsilon_d}$$

$$\Delta\rho_{mn} = \sqrt{\left(x_m - x'\right)^2 + \left(y_m - y'\right)^2}$$

$$\Delta C_n = \sqrt{\left(x_n^{(2)} - x_n^{(1)}\right)^2 + \left(y_n^{(2)} - y_n^{(1)}\right)^2}$$

$$D_{mn} = \hat{A}_{mn}^{ext} + \alpha\hat{A}_{mn}^{\text{int}} \qquad \text{(AIII-10)}$$

$$\hat{A}_{mn}^{ext} = \begin{cases} -\dfrac{1}{2} & m = n \\ \dfrac{k\Delta C_n}{4j}\displaystyle\int_{C'} (\hat{n}_n \cdot \Delta\hat{\rho}_{mn})H_1^{(2)}\left(k\Delta\rho_{mn}\right)dC' & m \neq n \end{cases} \qquad \text{(AIII-11)}$$

$$\hat{A}_{mn}^{\text{int}} = \begin{cases} \dfrac{1}{2} & m = n \\ \dfrac{k_d \Delta C_n}{4j} \displaystyle\int_{C'} (\hat{n}_n \cdot \Delta\hat{\rho}_{mn}) H_1^{(2)}\left(k_d \Delta\rho_{mn}\right) dC' & m \neq n \end{cases} \qquad \text{(AIII-12)}$$

where

$$\Delta\hat{\rho}_{mn} = \frac{\left(x_m - x'\right)\hat{x} + \left(y_m - y\right)\hat{y}}{\Delta\rho_{mn}}$$

$$\hat{n}_n = \frac{\left(x_n^{(2)} - x_n^{(1)}\right)\hat{x} + \left(y_n^{(2)} - y_n^{(1)}\right)\hat{y}}{\Delta C_n}$$

$$C_{mn} = \hat{D}_{mn}^{ext} + \alpha \hat{D}_{mn}^{\text{int}} \qquad \text{(AIII-13)}$$

$$\hat{D}_{mn}^{ext} = \begin{cases} -\dfrac{1}{2} & m = n \\ -\dfrac{jk\Delta C_n}{4} \displaystyle\int_{C'} (\hat{n}_m \cdot \Delta\hat{\rho}_{mn}) H_1^{(2)}\left(k\Delta\rho_{mn}\right) dC' & m \neq n \end{cases} \qquad \text{(AIII-14)}$$

$$\hat{D}_{mn}^{\text{int}} = \begin{cases} \dfrac{1}{2} & m = n \\ -\dfrac{jk_d\Delta C_n}{4} \displaystyle\int_{C'} (\hat{n}_m \cdot \Delta\hat{\rho}_{mn}) H_1^{(2)}\left(k_d\Delta\rho_{mn}\right) dC' & m \neq n \end{cases} \qquad \text{(AIII-15)}$$

where

$$\hat{n}_m = \frac{\left(y_m^{(2)} - y_m^{(1)}\right)\hat{x} - \left(x_m^{(2)} - x_m^{(1)}\right)\hat{y}}{\sqrt{\left(x_m^{(2)} - x_m^{(1)}\right)^2 + \left(y_m^{(2)} - y_m^{(1)}\right)^2}}$$

$$Y_{mn} = \hat{C}_{mn}^{ext} + \beta \hat{C}_{mn}^{\text{int}} \qquad \text{(AIII-16)}$$

$$\hat{C}_{mn}^{ext} = \begin{cases} \dfrac{1}{2\eta} H_1^{(2)}\left(\dfrac{k\Delta C_n}{2}\right) - \dfrac{k\Delta C_n}{4\eta}\left[1 - j\dfrac{2}{\pi}\ln\left(\dfrac{\gamma k \Delta C_n}{4e}\right)\right] & m = n \\ -\dfrac{\Delta C_n}{4\eta}\displaystyle\int_{C'} \left\{ \begin{array}{l} k(\hat{n}_n \cdot \Delta\hat{\rho}_{mn})(\hat{n}_m \cdot \Delta\hat{\rho}_{mn}) H_0^{(2)}\left(k\Delta\rho_{mn}\right) \\ \qquad + \left[(\hat{n}_n \cdot \hat{n}_m) - 2(\hat{n}_n \cdot \Delta\hat{\rho}_{mn})(\hat{n}_m \cdot \Delta\hat{\rho}_{mn})\right] \dfrac{H_1^{(2)}\left(k\Delta\rho_{mn}\right)}{\Delta\rho_{mn}} \end{array} \right\} dC' & m \neq n \end{cases}$$

(AIII-17)

$$\hat{C}_{mn}^{\text{int}} = \begin{cases} \dfrac{1}{2\eta_d} H_1^{(2)}\left(\dfrac{k_d\Delta C_{n'}}{2}\right) - \dfrac{k_d\Delta C_{n'}}{4\eta_0}\left[1 - j\dfrac{2}{\pi}\ln\left(\dfrac{\gamma k_0 \Delta C_n}{4e}\right)\right] & m = n \\ -\dfrac{\Delta C_n}{4\eta_d}\displaystyle\int_{C'} \left\{ \begin{array}{l} k_d(\hat{n}_n \cdot \Delta\hat{\rho}_{mn})(\hat{n}_m \cdot \Delta\hat{\rho}_{mn}) H_0^{(2)}\left(k_d\Delta\rho_{mn}\right) \\ \qquad + \left[(\hat{n}_n \cdot \hat{n}_m) - 2(\hat{n}_n \cdot \Delta\hat{\rho}_{mn})(\hat{n}_m \cdot \Delta\hat{\rho}_{mn})\right] \dfrac{H_1^{(2)}\left(k_d\Delta\rho_{mn}\right)}{\Delta\rho_{mn}} \end{array} \right\} dC' & m \neq n \end{cases}$$

(AIII-18)

III.1. 2 Excitation Vector Terms

If a TM plane wave is used as the incident field, then

$$V_{gm} = -A_0 e^{-jk\left(-x_m \cos\phi_{inc} + y_m \sin\phi_{inc}\right)} \tag{AIII-19}$$

and

$$I_{gm} = -\frac{A_0}{\eta_0 \Delta C_m}\left\{-[x_m^{(2)} - x_m^{(1)}]\sin\phi_{inc} + [y_m^{(2)} - y_m^{(1)}]\cos\phi_{inc}\right\} e^{-jk\left(x_m\cos\phi_{inc} + y_m \sin\phi_{inc}\right)} \tag{AIII-20}$$

where

$$\Delta C_m = \sqrt{\left(x_m^{(2)} - x_m^{(1)}\right)^2 + \left(y_m^{(2)} - y_m^{(1)}\right)^2}$$

ϕ_{inc} is the angle of incidence, and A_0 is the complex amplitude.

Note that the excitation vector whose elements are given by (AII-19) and (AII-20) will only be used to validate the code for this scattering problem. No excitation vector is needed in the eigenanalysis that gives us the characteristic modes.

III.1.3 Expressions For The Scattered Field In The Far-Zone

The scattered field due to the electric current density in the far zone is

$$E_z^{scat}\{\phi, J_z\} = -\frac{k\eta}{4}\sum_{n=1}^{N}\Delta C_n\, I_{fn}\, e^{jkx_n^{(1)}\cos\phi} e^{jky_n^{(1)}\sin\phi}\int_{C'} e^{jk\{x'\cos\phi + y'\sin\phi\}} dC' \qquad \text{(AIII-21)}$$

The scattered field due to the magnetic current density in the far zone is

$$E_z^{scat}\{\varphi, M_t\} = \frac{k}{4}\sum_{n=1}^{N}\Delta C_{n'}\, V_{fn}\, e^{jkx_n^{(1)}\cos\phi} e^{jky_n^{(1)}\sin\phi}\left\{[y_n^{(2)} - y_n^{(1)}]\cos\phi - [x_n^{(2)} - x_n^{(1)}]\sin\phi\right\}\int_{C'} e^{jk\{x'\cos\phi + y'\sin\phi\}} dC' \qquad \text{(AIII-22)}$$

The scattered electric field in the far zone can be evaluated using the following expression

$$E_z^{scat}(\phi) = E_z^{scat}\{\phi, J_z\} + E_z^{scat}\{\phi, M_t\} \qquad \text{(AIII-23)}$$

III.1.4 Verification of the Code *2DPBS*

In order to be sure of the validity of the above formulation, it is coded in MATLAB to enable us to calculate the operator matrix terms, current coefficients, excitation vector, and scattered electric fields. Once the operator matrix is completely available through the MATLAB calculation, CM analysis can be performed regardless of the specified incident field. In addition, the code is made to check the matrix symmetry, CM current orthogonality, and CM field orthogonality.

A circular cross-section cylinder filled with dielectric material whose permittivity is $\varepsilon_d = 4\varepsilon_o$, radius set to 0.1λ is considered for verification purposes. A TM plane wave is incident on the cylinder at $\phi_i = 0^o$. The following graph shows the scattered field in the far zone which compares to the result obtained using FEKO. The periodic boundary condition (PBC) feature, in FEKO, enables us to analyze infinite periodic structure by simulating a unit cell element which is equivalent to the 2-D infinitely long cylinder. Of course, only a plane wave is permitted with the use of this feature. Therefore, the result obtained in 2DPBS can be verified with that simulated in FEKO.

Fig.2 shows the far-zone scattered field pattern of two identical dielectric cylinders each of radius 0.2 λ filled with dielectric with permittivity $\varepsilon_d = 4\varepsilon_o$. The distance between the centers of the two cylinders is 0.8λ, and they are located symmetrically with respect to the x-axis and y-axis. The outcome of the coded formulation in MATLAB was compared to that found using FEKO.

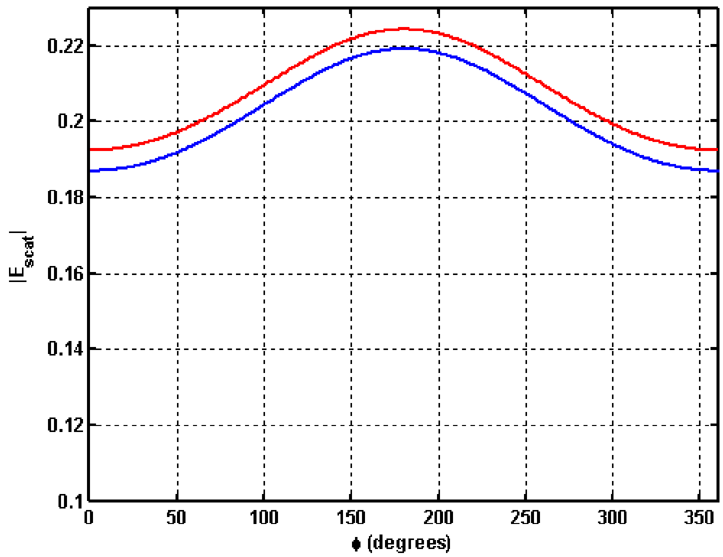

Fig. 1: the magnitude of the electric scattered field - 2-D circular cylinder. (——) 2DPBS (——) FEKO computation

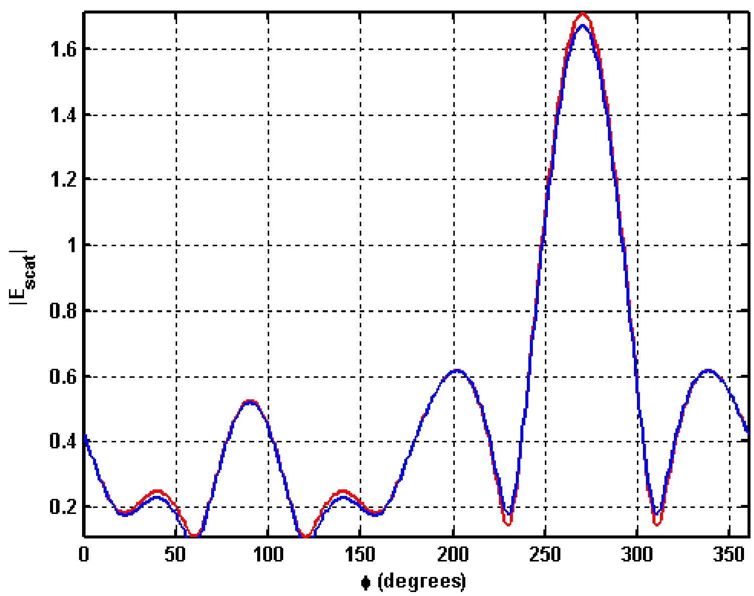

Fig. 2: the magnitude of the electric scattered field - two identical and parallel 2-D circular cylinders. (——) 2DPBS (——) FEKO computation

III. 2 TWO ELECTRIC CURRENT DENSITY FORMULATION - CODE 2DPBJ

III.2.1 Moment Method Operator Matrix Terms

We write the full matrix expressions discussed in Section 5.3.4 The various matrix equation terms are as follows

$$Z_{mn}^{\text{int}} = \begin{cases} -\frac{\eta k \Delta C_m}{4}\left[1 - j\frac{2}{\pi}\ln\left(\frac{\gamma k_d \Delta C_m}{4e}\right)\right] & m = n \\ -\frac{\eta k \Delta C_n}{8}\int_{-1}^{1} H_0^{(2)}\left(k_d \Delta\rho_{mn}\right) dC_n^{'} & m \neq n \end{cases} \tag{AIII-24}$$

$$Z_{mn}^{ext} = \begin{cases} -\frac{\eta k \Delta C_m}{4}\left[1 - j\frac{2}{\pi}\ln\left(\frac{\gamma k \Delta C_m}{4e}\right)\right] & m = n \\ -\frac{k\eta \Delta C_n}{8}\int_{-1}^{1} H_0^{(2)}\left(k \Delta\rho_{mn}\right) dC_n^{'} & m \neq n \end{cases} \tag{AIII-25}$$

$$Y_{mn}^{\text{int}} = \begin{cases} -\tfrac{1}{2} & m = n \\ \frac{k_d \eta \Delta C_{n'}}{8j}\int_{-1}^{1} (-t_m.\frac{\left(x_m - x'\right)}{\Delta\rho_{mn}}\hat{y} + t_m.\frac{\left(y_m - y\right)}{\Delta\rho_{mn}}\hat{\text{x}})\frac{H_1^{(2)}\left(k_d \Delta\rho_{mn}\right)}{\Delta\rho_{mn}} dC_n^{'} & m \neq n \end{cases} \tag{AIII-26}$$

$$Y_{mn}^{ext} = \begin{cases} \tfrac{1}{2} & m = n \\ \frac{k\eta \Delta C_{n'}}{8j}\int_{-1}^{1} (-t_m.\frac{\left(x_m - x'\right)}{\Delta\rho_{mn}}\hat{y} + t_m.\frac{\left(y_m - y\right)}{\Delta\rho_{mn}}\hat{\text{x}})\frac{H_1^{(2)}\left(k \Delta\rho_{mn}\right)}{\Delta\rho_{mn}} dC_n^{'} & m \neq n \end{cases} \tag{AIII-27}$$

$$V_m^i = A_0 e^{-jk\left(-x_m \cos\phi_{inc} + y_m \sin\phi_{inc}\right)} \qquad \text{(AIII-28)}$$

$$I_m^i = -\frac{A_0}{\Delta C_m}\left\{-[x_m^{(2)} - x_m^{(1)}]\sin\phi_{inc} + [y_m^{(2)} - y_m^{(1)}]\cos\phi_{inc}\right\} e^{-jk\left(x_m \cos\phi_{inc} + y_m \sin\phi_{inc}\right)} \qquad \text{(AIII-29)}$$

where

$\Delta C_m = \sqrt{\left(x_m^{(2)} - x_m^{(1)}\right)^2 + \left(y_m^{(2)} - y_m^{(1)}\right)^2}$

ϕ_{inc} is the incidence angle

A_0 is the complex amplitude of the incident plane wave.

III.2.2 Expressions For The Scattered Field In The Far-Zone

The scattered electric field due to the external electric current in the far zone is evaluated using

$$E_z^{scat}(\varphi) = -\frac{k\eta}{4}\sum_{n=1}^{N}\Delta C_n\, I_n^{ext}\, e^{jkx_n^{(1)}\cos\phi} e^{jky_n^{(1)}\sin\phi}\int_{C'} e^{jk\{x'\cos\phi + y'\sin\phi\}} dC' \qquad \text{(AIII-30)}$$

III.2.3 Verification Of The Code *2DPBJ*

The scattered field pattern for the same dielectric circular cylinder discussed in the previous section in this Appendix is depicted in Fig. 2.

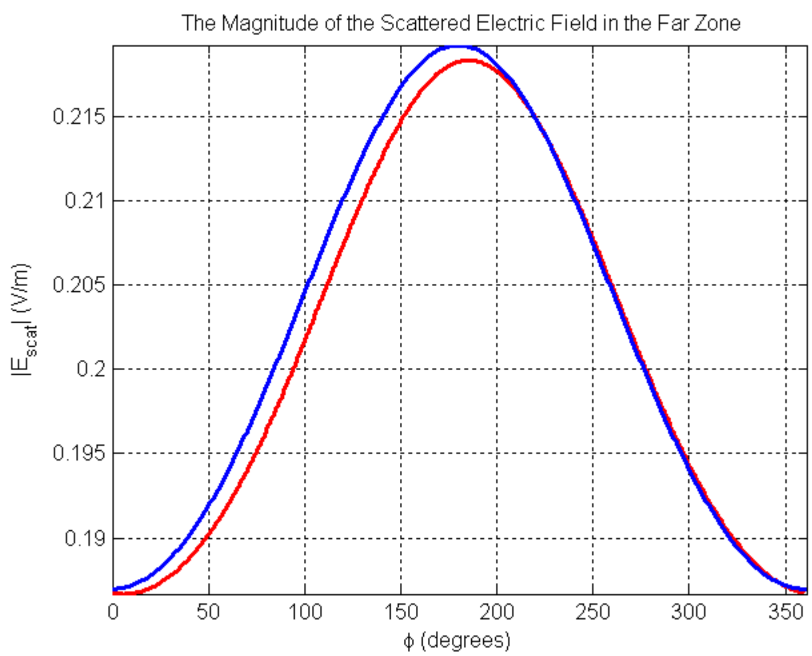

Fig. 3: : The magnitude of the electric scattered field in the far zone - 2-D circular cylinder. (———) 2DPBJ (———) FEKO computation

APPENDIX IV

Volume Integral Equation Models for Two-Dimensional Penetrable Cylinders of Arbitrary Cross-Section

IV.1 INTRODUCTION

The detailed expressions for the operator matrix and excitation vector terms discussed in Section 5.2-1 are presented here. The expansion and weighting functions is expressed as the following

$$J_{zn}\left(\bar{\rho}\right)=\begin{cases}1 & \text{if } \ \bar{\rho}\in\Delta S_n \\ 0 & \text{otherwise}\end{cases} \tag{AIV-1}$$

and

$$W_{zm}\left(\bar{\rho}\right)=\delta\left(\bar{\rho}-\bar{\rho}_m\right) \tag{AIV-2}$$

for $n=1,2,......N$, and $m=1,2,......N$, where $\bar{\rho}_m$ denotes the center of the *m-th* element and ΔS_n donates the n-th element.

IV.2 MOMENT METHOD MATRIX TERMS

A symmetric product between the weighting function and the L.H.S of the integral equation shown in (5.2-3) leads to the following expression

$$\begin{aligned}
Z_{mn} &= \left\langle \frac{\eta J_{zn}\left(\bar{\rho}\right)}{jk\left\{\varepsilon_d-\varepsilon_e\right\}} - E_{zn}^{scat}\left(\bar{\rho}\right), W_{zm}\left(\bar{\rho}\right)\right\rangle \\
&= \left\langle \frac{\eta J_{zn}\left(\bar{\rho}\right)}{jk\left\{\varepsilon_d/\varepsilon - \varepsilon_e/\varepsilon\right\}} + \frac{k\eta}{4}\iint_{S_d} J_z(\bar{\rho}')H_o^{(2)}\left(k\left|\bar{\rho}-\bar{\rho}'\right|\right)dS', \delta(\bar{\rho}_m-\bar{\rho})\right\rangle \qquad \text{(AIV-3)} \\
&= \frac{\eta J_{zn}\left(\bar{\rho}\right)}{jk\left\{\varepsilon_d/\varepsilon - \varepsilon_e/\varepsilon\right\}} + \frac{k\eta}{4}\iint_{S_d} J_z(\bar{\rho}')H_o^{(2)}\left(k\left|\bar{\rho}-\bar{\rho}'\right|\right)dS'
\end{aligned}$$

Since $J_{zn}(\bar{\rho})$ is non-zero only over ΔS_n, the term

$$J_{zn}(\bar{\rho}_m) = \delta_{mn} = \begin{cases} 1 & m = n \\ 0 & m \neq n \end{cases} \tag{AIV-4}$$

and hence,

$$\begin{aligned} Z_{mn} &= \frac{\eta\,\delta_{mn}}{jk\left\{ {\varepsilon_d}/{\varepsilon} - {\varepsilon_e}/{\varepsilon} \right\}} + \frac{k\eta}{4} \iint_{\Delta S_n} H_o^{(2)}\left(k\left|\bar{\rho} - \bar{\rho}'\right|\right) dS' \\ &= \frac{\eta\delta_{mn}}{jk\left\{ {\varepsilon_d}/{\varepsilon} - {\varepsilon_e}/{\varepsilon} \right\}} + \frac{k\,\eta}{4} \int_{y_n^{(1)}}^{y_n^{(2)}} \int_{x_n^{(2)}}^{x_n^{(1)}} H_o^{(2)}\left(k\rho_m\right) dx' dy' \end{aligned} \tag{AIV-5}$$

where

$$x_n^{(1)} = x_n - \frac{\Delta x_n}{2}$$

$$x_n^{(2)} = x_n + \frac{\Delta x_n}{2}$$

$$y_n^{(1)} = y_n - \frac{\Delta y_n}{2}$$

$$y_n^{(2)} = y_n + \frac{\Delta y_n}{2}$$

$$\rho_m = \sqrt{(x_m - x')^2 + (y_m - y')^2}$$

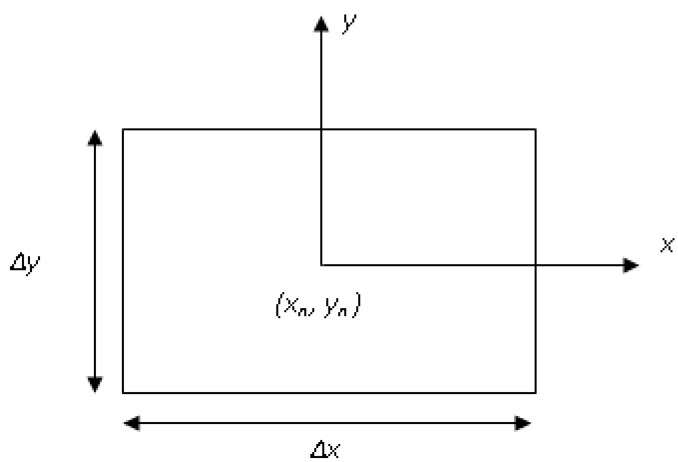

Fig. 4: Dielectric unit cell

IV.3 EXCITATION VECTOR

A symmetric product between the weighting function and the R.H.S of the integral equation shown in (5.2-3) leads to the following expression:

$$V_m = \left\langle E_z^{inc}(\bar{\rho}), W_{zm}(\bar{\rho}) \right\rangle \qquad \text{(AIV-6)}$$

The elements of $[V]$ can be numerically evaluated using

$$V_m = \left\langle E_z^{inc}(\bar{\rho}), W_{zm}(\bar{\rho}) \right\rangle = \iint_{\Delta S_m} \delta(\bar{\rho} - \bar{\rho}_m) E_z^{inc}(\bar{\rho})\, dS = E_z^{inc}(\bar{\rho}_m) \qquad \text{(AIV-7)}$$

A TM plane wave is used as an incident field.

$$E_z^{inc}(\bar{\rho}_m) = A_o e^{-jk(k_x\hat{x} + k_y\hat{y})} \qquad \text{(AIV-8)}$$

where A_o is the complex. The unit vector in the direction of a plane wave travelling towards the scatterer at an angle ϕ_i from the x axis is

$$\hat{k} = k_x\hat{x} + k_y\hat{y} = -\cos(\phi_i)\hat{x} - \sin(\phi_i)\hat{y} \qquad \text{(AIV-9)}$$

IV.4 EXPRESSION FOR THE FAR-ZONE SCATTERED FIELDS

The scattered electric field due to the volume current J_z in the far zone is expressed as follows

$$\begin{aligned} E_z^{scat}\{\varphi, J_z\} &= -j\omega\mu_o \Delta x \Delta y \sum_{n=1}^{N} I_n\, e^{jkx_n\cos\phi} e^{jky_n\sin\phi} \int_{C'} e^{jk\{x'\cos\phi + y'\sin\phi\}} dS' \\ &= -j\omega\mu\Delta x\Delta y\, I_n\, e^{jkx_n\cos\phi} e^{jky_n\sin\phi} \left[\mathrm{sinc}(k\frac{\Delta x}{2}\cos(\phi))\,\mathrm{sinc}(k\frac{\Delta y}{2}\sin(\phi)) \right] \end{aligned} \qquad \text{(AIV-10)}$$

IV.5 VERIFICATION OF THE CODE 2DPBV

In order to be sure of the validity of the above formulation, it is coded in MATLAB to enable us to calculate the operator matrix terms, current coefficients, excitation vector, and scattered electric fields. Once the operator matrix is completely available through the MATLAB calculation, CM analysis can be performed regardless of the specified incident field. In addition, the code is made to check the matrix symmetry, CM current orthogonality, and CM field orthogonality.

A circular cross-section cylinder filled with dielectric material whose permittivity is equal to $\varepsilon_d = 4\varepsilon$ and radius set to 0.1λ. A is considered for code verification purposes. A TM plane wave is incident on the cylinder at $\phi_i = 0^o$. Fig. 5 compares the scattered field in the far zone of that obtained using FEKO[1] to the one obtained using 2DPBV.

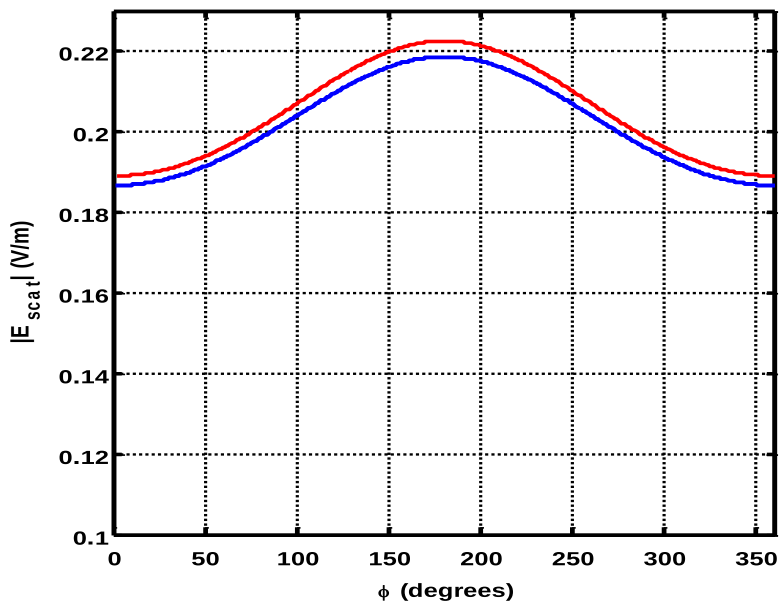

Fig. 5: the magnitude of the electric scattered field in the far zone - 2-D circular cylinder. (——) FEKO computation (——) our computation

[1] Reasons for using FEKO for a 2-D problem, and how to do it, are given in Appendix III

References

[ADAM11] J. Adams, J. Bernhard, “A Modal Approach to Tuning and Bandwidth Enhancement of an Electrically Small Antenna,” *IEEE Transactions on Antennas and Propagation*, Vol. 59, No. 4, pp 1085 – 1092, April 2011.

[AKKE05] K. Akkerman ,"The analysis and Control of Radiation from Conducting Structures using Characteristic modes”, Master Thesis, Dept. Electrical and Computer Engineering, University of Houston, USA, pp. 15-18, May 2005.

[ALRO 12] H.Alroughani, J.Ethier and D.A.McNamara, “An Appraisal of the Characteristic Modes of Dielectric Objects”, *URSI Radio Science Meeting Digest*, Chicago, USA, July 2012.

[AMEN97] G. Amendola, G. Angiulli, G. Di Massa, “Numerical and Analytical Characteristic Modes for Conducting Elliptic Cylinders,” *Microwave and Optical Technology Letters*, Vol. 16, No.4, pp. 243 – 249, November 1997.

[ANGU98] G.Angiulli and G. Di Massa, “Scattering from Arbitrarily Shaped Microstrip Patch Antennas using The Theory Of Characteristic Modes”, *IEEE Antennas and Propagation Society International Symposium*, pp. 1830-1833, 1998.

[ANTO03] E. Antonino-Daviu, M. Cabedo-Fabres, M. Ferrando-Bataller, A. Valero-Nogueira, “Wideband Double-fed Planar Monopole Antennas,” *Electronics Letters*, Vol. 39, No. 23, September 2003.

[ANTO04a] E. Antonino-Daviu, M. Cabedo-Fabres, M. Ferrando-Bataller, A. Valero-Nogueira, “A Discussion on the Feed Configuration of Planar Monopole Antennas to Obtain Ultra Wide Band Performance,” *IEEE Antennas and Propagation Society International Symposium*, Vol. 2, pp. 1867 – 1870, 2004.

[ANTO04b] E. Antonino-Daviu, M. Cabedo-Fabres, M. Ferrando-Bataller, J.I. Herranz-Herruzo, “Analysis of the Coupled Chassis-Antenna Modes in Mobile Handsets,” *IEEE Antennas and Propagation Society International Symposium*, Vol. 3, pp. 2751 – 2754, 2004.

[ANTO04c] E. Antonino-Daviu, M. Cabedo-Fabres, M. Ferrando-Bataller, A. Valero-Nogueira, “Resonant Modes in Antenna Handsets,” *Joint COST 273/284 Workshop*, Sweden, June 2004.

[ANTO05] E. Antonino-Daviu, M. Cabedo-Fabres, M. Ferrando-Bataller, A. Valero-Nogueira, M. Martinez-Vazquez, "Novel Antenna for Mobile Terminals based on the Chassis-Antenna Coupling," *IEEE Antennas and Propagation Society International Symposium*, Vol. 1A, pp. 503 – 506, 2005.

[ANTO06] E. Antonino-Daviu, C.A. Suarez-Fajardo, M. Cabedo-Fabres, M. Ferrando-Bataller, "Wideband Antenna for Mobile Terminals Based on the Handset PCB Resonance," *Microwave and Optical Technology Letters*, Vol. 48, No. 7, pp. 1408 – 1411, July 2006.

[AUST98] B.A. Austin, K.P. Murray, "The Application of Characteristic-Mode Techniques to Vehicle-Mounted NVIS Antennas," *IEEE Antennas and Propagation Magazine*, Vol. 40, Issue 1, pp. 7 – 21 & 30, February 1998.

[BALA89] C.A.Balanis, *Advanced Engineering Electromagnetics* (Wiley, 1989).

[BARB82] P.W.Barber, J.F.Owen and R.K.Chang, "Resonant Scattering for Characterization of Axisymmetric Dielectric Objects", *IEEE Trans. Antennas Propagat.*,Vol.30, No.2, pp.168-172, March 1982.

[BAUM76] C.E.Baum, "The Singularity Expansion Method" in L.B.Felsen (Edit.), *Transient Electromagnetic Fields* (Springer-Verlag, 1976) pp.129-179.

[BLAD07] J. van Bladel, *Electromagnetic Fields* (IEEE Press, 2007) 2nd Edition.

[CABE02] M. Cabedo-Fabres, A. Valero-Nogueira, M. Ferrando-Bataller, "Systematic Study of Elliptical Loop Antennas using Characteristic Modes," *IEEE Antennas and Propagation Society International Symposium*, Vol.1, pp. 156 – 159, 2002.

[CABE03b] M. Cabedo-Fabres, E. Antonino-Daviu, A. Valero-Nogueira, M. Ferrando-Bataller, "Analysis of Wide Band Planar Monopole Antennas using Characteristic Modes," *IEEE Antennas and Propagation Society International Symposium*, Vol. 3, pp. 733 – 736, 2003.

[CABE04a] M. Cabedo-Fabres, E. Antonino-Daviu, A. Valero-Nogueira, M. Ferrando-Bataller, "Optimization of the Polarization of Reflectarrays using Characteristic Modes," *IEEE Ant.and Propagation Society International Symposium*, Vol. 1, pp. 13 – 16, 2004.

[CABE04b] M. Cabedo-Fabres, A. Valero-Nogueira, J.I. Herranz-Herruzo, M. Ferrando-Bataller, "A Discussion on the Characteristic Mode Theory Limitations and its Improvement for the Effective Modeling of Antennas and Arrays," *IEEE Antennas and Propagation Society Intl. Symposium*, Vol. 1, pp. 121 – 124, 2004.

[CABE05] M. Cabedo-Fabres, E. Antonino-Daviu, A. Valero-Nogueira, M. Ferrando-Bataller, “Wideband Radiating Ground Plane with Notches,” *IEEE Antennas and Propagation Society International Symposium*, Vol. 2B, pp. 560 – 563, 2005.

[CABE06] M. Cabedo-Fabres, A. Valero-Nogueira, E. Antonino-Daviu, M. Ferrando-Bataller, “Modal Analysis of a Radiating Slotted PCB for Mobile Handsets,” *1st European Conference on Antennas and Propagation (EuCAP 2006)*, pp. 1 – 6, 2006.

[CABE07] M.Cabedo-Fabres et al., "The Theory Of Characteristic Modes Revisited : A Contribution to the Design of Antennas for Modern Applications, *IEEE Antennas Propagat. Mag.,*Vol.49, pp.52-68, Oct. 2007

[CABE03] M. Cabedo-Fabres, E. Antonino-Daviu, M. Ferrando-Bataller, A. Valero-Nogueira, “On the Use of Characteristic Modes to Describe Patch Antennas Performance,” *IEEE Antennas and Propagation Society International Symposium*, Vol. 2, pp. 712 – 715, 2003.

[CAPE11] M. Capek, P. Hazdra, and J. Eichler, “A Method of Tracking Characteristic Numbers and Vectors”, *Progress In Electromagnetics Research B*, Vol. 33, pp. 115-134, 2011.

[CART 43] P.S.Carter, “Antenna Arrays around Cylinders”, Proc.IRE, Vol.31, pp.671-693, Dec.1943.

[CHAD10] S. K. Chaudhury, H. J. Chaloupka, A. Ziroff, “Multiport Antenna Systems for MIMO and Diversity,” 4th *European Conference on Antennas and Propagation (EuCAP 2010)*, pp. 1 – 5, 2010.

[CHAL04] H. Chaloupka, X. Wang, “Novel Approach for Diversity and MIMO antennas at small Mobile Platforms,” *IEEE PIMRC-Symposium Digest*, Vol. 1, pp. 1229 – 1232, 2004.

[CHAL10] J. Chalas, K. Sertel, J. L. Volakis, “Antenna Optimization for UAV Platforms using Characteristic Modes,” *Antennas and Propagation Society International Symposium (APS*), 2010.

[CHAL11] J. Chalas, K. Sertel, J. L. Volakis, “Computation of the Q Limits for Arbitrary-Shaped Antennas using Characteristic Modes,” *Antennas and Propagation Society International Symposium (APS*), 2011.

[CHAN77] Y. Chang, R.F. Harrington, “A Surface Formulation for Characteristic

Modes of Material Bodies,” *IEEE Transactions on Antennas and Propagation*, Vol. 25, No. 6, pp 789 – 795, November 1977.

[CHAU07] J.Chauveau, N. de Beaucoudrey and J.Saillard, “Selection of Contributing Natural Poles for the Characterization of Perfectly Conducting Targets in Resonance Region”, *IEEE Trans. Antennas Propagat.*, Vol.55, No.9, pp.2610-2617, Sept.2007.

[CHAU07a] S. K. Chaudhury, W. L. Schroeder, H. J. Chaloupka, “Multiple Antenna Concept Based on Characteristic Modes of Mobile Phone Chassis,” 2nd *European Conference on Antennas and Propagation (EuCAP 2006)*, pp. 1 – 6, 2007.

[CHAU07b] S. K. Chaudhury, W. L. Schroeder, H. J. Chaloupka, “MIMO Antenna System Based on Orthogonality of the Characteristic Modes of a Mobile Device,” *2nd International ITG Conference on Antennas*, pp. 58 – 62, 2007.

[CHAU08] S. K. Chaudhury, H. J. Chaloupka, A. Ziroff, “Novel MIMO Antennas for Mobile Terminals,” *38th European Microwave Conference (EuMC)*, pp. 1751 – 1754, 2008.

[CHAU10] J.Chauveau, N. de Beaucoudrey and J.Saillard, “Resonance Behaviour of Radar Targets with Aperture : Example of an Open Rectangular Cavity”, *IEEE Trans. Antennas Propagat.*, Vol.58, No.6, pp.2060-2068, June 2010.

[CHO90] S.K.Cho, *Electromagnetic Scattering* (Springer-Verlag, 1990) pp.309

[CHUA85] C.Chuang, D.P.Nyquist, K.Chen and B.Drachman, “Singularity Expansion Method Formulation for Impulse Response of a Perfectly Conducting Thick Cylinder”, *Radio Science*, Vol.20, No.5, pp.1025-1030, 1985.

[COLL 91] R.E.Collin, *Field Theory of Guided Waves* (IEEE Press, 1991) 2nd Edition.

[COLL12] S.Collardey, P.Pouliguen, P.Potier and A.Sharaiha, “Characterization of UWB Antenna in Time Domain using the Complex Natural Resonances”, *IEEE Int. AP-S Symp. Digest*, Chicago, USA, 2009.

[DICH97] M. Dich, “Accurate Determination of Antenna Directivity”, *IEEE Transactions On Antennas And Propagation*, Vol.45, No.10, pp. 1502-1505, October 1997

[DOLP80] C.L.Dolph and S.K.Cho, "On the Relationship between the Singularity Expansion Method and the Mathematical Theory of Scattering", *IEEE Trans. Antennas Propagat.*, Vol.AP-28, No.6, pp.888-897, Nov.1980.

[EBER05] D. Eber, H. Chaloupka, "Design Approach for a Class of Compact Multiport Antennas," *Microwave, Antennas, Propagation and EMC Technologies for Wireless Comm.*, Vol. 1, pp 144 – 147, Aug 2005.

[ELHA92] A. El-Hajj, K. Kabalan, R.F. Harrington, "Characteristic Modes of a Slot in a Conducting Cylinder and their use for Penetration and Scattering, TE Case," *IEEE Transactions on Antennas and Propagation*, Vol. 40, No. 2, pp. 156 – 161, February 1992.

[ELSH92b] A. Elsherbeni and A. Kishk, "Modeling of Cylindrical by Circular Dielectric and Conducting Cylinders", *IEEE Transactions On Antennas And Propagation*, Vol.40, No.1, January 1992

[EOM04] H.J.Eom, *Electromagnetic Wave Theory for Boundary Value Problems* (Springer, 2004).

[ETHI08a] J. Ethier, "MIMO Antenna Design using Characteristic Mode Concepts," Masters Thesis, University of Ottawa, Canada, 2008.

[ETHI08b] J. Ethier, D. McNamara, "An Interpretation of Mode-Decoupled MIMO Antennas in Terms of Characteristic Port Modes", *13th Biennial IEEE Conference on Electromagnetic Field Computation Digest*, Athens, Greece, May 11 – 15, 2008.

[ETHI08c] J. Ethier, D. McNamara, "The Use of Generalized Modes in the Design of MIMO Antennas", *13th Biennial IEEE Conference on Electromagnetic Field Computation Digest*, Athens, Greece, May 11 – 15, 2008.

[ETHI08d] J. Ethier, E. Lanoue and D. McNamara, "MIMO Handheld Antenna Design Approach using Characteristic Mode Concepts", *Microwave and Optical Technology Letters*, Volume 50, No. 7, July 2008, pp.1724 – 1727.

[ETHI09a] J. Ethier, D. McNamara "The Use of Generalized Modes in the Design of MIMO Antennas", *IEEE Transactions on Magnetics*, Volume 45, Number 3, March 2009, pp. 1124 – 1127.

[ETHI09b] J. Ethier, D. McNamara, "An Interpretation of Mode-Decoupled MIMO Antennas in Terms of Characteristic Port Modes", *IEEE Transactions on Magnetics*, Volume 45, Number 3, March 2009, pp. 1128 – 1131.

[ETHI10a] J. Ethier and D. McNamara, “A Modal Significance Measure in the Characteristic Mode Analysis of Radiating Structures”, *Electronics Letters*, Vol. 46, No. 2, January 21, 2010.

[ETHI10b] J.Ethier and D.A.McNamara, “Multiband Antenna Synthesis using Characteristic Mode Indicators as an Objective Function for Optimization”, Proc. *2010 IEEE International Conference on Wireless Information Technology and Systems* (*ICWITS’2010*), USA, August/September 2010.

[ETHI10c] J.Ethier and D.A.McNamara, “Through the Looking Glass : A Characteristic Mode View of Electromagnetic Modeling & Design" , Proc. *14th Int. Symposium on Antenna Technology & Applied Electromagnetics (ANTEM’2010)*, Ottawa, July 2010.

[ETHI12a] J.Ethier & D.A.McNamara, "A Sub-Structure Characteristic Mode Concept for Antenna Shape Synthesis", *Electronics Letters*, Vol.48, No.9, April 2012.

[ETHI12b] J.Ethier & D.A.McNamara, “Predicting Infinite Periodic Structure Properties from Finite Structure Models”, *Microwave & Optical Technology Letters*, Vol.54, No.10, pp.2416-2420, Oct.2012.

[ETHI12c] J.Ethier and D.A.McNamara, “Further Applications of a Characteristic Mode Based Antenna Shape Synthesis Method”, Proc. *2012 IEEE International Conference on Wireless Information Technology and Systems* (*ICWITS’2012*), USA, Nov.2012.

[FAMD06] C.T. Famdie, W.L. Schroeder, K. Solbach, “Numerical Analysis of Characteristic Modes on the Chassis of Mobile Phones,” *1st European Conference on Antennas and Propagation (EuCAP 2006)*, pp. 1 – 6, 2006.

[FEKO] *FEKO*, EM Software & Systems Inc. (www.feko.info).

[GALL13] F.Gallée, T.Bernabeau, M. Cabedo-Fabres, E. Antonino-Daviu, A. Valero-Nogueira, “Application of the Theory of Characteristic Modes to the Design of Compact Metallic Strip Antenna with Multilayer Technology (LTCC)”, 7th *European Conference on Antennas and Propagation (EuCAP 2013)*, pp. 1891-1895, 2013.

[GARB65] R.J.Garbacz, “Modal Expansions for Resonance Scattering Phenomena,” *Proceedings of the IEEE*, pp. 856 – 864, August 1965.

[GARB68] R.J.Garbacz, "A Generalized Expansion for Radiation and Scattered Fields," Ph.D. Dissertation, Ohio State University, Columbus, 1968.

[GARB71] R.J.Garbacz and R.Turpin, "A Generalized Expansion for Radiated and Scattered Fields," *IEEE Transactions on Antennas and Propagation*, Vol. AP-19, No. 3, pp. 856 – 864, May 1971.

[GARB80] R. Garbacz, E.H. Newman, "Characteristic Modes of a Symmetric Wire Cross," *IEEE Transactions on Antennas and Propagation*, Vol. AP-28, No. 5, pp 712 – 715, September 1980.

[GARB82] R. Garbacz, D. Pozar, "Antenna Shape Synthesis using Characteristic Modes," *IEEE Transactions on Antennas and Propagation*, Vol. 30, No. 3, pp 340 – 350, May 1982.

[GAST67] M.Gastine, L.Courtois and J.L.Dormann, "Electromagnetic Resonances of Free Dielectric Spheres", *IEEE Trans. Microwave Theory Tech*., Vol.15, No.12, pp.694-700, Dec.1967.

[GIRI12] D.V.Giri and F.M.Tesche, "An Overview of the Natural Frequencies of A Straight Wire by Various Methods", *IEEE Trans. Antennas Propagat.,*Vol.60, No.12, pp.5859-5866, Dec.2012

[GLIS80a] A.W.Glisson and C.M.Butler, "Analysis of a Wire Antenna in the Presence of a Body of Revolution", *IEEE Transactions on Antennas and Propagation*, Vol. 28, No. 5, pp 604-609, Sept.1980.

[GLIS80b] A.W.Glisson and D.R.Wilton, "Simple and Efficient Numerical Methods for Problems of Electromagnetic Radiation and Scattering from Surfaces", *IEEE Trans. Antennas Propagat*., Vol.28, No.5, pp.593-603, Sept.1980.

[GLIS83] A.W.Glisson, D.Kajfez and J.James, "Evaluation of Modes in Dielectric Resonators using a Surface Integral Equation Formulation", *IEEE MTT-S Digest*, pp.409-411, 1983.

[GOGG90] P. Goggans ,"A Combined Method-of-Moments and Approximate Boundary Condition Solution For Scattering From Conducting Body with A Dielectric-Filled Cavity", Ph.D Dissertation, Department of Electrical Engineering, Auburn University, Mar 1990.

[GOLU 96] G.H.Golub and C.F. van Loan, *Matrix Computation* (John Hopkins University Press, 1996) Third Edition, pp.311.

[HANS02] G.W.Hanson and A.B.Yakovlev, *Operator Theory for Electromagnetics*

(Springer, 2002) pp.583-585.

[HARR 69] R.F.Harrington and J.R.Mautz, “Radiation and Scattering from Bodies of Revolution”, Appl. Sci. Res., pp.405-435, June 1969.

[HARR71a] R.F.Harrington and J.R.Mautz, “Theory of Characteristic Modes for Conducting Bodies,” *IEEE Transactions on Antennas and Propagation*, Vol. AP-19, No. 5, pp. 622 – 628, September 1971.

[HARR71b] R.F.Harrington and J.R.Mautz, “Computation of Characteristic Modes for Conducting Bodies,” *IEEE Transactions on Antennas and Propagation*, Vol. AP-19, No. 5, pp. 629 – 639, September 1971.

[HARR72a] R. F. Harrington, J. Mautz, Y. Chang, “Characteristic Modes for Dielectric and Magnetic Bodies,” *IEEE Transactions on Antennas and Propagation*, Vol. AP-20, No. 2, pp. 194 – 198, March 1972.

[HARR72b] R. F. Harrington, J. Mautz, “Control of Radar Scattering by Reactive Loading,” *IEEE Transactions on Antennas and Propagation*, Vol. AP-20, No. 4, pp 446 – 454, July 1972.

[HARR74a] R.F. Harrington, J. Mautz, “Pattern Synthesis for Loaded N-Port Scatterers”, *IEEE Transactions on Antennas and Propagation*, Vol. AP-22, No. 2, March 1974.

[HARR74b] R.F. Harrington, J. Mautz, “Optimization of Radar Cross Section of N-Port Loaded Scatterers”, *IEEE Transactions on Antennas and Propagation*, Vol. AP-22, No. 5, September 1974.

[HARR76] R.F.Harrington & J.R.Mautz, "A Generalised Network Formulation for Aperture Problems", *IEEE Trans. Antennas Propagat.*, Vol.AP-24, No.11, pp.870-873, Nov.1976.

[HARR80] J.R.Mautz and R.F.Harrington, "Boundary Formulation for Aperture Coupling Problems", Archiv für Elektronik und Übertragung (AEÜ), Vol.34, No.9, pp.377-388, 1980.

[HARR85] R.F. Harrington, J.R. Mautz, “Characteristic Modes for Aperture Problems,” *IEEE Transactions on Microwave Theory and Techniques*, Vol. 33, No. 6, pp. 500 – 505, 1985.

[HEYM 89] E.Heyman, G.Friedlander and L.B.Felsen, “Ray-mode Analysis of Complex Resonances of an Open Cavity”, *Proc. IEEE*, Vol.77, N.5, pp.780787, May 1989.

[HILB89] M. Hilbert, M.A. Tilston, K.G. Balmain, “Resonance Phenomena of Log-Periodic Antennas: Characteristic-Mode Analysis,” *IEEE Transactions on Antennas and Propagation*, Vol. 37, No. 10, pp. 1224 – 1234, October 1989.

[INAG82] N. Inagaki, R. Garbacz, “Eigenfunctions of Composite Hermitian Operators with Application to Discrete and Continuous Radiating Systems”, *IEEE Transactions on Antennas and Propagation,* Vol. AP-30, No. 4, pp 571 – 575, July 1982.

[JOHN90] W.A.Johnson, D.R.Wilton & R.M.Sharpe, "Modeling Scattering from and Radiation by Arbitrarily Shaped Objects with the Electric Field Integral Equation Triangular Surface Patch Code", *Electromagnetics,* Vol.10, pp.41-63, 1990.

[JONE64] D.S.Jones, *Theory of Electromagnetism* (MacMillan, 1964) pp.73

[KABA87a] K. Kabalan, R.F. Harrington, H. Auda, J.R. Mautz, “Characteristic Modes for Slots in a Conducting Plane, TE Case,” *IEEE Transactions on Antennas and Prop.*, Vol. 35, No. 2, pp. 162 – 168, February 1987.

[KABA87b] K. Kabalan, R.F. Harrington, H. Auda, J.R. Mautz, “Characteristic Modes for Slots in a Conducting Plane, TM Case,” *IEEE Transactions on Antennas and Prop.*, Vol. 35, No. 3, pp. 331 – 335, March 1987.

[KABA90] K. Kabalan, A. El-Hajj, R.F. Harrington, “Characteristic Mode Analysis of a Slot in a Conducting Plane Separating Different Media,” *IEEE Transactions on Antennas and Propagation*, Vol. 38, No. 4, pp. 476 – 481, April 1990.

[KAJF83] D.Kajfez, A.W.Glisson & J.James, “Evaluation of Modes in Dielectric Resonators using a Surface Integral Equation Formulation”, *IEEE Trans. Microwave Theory Tech.*, Vol.31, No.12, pp.1023-1029, Dec.1983.

[KAJF84] D.Kajfez, A.W.Glisson & J.James, “Computed Modal Field Distributions for Isolated Dielectric Resonators”, *IEEE Trans. Microwave Theory Tech.,* Vol.32, No.12, pp.1609-1616, Dec.1984.

[KRIS84] G.Kristensson, “Natural Frequencies of Circular Disks”, *IEEE Trans. Antennas Propagat.*, Vol.32, No.5, pp.442-448, May 1984.

[KUCH00a] A.A.Kucharski, “Resonances in Heterogeneous Dielectric Bodies with Rotational Symmetry – Volume Integral-Equation Formulation”, *IEEE Trans. Antennas Propagat.*, Vol.48, No.5, pp.766- 770, May 2000.

[KUCH00b] A.A.Kucharski, “A Method of Moments Solution for Electromagnetic Scattering by Inhomogeneous Dielectric Bodies of Revolution”, *IEEE Trans. Antennas Propagat.*, Vol.48, No.8, pp.1202-1210, Aug.2000

[KYRI 13] G.A.Kyriacou, C.S.Lavranos, P.C.Allilomes, C.Zekios, S.Lavdas and A.V.Kudrin, “Eigenanalysis of Open, Periodic, and Curved Waveguide structures”, *URSI, Radio Science Bulletin*, No.344, pp.13-31, March 2013.

[LAWR10] J.K.Lawrence, “On the Use of Natural-Mode Basis Functions for Electromagnetic Analysis of Arbitrary Conducting Surfaces”, Masters Thesis, Department of Electrical Engineering, Clemson University, USA, 2012.

[LAWR12] J.K.Lawrence and A.Q.Martin, “Using Natural-Mode Basis Functions to Represent Broadband Responses of a Thin-Wire Scatterer”, *IEEE Int. AP-S Symp. Digest*, Chicago, USA, 2012.

[LAZA10] M.Lazarus, "The great spectrum famine", *IEEE Spectrum*, Vol.47, No.10, pp.26-31, Oct.2010

[LIU01] Y. Liu, S. Safavi-Naeini, S. Chaudhuri, and R. Sabry, “On the Determination of Resonant Modes of Dielectric Objects using Surface Integral Equations”, *IEEE Transactions On Antennas And Propagation*, Vol.52, No.4, April 2001

[LIU04] Y.Liu, S.Safavi-Naeini, S.K.Chaudhuri and R.Sabry, "On the Determination of Resonant Modes of Dielectric Objects using Surface Integral Equations", *IEEE Trans. Antennas Propagat.*, Vol.52, pp.1062-1069, 2004.

[LIU90] D. Liu, R. Garbacz, D. Pozar, “Antenna Synthesis and Optimization using Generalized Characteristic Modes”, *IEEE Transactions on Antennas and Propagation*, Vol. 38, No. 6, pp 862 – 868, June 1990.

[LONG 94] Y.Long, “Determination of the Natural Frequencies for Conducting Rectangular Boxes”, *IEEE Trans. Antennas Propagat.*, Vol.42, No.7, pp.1016-1021, July 1994.

[LUCK51] W.S.Lucke, “Electric Dipoles in the Presence of Elliptic or Circular Cylinders”, *J. Appl. Physics*, Vol.22, No.1, pp.14-19, jan.1951.

[MAKA02] S.N.Makarov, *Antenna and EM Modeling with Matlab* (Wiley, 2002).

[MART72] L.Martin, “Representation of Transient Scattered Fields in Terms of Free Oscillations of Bodies”, *Proc. IEEE,* pp.640-641, May 1972.

[MAUT73] J.Mautz and R.F.Harrington, “Modal Analysis of Loaded N-Port Scatterers”, *IEEE Transactions on Antennas and Propagation*, Vol. AP-21, No. 2, March 1973.

[MAUT73] J. Mautz, R.F. Harrington, “Modal Analysis of Loaded N-Port Scatterers”, *IEEE Transactions on Antennas and Propagation*, Vol. AP-21, No. 2, March 1973.

[MAXI12] R.Maximidis, C.L.Zekios, P.C.Allilomes, A.V.Kudrin and G.A.Kyriacou, “A Characteristic Mode Eigenanalysis Exploiting FEM Features”, *Progress in Electromagnetics Research Symposium (PIERS),* Moscow, Aug. 2012.

[MAYH90] J.T. Mayhan, “Characteristic Modes and Wire Grid Modeling,” *IEEE Transactions on Antennas and Propagation,* Vol. 38, No. 4, pp. 457 – 469, April 1990.

[MONG94] R.K.Mongia, L.Larose, S.R.Mishra, and P.Bhartia, “Accurate Measurement of Q-Factors of Isolated Dielectric Resonators”, *IEEE Trans. Antennas Propagation,* Vol. 42, No. 8, pp.1463-1467, August 1994

[MURR94] K.P. Murray, B.A. Austin, “Synthesis of Vehicular Antenna NVIS Radiation Patterns using the Method of Characteristic Modes,” *IEE Proceedings of Microwaves, Antennas and Propagation,* Vol. 141, No. 3, pp. 151 – 154, June 1994.

[MYER11] J.M.Myers, S.S.Sandler and T.T.Wu, “Electromagnetic Resonances of a Straight Wire”, *IEEE Trans. Antennas Propagat.,*Vol.59, No.1, pp.129-134, Jan.2011.

[NALB82] A.H.Nalbantoğlu, “New Computation Method for Characteristic Modes”, Electronics Letters, Vol.18, No.23, pp.994-996, Nov.1982.

[NASH92] M.Nashimoto, H.Ikuno and M.Kawano, “On Natural Modes Excited by Incident Pulse”, *Proc. ISAP'92,* pp.597-600, Japan, 1992.

[NEWM77] E.H. Newman, “Small Antenna Location Synthesis using Characteristic Modes,” *IEEE Transactions on Antennas and Propagation*, Vol. AP-25, No. 4, pp 530 – 795, November 1977.

[OBEI08] K. Obeidat, B. Raines, R.G. Rojas, “Design and Analysis of a Helical

Spherical Antenna using the Theory of Characteristic Modes," *Antennas and Propagation Society International Symposium (APS*), pp. 1 – 4, 2008.

[OBEI10] K. Obeidat, B. Raines, R.G. Rojas, "Application of Characteristic Modes and Non-Foster Multiport Loading to the Design of Broadband Antennas," *IEEE Transactions on Antennas and Propagation,* Vol. 58, Issue 1, pp 203 – 207, 2010.

[PETE97] A.Peterson, S.Ray and R.Mittra, *Computational Methods for Electromagnetics* (IEEE Press, 1997).

[PETO07] A.Petosa, *Dielectric Antenna Handbook* (Artech House, 2007)

[POZA84] D. Pozar, "Antenna Synthesis and Optimization using Weighted Inagaki Modes", *IEEE Transactions on Antennas and Propagation*, Vol. AP-32, No. 2, pp 159 – 165, February 1984.

[RAIN10] B. Raines, R.G. Rojas, "Design of Multiband Reconfigurable Antennas," 4th *European Conference on Antennas and Propagation (EuCAP 2010)*, pp. 1 – 5, 2010.

[RAIN12] B. Raines, and Roberto Rojas, "Wideband Characteristic Mode Tracking", *IEEE Transactions On Antennas And Propagation*, Vol. 60, No. 7, pp.3537-3541, July 2012.

[RICH39] D.Richtmyer, "Dielectric Resonators", *J.Appl.Phys*., Vol.10, pp.391-398, June 1939.

[ROTH 99] E.Rothwell and M.Cloud, "Natural Frequencies of a Conducting Sphere with a Circular Aperture", *J. Electromagnetic Waves Applications*, Vol.13, pp.729-755, 1999.

[SAFI 13] E.Safin and D.Manteuffel, "Reconstruction of the Characteristic Modes on an Antenna based on the Radiated far Field", *IEEE Transactions on Antennas and Propagation*, Vol. 61, No.6, pp.2964-2971, June 2013.

[SAHA 09] A.Sahai, S.M.Mishra, R.Tandra & K.A.Woyach, "Cognitive Radios for Spectrum Sharing", *IEEE Signal Processing Magazine*, pp.140-145, Jan.2009

[SCHAU84] D.H.Schaubert, D.R.Wllton, and A. W.Glisson, "A Tetrahedral Modeling for Electromagnetic Scatterlng by Arbitrary Shaped Homogeneous Dielectrlc Bodies", *IEEE Trans. Antennas Propagat*., Vol. AP-32. pp 77-85, 1984.

[SCHR05] W.L. Schroeder, C.T. Famdie, K. Solbach, "Utilisation and Tuning of the Chassis Modes of a Handheld Terminal for the Design of Multiband Radiation Characteristics," *IEE Wideband and Multi-band Ant. and Arrays*, pp. 117 – 121, 2005.

[SCHR06] W.L. Schroeder, A.A. Vila, C. Thome, "Extremely Small, Wide-band Mobile Phone Antennas by Inductive Chassis Mode Coupling," *Proceedings of the 9th European Conference on Wireless Technology*, pp. 407 – 410, 2006.

[STRA41] J.A.Stratton, *Electromagnetic Theory* (McGraw-Hill, 1941).

[SUN89] W.Sun, K.Chen, D.Nyquist and E.Rothwell, "The Natural Oscillations of an Infinitely Long Cylinder with Lossy Material", *Radio Science,* Vol.24, No.3, pp.369-380, May-June 1989.

[SUN90] W.Sun, K.Chen, D.Nyquist and E.Rothwell, "Determination of The Natural Modes for a Rectangular Plate", *IEEE Trans. Antennas Propagat.,*Vol.38, pp.643-652, May 1990.

[SURI04] N. Surittikul, R.G. Rojas, "Analysis of Reconfigurable Printed Antenna using Characteristic Modes: FDTD Approach," *IEEE Antennas and Propagation Society Intl Symposium*, Vol. 2, pp. 1808 – 1811, 2004.

[SURI05] N. Surittikul, R.G. Rojas, "Time Domain Method of Characteristic Modes for the Analysis / Design of Reconfigurable Antennas," *IEEE Antennas and Propagation Society International Symposium*, Vol. 2B, pp. 585 – 588, 2005.

[TAYL82] A.W.Naylor and G.R.Sell, *Linear Operator Theory in Engineering and Science* (Springer-Verlag, 1982)

[TYRA69] G.Tyras, *Radiation and Propagation of Electromagnetic Waves* (Academic Press, 1969)

[UMAS86] K.A.Umashankar, A. Taflove and S. M. Rao, "Electromagnetic Scattering By Arbitrary Shaped Three-Dimensional Homogeneous Lossy Dielectric Bodies," *IEEE Trans. Antennas Propagat.,* Vol.34, No. 6, pp.758–766, June 1986.

[VAIN09] P.Vainikainen, J.Holopainen, C.Icheln, O.Kivekas, M.Kyro, M.Mustonen, S.Ranvier, R.Valkonen and J.Villanen, "More Than 20 Antenna Elements in Future Mobile Phones : Threat or Opportunity?", *3rd European Conf. Antennas Propagation (EuCAP)*, pp.2940-2943, March 2009

[VANN12] C. van Niekerk and J.T.Bernhard, “Characteristic Mode Analysis of a Shorted Microstrip Patch Antenna”, *IEEE Antennas and Propagation Society International Symposium*, 2012.

[VECH 90] S.R.Vechinski and T.H.Shumpert, “Natural Resonances of Conducting Bodies of Revolution”, *IEEE Trans. Antennas Propagat.*, Vol.38, No.7, pp.1133-1136, July 1990.

[VESC89] R.Vescovo, “Characteristic Modes for Bodies Endowed with Mutually Orthogonal Symmetry Planes”, *Microwave & Optical Technology Letters*, Vol.2, No.11, pp.390-393, Nov.1989.

[VESC90] R.Vescovo and T.Corzani, “Characteristic Modes for Non-Conducting Bodies Having Mutually Orthogonal Symmetry Planes”, *Microwave & Optical Technology Letters*, Vol.3, pp.124-127, April 1990.

[WILT82] D.R.Wilton and C.M.Butler, “Observations Resulting from Eigensolutions of Integral Equations”, *URSI National Radio Science Meeting Digest*, Albuquerque, USA, pp.36, 1982 (Presentation Slides Provided by D.R.Wilton).

[YEE73] A. Yee, R. Garbacz “Self- and Mutual-Admittances of Wire Antennas in Terms of Characteristic Modes,” *IEEE Transactions on Antennas and Propagation*, Vol. 21, No. 6, pp 868 – 871, November 1973.

[YUAN87] X. Yuan, R. F. Harrington, and S. S. Lee, “Electromagnetic Scattering by a Dielectric Cylinder Partially Covered by Conductors”, *Journal Of Electromagnetic Wave And Application*, Vol.2,No.1, pp.21-44, 1987

[ZEKI13] C.L.Zekios, P.C.Allilomes and G.A.Kyriacou, “Eigenanalysis of Electromagnetic Structures Based on the Finite Element Method, *Applied Mathematics*, Vol.4, pp.1009 – 1022, July 2013.